Design of Steel Plate Shear Wall Systems with Explicit Consideration of Drift Demands and Frame Action

by

Meisam Safari Gorji

A thesis submitted in partial fulfillment of the requirements for the degree of

Doctor of Philosophy

in
Structural Engineering

Department of Civil and Environmental Engineering
University of Alberta

Abstract

This research presents a performance-based design procedure for steel plate shear wall (SPSW) systems with explicit consideration of plastic mechanisms, inelastic drift demands and frame actions. The proposed design procedure generally adopts the philosophy of a recently developed performance-based plastic design (PBPD) methodology in which an energy-work balance concept is employed to produce structures with targeted seismic performance, taking advantage of plastic analysis method and capacity design principles. The intention is to address some of the shortcomings of current SPSW design practice.

Based on extensive nonlinear response-history analyses of SPSWs having different bay widths and overall heights, a simple empirical expression was proposed for predicting yield drift ratio, which is an essential parameter to be used at the beginning of the design process. A step-by-step design procedure was presented and various design parameters were studied. The validity of the proposed design approach was tested by evaluating the seismic behaviour of case study SPSWs designed for buildings located in Canada and the U.S. having different seismic hazard levels.

Next, the proposed approach was used as a reliable design procedure to perform a comprehensive study of alternative SPSW configurations, aiming to improve some of the drawbacks of the conventional SPSW systems. As such, the design procedure was further extended to include two other SPSW configurations,

namely (1) SPSW with Outriggers (SPSW-O) and (2) Coupled SPSW (C-SPSW). The above-mentioned SPSW configurations are intended to enhance the overturning stiffness of SPSWs, while improving material efficiency and providing architectural flexibility. The plastic method of structural analysis was used to investigate the behaviour, mechanisms and efficiency of these SPSW configurations, and to develop procedures for efficient design of such structural systems.

Four different SPSW-O options were discussed and their structural characteristics were investigated in terms of lateral load resistance and overturning stiffness. A simple parameter called the outrigger efficiency factor (OEF) was defined to quantify the level of the overturning stiffness provided by the outrigger system; this allows for the comparison of various SPSW-Os on a consistent basis. Closed form analytical expressions that capture the ultimate lateral strength and OEF SPSW-Os were developed and compared with numerical simulations with reasonable agreement. Furthermore, a comprehensive parametric study was conducted to investigate the influence of a number of parameters on the behaviour of SPSW-O systems. Parameters subjected to investigation included the height of the systems, the length and properties of the outrigger beams, and the types of beam-to-column connections used in the systems. Subsequently, 12- and 20-story SPSW-O systems were designed using the proposed design procedure; and their seismic performances were evaluated under a suite of 20 ground motions representing the design-level earthquakes.

Further, the proposed design approach was extended to the coupled SPSW systems considering two different options, namely (1) C-SPSW with simple boundary frame connections and (2) C-SPSW with moment-resisting boundary frame connections. The C-SPSW configuration constitutes a dual system in which a substantial proportion of the story shear is resisted through the moment-resisting actions of the coupling beams and boundary frame elements. The principles of plastic analysis and capacity design were used to develop procedures for efficient designs of the two C-SPSW options by explicitly considering the contributions of the frame actions to the overall lateral strengths of such systems. This was done by estimating an appropriate proportion of the design force that should be used to size the infill plates within each system. Eight and 12-story C-SPSWs were designed using the proposed procedures, along with two uncoupled pairs of SPSWs designed for comparison. A series of nonlinear response history and pushover analyses were conducted to evaluate and compare the seismic performances of the prototypes.

Dedicated to my loving parents, Hosseinali and Ehteram,
who have taught me the value of education and
the essence of “Never Give Up” in life.

Acknowledgements

I would like to acknowledge the many people in my life who have supported me, not only in writing this thesis but in my journey to pursue my dream.

I am extremely grateful to my supervisor, Professor J.J.Roger Cheng, for his valuable advice not only related to research and teaching, but also that to my career and life in general. He has kindly supported me throughout my thesis with his knowledge and encouragement, while providing me with the freedom to conduct my PhD research in my own way.

I would like to express my appreciation to my doctoral committee, Professors Robert G. Driver, Samer Adeeb, Lijun Deng, and Xiaodong Wang for making time to serve on my doctoral committee. I would also like to thank Professor Tony Yang from the University of British Columbia for serving as my external committee member.

Many thanks are due to my friends and colleagues who shared their thoughts and resources.

The financial support provided through my supervisor and the Faculty of Graduate Studies and Research of the University of Alberta is greatly appreciated. I am also thankful to the friendly staff of the Department of Civil and Environmental Engineering at the U of A. Their services are gratefully appreciated and acknowledged.

In addition, I would like to immensely thank my dear parents, for their endless love, support and self-sacrifices, without which I would have lost the track of my life. To my dear brother and sister, Arash and Alaleh, thanks for always being there for me. I am also thankful to my friends and extended family back home, for their mental support and encouragements. Also, a warm and heartfelt thought to my late grandparents—sadly they will not see the end of this work.

Last, but certainly not the least, to my dear fiancée Alisa: you sustain me with the unconditional love you give. “After all I’m forever in your debt…”

Contents

List of Tables

List of Figures

List of Abbreviations and Symbols

Abbreviations

BRB	Buckling restrained brace
C-SPSW	Coupled steel plate shear wall
D	Ductile
DBE	Design basis earthquake
DBD	Displacement-based design
DC	Degree of coupling
DDBD	Direct displacement-based design
EP	Elastic-plastic
HBE	Horizontal boundary element
LD	Limited ductility
MCE	Maximum considered earthquake
MDOF	Multi-degree-of-freedom
OEF	Outrigger efficiency factor
PBOD	Performance-based optimum design
PBPD	Performance-based plastic design
RBS	Reduced-beam section
SDOF	Single-degree-of-freedom
SPSW	Steel plate shear wall
SPSW-O	Steel plate shear wall with outrigger
VBE	Vertical boundary element

Symbols

A_b	Cross-sectional area of beam
A_c	Cross-sectional area of VBE
DC	Degree of coupling
E	Young's modulus
E_e	Elastic component of the internal work

e_{max}	Maximum elongation of the strip elements
E_p	Plastic component of the internal work
e_y	Yield elongation of the strip elements
F_D	Design lateral force
F_{Di}	Lateral design force at story i
F_i	Lateral force at story i
F_p	panel plastic strength
F_{Pi}	Lateral force at needed at level i to develop plastic mechanism
F_y	Yield stress of steel
g	Gravitational acceleration
H	Height of the structure
h_i	Elevation of story level i from ground
h_n	Elevation of story level n from ground
h_{si}	Height of the story i
I_b	Moment inertia of beam
I_c	Moment inertia of column
I_e	Seismic importance factor
L	Bay width of the steel plate shear wall
L'	Outrigger bay width
M	Total mass of the system
M_{CB}	Plastic moment capacity of coupling beam
M_{CBi}	Plastic moment capacity of coupling beam at level i
$M_{Coupling}$	Moment resistance due to coupling action
M_{EVBE}	Plastic moment capacity of external VBE
M_{IVBE}	Plastic moment capacity of internal VBE
M_{HBE}	Plastic moment capacity of HBE
M_{HBEi}	Plastic moment capacity of HBE at story i
M_{OB}	Plastic moment capacity of outrigger beam

$M_{(OB)i}$	Plastic moment capacity of outrigger beam at level i
M_{OC}	Plastic moment capacity of outrigger column
$M_{OC\,i}$	Plastic moment capacity of outrigger column at story i
M_{OBi}	Plastic moment capacity of outrigger beam at level i
$M_{Outrigger}$	Moment resistance due to outrigger system
M_{Pier}	Overturning resistance in SPSW pier
M_{SPSW}	Moment resistance at the base of SPSW
M_v	Higher mode factor
M_{VBE}	Plastic moment capacity of VBE
$M_{VBE\,(Ext)}$	Plastic moment capacity of external VBEs in coupled SPSW
$M_{VBE\ i}$	Plastic moment capacity of VBE at story i
$M_{VBE(Int)}$	Plastic moment capacity of internal VBE
N	Number of stories
OEF	Outrigger efficiency factor
P_{LVBE}	Axial force in the left VBE
P_{OC}	Axial force in the outrigger column
P_{RHBE}	Axial force in the right VBE
R	Response modification factor
R_d	Ductility-related force modification factor
R_o	Overstrength-related force modification factor
R_μ	Ductility reduction factor
S_a	Pseudo spectral acceleration
S_{DS}	Design spectral acceleration parameter at short periods
S_{D1}	Design spectral acceleration parameter at period of 1 sec
S_v	Design spectral pseudo-velocity
T	Fundamental period of structure
t_i	Thickness of infill panel of story i
t_w	Infill panel thickness

V_{OB}	Shear force in outrigger beam
V_e	Elastic base shear
V_i	Story shear at level i
V_{LHBE}	Plastic moment capacity of left HBE
V_P	Plastic strength of the system
V_r	Shear resistance
V_y	Base shear at yield
W	Total seismic weight of the system
W_{Ex}	Work due to external forces
w_i	Weight of the structure at level i
w_n	Weight of the structure at level n
Z	Plastic section modulus
Z_{RBS}	plastic section modulus of reduced beam section

Greek Symbols

α	Design base shear parameter
α_i	Tension field inclination angle at story level i
Δ_u	Maximum drift
Δ_y	Yield drift
Φ	Resistance factor for steel
Ω	System overstrength
γ	Energy modification factor
κ	Percentage of the total lateral design force assigned to infill panel
$\kappa_{balanced}$	Percentage of the total lateral design force assigned to infill panel in balanced condition
$\kappa_{optimum(P)}$	Percentage of the total lateral design force assigned to infill panel to achieve optimum design in C-SPSW (P) system
$\kappa_{optimum\ (PP)}$	Percentage of the total lateral design force assigned to infill panel to achieve optimum design in SPSW-O (PP) system

$\kappa_{optimum\ (PR)}$	Percentage of the total lateral design force assigned to infill panel to achieve optimum design in SPSW-O (PR) system
$\kappa_{optimum\ (R)}$	Percentage of the total lateral design force assigned to infill panel to achieve optimum design in C-SPSW (R) system
$\kappa_{optimum\ (RP)}$	Percentage of the total lateral design force assigned to infill panel to achieve optimum design in SPSW-O (RP) system
$\kappa_{optimum\ (RR)}$	Percentage of the total lateral design force assigned to infill panel to achieve optimum design in SPSW-O (RR) system
κ_{P}	Percentage of the total lateral design force assigned to infill panel in C-SPSW-O (P) system
κ_{PP}	Percentage of the total lateral design force assigned to infill panel in SPSW-O (PP) system
κ_{PR}	Percentage of the total lateral design force assigned to infill panel in SPSW-O (PR) system
κ_{R}	Percentage of the total lateral design force assigned to infill panel in C-SPSW (R) system
κ_{RP}	Percentage of the total lateral design force assigned to infill panel in SPSW-O (RP) system
κ_{RR}	Percentage of the total lateral design force assigned to infill panel in SPSW-O (RR) system
λ	Ratio of plastic section modulus of outrigger beam to that of HBE; ratio of plastic section modulus of coupling beam to that of HBE
λ_{i}	Proportioning factor of the equivalent lateral force at level i
μ_{s}	Structural ductility factor
μ_{max}	Maximum plate ductility
θ_{p}	Plastic rotation, Inelastic drift
θ_{u}	Target drift
θ_{y}	Yield drift ratio

ω_h	Horizontal component of tension field force along HBE
$\omega_{h(i)}$	Horizontal component of tension field force along HBE level i
ω_v	Vertical component of the tension field force along HBE

1. INTRODUCTION

1.1 Motivation and Background

Numerous experimental and analytical research over the past three decades have proven that steel plate shear walls (SPSWs) are one of the most effective lateral force resisting systems. Our knowledge of the behaviour and design principles of thin unstiffened SPSWs has been evolving since the researchers at the University of Alberta pioneered the research into this structural system in the early 1980s (Thorburn et al. 1983; Timler and Kulak 1983; Tromposch and Kulak 1987). Based on these key studies the CSA S16-94 Standard (Canadian Standards Association 1994) provided first design requirements for thin unstiffened SPSWs taking into account the post-buckling strength and tension field action mechanism of the infill panels. Similar design requirements were then adopted by other codes and standards (e.g., AISC 341 2005 and 2010; NEHRP 2003).

Although the general behaviour of conventional SPSWs is reasonably well understood and their design provisions have been extensively developed, the quest for innovative and efficient design procedures is an ongoing process. The intention is to develop state-of-the-art design methodologies that can address the shortcomings of the current SPSW design practice and avoid unnecessary conservatism that exists in the design process.

SPSWs have commonly been designed using conventional force-based design approach prescribed by the codes, where the design base shear is calculated for an initially assumed elastic system followed by modifications (i.e., force reduction factors), which implicitly account for the inelastic response. However, like other seismic force resisting systems, SPSWs are expected to experience significant inelastic deformations during major earthquakes. Therefore, designing such a structural system having a highly nonlinear seismic behaviour using the elastic analysis approach would inevitably involve many design iterations to achieve final design that meets strength and drift requirements.

As the demands of regulators and consumers for higher levels of safety, reliability and economy have increased, modern building codes have shifted towards the performance-based design (PBD) concept in the past two decades. Although, the conventional force-based design approach commonly used in the PBD practice has served the structural engineering community relatively well, the development of more rational and direct design approaches is still needed. Such desirable design approaches could facilitate the achievement of performance objectives, while eliminating or minimizing the need for an iterative design process. As such, it is necessary to have PBD tools and procedures for SPSWs to enable structural engineers to meet desired performance objectives in a reliable and cost-effective manner.

In SPSWs, the horizontal boundary element (HBE) to vertical boundary element (VBE) connections in a SPSW can be pinned (i.e., simple shear connection), rigid (i.e., moment-resistant) or semi-rigid. SPSWs with rigid HBE-to-VBE connections are inherently dual systems in which the moment-resisting action of the boundary frame provides substantial lateral load resistance to the system. However, SPSWs have been traditionally designed by assuming that the infill panel resists 100% of the design story shear. As such, the lateral load resistance of the boundary frame introduces substantial overstrength to the system. Past experimental and analytical research (Driver et al. 1997; Berman and Bruneau 2005; Qu and Bruneau 2009) has indicated that the boundary frame action can substantially contribute (ranging from 25% to 50%) to the overall strength of the system, depending on the type of HBE-to-VBE connections used and the infill panel aspect ratio. Therefore, the proper use of such overstrength, by explicitly considering this sharing of shear resistance, could result in material efficiency and economic savings.

On the other hand, the lateral loads in a SPSW with simple shear HBE-to-VBE connections are essentially resisted through the tension field action of the infill panels. While the AISC Seismic Provisions (2010) require moment-resisting boundary frames in SPSWs for seismic applications, S16-14 (CSA 2014) permits

the use of simple shear HBE-to-VBE connections in the limited-ductility (Type LD) category of SPSWs. Moghimi and Driver (2013) tested a full-scale modular SPSW with simple boundary frame connections and reported a stable cyclic performance with high levels of ductility. The specimen exhibited hysteresis loops comparable with those of a SPSW with a moment-resisting frame. Although such a SPSW option could result in potential cost savings due to the use of simple connections, its seismic performance under earthquake excitations has not been sufficiently investigated. Furthermore, the use of simple HBE-to-VBE connections in alternative SPSW configurations such as coupled steel plate shear walls (C-SPSW) ―consisting of a pair of SPSWs that are interconnected by coupling beams at floor levels―and steel plate shear wall with outriggers (SPSW-O)―composed of a SPSW and rigidly connected adjacent beams―which are inherently dual systems, also merit investigation.

Moreover, despite the exemplary seismic performance of SPSWs, as commonly reported by researchers, they are not widely used, especially in mid- to high-rise buildings. Two major detractions to the system's use in taller buildings are recognized as follows: (1) their relatively low overturning stiffness compared to reinforced concrete shear walls; and (2) the fact that large column sections are needed to satisfy capacity design requirements (Berman et al. 2008). Therefore, practical and cost-effective solutions are needed to address the above-mentioned issues to advance the implementation of the SPSW systems in modern structures, particularly in mid- to high-rise buildings.

1.2 Scope and Objectives

This research firstly presents a performance-based design procedure for SPSW systems with the primary aim of achieving predictable and targeted seismic performance, while improving design economy (i.e., achieving more material-efficient SPSW designs). Specifically, this is done by explicitly accounting for the frame strength and incorporating the performance criteria into the design process right from the start. The intention is to address current SPSW design issues partly

related to the conventional force-based design philosophy (e.g., heavily relying on iterative design process) and partly due to some conservative assumptions used in conventional design of SPSWs (e.g., neglecting the strength of the boundary frame). For this purpose, procedures for explicit consideration of the lateral strength provided by the frame actions in different SPSW configurations are studied and incorporated into the design process.

Secondly, the proposed design is further extended to include two alternative SPSW configurations that are aimed at improving the structural characteristics of traditional SPSWs and providing more architectural flexibility. The two SPSW configurations under investigation are (1) SPSW with outriggers (SPSW-O) and (2) coupled SPSW (C-SPSW). The proposed design procedure is used as a reliable tool to investigate the seismic performances of several potential options proposed for each of these configurations, allowing for their comparison on a consistent basis. The goal is to provide design recommendations for such systems to advance the implementation of SPSW systems, especially in mid- to high-rise buildings.

To achieve the first objective, it is necessary to examine the applicability and expediency of various design philosophies (e.g., performance-based design, displacement-based design, plastic design and capacity design) for SPSW structures, and the potential approaches that can be taken to effectively make use of boundary frame strength and incorporate it into the design. This research extensively benefits from the performance-based plastic design (PBPD) concept and employs the principles of plastic analysis and capacity design to produce SPSW systems with predictable and targeted seismic performance, while minimizing unnecessary system overstrength. A step-by-step design procedure is presented; various essential design parameters are investigated, and appropriate recommendations are provided. Subsequently, in order to verify the validity of the proposed design, several case study SPSWs are designed for two different earthquake hazard levels. The seismic performances of the SPSW designs are evaluated using nonlinear response history analyses and are compared with those designed using governing codes.

Next, this research investigates the plastic behaviour and mechanisms of SPSW-O systems, and discusses their effectiveness in improving the overturning stiffness of conventional SPSWs. Several potential SPSW-O options that are specifically designed to improve the flexural stiffness by means of moment-connected adjacent beams/girders are discussed. The level of overturning stiffness and lateral load resistance provided by each of these options are investigated. A simple metric is defined to quantify the contribution of the outrigger elements to the overall overturning stiffness of the system. This parameter, herein referred to as the outrigger efficiency factor (OEF), allows for the comparison of various SPSW-O systems on a consistent basis. Analytical expressions are derived for lateral load resistance and for the OEF of several SPSW-O options by employing the principles of plastic analysis and virtual work. The validity of these analytical expressions is verified using numerical simulations with reasonable agreement. These expressions, which represent two of the key design parameters in SPSW-Os, can be used to facilitate the design process when proportioning such systems. Subsequently, extensive parametric study is conducted to investigate the impact of several parameters on the behavioural characteristics of SPSW-O systems. Parameters subject to investigation include the length and strength of outrigger beams, height of the system, and beam-to-column connection types (i.e., pinned or rigid).

The knowledge generated herein is used to develop design procedures for SPSW-O systems. Since the SPSW-O configuration is inherently a dual system, a substantial portion of the lateral load is carried by the moment-resisting actions of the boundary frame and outrigger elements. Therefore, to achieve an efficient design approach for such systems it is necessary to quantify the level of strength provided by the frame action in each of the SPSW-O options discussed in this research. This is done specifically by investigating the relative contributions of the tension field action of the infill plates and moment-resisting action of the connections using plastic analyses of single- and multiple-story SPSW-Os. For each of the SPSW-O options, an appropriate share of the design lateral load that should

be assigned to the infill plates to achieve a material-efficient design is estimated, and the corresponding design procedures are discussed. To study the validity of the design procedure several mid- and high-rise SPSW-O systems are designed using the proposed design approach. The seismic performances of the case study SPSW-O designs are evaluated using nonlinear response history analyses, and are compared with those of the free-standing SPSWs (i.e., SPSWs without outriggers).

Finally, a seismic design procedure is presented for coupled SPSW systems by explicitly taking into consideration the wall-frame dual action (i.e., frame action and infill panels' tension field action). Two potential C-SPSW options are considered herein, namely: (1) C-SPSW with simple boundary frame connections and (2) C-SPSW with moment-resisting boundary frames. Again, the principles of plastic analysis and capacity design are employed to quantify the strength provided by the boundary frames and coupling actions for each of these C-SPSW configurations. To investigate the effectiveness of the proposed design approach and to evaluate the behaviour of the two C-SPSW options, several case studies are considered in this research. The seismic performances of the case study designs are assessed using nonlinear static and response history analyses, and are compared with those of the uncoupled walls.

1.3 **Thesis Outline**

This thesis consists of seven chapters:

Chapter 1 provides the background to and research motivation for the project; its objectives and scope; and an outline of the thesis.

Chapter 2 presents a review of the current seismic design practice and, more specifically, of SPSW design requirements. The major shortcomings of the traditional SPSW design, and the potential detractions to the system's use, are reviewed. Brief reviews of various design approaches proposed by previous researchers are provided, with an emphasis on a recently developed performance-

based plastic design (PBPD) methodology. Subsequently, a seismic design procedure is proposed for SPSWs to tackle some of the shortcomings of current design practice.

Chapter 3 evaluates seismic performances of several case study SPSWs that are designed using the approach presented in Chapter 2. For this purpose, two case study SPSW structures are considered. The prototype buildings are assumed to be located in Vancouver, BC and Los Angeles, CA, with different seismic hazard levels and governing codes (i.e., Canadian codes and U.S. codes). The performances of code-designed SPSWs are also discussed for the purpose of comparison.

Chapter 4 investigates the plastic mechanisms and behaviour of steel plate shear wall with outriggers (SPSW-O) systems. Several potential SPSW-O options are discussed, and their structural characteristics and effectiveness in improving the overturning stiffness of SPSWs are studied. A parameter called the outrigger efficiency factor (OEF) is defined to quantify the proportion of the overall overturning stiffness provided by the outrigger elements. Analytical expressions for overall lateral load resistance and OEF are derived, and compared with numerical simulations. A total of 64 SPSW-O systems (8- and 12-story) are designed to carry out a comprehensive parametric study that aims to investigate the impact of a number of parameters on SPSW-O characteristics.

Chapter 5 presents seismic design procedures for the SPSW-O systems covering several configurations discussed in Chapter 4. Twelve- and 20-story prototype designs are considered to verify the validity of the proposed design approach. Nonlinear response history analyses are conducted to evaluate and compare seismic performances of different SPSW-O systems. The seismic behaviour of the case studies is evaluated in terms of story drifts, outrigger column and VBE (i.e., SPSW

column) demands, infill plate ductility demands, and outrigger beam inelastic rotation demands.

Chapter 6 discusses two coupled SPSW options and presents design procedures for each of these options. Plastic analyses of single- and multiple-story C-SPSWs are performed to estimate the share of the design lateral load that should be assigned to the infill plates in each of these options in order to achieve an optimum design for lateral load resistance in such systems. Eight- and 12-story C-SPSWs are designed using the proposed design approach, and are analysed using nonlinear static and response history analyses. The seismic performances of the two C-SPSW options are evaluated and compared with those of the uncoupled walls.

Chapter 7 presents the research summary and discusses the outcome of the thesis. Furthermore, research needs and future considerations are pointed out.

1.4 References

AISC (2010). Seismic Provisions for Structural Steel Buildings. ANSI/AISC 341-10, American Institute of Steel Construction, Incl., Chicago, Illinois.

Berman, J.W. and Bruneau, M. (2005). Experimental Investigation of Light-Gauge Steel Plate Shear Walls. Journal of Structural Engineering, 131 (2), 259-267.

Berman, J.W., Lowes, L.N., Okazaki, T., Bruneau, M, Tsai, K-C., Driver, R.D., Sabelli, R. (2008). Research needs and future directions for steel plate shear walls. ASCE Structures Congress: Crossing Borders.

CSA (1994). Design of Steel Structures. CAN/CSA S16-94, Canadian Standards Association, Mississauga, ON, Canada.

CSA (2014). Design of Steel Structures. CAN/CSA S16-14, Canadian Standards Association, Mississauga, ON, Canada.

Driver, R.G., Kulak, G.L., Kennedy, D.J.L., and Elwi, A.E., (1997). Seismic Behaviour of Steel Plate Shear Walls. Structural engineering rep. no. 215. Dept. of Civil Engineering Universityof Alberta.

FEMA (2003). NEHRP Recommended Provisions for Seismic Regulations for New Buildings and Other Structures. FEMA Report No. 450, Building Safety Council for FEMA, Washington, D.C.

Moghimi, H., and Driver, R. G. (2013). Economical Steel Plate Shear Walls for Low Seismic Regions. Journal of Structural Engineering, 139, 379–388.

Qu, B., and Bruneau, M. (2009). Design of Steel Plate Shear Walls Considering Boundary Frame Moment resisting Action. Journal of Structural Engineering, ASCE, Vol. 135, No. 12, pp. 1511-1521.

2. PERFORMANCE-BASED OPTIMUM DESIGN OF STEEL PLATE SHEAR WALLS

2.1 Introduction

Steel plate shear walls (SPSWs) have been widely accepted by the structural engineering community as an economical and effective lateral force resisting system for buildings in high seismic zones. The lateral load resistance in SPSWs is provided primarily by the tension field action of the thin infill plates, which buckle in shear at low load levels. The boundary frame, consisting of horizontal and vertical boundary elements (HBEs and VBEs), provides additional strength to the system through moment-resisting action if rigid connections are used. When subjected to cyclic loading, the system exhibits ductile behaviour and develops stable hysteretic loops due to a high level of inherent redundancy. Previous research has shown that SPSWs possess excellent ductility, which allows the system to undergo large inelastic deformation without losing its strength. Thus, the system is capable of dissipating a significant amount of energy when subjected to severe earthquake excitations.

However, SPSWs have been traditionally designed using the elastic analysis approach suggested by the codes where the inelastic behaviour and characteristics of the system are captured in an indirect manner. Just as in other seismic force resisting systems, the seismic design base shear for SPSWs is obtained from spectral response acceleration provided by the codes assuming an elastic system behaviour. Then, several code-prescribed force modification factors (e.g., overstrengh-related and ductility-related force modification factors) are employed to account for the nonlinearity of the system in an implicit manner.

In modern building codes, in order to control the degree of damage to both the structural and non-structural elements of the systems during earthquakes, drift limits are imposed for specified hazard levels. Once the structure is preliminarily designed using a lateral force distribution pattern given by the code, an elastic

analysis is performed and the resulting elastic drifts are multiplied by a response amplification factor to calculate the corresponding inelastic drifts, which are then checked against the prescribed drift limits. However, since the design procedure is based primarily on an elastic analysis approach involving various modification factors, many design iterations may be needed to achieve the desired level of strength while meeting drift requirements.

The high human and economic cost of earthquakes in the last two decades have highlighted the need to develop the concepts of objective-oriented design and performance-based design, which have been adopted in current building codes such as NBCC (2010) and IBC (2012). Although the current design practice has been relatively successful in providing life safety as its primary objective, the quest for achieving higher levels of performance, reliability and economy is a continuous process.

SPSWs are inherently dual systems in which the infill plates and boundary moment frame work together to resist lateral loads. Experimental and analytical studies have shown that the contribution of the boundary frame action to the global strength of a ductile SPSW is significant, especially in walls with larger infill panel aspect ratios (Qu and Bruneau 2009). However, North American steel design codes have conventionally assumed that the total design storey shear in a SPSW is resisted by the infill plates, while neglecting the share of the frame action in lateral load resistance. Although the substantial overstrength provided by the frame action positively affects SPSW's seismic performance, it leads to a conservative and likely more expensive design.

On the other hand, SPSWs may be used in alternative configurations to improve their structural characteristics and architectural flexibility. These include Coupled SPSW (C-SPSW) and SPSW with Outriggers (SPSW-O), in which the contribution of the moment-resisting action to overall strength becomes even more significant. Hence, neglecting the share of the frame action and designing the infill plates for 100% of the story shear within such systems would result in overly conservative design.

Therefore, efficient design methods are needed for the SPSW systems; these must explicitly account for the inelastic characteristics of the SPSW behaviour and the infill panel-frame dual action in order to achieve optimal design, while meeting desired performance levels.

2.2 **Background**

To overcome the shortcomings arising from the conventional force-based design approach prescribed by the codes, various displacement-based design (DBD) methodologies have been developed by researchers (e.g., Panagitakos and Fardis 1999; Browning 2001; Aschheim and Black 2000; Chopra and Goel 2001; Feeman 1998; Priestly and Kowalsky 2000 and 2007). Among the many DBD methods, the direct displacement-based design (DDBD) approach developed by Priestly et al. (2007) has gained more popularity among researchers. DDBD was first developed for the design of reinforced concrete structures and was later applied to the design of various steel seismic force resisting systems (Della Corte and Mazzolani 2008; Wijesundara 2009; Goggins and Sulivan 2010, Salawdeh, 2012; Sulivan et al. 2011; Sulivan 2012). The DDBD methodology adopts the concept of substitute structure (Shibata and Sozen 1976) and uses target displacement as the starting point of the design. Next, the structure is transferred to a single degree of freedom system and is characterized by defining ductility-dependent equivalent viscous damping and using secant stiffness corresponding to the elastic response spectra. The necessary design forces are then obtained by considering the effective damping and stiffness. However, iteration may be needed using a revised damping if the damping check is not satisfied.

Although most of the DBD approaches developed by researchers are effective in providing appropriate design base shear considering the inelastic state of the structures and their modal properties (e.g., yield displacement, effective period, ductility, viscous damping, and effective stiffness), the design of the designated yielding elements (e.g., beams in moment frames) and columns still follow the conventional elastic analysis approach and capacity design, which may

involve a lengthy iterative process. On the other hand, the relative complexity of the above-mentioned procedures compared to the current practice is a barrier, reducing their desirability among practicing engineers and designers. However, since modern building codes have been moving towards performance-based design, the displacement-based design concept has gained popularity among researchers and its improvement is an ongoing process.

Another rational displacement-based design methodology, called the performance-based plastic design (PBPD), was proposed by Goel and his co-investigators. PBPD has been under development, and has been gradually improved, over the last two decades (Leelataviwat et al. 1999 and 2007; Lee and Goel 2001; Dasgupta et al. 2004; Chao and Goel 2006a, 2006b and 2008; Chao et al 2007; Goel and Chao 2008). The PBPD methodology, which is based on an energy-work balance concept in a given structure (Housner 1956), employs basic principles of plastic analysis and capacity design to achieve a pre-selected target drift and yield mechanism. It has been extensively shown that the PBPD method is capable of producing structures with well controlled and predictable seismic performance, while eliminating or minimizing the need for the conventional iterative (trial-and-error) design process.

PBPD was first developed for the design of steel moment frames (Lee and Goel 2001) and has since been successfully applied to the design of various seismic force resisting systems such as eccentrically braced frames (Chao and Goel 2006a), concentrically braced frames (Chao and Goel 2006b), buckling restrained braced frames (Sahoo and Chao 2010), special truss moment frames (Chao and Goel 2008) and reinforced concrete moment frames (Liao and Goel 2012). However, the application of PBPD to steel plate shear walls is limited and is still under development. Since SPSW is inherently a dual system where the earthquake-induced forces are resisted through the tension field and frame actions, challenges exist in estimating their relative contributions to the overall strength as well as in the proper design of non-yielding elements.

Ghosh et al. (2009) and Bayat (2010) investigated the use of PBPD in the design of four-story SPSWs with simple (pinned) beam-to-column connections, taking into consideration the fact that the boundary frame within such a system does not contribute to its lateral load resistance, and thus simplifying the design approach. Safari Gorji and Cheng (2013) studied the application of PBPD to SPSWs with rigid boundary frame connections and attempted to explicitly account for the frame strength by employing a "balanced design" concept (Qu and Bruneau 2009) in the design process to achieve an efficient design. The balanced condition refers to a design case in which the infill panel is designed for an optimum percentage of the lateral load such that the capacity design of the boundary frame results in no additional overstrength for the system (Qu and Bruneau 2009). Kharmale and Ghosh (2013) investigated the PBPD methodology for SPSWs with moment-resisting boundary frames by considering the desired yield mechanism and target structural ductility as performance objectives. However, since a SPSW with rigid beam-to-column connections is inherently a dual system, in which the boundary moment frame provides substantial strength to the system, a few simplifying assumptions were made resulting in an iterative design process to achieve the final design. In this method, the initial plate thicknesses are calculated assuming that the total story shear is carried by the infill panel, and are further revised through an iterative design process. The boundary frame elements (i.e., HBE and VBE) are sized through several iterations accordingly. Although the proposed PBPD approach has been shown to achieve desired performance objectives in terms of ductility and yield mechanism (Kharmale and Ghosh (2013), there are a few shortcomings that need to be addressed for possible improvement of the design and its applicability to other SPSW configurations (e.g., coupled SPSWs and SPSW-Os). Some of these issues are pointed out as follows:

1- Since the plate thickness and the boundary frame elements are initially designed assuming that the infill plates resist 100% of the design story shear, many design iterations are needed to arrive at the final design that meets the desired

performance objectives. However, one of the main objectives of the original PBPD methodology is to eliminate or minimize the number of design iterations by incorporating the key performance objectives into the design process from the initial stage. As such, procedures are needed to explicitly account for the strength provided by the boundary moment frame, which could shorten the lengthy iterative design process.

2- Previous research has shown that SPSWs exhibit a pinched hysteretic response, especially when simple HBE-to-VBE connections are used. Since the shear resistance of the SPSW is provided primarily by the tension field action, and the plates have negligible resistance in compression, progressive yielding and buckling in the thin infill panels result in pinched hysteresis loops when subjected to cyclic loading. Hence, assuming an elasto-plastic system behaviour with full hysteresis loops (when employing the energy-work equation for SPSWs) can lead to unconservative design base shear, and may increase the number of design iterations. Therefore, further modification is needed to account for the reduced energy dissipation due to the pinched response.

3- As mentioned earlier, yield drift ratio is an essential parameter used at the beginning of the PBPD process to calculate design base shear. Notably, the energy balance equation is very sensitive to variation of the yield drift ratio, and as such, slightly different yield drift ratios would result in significantly different design base shears. On the other hand, in contrast with moment-resisting frames in which the yield drift ratio is somewhat independent of the height of the structure due to the predominant racking-type lateral deformation, the yield drift in SPSWs varies for different heights and infill panel aspect ratios. Similar to a plate girder cantilevered from its base, the lateral drift in a SPSW is comprised of flexural and shear components. The flexural component of the drift results from the elongation and shortening of the columns; therefore, it becomes significant in taller walls and can even dominate over shear, especially in

slender walls. However, no expedient tool is available for the design engineer to estimate a proper yield drift ratio without performing a pushover analysis or employing trial-and-error methods. Therefore, an appropriate technique for estimating the yield drift ratio in SPSWs is necessary in order to achieve a reasonable design base shear in the PBPD method.

4- As discussed by the researchers, although the proposed PBPD method is effective in achieving the pre-selected design objectives in terms of ductility and yield mechanism, it fails to provide an expedient method for the design of HBEs in the system (Kharmale and Ghosh 2013).

5- The PBPD approach proposed by these researchers uses ductility ratio (in lieu of drift ratio) as the target performance objective. However, since the original PBPD methodology, as applied to various structural systems, uses pre-selected target drift as one of the two key performance limit states, it would be more desirable to keep the SPSW design consistent with the original PBPD. In addition, as previously discussed, modern codes impose drift limits on building structures for a given seismic hazard level with the primary aim of controlling the degree of damage in structural and non-structural components. As such, it would be more convenient for the design engineer to have control over drift from the beginning of the design process.

The above-mentioned issues will be dealt with in this chapter, which aims to provide a direct performance-based seismic design procedure for SPSW systems. Since the current research project extensively adopts the philosophy of PBPD, the concepts underlying this approach are described in more detail in the next section.

2.3 **Performance-Based Plastic Design Concept**

The PBPD methodology uses an energy-work balance concept (Figure 2.1; Equation 2.1) and employs the principles of plastic analysis and capacity design to

produce structures with predictable seismic performance. The desired target drift ratio and yield mechanism are pre-selected as essential performance objectives through which the degree and distribution of damage in a structure are controlled from the beginning of the design process.

According to a preliminary observation by Housner (1950), there is a relationship between the amount of work needed to monotonically push the structure up to a target drift and the elastic input energy in the system. In the PBPD method, this relationship is built by employing an appropriate inelastic response spectrum for an equivalent elastic-plastic single degree of freedom (EP-SDOF) system, and is used to derive the design base shear for a given hazard level (Goel and Chao, 2008). In this regard, it is assumed that the amount of earthquake-induced energy for an elastic-plastic single degree of freedom system is calculated as a fraction of that for an elastic system obtained from the design pseudo-velocity spectrum (i.e., $E = \frac{1}{2}MS_v^2$).

$$\left(E_e + E_p\right) = \gamma\, E = \gamma \left(\frac{1}{2} M {S_v}^2\right) \tag{2.1}$$

where γ is the energy modification factor; S_v is the design spectral pseudo-velocity; M is the total mass of the system; and E_e and E_p are the elastic and plastic components of the work, respectively. Earlier research has shown that the above-mentioned principle is also valid for multi degree of freedom (MDOF) systems (Leelataviwat et al., 2008). To calculate the design base shear, the amount of work required to monotonically push the structure up to a selected target drift (appropriate for the given hazard level), while forming a desired yield mechanism, is equated to the amount of energy needed for an equivalent EP-SDOF system to reach the same target value. It should be mentioned that the basic concept of virtual work (Neal 1977) is used to calculate the work due to plastic deformations and rotations in the system and no pushover analyses is performed at this stage (Goel and Chao 2008). The right hand side of the Eq. (2.1) can be written in terms of pseudo-spectral acceleration:

$$\left(E_e + E_p\right) = \gamma.\left(\frac{1}{2}M.{S_v}^2\right) = \frac{1}{2}\gamma.M.\left(\frac{T}{2\pi}S_a.g\right)^2 \quad (2.2)$$

where S_a is the pseudo-spectral acceleration, which (for the design purpose) can be read from seismic design response spectrums provided by the codes (e.g., NBCC 2010; ASCE-7 2010) for a given hazard level.

The energy modification factor γ is a function of the ductility reduction factor ($R_\mu = V_e/V_y$) and structural ductility factor ($\mu_s = \Delta_u/\Delta_y$), and is defined as follows:

$$\gamma = \frac{2\mu_s - 1}{{R_\mu}^2} \quad (2.3)$$

In order to relate the ductility reduction factor to the structural ductility factor any inelastic spectra for elastic-plastic SDOF system can be used; however, as suggested by Goel and Chao (2008), the inelastic spectra proposed by Newmark and Hall (1982) is used in PBPD for simplicity (Table 2.1 and Figure 2.2). As a result, the energy modification factor inelastic spectra ($\gamma - \mu_s - T$) can be obtained, as shown in Figure 2.3. Considering the relationship between various terms using inelastic spectra, the work-energy equation takes the following format (Goel and Chao 2008):

$$\frac{1}{2}\left(\frac{W}{g}\right).\left(\frac{T}{2\pi}\frac{V_y}{W}g\right)^2 + V_y\left(\sum_{i=1}^{N}\lambda_i h_i\right)\theta_p = \frac{1}{2}\gamma\left(\frac{W}{g}\right).\left(\frac{T}{2\pi}S_a g\right)^2 \quad (2.4)$$

Solving for V_y the base shear coefficient is calculated as:

$$\frac{V_y}{W} = \frac{-\alpha + \sqrt{\alpha^2 + 4\gamma{S_a}^2}}{2} \quad (2.5)$$

In Eq. (2.5), α is a dimensionless parameter, which depends on the modal properties of the system and the plastic drift ratio as well as the lateral load distribution method used in the design, and can be calculated using Eq. (2.6), in which $h^* = \sum_{i=1}^{N}\lambda_i h_i$.

$$\alpha = \left(h^* \frac{\theta_p 8\pi^2}{T^2 g} \right) \tag{2.6}$$

As suggested by Goel and Chao (2008), the lateral load distribution method proposed by Chao et al. (2007), which has been developed based on nonlinear response of variety of seismic force resisting systems, is used in the PBPB method. In contrast with those suggested by the codes (e.g., NBCC 2010), which are primarily based on the first-mode deflection of the structure, the lateral force distribution given by equations 2.7-2.9 explicitly accounts for the higher mode effects and has been shown to result in a more uniform inelastic response along the height of the system (Chao et al. 2007).

$$F_i = \lambda_i V_y \tag{2.7}$$

$$\lambda_i = (\beta_i - \beta_{i+1}) \left(\frac{w_n h_n}{\sum_{j=1}^{n} w_j h_j} \right)^{0.75T^{-0.2}} \tag{2.8}$$

$$\beta_i = \frac{V_i}{V_n} = \left(\frac{\sum_{j=i}^{n} w_j h_j}{\omega_n h_n} \right)^{0.75T^{-0.2}} \tag{2.9}$$

$$h^* = \sum_{i=1}^{N} \lambda_i h_i = \left(\sum_{i=1}^{n} (\beta_i - \beta_{i+1}) h_i \right) \left(\frac{w_n h_n}{\sum_{j=1}^{n} w_j h_j} \right)^{0.75T^{-0.2}}$$

$$\alpha = \left(\frac{\theta_p 8\pi^2}{T^2 g} \right) \left(\sum_{i=1}^{n} (\beta_i - \beta_{i+1}) h_i \right) \left(\frac{w_n h_n}{\sum_{j=1}^{n} w_j h_j} \right)^{0.75T^{-0.2}} \tag{2.10}$$

Where β_i is the shear distribution factor at level i; $h_n$and h_j are the elevations of the floors level n and j, respectively; and $w_n$and w_j are the seismic weights of the floors n and j, respectively.

2.4 **Design Procedure**

A seismic design procedure, which explicitly considers the boundary frame action and inelastic drift demands, is presented for the SPSW systems. The proposed

design procedure generally adopts the philosophy of PBPD methodology and provides a reliable approach to design SPSW structures with targeted seismic performance, while optimizing material efficiency. A step-by-step outline of the design procedure for a typical SPSW system is summarized here; detailed discussions are presented in the sub-sections that follow.

1- Select a yield mechanism for the system, considering the most desirable distribution of damage along the height of the structure during a seismic event. Select a target drift ratio (θ_u) corresponding to the acceptable degree of damage in the structure for a specified hazard level.
2- Estimate the yield drift ratio of the SPSW structure (θ_y) assuming a uniform yield mechanism and idealized elastic-plastic system behaviour. Calculate the plastic drift ratio (θ_p) by subtracting the yield drift ratio from target drift ratio (i.e., $\theta_p = \theta_u - \theta_y$).
3- Estimate the natural period of the structure (T) and compute the design base shear using the energy-work balance equation. Distribute the design shear over the height of the system considering the lateral force distribution pattern proposed by Chao et al. (2007).
4- Modify lateral design forces to size the infill plates by explicitly taking into account the contribution of the frame action to the lateral load resistance of the system. The "balanced" design concept proposed by Qu and Bruneau (2009) (which is further expanded to develop optimum design expressions for other SPSW configurations in Chapters 5 and 6) is employed in this step to determine an appropriate proportion of the story shear that should be assigned to the infill panel such that an optimum design is achieved. Calculate plate thickness using the modified design loads.
5- Design boundary frame elements according to the capacity design procedure.
6- Update infill panel thickness to further minimize unnecessary system overstrength and revise the design.

2.4.1 Yield Mechanism and Target Drift Ratio

As mentioned earlier, the proper selection of a yield mechanism and target drift are essential design criteria that need to be considered at the beginning of the design process. Figures 2.4-2.6 illustrate desirable yield mechanisms in three different SPSW configurations considered in this research, namely (1) conventional (planar) SPSW, (2) coupled SPSW (C-SPSW), and (3) SPSW with outriggers (SPSW-O) systems. The C-SPSW system consists of a pair of SPSWs that are linked together by the coupling beams at floor levels. Also, the SPSW-O configuration consists of a SPSW and rigidly connected adjacent beams, which act as outriggers for the SPSW. As shown in Figure 2.4, the desirable yield mechanism in conventional SPSW involves uniform yielding of all infill plates and formation of plastic hinges at HBE ends and VBE bases. The infill plates and HBEs are the designated energy dissipating elements in a typical SPSW with a moment-resisting boundary frame. However, in the limited-ductility (Type LD) category of SPSWs (CSA S16-14), the boundary frame may be designed using pinned HBE-to-VBE connections. In such SPSW systems, the yield mechanism only involves uniform yielding of the infill plates through which the earthquake-induced energy is dissipated.

In the SPSW-O configuration, which can be used to improve the overturning stiffness of SPSWs by means of outrigger beams, in addition to the inelastic activities within SPSW as described above, plastic hinges must form at outrigger beam (OB) ends and outrigger column bases in order to develop a desirable sway mechanism (Figure 2.5). It should be mentioned that the HBE-to-VBE connections within a SPSW-O can be either pinned or rigid; this will be discussed in detail in Chapter 4.

The intended yield mechanism for the coupled SPSW systems, as shown in Figure 2.6, consists of uniformly yielded infill plates at all stories of both SPSW piers and plastic hinges formed at the ends of HBEs and coupling beams (CBs) as well as at the bases of both the internal and external VBEs.

As mentioned earlier, the target drift ratio, which is related to the degree of damage in the structure, needs to be selected in the initial stage of the design. Modern building codes impose limitations on design story drifts as a means of controlling damage to structural and non-structural elements of the building structures. The applicable drift limits prescribed by the codes can vary depending on the occupancy category of the building as well as the seismic hazard levels considered in the design. A 2% story drift limit is prescribed by ASCE-7 (2010) when designing ordinary buildings; this is based on an earthquake hazard corresponding to two-thirds of the maximum considered earthquake (MCE). However, NBCC (2010) considers seismic design force based on MCE and permits a maximum drift of 2.5% for seismic load applications.

Goel and Chao (2008) suggested target drift ratios of 2% and 3% for the seismic hazard levels associated with the design-basis earthquake (DBE) (i.e., the earthquake with 10% probability of exceedance in 50 years) and MCE (i.e., 2% probability of exceedance in 50 years), respectively.

2.4.2 Estimation of Yield Drift in SPSW

A proper estimation of the structure's yield drift ratio is required at the beginning of the PBPD design process in order to calculate design base shear. The nonlinear static analysis procedure or so-called "pushover" analysis is an expedient way to estimate the yield drift ratio of the structures. In a pushover analysis, the analytical model of the structure incorporating material nonlinearity is monotonically pushed by a set of invariant lateral force patterns until a predefined target displacement is achieved at a given location. Most modern seismic design codes specify an inverted triangular distribution of the lateral loads corresponding to the first vibrational mode of the structure. While performing pushover analysis employing this load distribution provides acceptable estimates of the nonlinear response for low-rise structures with short natural periods, the nonlinear response estimated by this procedure becomes erroneous for high-rise structures having significant higher mode contributions. To address the shortcomings of the conventional pushover

analysis procedure, various improved pushover methods have been proposed by researchers incorporating higher mode effects into the analysis (Chopra and Goel, 2002; Kalkan and Kunnath, 2006). These methods have been shown to result in a considerable reduction of errors and approximations in estimating the nonlinear response of the structures using pushover analysis.

The lateral deflection of the SPSWs subjected to lateral load is similar to that of a plate girder cantilevered from its base, and is comprised of two terms, namely (1) shear-sway (racking-type drift) resulting from the uniform yielding of web plates and (2) cantilever bending (flexural-type drift) due to axial deformation of VBEs. The contribution of each of these components to lateral drift is dependent on the height-to-width ratio of the SPSW, as well as the relative rigidity of the boundary frame elements and their connections. For tall and slender walls the flexural component of the lateral drift typically dominates over shear-sway (Taranath 2011). Pushover analysis of the wall subjected to the lateral load distribution corresponding to the first vibrational mode usually overestimates the yield drift ratio because it neglects higher mode effects (as shown in Figure 2.7). Since the cumulative axial deformation (elongation and shortening) of the VBEs results in significant elastic lateral deformation, the first yielding in the SPSW occurs at a large drift. In reality, however, when the structure is subjected to earthquake excitation, the effects of higher modes significantly reduce the cumulative axial deformation of the VBEs, resulting in smaller yield drift.

Therefore, in order to better predict yield drift ratio in SPSWs nonlinear response history analysis of the system subjected to earthquake ground motions is warranted. Such work is conducted in this section, which considers several SPSW systems with various height and infill panel aspect ratios as described below.

2.4.2.1. **Case Study Designs**

Three-, 9-, 14- and 20-story SPSWs with three different bay widths, previously designed by Berman (2011) for modified versions of the SAC model buildings (FEMA 2000), are considered herein to investigate the yield drift ratio in SPSWs.

All SPSWs were designed for site class D (i.e., stiff soil according to ASCE 2005) located in Los Angeles, and are representative of typical low-rise, mid-rise and high-rise SPSWs designed according to the AISC Seismic Provisions (2005). The SPSW characteristics and component design summaries are presented in Table 2.2 and Tables 2.3-2.6, respectively, and all other details of the designs can be found elsewhere (Berman 2011). The modelling assumptions and loadings are exactly matched with those reported by Berman (2011).

2.4.2.2. **Analytical Models**

A series of nonlinear response history analyses were conducted to investigate the yield drift ratios of the SPSW systems. The analytical models developed for this purpose were dual-strip models that are capable of capturing the tension field action in both directions as the loading direction changes during earthquakes. In the strip modelling approach, infill plates are represented by a series of discrete tension-only members that are pinned to the boundary frame, and the boundary elements (HBEs and VBEs) are represented using regular frame elements. As suggested by Berman (2011), the strip modelling approach was selected because of the large number of SPSWs and earthquake time histories considered for the nonlinear analyses. Furthermore, the strip modelling technique is computationally expedient and accurately captures the nonlinear response of SPSWs (Driver et al. 1997, 1998; Elgaaly 1998; Berman and Bruneau 2003, 2005; Qu and Bruneau 2008; Berman 2011; Purba and Bruneau 2012). Figure 2.8 shows the strip models created for the three-story SPSWs considered in this study. As shown, the 3N, 3M and 3W models, respectively, employ 13, 17 and 15 inclined strips in each direction at every story. Previous research has shown that a minimum of 10 strips are adequate to capture tension field action of the infill plates (Thurburn et al. 1983; Driver et al. 1997). For each SPSW model a single inclination angle for the strips (close to the average tension field angle of all plates) was selected for modelling expediency. The inclination angles used herein ranged between 42º and 45º, with the average being 43º. For analysis purpose and modelling simplicity, S16-14 (CSA 2014) permits the

use of an averaged inclination angle for the strips in the model. In addition, previous research has indicated that the response of SPSWs predicted using the strip model is fairly insensitive to slight variations (between 38º and 50º) in the tension field angle (e.g., Shishkin et al. 2009). The cross-hatching modelling method (Timler et al. 1998), in which the strips from two adjacent stories share the same nodes at HBE levels, was employed in order to simplify the generation of the models and reduce the number of nodes. It should be recognized that, the strip elements have strength only in tension and their compressive strength was set to zero. To capture infill panel yielding, lumped axial hinges (i.e., the Axial-P hinge in SAP2000) were inserted at the midpoints of the strips. The capability of such axial hinges to accurately simulate the hysteretic tension-only behaviour of the strips has also been verified and reported by other researchers (e.g., Purba and Bruneau 2012). The HBEs and VBEs were modelled using regular frame elements, where axial-flexural fiber hinges (i.e., Fiber P-M2-M3 hinge in SAP2000) were defined in the potential regions of inelastic deformations in these elements. Hence, such plastic hinges, which account for the interaction between the axial forces and bending moments, were inserted at the ends of all frame elements in the models. ASTM A572 Gr. 50 steel and A36 steel were used for the frame elements and the infill plates, respectively. As commonly done in simple plastic theory, an idealized elastic-perfectly plastic stress-strain material models were used for both steel materials in the numerical simulations assuming no degradation. It should be mentioned that the adequacy of the strip models described above in capturing the nonlinear behaviour of SPSWs was verified against cyclic test results of a four-story SPSW conducted by Driver et al. (1997) with reasonable agreement.

The structures considered were nonlinearly analysed under a suite of 20 earthquake ground motions representing the seismic hazard with a 10% probability of exceedance in 50 years (10/50). The ground motions time histories used in this research were the 10/50 Los Angeles earthquake acceleration time histories developed by Somerville et al. (1997) for the SAC steel project (Gupta and Krawinkler 1999). The details of the ground motions and the associated

acceleration response spectra can be found in (Somerville et al. 1997; Gupta and Krawinkler 1999)

The fundamental periods of the protype SPSWs calculated using the strip models are summarized in Table 2.7. A reasonable agreement is observed between the periods calculated herein and those reported in past research (Berman 2011). It should be mentioned that the periods reported by Berman (2011) were calculated using the strip models developed in OpenSees (Mazzoni et al. 2006). Although the basic modelling assumptions, SPSW geometries and seismic masses considered in this study were the same as those used by Berman, the slight discrepancies could be attributed partly to some modelling details that were not reported by the researcher (e.g., the number of strips used for each SPSW and tension field inclination angles), and partly to the solution techniques used for numerical simulations in the two programs. In addition, the use of axial-flexural fiber plastic hinges in the boundary frame elements introduces a slight softening to the model, which results in slightly larger periods, especially in taller walls with larger VBE depths.

Table 2.7 also presents the maximum roof drift ratios at the time that the first yielding occurs in the structures during earthquakes. As expected, the yield drift ratios are positively correlated to the height of the walls and inversely correlated to the width of the walls. As shown, the yield drift ratios for SPSWs of the same heights can vary significantly when the infill panel aspect ratio is changed. This is due primarily to the greater contributions of the flexural-type component of the drift in more slender walls (i.e., the larger H/L ratio). Therefore, first yielding occurs at relatively larger drifts when the wall flexure dominates over shear.

Figure 2.9 shows yield drift ratio versus SPSW slenderness ratio (x) for all SPSWs considered in this study. A simple expression is suggested for estimating yield drift ratio of SPSWs based on a linear regression analysis of the results:

$$\theta_y = 0.0005\frac{H}{L} + 0.003 \qquad (2.11)$$

where H and L are the height and bay width of the SPSW in meters, respectively. It should be mentioned that the yield drift ratios estimated using Eq. (2.11) are slightly conservative, because the yield ratios for the systems were selected as the maximum values experienced during 20 earthquake excitations. Since the higher yield drift results in smaller inelastic drift demand in the energy-work equation, the yield drift ratios estimated using Eq. (2.11) would result in slightly conservative design base shears, especially in taller walls. On the other hand, the yield drift in this study was defined as the drift corresponding to the first yield in the structure instead of that conventionally defined in pushover analysis as the intersection of elastic and post-elastic curves. This definition of the yield drift generally results in slightly smaller values for θ_y, which would partly offset the overestimation of this parameter for the design purpose.

2.4.3 Estimation of Fundamental Period of the Systems

An appropriate estimation of the fundamental period of the structure is necessary to calculate the design base shear. According to NBCC (2010), the first-mode period of SPSWs can be approximated using Eq. (2.12), which is based on the work of Saatcioglu and Humar (2003):

$$T_a = 0.05(h_n)^{3/4} \quad (2.12)$$

where h_n is the height of the structure in meters. The fundamental periods can also be estimated using a proper structural model; however, NBCC (2010) considers the upper limit for the fundamental period of shear wall structures to be $2T_a$. Bhowmick et al. (2009) and Topkaya and Kurban (2009) showed that the above-mentioned equation provides low estimates of the fundamental periods of SPSW structures, as it was developed for reinforced concrete shear wall structures. Using detailed finite element analyses of SPSWs, Bhowmick et al. (2009) proposed the following equation to better estimate the fundamental periods of structures having SPSWs as their seismic force resisting system:

$$T_a = 0.03h_n \quad (2.13)$$

2.4.4 Design Base Shear

As previously discussed, infill plates are the main energy dissipating elements of a SPSW. Given that the infill plates yield only in tension and have negligible strength in compression, when subjected to cyclic loading, the system exhibits a pinched hysteretic response (Figure 2.10a). When the boundary frame of a SPSW is moment-resistant, although the rigid HBE-to-VBE connections provide complementary strength and additional energy dissipation during load reversals, progressive yielding and buckling of the infill plates do not allow for the development of full hysteretic loops. Since the design base obtained from the energy-work equation was originally derived assuming full hysteretic loops for the system, the reduced area of cyclic loops due to the pinched hysteresis curves of the SPSWs should be taken into consideration in the design process.

Figure 2.10 shows a comparison between the inelastic response characteristics of a buckling restrained brace (BRB) and a SPSW subjected to cyclic loading. Since buckling is prevented in a BRB system, the energy-dissipating element yields in both tension and compression resulting in full hysteretic loops. However, the characteristics of the hysteresis curves in SPSWs depend largely on the rigidity of the boundary frame and ductility detailing provided. A SPSW is considered a dual system in which the overall response is a combination of the behaviours of the boundary moment frame and the infill panel system. If the HBE-to-VBE connections were purely pinned, the response of the system would be similar to that of a tension-only system in which the boundary frame provides no strength and energy dissipation to the system.

Figure 2.11 shows a qualitative comparison between cyclic response of a full-scale test of a four-story SPSW with moment-resisting boundary frame (Driver et al. 1997) and that of a two-story modular SPSW with simple shear HBE-to-VBE connections (Moghimi and Driver 2013). As discussed by Moghimi and Driver (2013), while the modular SPSW demonstrated lower yield strength, larger yield drift and smaller initial stiffness due to differences in their structural characteristics

(e.g., simple HBE-to-VBE connections and bolted infill plates) and geometries, the two systems exhibited similar overall behaviour in terms of robustness and ductility. Note that, although the conventional double-angle shear connections were used in the specimen, the cyclic response was far from that of a tension-only system (with purely pinned connections). This indicates that the simple boundary frame in the test specimen made non-negligible contribution to the overall lateral load resistance.

As suggested by Goel and Chao (2008), the energy-work equation can be modified by an energy reduction factor (η) to account for the reduced area of the cyclic loops, as follows:

$$\eta\left(E_e + E_p\right) = \gamma\, E = \gamma \left(\frac{1}{2} M {S_v}^2\right) \tag{2.14}$$

Accordingly, the base shear equation is modified (Goel and Chao 2008):

$$\frac{V_y}{W} = \frac{-\alpha + \sqrt{\alpha^2 + 4\left(\frac{\gamma}{\eta}\right){S_a}^2}}{2} \tag{2.15}$$

Given the experimental test results of the past research (Driver et al. 1997; Berman and Bruneau 2005; Vian and Bruneau 2005; Qu et al. 2008; Choi and Park 2008, 2009, 2010; Moghimi and Driver 2013), and based on preliminary studies of single-story and multiple-story SPSWs subjected to cycling loading, slightly conservative values of $\eta = 0.5$ and $\eta = 0.75$ are suggested for SPSWs with pinned HBE-to-VBE connections and those with moment-resisting connections (Figure 2.12), respectively (Safari Gorji and Cheng 2013).

2.4.5 Design of Infill Plates

In the conventional design of SPSWs according to North American design standards, the infill plate at every story is designed to resist 100% of the factored story shear force. Hence, the lateral load resistance provided by the moment-resisting action of the boundary frame is neglected, typically resulting in a

conservative and likely more expensive design. A large-scale test of a multi-storey steel plate shear wall conducted by Driver et al. (1997), and many subsequent experimental and analytical investigations have shown that the strength contribution of the boundary frame action to the overall lateral load resistance of SPSWs is significant. Figure 2.13 shows the hysteresis curves from the full-scale cyclic test of a four-story SPSW with moment-resisting connections conducted by Driver et al. (1997) at the University of Alberta. As shown, the wall exhibited excellent ductility, energy dissipation and robustness. The ultimate strength of the system was predicted using nonlinear static analysis with good agreement. In addition, an analysis was performed to estimate the strength of the bare frame (i.e., without infill plates), and the results are shown in the figure. As shown, the boundary frame of the SPSW in the specimen contributes about 25% to the overall lateral load resistance of the system (Driver et al. 1997).

Figure 2.14 (left side) shows the cyclic test results of a single-story SPSW with light-gauge infill panel and shear HBE-to-VBE connections (Berman and Bruneau 2005). The researchers used a numerical method to subtract the contribution of the frame action from the overall hysteretic response, as shown in Figure 2.14 (right side). Considering the curves, it is recognized that although the conventional web-angle shear connections were used in the specimen, their moment-resisting capacity was substantial, as the presence of these connections added more than 60% to the overall lateral load resistance (645 kN versus 400 kN).

As discussed above, SPSWs are considered dual systems in which the strength due to the frame action can significantly vary depending on the rigidity of the beam-to-column connections (e.g., pinned, rigid and semi-rigid) as well as the wall's geometry (e.g., infill panel aspect ratio) and configuration (e.g., planar SPSW, coupled SPSW and SPSW-O). As such, when the boundary frame strength is significant, especially for taller walls, there is a considerable incentive to make use of the system overstrength and achieve more efficient design by explicitly taking into consideration the share of the frame action in shear resistance of the system.

Qu and Bruneau (2009), following a detailed plastic analysis of conventional SPSWs, investigated the relative and respective contributions of infill plates and boundary frame moment-resisting action to the overall strength of the system. To explicitly account for the strength provided by the frame action in a multi-storey SPSW, the researchers proposed the approach illustrated in Figure 2.15. As shown, a percentage of the lateral design force ($\kappa_i F_{Di}$) at story level *i* is assigned to the infill panel, and the remaining lateral design force on that level $(1-\kappa_i)F_{Di}$ is carried by the frame action. Furthermore, the boundary frame must have adequate strength to resist the tension field forces resulting from fully yielded infill panels. Obviously, when $\kappa_i = 1$, 100% of the design story shear is assigned to the infill panel, as commonly done in the conventional design of SPSWs (CSA S16 2014 and AISC 2010).

To achieve the optimum design for lateral load resistance, a proper value of κ should be selected considering the amount of overstrength available in the SPSW system. Employing the principles of plastic analysis and capacity design, Qu and Bruneau (2009) derived the following expression for the overstrength of planar SPSWs at the story level *i*.

$$\Omega_{\kappa i} = \frac{F_{Pi}}{F_{Di}} = \kappa_i\left[1 + \frac{L}{2h_i}\tan^{-1}(\alpha_i)\right] \tag{2.16}$$

where F_P and F_D are the plastic strength of the system and design lateral force, respectively; Ω_κ is the SPSW overstrength; α is the tension field inclination angle; L is the width of the panel; and h_i is the elevation of the i-th story calculated from the base. The notations defined herein are related to the i-th story.

Figure 2.16 shows the relationship between overstrength and κ for a single-story SPSW considering various infill panel aspect ratios. Given this plot, as discussed by Qu and Bruneau (2009), three design cases are recognized as follows:

1- In the first scenario, the systems possess overstrength ($\Omega_\kappa > 1$) caused by the boundary frame moment-resisting action, which is usually the case in typical SPSWs designed according to current codes. As shown, the amount of overstrength

is a function of κ, panel aspect ratio and α (which was assumed to be constant in this plot). For a constant κ the value of overstrength is greater for a larger infill panel aspect ratio.

2- The second case corresponds to the case where Ω_κ is equal to unity. These design cases (marked by the circles) in Figure 2.16, were referred to as the "balanced design" case by these researchers. The balanced design case refers to a condition in which the SPSW design is optimized to eliminate system overstrength so that the sum of the plastic strength provided by the tension field and boundary frame moment-resisting actions is exactly equal to that theoretically required to resist design load ($\Omega_\kappa = 1$). By setting the overstrength of the system (Equation 2.16) equal to unity, Qu and Bruneau derived the following equation to determine the percentage of the lateral force that should be assigned to the infill panel (κ_{balanced}), such that the optimum design case can be achieved.

$$\kappa_{\text{balanced i}} = \left[1 + \frac{L}{2h_i}\tan^{-1}(\alpha_i)\right]^{-1} \qquad (2.17)$$

3- The third category of designs as depicted by the lines corresponding to $\kappa < \kappa_{\text{balanced}}$, indicates the SPSW designs in which the infill panels selected are thinner than those required in the balanced condition. This undesirable design case, which is referred to as "SPSW having weak infill panel" (Qu and Bruneau 2009), will not have enough strength to carry design loads if the boundary frame is designed only to resist the tension field forces (i.e., designed using capacity design procedure).

The "balanced" design concept discussed above, which corresponds to the optimum design of a planar SPSW in terms of material efficiency, can be further extended to other SPSW configurations shown in Figures 3.5 and 3.6 (i.e., C-SPSW and SPSW-O). However, since such structural systems are considered dual systems in which significant portions of the story shears are resisted by the frame actions due to the high number of rigid connections used (i.e., coupling beam connections, outrigger beam connections and SPSW boundary frame connections), challenges

exist in terms of estimation of optimum percentage of lateral force to be used for the plate design (i.e., $\kappa_{optimum}$) as well as proper design of frame elements (i.e., HBEs, VBEs, outrigger beams and coupling beams). The procedures to achieve optimum designs for such SPSW configurations are developed in this research (Chapters 5 and 6) by using the principles of plastic analysis and are incorporated into the design approach presented, hereinafter referred to as performance-based optimum design (PBOD). The design procedure aims to achieve optimum designs for SPSW systems in terms of material efficiency, while meeting the desired seismic performance objectives. For this purpose, the infill plates in any of the SPSW configurations discussed above are designed for a modified story shear corresponding to the optimum design cases (i.e., $\kappa_{optimum}$). As such, the required plate thickness at *i*-th story can be calculated as follows:

$$t_{wi} = \frac{2\sum_{j=i}^{n} \kappa_{optimum\,j} F_j}{F_y L \sin(2\alpha_i)} \tag{2.18}$$

where F_y is the yield strength of the infill plate and α is the angle of inclination of the tension field, calculated as follows (Timler and Kulak 1983):

$$\tan^4_{\alpha} = \frac{1 + \frac{t_w L}{2A_c}}{1 + t_w h\left(\frac{1}{A_b} + \frac{h^3}{360 I_c L}\right)} \tag{2.19}$$

where t_w is the thickness of the infill plate, h is the story height, L is the bay width, I_c is moment of inertia of the VBE, and $A_b$is the cross-sectional area of the HBE. For planar SPSWs the value of $\kappa_{optimum}$ in Eq. (2.18) refers to the balanced design expression presented in Eq. (2.17). Note that the expressions of $\kappa_{optimum}$ for the SPSW-O and C-SPSW systems will be presented in Chapter 5 and 6, respectively. It should be recognized that, the value of $\kappa_{optimum}$ for SPSWs with pinned HBE-to-VBE connections is equal to unity, resulting in 100% of the design story shear being assigned to the infill panel (Qu and Bruneau 2009).

Although the optimum design expressions for the three SPSW configurations were developed by setting system overstrength equal to unity, the capacity design procedure would still result in slight overstrength. However, where practicable, attempts can be made to further revise the infill plate thicknesses in an effort to minimize the unnecessary overstrength. The principles of plastic analysis and virtual work can be used to calculate the share of the frame action in overall strength and determine the portion of the story shear that needs to be resisted by the infill plates (V_i) considering the plastic mechanisms shown in Figures 2.4-2.6. For this purpose, Equations 2.20, 2.21 and 2.22 can be used for planar SPSWs, SPSWs with outriggers (SPSW-O) and coupled SPSWs (C-SPSW), respectively.

$$\left(\sum_{i=1}^{n} F_i h_i\right) = 2M_{VBE} + 2\sum_{i=1}^{n} M_{HBEi} + \sum_{i=1}^{n} V_i h_{si} \tag{2.20}$$

$$\left(\sum_{i=1}^{n} F_i h_i\right) = 2M_{OC} + 2M_{VBE} + 4\sum_{i=1}^{n} M_{OBi} + 2\sum_{i=1}^{n} M_{HBEi} + \sum_{i=1}^{n} V_i h_{si} \tag{2.21}$$

$$\left(\sum_{i=1}^{n} F_i h_i\right) = 2M_{VBE\,(Ext)} + 2M_{VBE(Int)} + 4\sum_{i=1}^{n} M_{HBEi} + 2\sum_{i=1}^{n} M_{CBi} + \sum_{i=1}^{n} V_i h_{si} \tag{2.22}$$

Where $M_{VBE\,(Ext)}$ and $M_{VBE(Int)}$ are the plastic moments at the bases of external and internal VBEs, respectively; M_{OC} is the plastic moment at the base of outrigger columns; h_{si} is the height of the i-th story; h_i is the elevation of the i-th floor; and M_{HBEi} , M_{CBi} and M_{OBi} are plastic moments of HBE, coupling beams and outrigger beams (i-th level), respectively.

2.4.6 Design of Boundary Elements

Once the infill plate thicknesses are selected using the modified story shear associated with the optimum design condition (i.e., $\Omega = 1$) , the boundary frame elements are proportioned employing the capacity design principles. To achieve the desired yield mechanism shown in Figure 2.4, the HBEs are required to have adequate strength to anchor the fully yielded infill plates at all stories. As such, they

are designed to resist the combined effects of bending moments and axial and shear forces arising from tension field and boundary frame action (Figure 2.17). Hence, the designer must ensure that the HBEs will not develop plastic hinges along their lengths, with the exception of their ends, to allow the formation of the desirable sway mechanism.

As described by Vian and Bruneau (2005), in order to prevent the formation of in-span plastic hinges along HBEs, these elements should be proportioned to resist the flexural demand given by:

$$M_{HBE} = \frac{1}{4}\omega_v L^2 \times \frac{\eta}{1+\sqrt{1-\eta^2}} \tag{2.23}$$

where ω_v is the resultant of the vertical uniformly distributed forces resulting from the tension fields on the top and bottom of HBEs; η is the plastic section modulus reduction ratio in cases where reduced beam section (RBS) HBE-to-VBE connections are used, and is defined as $\eta = Z_{RBS}/Z$. Additionally, in order to develop uniform tension fields in the top and bottom panels, HBEs at these levels are required to be sufficiently stiff. To meet this requirement, Dastfan and Driver (2008) derived the following limits for the moments of inertia of the top and bottom HBEs, respectively:

$$I_b = \frac{t_w L^4}{650L - (\frac{t_w h^4}{I_c})} \tag{2.24}$$

$$I_b = \frac{t_w L^4}{267L - (\frac{t_w h^4}{I_c})} \tag{2.25}$$

where t_w is the plate thickness; L is the width of the bay; h is the story height; and I_b and I_c are the moment of inertia of HBE and VBE, respectively.

The VBEs are required to resist axial, flexural and shear demands resulting from the tension fields as well as the frame action (in case of moment-resisting boundary frames). The intention is to limit the inelastic deformation of VBEs only at the bases, while allowing the wall to develop sway plastic mechanism. As

recommended by Berman and Bruneau (2008), the capacity design of VBEs can be facilitated by considering the free body diagram of each VBE with the forces and moments that will develop assuming the formation of the intended uniform sway plastic mechanism (Figure 2.18).

In addition to their strength requirement, VBEs are required to have sufficient stiffness to enable the infill plates to develop their full plastic strength. To ensure that VBEs meet this requirement, S16-14 (CSA 2014) imposes a minimum value for the moment of inertia of these elements as follows:

$$I_c = 0.000307 t_w \frac{h^4}{L} \tag{2.26}$$

The detailed capacity design procedures for the design of boundary frame elements can be found elsewhere (AISC 2007; Berman and Bruneau 2008; Qu and Bruneau 2009; Bruneau et al. 2011).

2.4.7 Consideration of P-Delta Effects

It is recognized that the P-Delta effect was not included in the design base shear calculated using the energy-work equation; therefore, further consideration is needed to account for the effects of gravity loads on laterally displaced SPSWs. As suggested by Goel and Chao (2008), the P-Delta effect can be incorporated into the design by adding "P-Delta" lateral forces to those initially calculated using Eq. (2.15).

As schematically shown in Figure 2.19, a lean-on gravity column with tributary weights is added to the model, and is connected to the SPSW using pin-ended rigid links. The P-Delta lateral forces are then calculated assuming that the wall has uniformly deflected to the pre-selected target drift, while the gravity loads are directly applied to the lean-on column.

Assuming that the desired uniform sway yield mechanism has formed, the associated P-Delta lateral force at story level *i* is calculated as $W_i \theta_u$, where W_i is the tributary gravity load applied on the lean-on column at i-th floor and θ_u is the target drift ratio as previously defined. Considering the entire system, the total force

due to the P-Delta effects in the wall, which is additive to the design base shear calculated by Eq. (2.15), can be taken as $W\theta_u$. Where W is the total seismic weight of the structure assigned to the SPSW.

2.5 Summary and Conclusion

This chapter has firstly reviewed the shortcomings of conventional SPSW design and pointed out possible areas of improvement. A performance-based design approach was then presented for SPSWs, with the primary aim of addressing some of these shortcomings.

SPSWs have been conventionally designed using the force-based design approach prescribed by the codes (e.g., NBCC 2010 and ASCE-7 2010), in which the inelastic behaviour of the system is taken into account in an implicit manner by employing various modification factors (e.g., overstrength-related (R_o) and ductility-related (R_d) force modification factors). Although this design approach has been relatively successful in the past, demands for higher levels of safety, performance and economy continue to increase. In this regard, the concept of performance-based design (PBD) has been developed, and adopted as an essential part of modern building codes. However, the existing force-based design procedure to achieve PBD objectives employing "indirect" methods (i.e., the elastic analysis approach) often becomes a lengthy iterative process. In addition, predicting the behaviour of a structure with highly nonlinear response based on the elastic analysis approach would involve significant approximation and could result in potential safety and cost consequences. Therefore, the need for innovative tools and more rational approaches to achieving performance objectives is a continuous process through which PBD could be further implemented.

Brief reviews of the design approaches that have been proposed by researchers to tackle the shortcomings of force-based design were briefly discussed, with an emphasis on a recently developed performance-based plastic design (PBPD) methodology. The philosophy of PBPD, which has been largely adopted in this research, was described in more detail. The PBPD methodology uses

intended yield mechanism and target drift as key performance limit states, and employs an energy-work balance equation and the principles of plastic design to achieve structures with predictable seismic performances. PBPD has gained popularity among researchers and practicing engineers in the last decade due to its relative simplicity and effectiveness in achieving pre-selected performance objectives, while eliminating or minimizing the need for an iterative design process.

A design procedure, called performance-based optimum design (PBOD), was presented for SPSW systems, with explicit consideration of boundary frame strength and inelastic drift demands. The presented design approach, which generally adopts the philosophy of PBPD, aims to tackle some of the shortcomings of the conventional SPSW design. In this procedure, an "optimum design concept" was employed, in which the infill panel within a SPSW system is designed with a modified lateral design load that is estimated by setting the overstrength of the system equal to unity. The applicability of the proposed design approach for three SPSW configurations, namely (1) planar SPSWs, (2) SPSW with outriggers (SPSW-O) and (3) coupled SPSW (C-SPSW) were discussed. The step-by-step process of the design was outlined and the description of each step was further discussed in detail. Based on extensive nonlinear response history analyses, a simple empirical equation was proposed to estimate the yield drift ratio in SPSW systems, which is an essential part of the design process. Various parameters of the design were investigated and appropriate considerations were suggested.

Table 2.1 Ductility reduction factor for various range of structural period

Period Range	Ductility Reduction Factor
$0 \le \frac{T_1}{10}$	$R_\mu = 1$
$\frac{T_1}{10} \le T \le \frac{T_1}{4}$	$R_\mu = \sqrt{2\mu_s - 1}\left(\frac{T_1}{4T}\right)^{2.513 \log\left(\frac{1}{\sqrt{2\mu_s - 1}}\right)}$
$\frac{T_1}{4} \le T \le T_1'$	$R_\mu = \sqrt{2\mu_s - 1}$
$T_1' \le T \le T_1$	$R_\mu = \frac{T\mu_s}{T}$
$T_1 \le T$	$R_\mu = \mu_s$

Note: $T_1 = 0.57$ sec; $T_1' = T_1\left(\sqrt{2\mu_s - 1}/\mu_s\right)$ sec

Table 2.2 SPSW characteristics (Berman 2011)

Name	Number of stories	Bay width (m)	Number of SPSW in each direction
1	3	3.05	4
2	3	4.57	4
3	3	6.10	2
4	9	3.05	8
5	9	4.57	6
6	9	6.10	4
7	14	4.57	6
8	14	6.10	6
9	14	7.62	4
10	20	4.57	6
11	20	6.10	6
12	20	7.62	4

Table 2.3 Three-story SPSW member sizes and plate thicknesses (Berman 2011)

	3N			3M			3W		
Story	Plate	HBE	VBE	Plate	HBE	VBE	Plate	HBE	VBE
1	4.76	W18×97	W14×370	3.18	W16×57	W14×398	4.76	W24×192	W14×605
2	3.18	W18×97	W14×211	3.18	W21×122	W14×233	3.18	W24×192	W14×311
2	1.59	W18×71	W14×211	1.59	W21×122	W14×233	1.59	W24×146	W14×311

Table 2.4 Nine-story SPSW member sizes and plate thicknesses (Berman 2011)

	3N			3M			3W		
Story	Plate	HBE	VBE	Plate	HBE	VBE	Plate	HBE	VBE
1	6.35	W18×71	W14×730	6.35	W18×86	W14×730	6.35	W18×86	W14×730
2	6.35	W18×71	W14×730	6.35	W18×86	W14×730	6.35	W18×86	W14×730
3	6.35	W18×71	W14×730	6.35	W24×146	W14×500	6.35	W18×86	W14×730
4	6.35	W21×111	W14×455	6.35	W18×86	W14×500	6.35	W18×207	W14×730
5	4.76	W18×71	W14×455	4.76	W18×86	W14×500	4.76	W18×86	W14×730
6	4.76	W21×111	W14×342	4.76	W24×146	W14×500	4.76	W24×207	W14×605
7	3.18	W14×48	W14×342	3.18	W16×57	W14×370	3.18	W16×57	W14×605
8	3.18	W18×86	W14×342	3.18	W18×146	W14×370	3.18	W24×176	W14×455
9	1.59	W18×71	W14×342	1.59	W18×106	W14×370	1.59	W24×162	W14×455

Table 2.5 Fourteen-story SPSW member sizes and plate thicknesses (Berman 2011)

	3N			3M			3W		
Story	Plate	HBE	VBE	Plate	HBE	VBE	Plate	HBE	VBE
1	6.35	W14×82	W36×800	4.76	W14×68	W36×800	6.35	W16×89	W36×800
2	6.35	W14×82	W36×800	4.76	W14×68	W36×800	6.35	W16×89	W36×800
3	6.35	W14×82	W36×800	4.76	W14×68	W36×800	6.35	W16×89	W36×800
4	6.35	W14×82	W36×800	4.76	W14×68	W36×800	6.35	W16×89	W36×800
5	6.35	W14×82	W36×800	4.76	W14×68	W36×800	6.35	W30×235	W36×800
6	6.35	W14×82	W36×800	4.76	W14×68	W36×800	4.76	W16×89	W36×800
7	6.35	W24×162	W36×800	4.76	W14×68	W36×800	4.76	W16×89	W36×800
8	4.76	W14×82	W36×800	4.76	W24×192	W36×800	4.76	W16×89	W36×800
9	4.76	W14×82	W36×529	3.18	W12×50	W36×652	4.76	W30×235	W36×800
10	4.76	W24×162	W36×529	3.18	W12×50	W36×652	3.18	W14×53	W36×652
11	3.18	W12×45	W36×330	3.18	W12×50	W36×652	3.18	W14×53	W36×652
12	3.18	W21×132	W36×330	3.18	W24×192	W36×441	3.18	W30×235	W36×652
13	1.59	W12×45	W36×330	1.59	W12×50	W36×441	1.59	W14×53	W36×487
14	1.59	W21×111	W36×330	1.59	W24×162	W36×441	1.59	W27×217	W36×487

Table 2.6 Twenty-story SPSW member sizes and plate thicknesses (Berman 2011)

	3N			3M			3W		
Story	Plate	HBE	VBE	Plate	HBE	VBE	Plate	HBE	VBE
1	4.76	W14×61	W36×800	3.18	W14×48	W36×800	3.42	W14×61	W36×800
2	4.76	W14×61	W36×800	3.18	W14×48	W36×800	3.42	W14×61	W36×800
3	4.76	W14×61	W36×800	3.18	W14×48	W36×800	3.42	W14×61	W36×800
4	4.76	W14×61	W36×800	3.18	W14×48	W36×652	3.42	W21×122	W36×800
5	4.76	W21×132	W36×800	3.18	W21×147	W36×652	3.18	W14×61	W36×800
6	3.41	W14×48	W36×800	2.68	W14×48	W36×652	3.18	W14×61	W36×800
7	3.41	W14×48	W36×529	2.68	W14×48	W36×652	3.18	W14×61	W36×800
8	3.41	W18×86	W36×529	2.68	W14×48	W36×652	3.18	W21×122	W36×800
9	3.18	W14×48	W36×529	2.68	W14×48	W36×652	3.18	W14×48	W36×800
10	3.18	W14×48	W36×529	2.68	W14×48	W36×652	2.68	W14×48	W36×800
11	3.18	W18×86	W36×529	2.68	W14×48	W36×652	2.68	W14×48	W36×800
12	2.68	W12×40	W36×529	2.68	W14×48	W36×652	2.68	W14×48	W36×800
13	2.68	W12×40	W36×395	2.68	W21×147	W36×652	2.68	W14×48	W36×800
14	2.68	W12×40	W36×395	1.59	W12×40	W36×652	2.68	W27×176	W36×800
15	2.68	W21×111	W36×395	1.59	W12×40	W36×652	2.68	W24×40	W36×800
16	1.59	W12×40	W36×395	1.59	W12×40	W36×441	1.59	W12×40	W36×800
17	1.59	W12×40	W36×395	1.59	W12×40	W36×441	1.59	W12×40	W36×529
18	1.59	W12×40	W36×395	1.59	W12×40	W36×330	1.59	W12×40	W36×529
19	1.59	W12×40	W36×395	1.59	W12×40	W36×330	1.59	W12×40	W36×395
20	1.59	W21×111	W36×395	1.59	W24×162	W36×330	1.59	W27×217	W36×395

Table 2.7 Fundamental periods and maximum yield drift

SPSW	Yield drift ratio	Period (sec)^a	Period (sec)^b
3N	0.0045	0.62	0.66
3M	0.0040	0.52	0.57
3W	0.0038	0.55	0.60
9N	0.0097	1.66	1.67
9M	0.0067	1.35	1.36
9W	0.0054	1.24	1.37
14M	0.0083	2.55	2.50
14W	0.0068	2.10	2.06
14WW	0.0065	2.01	2.03
20M	0.0110	3.82	3.78
20W	0.0089	3.15	3.10
20WW	0.0063	3.02	2.97

^{a}Fundamental period calculated using strip models in this research

^{b}Fundamental period reported by Berman (2011)

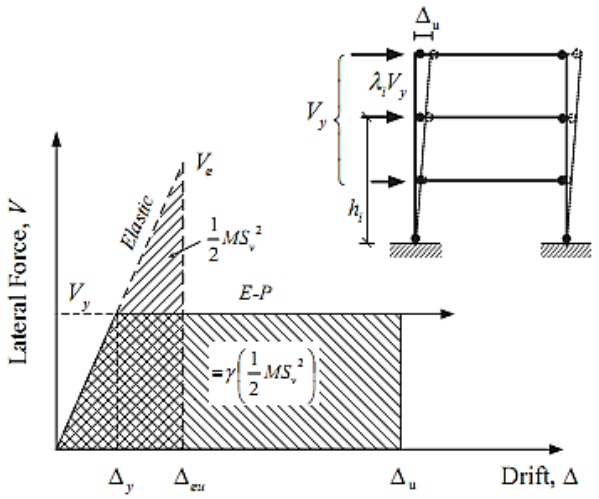

Figure 2.1 Energy-work balance used in PBPD

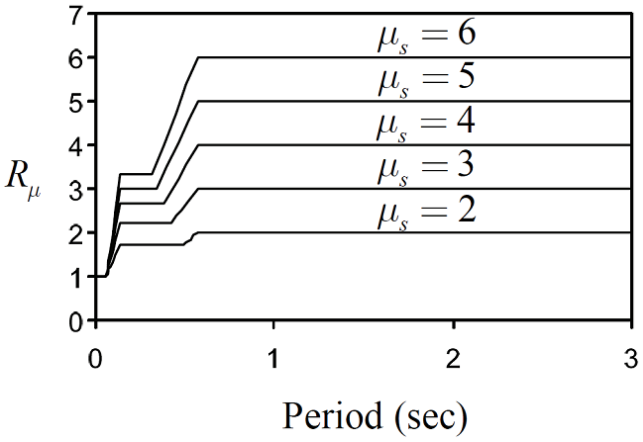

Figure 2.2 Idealized inelastic spectra for EP-SDOF systems (Newmark and Hall 1982)

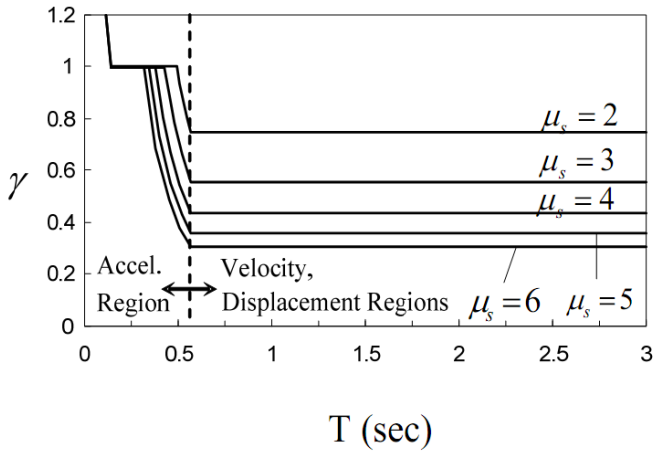

Figure 2.3 Energy modification factor inelastic spectra (Lee and Goel 2001)

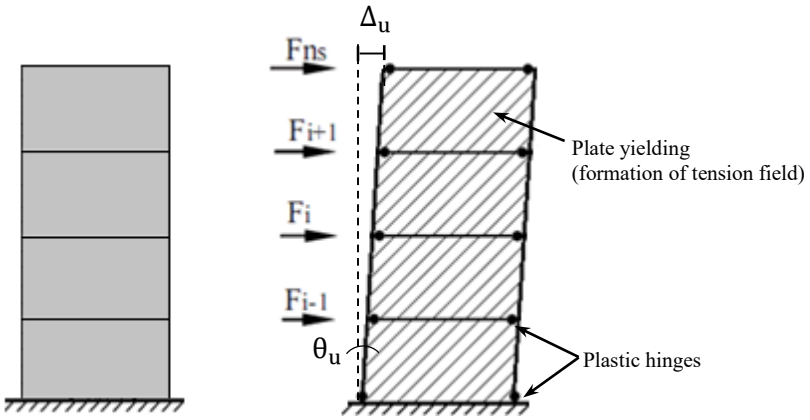

Figure 2.4 Desirable yield mechanism for conventional SPSW with moment-resisting boundary frame

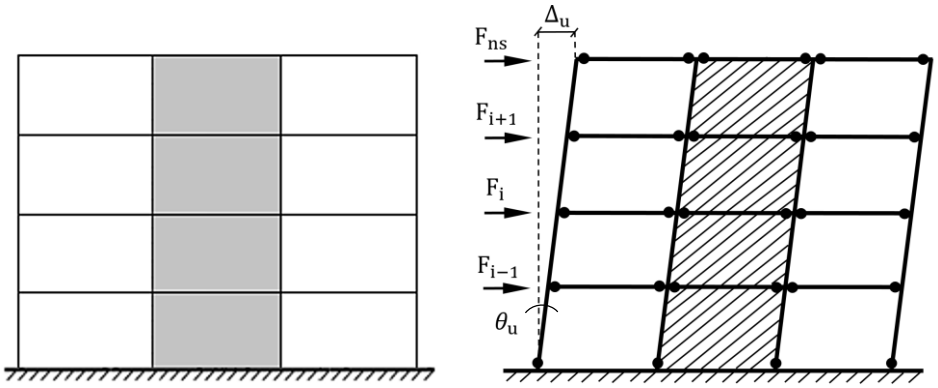

Figure 2.5 Desirable yield mechanism for SPSW with outriggers (SPSW-O) system

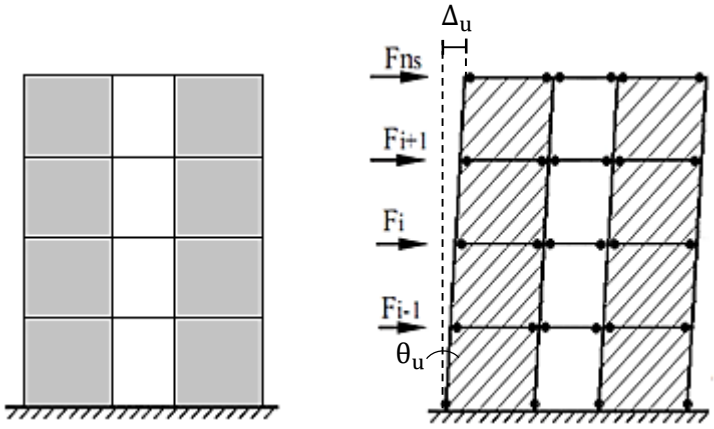

Figure 2.6 Desirable yield mechanism for coupled SPSW (C-SPSW) configuration

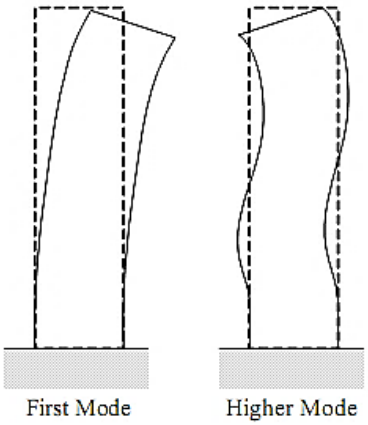

Figure 2.7 Higher mode effects in SPSW systems

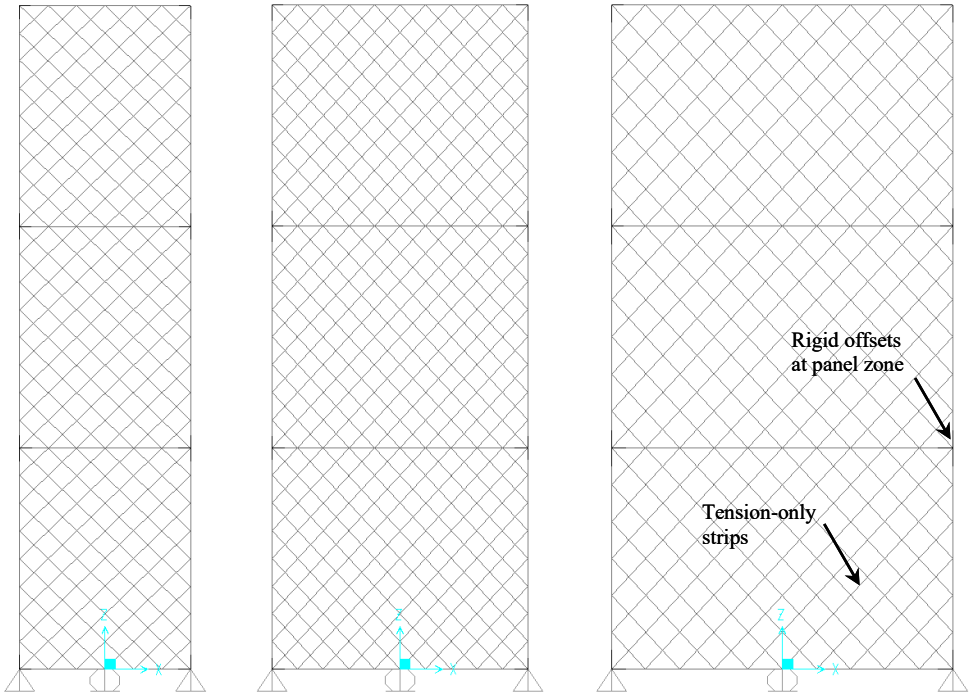

Figure 2.8 Dual strip models created in SAP2000

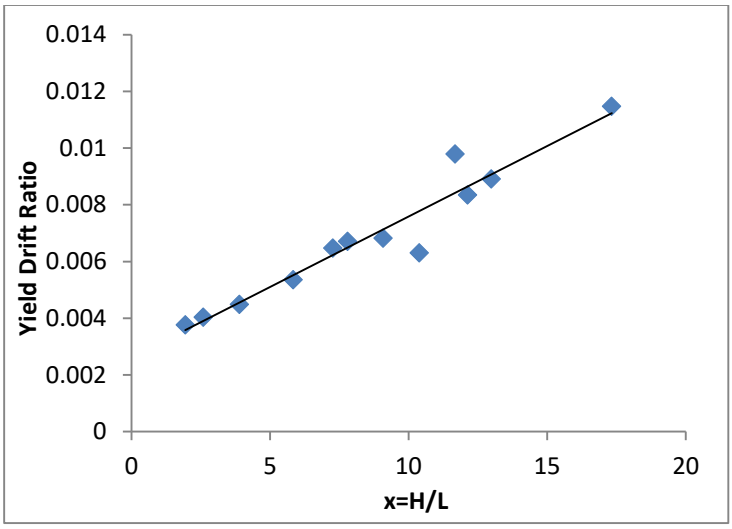

Figure 2.9 Yield drift ratios from nonlinear response history analyses

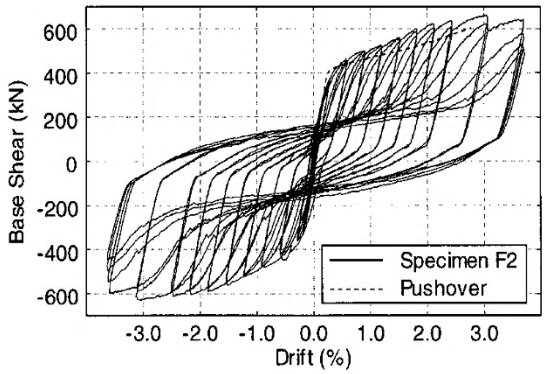

(a) Berman and Bruneau (2005)

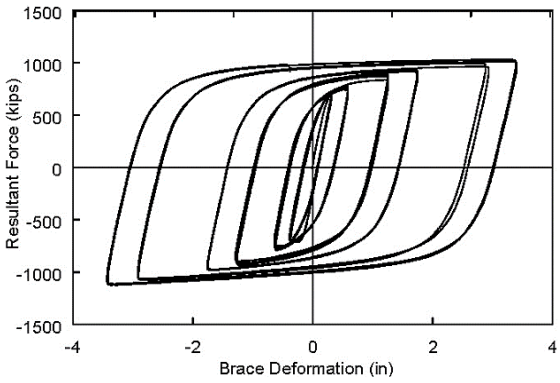

(b) Merritt et al. (2003)

Figure 2.10 Cyclic responses of seismic force resisting systems: (a) Steel plate shear wall; (b) Buckling restrained brace

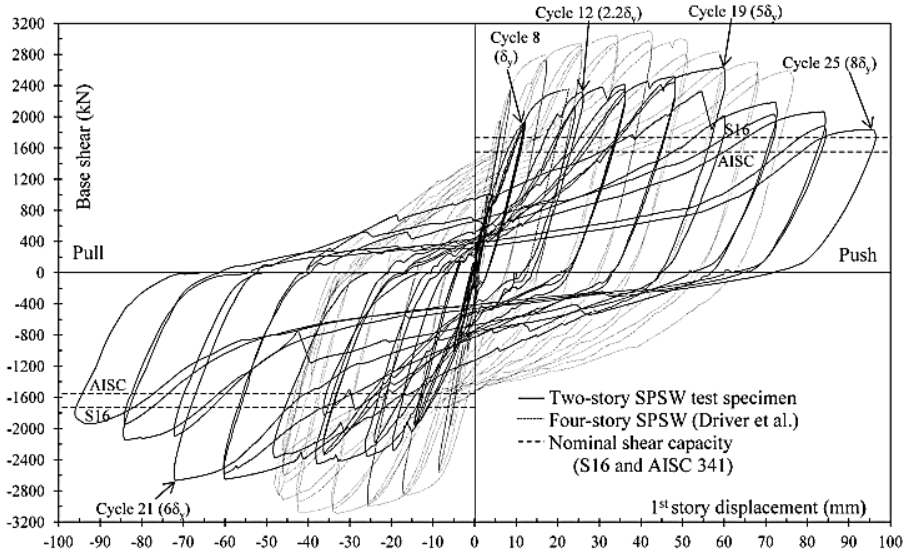

Figure 2.11 Cyclic test results for the first story lateral displacement versus base shear (Moghimi and Driver 2013)

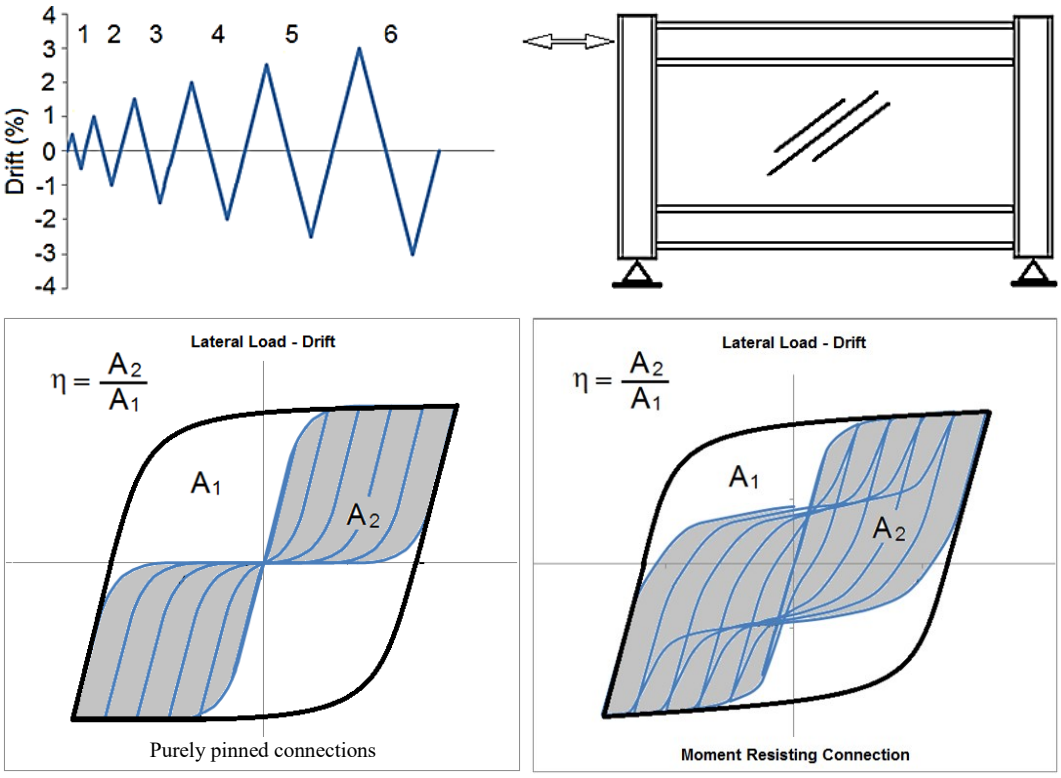

Figure 2.12 Dissipated energy by SPSWs, and the definition of the energy reduction factor (η)

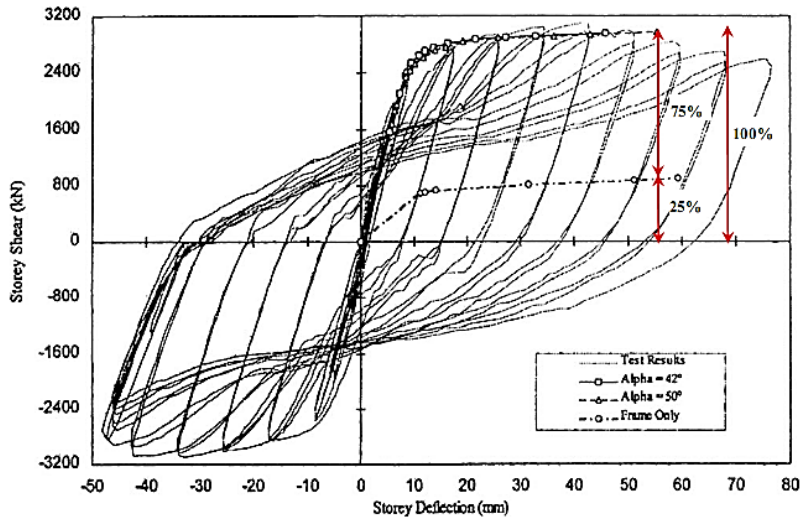

Figure 2.13 large scale test results of a four story SPSW with moment-resisting boundary frame (Driver et al. 1997)

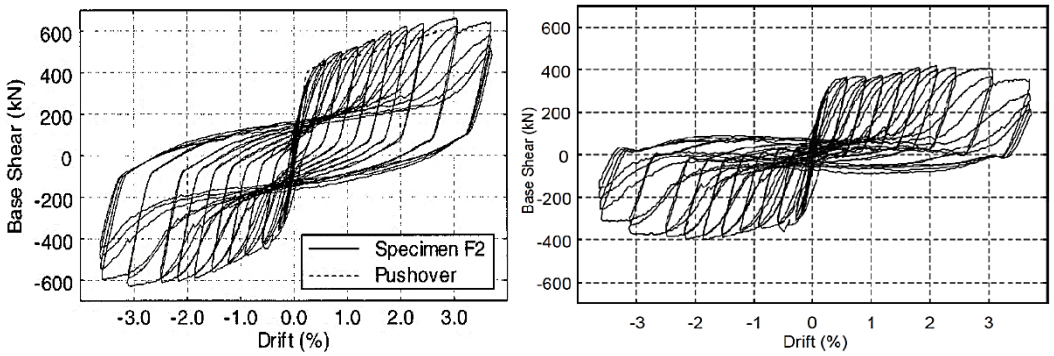

Figure 2.14 Cyclic test results of a single-story SPSW (Berman and Bruneau 2005)

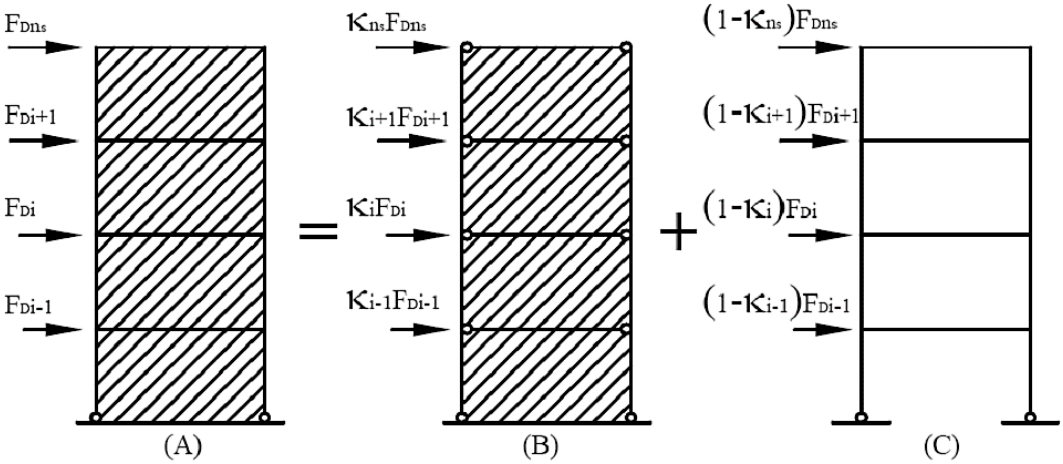

Figure 2.15 Design of SPSWs considering boundary frame action (Qu and Bruneau 2009)

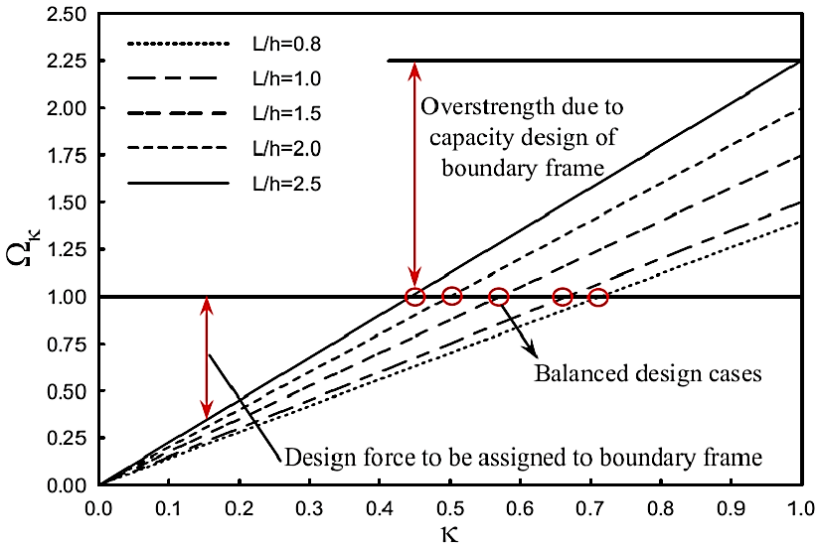

Figure 2.16 Relationship between Ω_κ and κ for various infill panel aspect ratios assuming α=45° (Qu and Bruneau 2009)

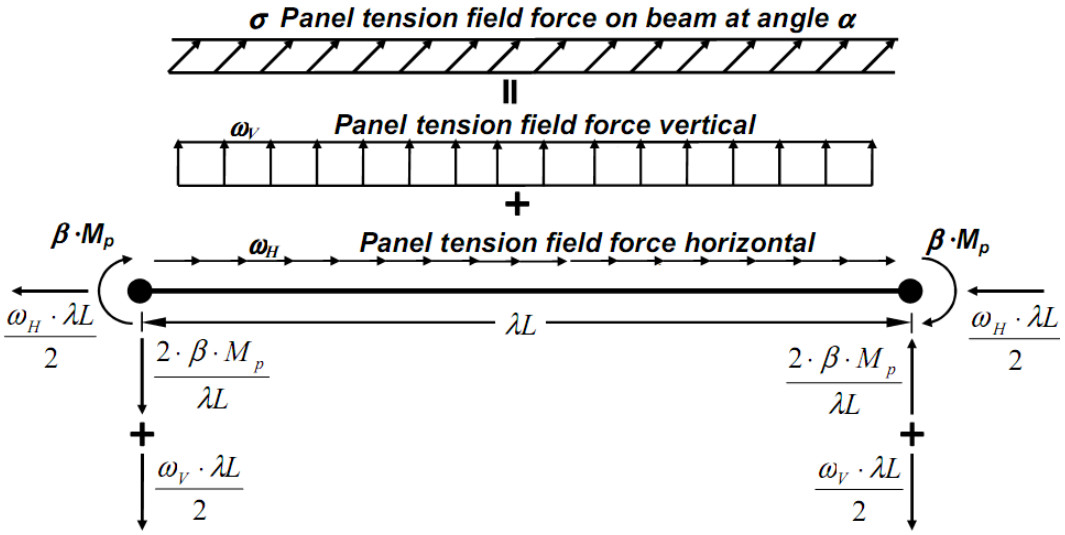

Figure 2.17 Free-body diagram of the bottom HBE (Vian and Bruneau 2005)

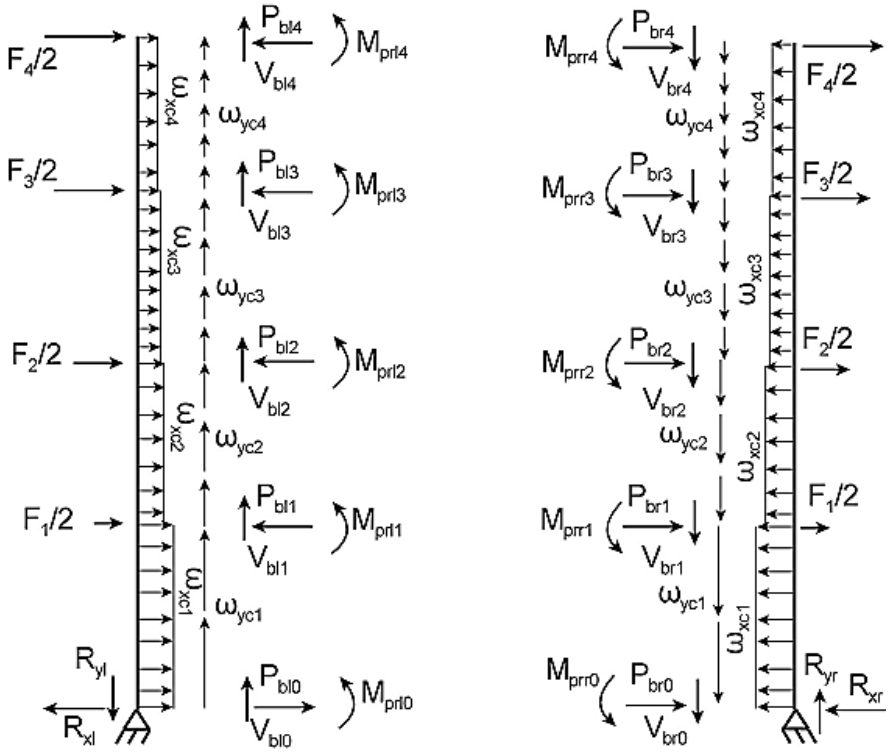

Figure 2.18 Free-body diagrams of VBEs (Berman and Bruneau 2008)

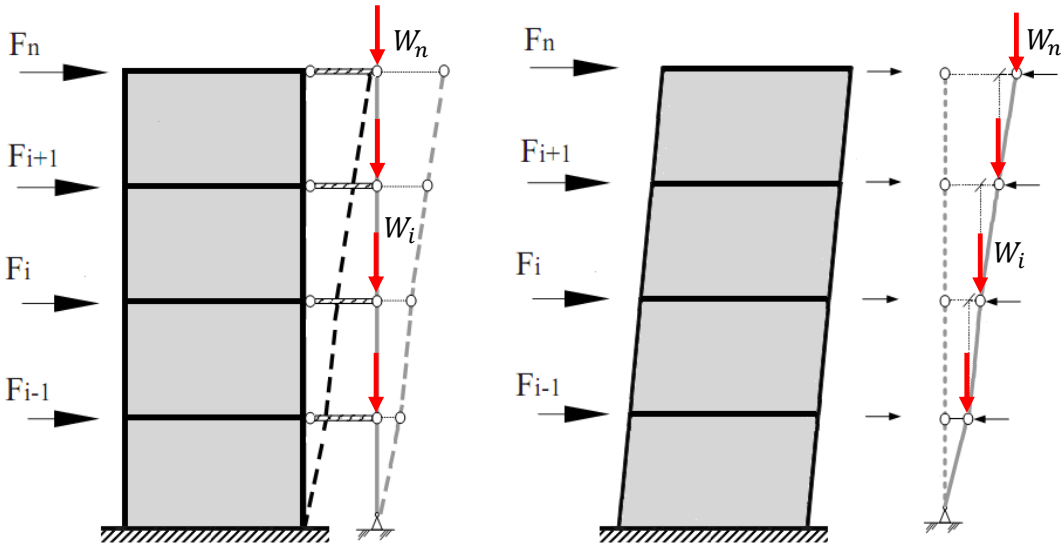

Figure 2.19 Consideration of P-Delta effects using a lean-on column

2.6 References

Aschheim, M.A., and Black, E.F. (2000). Yield point spectra for seismic design and rehabilitation. Earthquake Spectra, Vol. 16, No. 2, 317-336.

Bayat, M.R. (2010). Performance-based plastic design of earthquake resistant steel structures: concentrically braced frames, tall moment frames, plate shear wall frames. Ph.D. dissertation, Department of Civil Engineering, The University of Texas at Arlington, Texas.

Berman, J.W., and Bruneau, M. (2005). Experimental investigation of light-gauge steel plate shear walls. Journal of Structural Engineering, 131 (2), 259-267.

Berman, J.W. (2011). Seismic behaviour of code designed steel plate shear walls., Engineering Structures, 33(1), 230–244.

Bhowmick, A.K., Grondin, G.Y., and Driver, R.G. (2011). Estimating fundamental periods of steel plate shear walls., Engineering Structures, 33(6), 1883-1893.

Browning, J.P. (2001). Proportioning of earthquake-resistant RC building structures. Journal of the Structural Division, ASCE, Vol. 127, No.2, 145-151.

Chao, S-H., and Goel, SC. (2006a). Performance-based design of eccentrically braced frames using target drift and yield mechanism. AISC Engineering Journal, Third quarter: 173–200.

Chao, S-H., and Goel, SC. (2006b). A seismic design method for steel concentric braced frames (CBF) for enhanced performance. In Proceedings of Fourth International Conference on Earthquake Engineering, Taipei, Taiwan, 12–13 October, Paper No. 227.

Chao, S-H., and Goel, SC. (2008). Performance-based plastic design of seismic resistant special truss moment frames. AISC Engineering Journal, Second quarter: 127–150.

Chao, S-H., Goel, SC., and Lee, S-S. (2007). A seismic design lateral force distribution based on inelastic state of structures. Earthquake Spectra 23: 3, 547–569.

Choi, I-R., and Park, H-G. (2008). Ductility and energy dissipation capacity of shear-dominated steel plate walls. Journal of Structural Engineering, ASCE, Vol. 134, No. 9, pp. 1495-1507.

Choi, I-R., and Park, H-G. (2009). Steel plate shear walls with various infill plate designs. Journal of Structural Engineering, ASCE, Vol. 135, No. 7, pp. 785-796.

Choi, I-R., and Park, H-G. (2010). Hysteresis model of thin infill plate for cyclic nonlinear analysis of steel plate shear walls." Journal of Structural Engineering, ASCE, Vol. 136, No. 11, pp. 1423-1434.

Chopra, A.K., and Goel, R.K. (2001). Direct displacement-based design: use of inelastic vs. elastic design spectra. Earthquake Spectra, Vol. 17, No.1, 47-65.

Chopra, A.K., and Goel, R.K. (2002). A modal pushover analysis procedure for estimating seismic demands for buildings. Earthquake Engineering & Structural Dynamics, 31 (3), 561-582.

Dasgupta, P., Goel, S.C., and Parra-Montesinos, G. (2004). Performance-based seismic design and behaviour of a composite buckling restrained braced frame (BRBF). In Proceedings of Thirteenth World Conference on Earthquake Engineering, Vancouver, Canada, 1–6 August 2004, Paper No. 497.

Dastfan, M., and Driver, R.G. (2008), Flexural stiffness limits for frame members of steel plate shear wall systems, Proceedings of Annual Stability Conference, Nashville, Structural Stability Research Council, Rolla, MO.

Della Corte, G. and Mazzolani, F.M. (2008). Theoretical developments and numerical verification of a displacement-based design procedure for steel braced structures. 14th World Conference on Earthquake Engineering, Beijing, China.

Driver, R.G., Kulak, GL., Kennedy, D.J.L., and Elwi, A.E. (1997). Seismic behaviour of steel plate shear walls. Structural engineering report no. 215. Deptartment of Civil Engineering University of Alberta.

Driver, R.G., Kulak, G.L., Kennedy, D.J.L., and Elwi, A.E. (1998). Cyclic test of a four-story steel plate shear wall. Journal of Structural Engineering; 124(2):112–30.

Freeman, S.A. (1998). The capacity spectrum method as a tool for seismic design, Proceedings of the 11th European Conference on Earthquake Engineering, Sept 6-11, Paris.

Goel, S.C., and Chao, S-H. (2008). Performance-based plastic design: earthquake resistant steel structures. International Code Council: Washington, DC.

Ghosh, S., Adam, F., and Das, A. (2009). Design of steel plate shear walls considering inelastic drift demand. Journal of Constructional Steel Research, Vol. 65, pp. 1431–1437.

Goggins, J.G., and Sullivan, T.J. (2009). Displacement-based seismic design of SDOF concentrically braced frames, in STESSA 2009, Mazzolani, Ricles & Sause (eds), Taylor & Francis Group, pp. 685-692.

Gupta, A., and Krawinkler, H. (1999). Seismic demands for performance evaluation of steel moment resisting frame structures. Report no. 132. John A. Blume earthquake engineering center. Stanford University.

Housner, G.W. (1956). Limit design of structures to resist earthquakes. In Proceedings of First World Conference on Earthquake Engineering, Earthquake Engineering Research Institute, Berkeley, CA, June; Part 5: 1–11.

International Building Code (IBC), (2012).

Kalkan, E., and Kunnath, S.K. (2006). Adoptive modal combination procedure for nonlinear static analysis of building structures. Journal of Structural Engineering. 132:11, 1721-1731.

Kharmale, S.B., and Ghosh, S. (2013). Performance-based plastic design of steel plate shear walls. Journal of Constructional Steel Research, Vol. 90, pp. 85–97.

Leelataviwat, S., Saewon, W., and Goel, SC. (2007). An energy based method for seismic evaluation of structures. In Proceedings of Structural Engineers Association of California Convention, SEAOC 2007, Lake Tahoe, CA, September 26–29, 2007; 21–31.

Lee, S-S., and Goel, S.C. (2001). Performance-based design of steel moment frames using target drift and yield mechanism. Research Report no. UMCEE 01-17, Dept. of Civil and Environmental Engineering, University of Michigan, Ann Arbor, MI.

Leelataviwat, S., Goel, S.C., and Stojadinovic, B. (1999). Toward performance-based seismic design of structures. Earthquake Spectra 15(3): 435–461.

Liao, W-C., and Goel, S.C. (2012). Performance-based plastic design and energy-based evaluation of seismic resistant RC moment frame. Journal of Marine Science and Technology, Vol. 20, No. 3, pp. 304-310

Mazzoni, S., McKenna, F., Scott, M.H., and Fenves, GL. (2006). Open system for earthquake engineering simulation user command-language manual-opensees version 1.7.3. Pacific earthquake engineering research center.

Moghimi, H., and Driver, R.G. (2013). Economical steel plate shear walls for low seismic regions. Journal of Structural Engineering, 139, 379–388.

National Building Code of Canada (NBCC), (2010).

Newmark, N.M., and Hall, W.J. (1982). Earthquake spectra and design, Engineering Monographs on Earthquake Criteria, Structural Design, and Strong Motion Records, Vol 3, Earthquake Engineering Research Institute, University of California, Berkeley, CA.

Neal, B.G. (1977). The plastic method of structural analysis, Chapman & Hall, London.

Panagiotakos, T.B., and Fardis, M.N. (1999). Deformation-controlled earthquake-resistant design of RC buildings. Journal of Earthquake Engineering, Vol. 3 No. 4, 498-518.

Priestley, M.J.N., and Kowalsky, M.J. (2000). Direct displacement-based design of concrete buildings. Bulletin of the New Zealand National Society for Earthquake Engineering, New Zealand National Society for Earthquake Engineering, Silverstream. Vol. 33, No.4.

Priestley, M.J.N., Calvi, G.M., and Kowalski, M.J. (2007). Displacement based seismic design of structures, IUSS Press, Pavia, Italy.

Purba, R., and Bruneau, M. (2012). Case study on the impact of horizontal boundary elements design on seismic behaviour of steel plate shear walls. Journal of Structural Engineering, Vol. 138, No. 5, 645-657.

Qu, B., and Bruneau, M. (2009). Design of steel plate shear walls considering boundary frame moment-resisting action. Journal of Structural Engineering, ASCE, Vol. 135, No. 12, pp. 1511-1521.

Qu, B., Bruneau, M., Lin, C.H., and Tsai, K.C. (2008). Testing of full scale two-story steel plate shear walls with RBS connections and composite floor. Journal of Structural Engineering, 134 (3), 364–373.

Saatcioglu, M., and Humar, J. (2003). Dynamic analysis of building for earthquake resistant design. Canadian Journal of Civil Engineering, 30:338-359.

Safari Gorji, M. and Cheng, J.J.R. (2013). Performance-based plastic design of Type D steel plate shear walls. Proc. Canadian Society for Civil Engineering Annual Conference, Montreal.

Sahoo, D.R., and Chao, S-H. (2010). Performance-based plastic design method for buckling-restrained braced frames. Engineering Structures, Vol. 32: 2950-2958.

Salawdeh, S. (2012). Seismic design of concentrically braced steel frames. PhD thesis, National University of Ireland, Galway, Ireland, 280 pages.

Shibata, A., and Sozen, M.A. (1976). Substitute structure method for seismic design in RC. Journal of Structural Division, ASCE, Vol. 102, ST1.

Shishkin, J.J., Driver, R.G., and Grondin, G.Y. (2009). Analysis of steel plate shear walls using the modified strip model. Journal of Structural Engineering, ASCE, Vol. 135, No. 11.

Somerville, P., Smith, N., Punyamurthula, S., and Sun, J. (1997). Development of ground motion time histories for phase 2 of the FEMA/SAC steel project. SAC background document. Report no. SAC/BD-97/04. SAC Joint Venture. 1997.

Sullivan, T.J., Maley, T., and Calvi, G.M. (2011). Seismic response of steel moment-resisting frames designed using a Direct DBD procedure. 8th International Conference on Structural Dynamics, Eurodyn2011, paper No.730.

Sullivan, T.J. (2012). Formulation of a direct displacement-based design procedure for steel eccentrically braced frame structures. 15th World Conference on Earthquake Engineering, Lisbon, Portugal.

Thorburn, L.J., Kulak, G.L., and Montgomery, C.J. (1983). Analysis of steel plate shear walls. Structural Engineering Report No. 107, Department of Civil Engineering, University of Alberta, Edmonton, Alberta, Canada.

Timler, P.A., and Kulak, G.L. (1983). Experimental study of steel plate shear walls. Structural Engineering Rep., No. 114, Department of Civil Engineering, University of Alberta, Edmonton, AB, Canada.

Topkaya, C., and Kurban, C.O. (2009). "Natural periods of steel plate shear wall systems." Journal of Constructional Steel Research, 65(3), 542-551.

Vian, D., and Bruneau, M. (2005). Steel plate shear walls for seismic design and retrofit of building structure. Technical Report No. MCEER-05-0010, Multidisciplinary Center for Earthquake Engineering Research, Buffalo, New York.

Wijesundara, K. (2009). Design of concentrically braced steel frame with RHS shape braces. PhD thesis, ROSE School, IUSS Pavia, Italy, 345pages.

3. SEISMIC PERFORMANCE EVALUATION OF STEEL PLATE SHEAR WALL DESIGNS

3.1 Steel Plate Shear Wall Designs

To evaluate the effectiveness of the design procedure presented in Chapter 2, two eight-storey prototype buildings that use steel plate shear walls as their seismic force resisting systems are considered. The prototype buildings are assumed to be located in the cities of Vancouver, BC and Los Angeles, CA. The intention is to evaluate the seismic performances of SPSWs that are designed using the proposed PBOD approach for different seismic hazard levels. Furthermore, the seismic performances of the SPSWs designed using the proposed approach (herein referred to as PBOD-SPSWs) are compared with those of the SPSWs designed according to the governing codes in Canada and the United States.

3.1.1 Case Study I: SPSW Designs in Canada

The proposed approach was used to design SPSWs as the seismic force resisting system for a hypothetical office building located in Vancouver, BC. SPSWs with moment-resisting boundary frames, herein referred to as Type D (ductile, CSA S16-14 2014), are considered in this study. Also, the prototype SPSW was separately designed according to the Canadian codes and standards (i.e., CSA S16 2014 and NBCC 2010) for the purpose of comparison. In order to evaluate the seismic behaviour of the plate walls, a series of nonlinear response history analyses were conducted under spectrum-compatible earthquake records for Vancouver, BC. Furthermore, pushover analyses were performed to estimate the overall strength of the systems. The building descriptions and design assumptions are briefly summarized in the following sub-section.

3.1.1.1. **Assumptions and Design Summary**

The eight-story building under investigation was adapted from Bhowmick et al. (2009), and was assumed to be located on rock (i.e., Site Class B, NBCC 2010) in Vancouver, BC. The building has two identical SPSWs aligned in each direction to resist lateral loads, as shown in Figure 3.1. Considering the plan symmetry and neglecting the effect of torsion, each wall was designed to resist one half of the design seismic loads. The bay width and constant story height were assumed to be 6 m and 3.8 m, respectively, resulting in an infill panel aspect ratio of 1.58. A dead load of 4.26 kPa was used for all floors and the roof. The live load and snow load were taken as 2.4 kPa and 1.66 kPa, respectively. The nominal yield strengths of boundary elements and infill plates were assumed to be 350 MPa (Grade 350W) and 248 MPa (A36, ASTM 2008), respectively. All steel members were assumed to have a modulus of elasticity of 200000 MPa. Low-yield steel was selected for the infill plates in order to preclude design cases that are governed by minimum plate thickness, thus avoiding any unnecessary overstrength due to the capacity design requirements. Notably, even a slightly thicker plate would result in a shear resistance that is significantly higher than that required to resist the seismic force demands. In addition, for the purpose of comparison, it was assumed that the calculated infill plate thicknesses are available in all cases. Specifically, this assumption was made to ensure that the proposed design approach is effectively capable of producing SPSWs that meet strength and drift requirements without any increased shear resistance due to other limitations (e.g., plate availability, welding and handling requirements). It should be mentioned that past experimental tests have demonstrated that infill plates as thin as 0.7 mm can be effectively used in SPSWs with reasonable seismic performance (Berman and Bruneau 2005; Neilson et al. 2010). On the other hand, the shear capacity of the infill panel can be reduced to a desired level by introducing regular circular perforations in the plate (Roberts and Sabouri-Ghomi 1992; Purba and Bruneau 2009; Vian et al. 2009).

A ductility-related force modification factor (R_d) of 5 and an overstrength-related force modification factor (R_o) of 1.6 were used for the code-designed SPSWs (NBCC 2010). Summaries of the key parameters used in different design approaches are given in Tables 3.1 and 3.2.

3.1.1.2. **Nonlinear Models and Spectrum Compatible Ground Motions**

NBCC (2010) suggests the use of multiple time-history earthquake records for seismic evaluation purposes, and indicates that the ground motions must be spectrum-compatible. This is done by scaling the available time history records such that their resulting response spectrum matches or exceeds the target spectrum for a given location (Saatcioglu and Humar 2003). The number of earthquake records to be used for response history analyses was not specified by NBCC. However, a minimum of three earthquake records is suggested by NEHRP (2000) for seismic analyses. Four earthquake time-history records that were specifically scaled to be compatible with the design spectrum in Vancouver, BC were considered in this study. The original ground motions (i.e., unscaled) and the spectrum compatible time history acceleration records, which were previously used for seismic evaluation of SPSWs (Bhowmick et al. 2009), are shown in Figure 3.2 and Figure 3.3, respectively.

As described in Chapter 2, the popular strip model was employed for numerical simulations of SPSWs in this research. The numerical models of the SPSWs considered in this section consisted of 15 strip elements oriented in both directions at each story (with a constant inclination angle of 43° from the vertical) representing the infill plates, and regular frame elements used for the boundary frame members. To simulate the inelastic deformation of the infill plates axial hinges were inserted at the mid-pint of all strips. Also, axial-flexural fiber hinges, as described in the previous chapter, were defined along the HBEs and VBEs to capture any nonlinear deformations in these elements. All other modeling assumptions were similar to those used in Chapter 2.

3.1.1.3. **Nonlinear Analysis Results and Discussion**

Nonlinear static analyses (pushover) were performed to investigate the lateral load resistance, stiffness and yield drift ratio of the SPSWs considered. Both systems were subjected to the lateral force distribution patterns used in their designs and were pushed to the roof drift ratio of 2.5% (code limit, NBCC 2010). Figure 3.4 shows the pushover curves from nonlinear static analyses of the SPSWs considered. Although both design approaches resulted in very close design base shears, the code-designed SPSW possesses significantly higher lateral load resistance and initial stiffness compared to those of the SPSW designed using the proposed PBOD procedure. The estimated overstrengths of the systems were approximately 1.8 and 1.1 for the code-designed SPSW and PBOD-SPSW, respectively. The higher overstrength of the code-designed SPSW stems from two main reasons: (1) neglecting the strength provided by the moment-resisting action of the boundary frame, and (2) using a reduction factor embedded in the design equation provided by the code (Equation 3.2, CSA S16 2014). Assuming that the infill panel has fully yielded, the shear yielding capacity of the plate can be calculated using the following equation (Berman and Bruneau 2003, Sabouri-Ghomi and Roberts 1991):

$$V_y = 0.5 F_y t_w L \sin(2\alpha) \tag{3.1}$$

where F_y is the yield stress of the infill plate, t_w is the plate thickness and α is the tension field inclination angle. Based on this equation and assuming that 100% of the story shear is resisted by the infill panel, CSA S16-14 (2014) standard provides Eq. (3.2) to calculate the factored shear resistance of a SPSW.

$$V_r = 0.4 \Phi F_y t_w L \sin(2\alpha) \tag{3.2}$$

Where Φ is the resistance factor of steel ($\Phi = 0.9$). Note that the 0.5 factor in Eq. (3.1) is replaced by 0.4 to account for SPSW overstrength and consistency with other code assumptions (CSA S16-14). As previously mentioned, the portion of the unintended overstrength that usually exists in SPSW systems due to the limitation of the plate thickness available in the market was precluded by assuming that the

theoretically required plate thicknesses are available in all cases. Therefore, the overstrength shown in Figure 3.4 stems only from the assumptions made in the design approach. It is recognized that the slight overstrength of the PBOD-SPSW stems from the resistance factor (0.9) used for steel when designing the infill panel.

As shown in Figure 3.4, the empirical expression of the yield drift (Equation 2.11) proposed in Chapter 2 provided a good estimate of this parameter for the SPSW systems, and can be used as an effective tool to facilitate the design process. Figures 3.5 and 3.6 show the maximum story drifts observed during the nonlinear response history analyses of the SPSWs considered in this section. As shown, the nonlinear responses for the both SPSWs considered were well within the NBCC limit (i.e., 2.5% of the story height) under all spectrum-compatible earthquakes. The mean response of the PBOD-SPSW was well within the target value of 2% with reasonably uniform drift distribution. This indicates that a targeted seismic performance was achieved in terms of drift, even without the need for any design iteration. As expected, the PBOD-SPSW experienced larger inelastic drifts compared to those of the code-designed SPSW. It is recognized that the larger deformations observed in the former system are attributed to its thinner infill plate thicknesses and lighter boundary frame elements, compared to those in the SPSW designed using code method (i.e., designing plates for 100% of the design shear). As mentioned earlier, the plate thicknesses in the PBOD-SPSW were specifically calculated for the desired target drift ratio of 2%, while explicitly taking into consideration the boundary frame action. Consequently, lighter boundary frame elements were needed to satisfy capacity design requirements in this case (Tables 3.3 and 3.4). As a result, the SPSW designed using the proposed approach underwent larger inelastic deformations to dissipate earthquake-induced energy, imposing greater ductility demands on the infill plates and HBEs.

Figures 3.7 and 3.8 show the axial plastic hinges formed in the strip elements under the four earthquake excitations considered in this section. These plastic hinges represent the inelastic deformations in the infill plates of the walls. Clearly, the infill plates in the PBOD-SPSW experienced relatively larger ductility

demands, especially in the lower stories, compared to those in the code-designed wall. The extents and distributions of the inelastic ductility demands on the infill plates generally followed the drift distribution patterns shown in Figures 3.5 and 3.6.

Figures 3.9 and 3.10 present the nonlinear rotations of the HBEs during the spectrum-compatible Nahanni earthquake. For the given earthquake, the HBEs at the upper stories (6^{th}, 7^{th} and 8^{th} levels) of the code-designed SPSW experienced larger inelastic rotation demands compared to those of the PBOD-SPSW. Comparisons of the results indicated that most of the HBEs in the code-designed SPSW experienced relatively smaller inelastic rotation demands during the earthquakes, with the exception of those at the upper stories. Furthermore, the HBEs at the lower half of the wall in the code-designed system remained elastic or experienced small inelastic rotations. For the PBOD-SPSW, the maximum HBE inelastic rotation was 0.018 radians (at the 3^{rd} floor level), experienced during the modified Parkfield earthquake. However, the maximum HBE inelastic rotation demand in the code-designed SPSW was 0.012 radians (at the 3^{rd} floor level), which was observed during the Nahanni earthquake.

Inspecting the nonlinear hinges defined in the SPSW models revealed that the inelastic activities in both systems were limited to the infill plates and HBE ends as intended. Therefore, the proposed design approach was effective in achieving the intended performance objectives without the need for design iteration, while maximizing material efficiency.

3.1.1.4. **Comparison of System Weight**

Figure 3.12 shows a comparison of steel weights for elements of the SPSWs designed using two different approaches. As mentioned earlier, the explicit consideration of the boundary frame strength in the proposed PBOD approach resulted in a SPSW with substantially thinner infill panels and consequently lighter boundary frame elements to satisfy the capacity design requirements. The overall weight of the system in this case is about 71% of that designed using the Canadian

codes, in which the lateral load resistance of the boundary moment frame is not explicitly accounted in the design process.

3.1.2 Case Study II: SPSW Designs in the U.S.

In order to further assess the effectiveness of the proposed design approach for SPSWs subjected to higher levels of earthquake hazards, two 8-story SPSW systems were designed for a prototype building structure that is assumed to be located in a region of high seismicity in the U.S..

3.1.2.1. **Building Description and Design Assumptions**

The building under consideration was a hypothetical office building founded on a Class D site (ASCE 7 2010) located in Los Angeles. The plan dimensions, gravity loads and story masses were matched with those of the 9-story SAC buildings (FEMA 2000). As shown in Figure 3.11, the seismic force resisting system in the north-south direction consists of two SPSWs placed in the perimeter frames. Considering rigid floor diaphragms and neglecting building torsion (for simplicity), it is assumed that each wall resists one half of the design lateral forces in this direction.

The SPSWs considered in this section were separately designed according to the proposed design approach and the methods prescribed by the American codes (i.e., ASCE 7 [2010] and AISC Seismic Provisions [2010]). For the code-designed SPSWs, the equivalent lateral force procedure was used to determine design seismic loads considering the shape of the design response spectrum provided in ASCE 7 (2010). ASTM A572 Gr. 50 and A36 steels were selected for frame elements and infill panels, respectively. The idealized elasto-plastic material model was considered for all elements, assuming no strain hardening. For the same reasons as described in previous case study, the calculated plate thicknesses were used in the design and analysis (i.e., they were not rounded to the nearest plate thickness available in the market).

3.1.2.2. **Design Summary**

Tables 3.5 and 3.6 summarize various key parameters used in the two different design approaches. Summary of the component designs for the SPSWs designed using the proposed procedure and code method are presented in Tables 3.7 and 3.8, respectively.

3.1.2.3. **Nonlinear Analysis and Earthquake Time-History Records**

The prototype SPSW structures were nonlinearly analysed under a series of earthquake acceleration time-histories developed by Somerville et al. (1997) for the SAC steel project (FEMA 2000). Also, nonlinear static analyses were conducted for comparison purpose. The suite of 20 ground motions considered herein were those associated with the design basis earthquake (DBE), with a 10% probability of exceedance in 50 years (10/50). It should be mentioned that, in order to use the pre-scaled SAC ground motions (Somerville et al. 1997) for seismic performance evaluation purposes, the spectral ordinates were matched with those used in FEMA-355C (FEMA 2000). The basic characteristics of the considered earthquakes and their elastic acceleration spectra are shown in Table 3.9 and Figure 3.14, respectively.

The infill panels at all stories were represented by 13 pin-ended tension-only strips, where the compression strength of these elements was set to zero. The HBEs and VBEs were modeled using regular frame elements. A constant tension field angle of 42.7° was used for modeling simplicity. All other modeling assumptions were the same as those considered in the previous case study.

3.1.2.4. **Analysis Results**

Figure 3.13 shows the pushover curves from nonlinear static analysis of the SPSWs subjected to lateral design force distribution used in the design. As shown, although the design base shear calculated using the proposed approach was slightly higher (11%) than that of the code method, the overall lateral load resistance of the PBOD-SPSW was about 72% of that of the code-designed wall. As discussed earlier, this

is due mainly to the conservative design assumptions used in the code method. Again, in contrast with the code method, the proposed design approach results only in a slight overstrength (approximately 1.1) by explicitly taking into account the shear resistance provided by the frame action in the design process. The proposed equation of the yield drift (Equation 2.11) provided a good estimation of this quantity for the SPSWs, leading to an appropriate design base shear for the selected target drift and earthquake hazard level.

Figures 3.15 and 3.16 show the mean maximum story drifts from nonlinear response history analyses of the 20 ground motions. As shown, the PBOD-SPSW experienced larger story drifts at stories below the mid-height of the wall, where the mean maximum drift ratio was 1.77% (at the 3rd story). Conversely, the code-designed SPSW underwent larger inelastic deformations at story levels above the mid-height of the wall, with the maximum drift ratio of 1.70% experienced at the 7th story. The mean and mean-plus-standard deviation values of drift ratios for the former SPSW varied from 1.32% to 1.77%, and 1.73% to 2.40%, respectively, while these quantities for the code-designed SPSW ranged from 0.95% to 1.7%, and 1.26% to 2.30%, respectively. The average maximum drift demand for the SPSW designed using the proposed method was 0.02. Hence, the PBOD-SPSW met the performance objective in terms of drift, which is related to the degree of damage in the system. As in the Case Study I presented earlier, the SPSW designed using the proposed approach exhibited relatively larger drift demands (still within the target value), compared to those of the code-designed SPSW. Again, this is due to the considerably thinner plate thicknesses (e.g., 4.4 mm versus 6.1 mm [Tables 3.7 and 3.8]) selected for such systems, considering the desired target drift for the given earthquake hazard level. A careful inspection of the axial hinges of the strip elements and axial-flexural fiber hinges of the boundary elements revealed that the inelastic deformations were limited to the infill plates and HBE ends. Furthermore, the distribution of the drift demands was fairly uniform over the height of the wall. This indicates that the second design objective (i.e., achieving pre-selected yield mechanism), which is related to the distribution of damage in the system, was met.

While the response history analysis results showed that both systems performed well within the 2% drift limit, a targeted and material-efficient design can be achieved by using the proposed design approach, while eliminating the need for any design iteration. In contrast, the code design approach resulted in a conservative design, which would need further design revisions and evaluations to achieve a higher level of efficiency, while meeting the drift requirement.

3.2 Summary and Conclusion

Two case studies investigating the seismic behaviour of SPSWs designed according the design procedure presented in Chapter 2, and those designed using code methods, were conducted. The prototype buildings were assumed to be located in Los Angeles, CA, and Vancouver, BC, with different earthquake hazard levels, and applicable design codes and standards.

The results indicated that both case study SPSWs designed using the proposed PBOD approach performed well under the considered earthquakes and were effective in controlling story drifts within the pre-selected target values. Furthermore, the intended yield mechanism was achieved by limiting the inelastic activities to the infill plates and HBE ends, with fairly uniform distribution of drifts over the height of the systems. Thus, the key performance objectives were met without the need for further design iterations.

Although the SPSWs designed using the proposed method generally experienced slightly larger drifts and ductility demands compared to those of the code-designed walls, these quantities were well within the desired limits. With the drift control built in, the proposed design approach would allow the designer to effectively make use of the SPSW system's ductility for a given earthquake hazard level and avoid unnecessary conservatism in the design. While the proposed approach resulted in similar design base shears compared to those calculated using applicable code methods, the infill plates selected for the systems were generally thinner than those of the code-designed SPSWs. This is due primarily to the explicit consideration of the frame strength to the lateral load resistance of the system in the

proposed approach, which minimizes unnecessary system overstrength. Hence, a targeted and material-efficient design can be achieved for SPSW systems using the proposed approach considering the expected degree of damage for a given hazard level, while eliminating the need for iterative design process commonly needed in force-based code procedures.

Table 3.1 Code design parameters for 8-story SPSW

No.	Parameters	Values
1	Ductility-related force modification factor (R_d)	5
2	Overstrength-related force modification factor (R_o)	1.6
3	Seismic importance factor (I_e)	1
4	Higher mode factor (M_v)	1
5	Design spectral acceleration	0.4
6	Base shear coefficient	0.05
7	Design base shear (kN)	1727

Table 3.2 PBPD parameters for 8-story SPSW

No.	Parameters	Values
1	Target drift ratio (θ_u)	2%
2	Yield drift ratio (θ_y)	0.55%
3	Energy reduction factor (η)	0.75
4	Structural ductility factor (μ_s)	3.6
5	Ductility reduction factor (R_μ)	3.6
6	Energy modification factor (γ)	0.48
7	Design spectral acceleration	0.4
8	Design base shear (kN) (P-Delta included)	1763

Table 3.3 Design lateral forces and design summary (Code method)

Story	Seismic weight (kN)	Lateral force (kN)	Plate Thickness (mm)	HBE	VBE
1	4260	44.8	3.8	W460×97	W840×527
2	4260	89.6	3.7	W460×106	W840×527
3	4260	134.5	3.5	W460×106	W840×433
4	4260	179.3	3.2	W460×113	W840×433
5	4260	224.1	2.7	W460×113	W760×284
6	4260	268.9	2.3	W460×128	W760×284
7	4260	313.8	1.7	W460×128	W760×196
8	4680	472.2	1.0	W460×144	W760×196

Table 3.4 Design lateral forces and design summary (proposed method)

Story	Seismic weight (kN)	Lateral force (kN)	Plate Thickness (mm)	HBE	VBE
1	4260	36.7	2.3	W460×68	W840×359
2	4260	74.2	2.2	W460×74	W840×359
3	4260	113.3	2.1	W460×74	W840×299
4	4260	155.2	2.0	W460×82	W840×299
5	4260	202.0	1.8	W460×82	W760×220
6	4260	257.8	1.5	W460×82	W760×220
7	4260	333.4	1.2	W460×97	W760×161
8	4680	590.7	0.8	W460×113	W760×161

Table 3.5 PBPD parameters for 8-story SPSW

No.	Parameters	Values
1	Target drift ratio (θ_u)	2%
2	Yield drift ratio (θ_y)	0.47%
3	Energy reduction factor (η)	0.75
4	Structural ductility factor (μ_s)	4.2
5	Ductility reduction factor (R_μ)	4.2
6	Energy modification factor (γ)	0.42
7	Design spectral acceleration	0.83
8	Design base shear (kN) (P-Delta included)	5200

Table 3.6 Code design parameters for 8-story SPSW

No.	Parameters	Values
1	Fundamental Period (sec)	0.95
2	Response modification factor (R)	7
3	Seismic importance factor (I_e)	1
4	Design spectral acceleration	0.83
5	Design spectral acceleration parameter at short periods (S_{DS})	1.07
6	Design spectral acceleration parameter at period of 1 sec (S_{D1})	0.79
7	Base shear coefficient	0.119
8	Design base shear (kN)	4670

Table 3.7 Story shears and design summary (proposed procedure)

Story	Seismic weight (kN)	Lateral force (kN)	Plate Thickness (mm)	HBE	VBE
1	4940	109.8	4.4	W24×76	W36×441
2	4856	218.1	4.3	W24×84	W36×441
3	4856	333.1	4.1	W24×94	W36×361
4	4856	456.9	3.8	W24×103	W36×361
5	4856	595.4	3.4	W24×117	W33×263
6	4856	761.3	2.9	W24×117	W33×263
7	4856	988.5	2.3	W24×146	W33×201
8	5230	1736.9	1.4	W24×192	W33×201

Table 3.8 Story shears and design summary (Code method)

Story	Seismic weight (kN)	Lateral force (kN)	Plate Thickness (mm)	HBE	VBE
1	4940	88.9	6.1	W27×84	W36×529
2	4856	204.2	6.0	W27×102	W36×529
3	4856	335.6	5.7	W27×114	W36×487
4	4856	477.4	5.3	W27×129	W36×487
5	4856	627.5	4.7	W27×146	W36×330
6	4856	784.5	3.8	W27×178	W36×330
7	4856	947.5	2.8	W27×178	W36×231
8	5230	1202.0	1.6	W27×194	W36×231

Table 3.9 Characteristics of 10/50 Los Angeles ground motions used for seismic evaluation of SPSWs (Gupta and Krawinkler 1999)

Designation	Record information	Duration (sec.)	Magnitude	R (km)	Scale	PGA (in/sec^2)
LA01	Imperial Valley, 1940	39.38	6.9	10	2.01	178.0
LA02	Imperial Valley, 1940	39.38	6.9	10	2.01	261.0
LA03	Imperial Valley, 1979	39.38	6.5	4.1	1.01	152.0
LA04	Imperial Valley, 1979	39.38	6.5	4.1	1.01	188.4
LA05	Imperial Valley, 1979	39.08	6.5	1.2	0.84	116.4
LA06	Imperial Valley, 1979	39.08	6.9	1.2	0.84	90.6
LA07	Landers, 1992	79.98	7.3	36.0	3.2	162.6
LA08	Landers, 1992	79.98	7.3	36.0	3.2	164.4
LA09	Landers, 1992	79.98	7.3	25.0	2.17	200.7
LA10	Landers, 1992	79.98	7.3	25.0	2.17	139.1
LA11	Loma Prieta, 1989	39.98	7.0	12.4	1.79	256.9
LA12	Loma Prieta, 1989	39.98	7.0	12.4	1.79	374.4
LA13	Northridge, 1994 Newhall	59.98	6.7	6.7	1.03	261.8
LA14	Northridge, 1994 Newhall	59.98	6.7	6.7	1.03	253.7
LA15	Northridge, 1994 Rinaldi	14.95	6.7	7.5	0.79	206.0
LA16	Northridge, 1994 Rinaldi	14.95	6.7	7.5	0.79	223.9
LA17	Northridge, 1994 Sylmar	59.98	6.7	6.4	0.99	219.9
LA18	Northridge, 1994 Sylmar	59.98	6.7	6.4	0.99	315.5
LA19	North Palm Springs, 1986	59.98	6.0	6.7	2.97	393.5
LA20	North Palm Springs, 1986	59.98	6.0	6.7	2.97	380.9

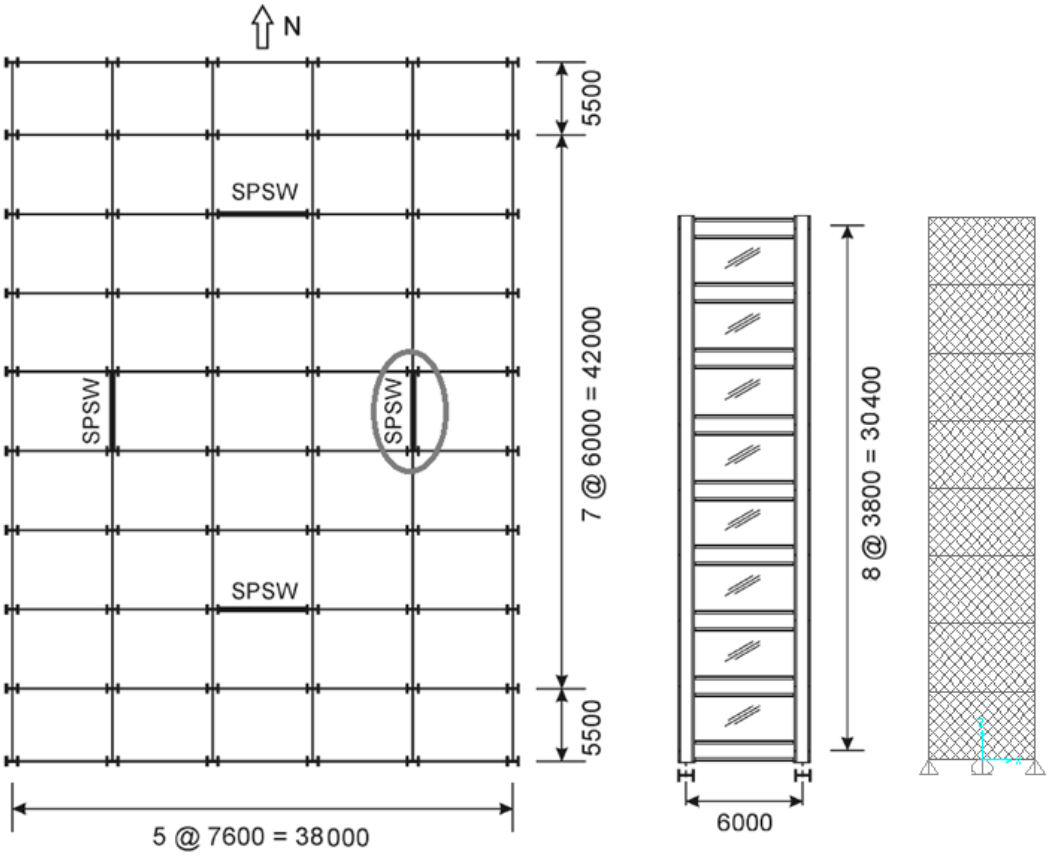

Figure 3.1 Floor plan, SPSW dimensions and dual strip model

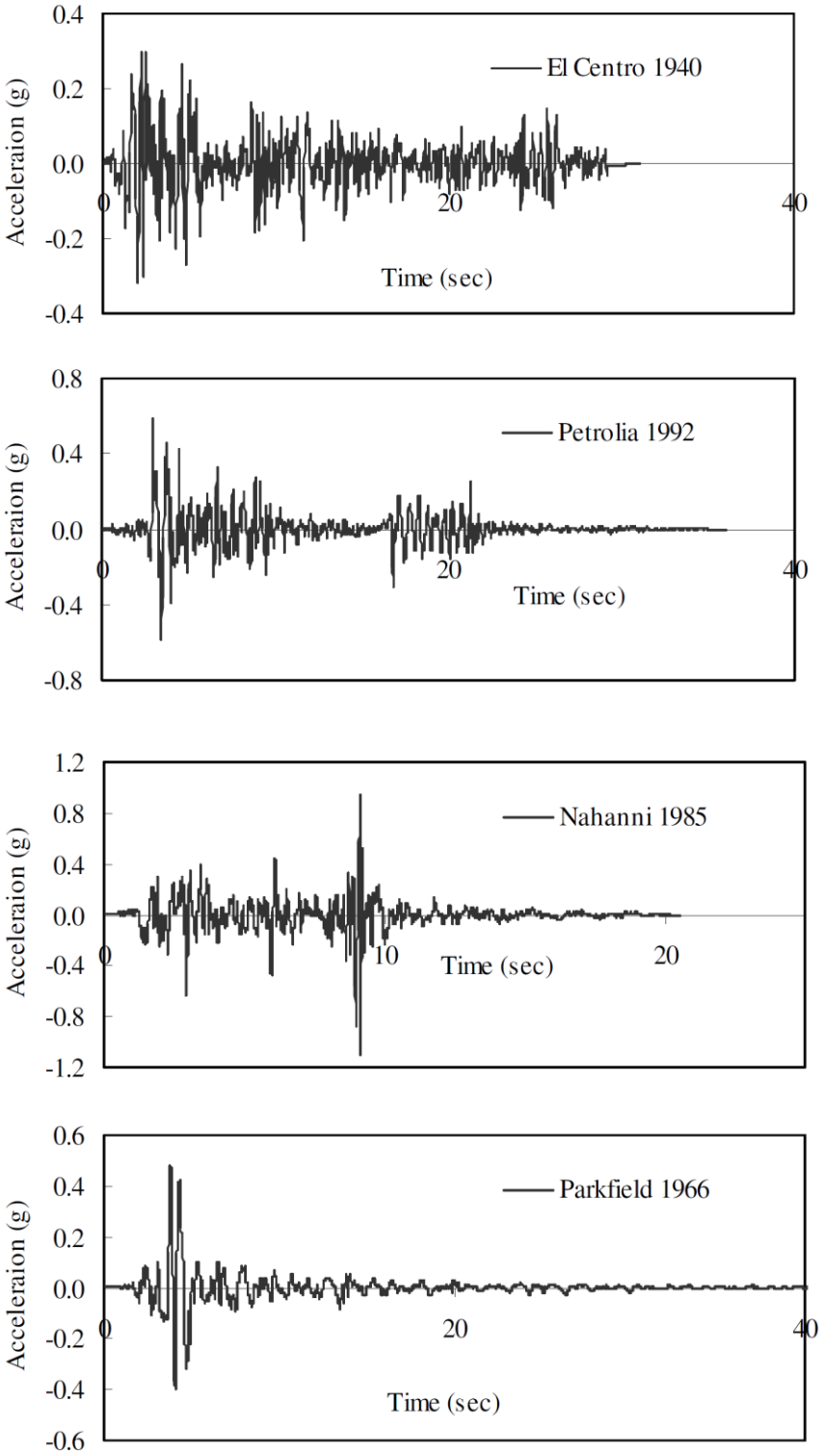

Figure 3.2 Original earthquake ground motions selected for seismic analysis (Bhowmick 2009)

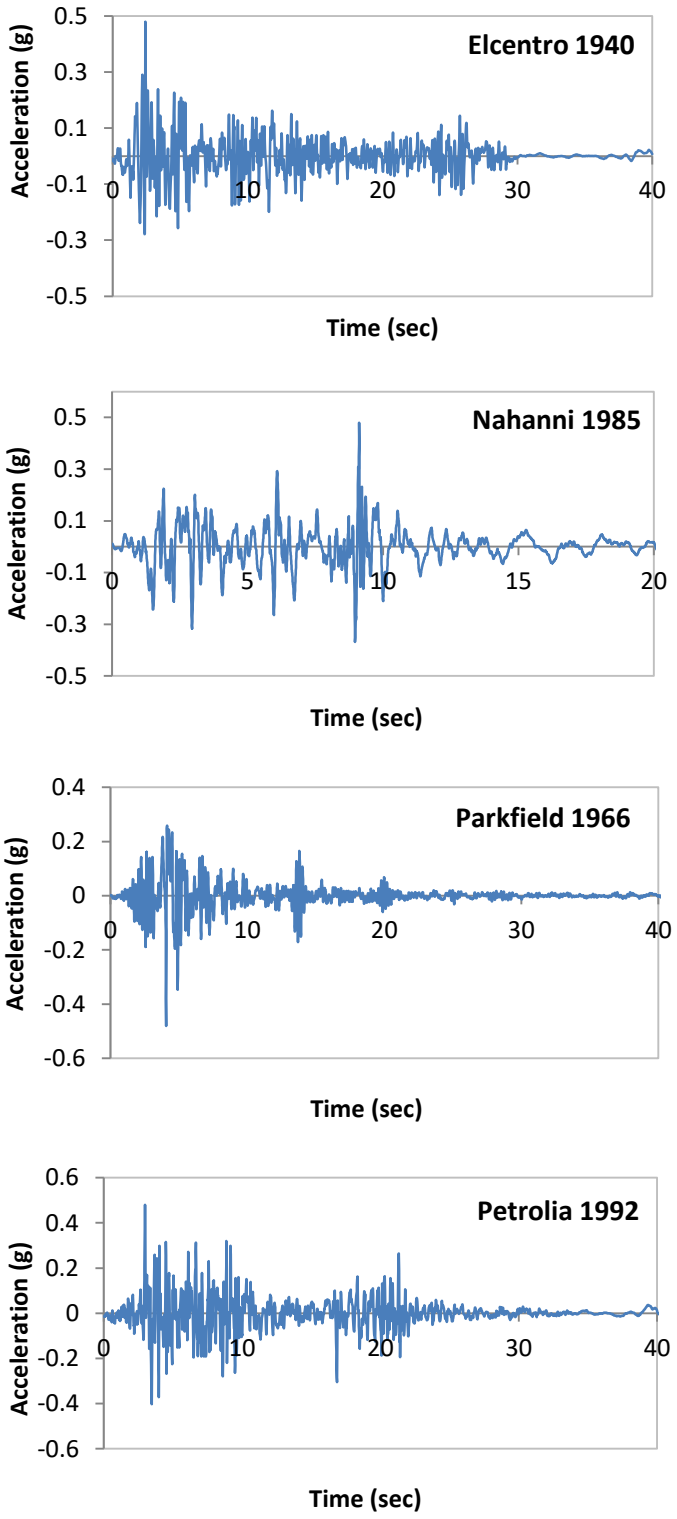

Figure 3.3 Spectrum-compatible earthquake records used for seismic analysis (Bhowmick 2009)

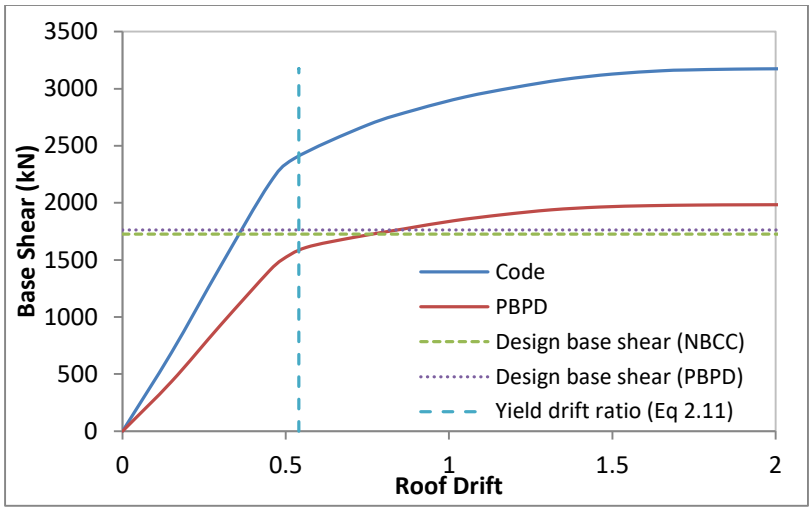

Figure 3.4 Pushover curves from nonlinear static analyses

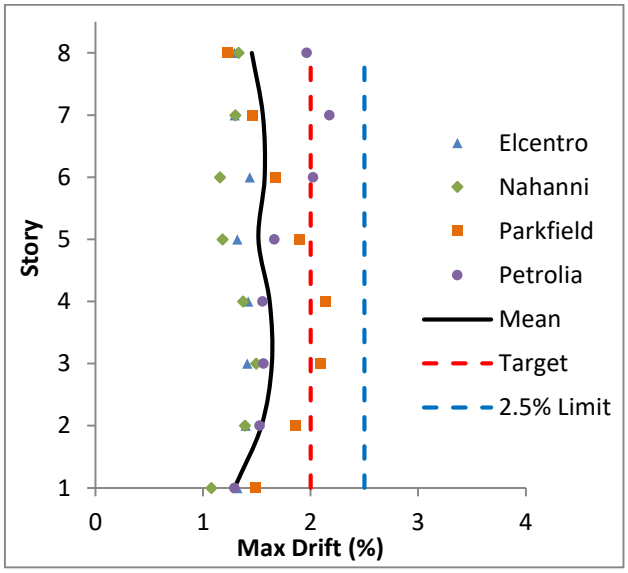

Figure 3.5 Story drift from nonlinear response history analyses of the PBOD-SPSW

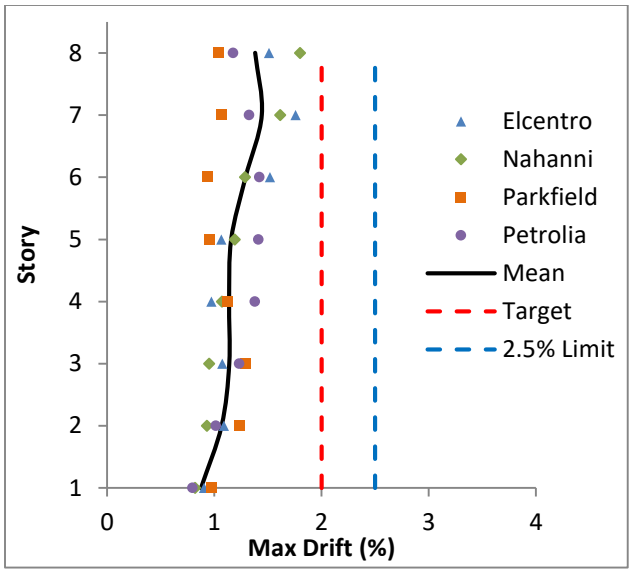

Figure 3.6 Story drift from nonlinear response history analyses of code designed SPSW

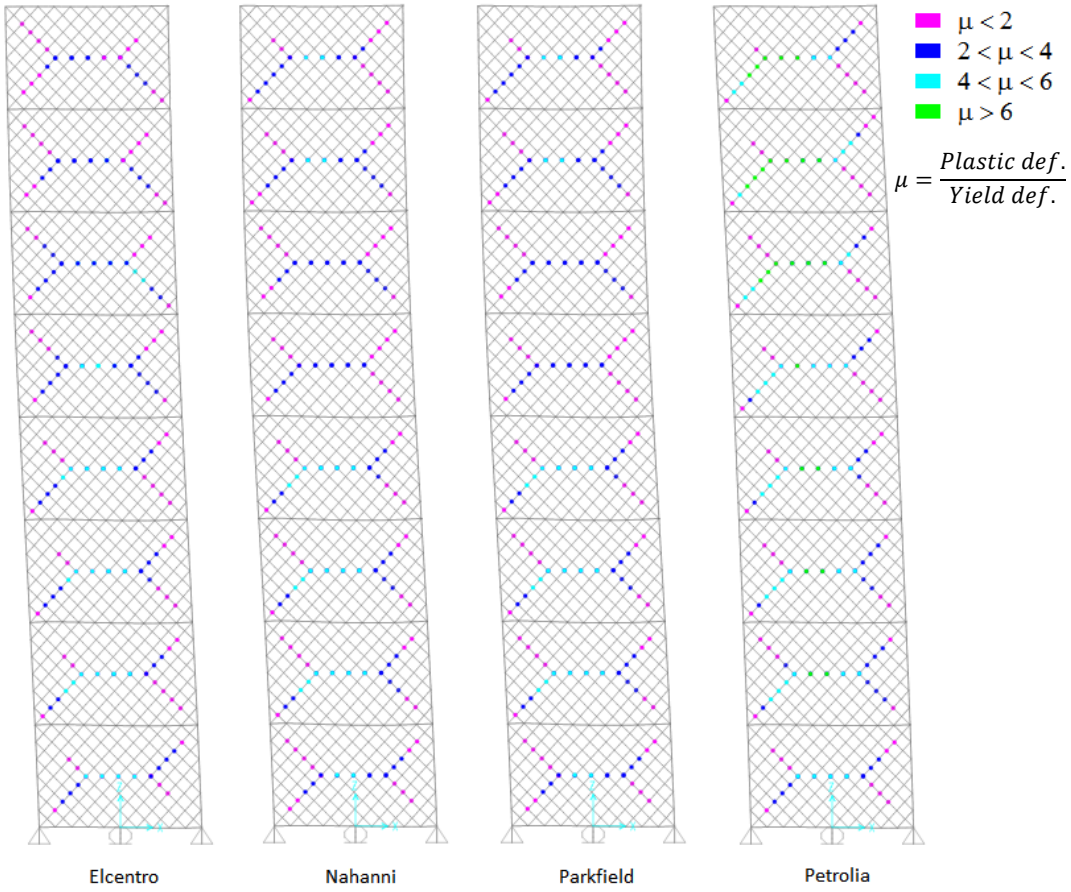

Figure 3.7 Plastic hinges in strip elements for the PBOD-SPSW

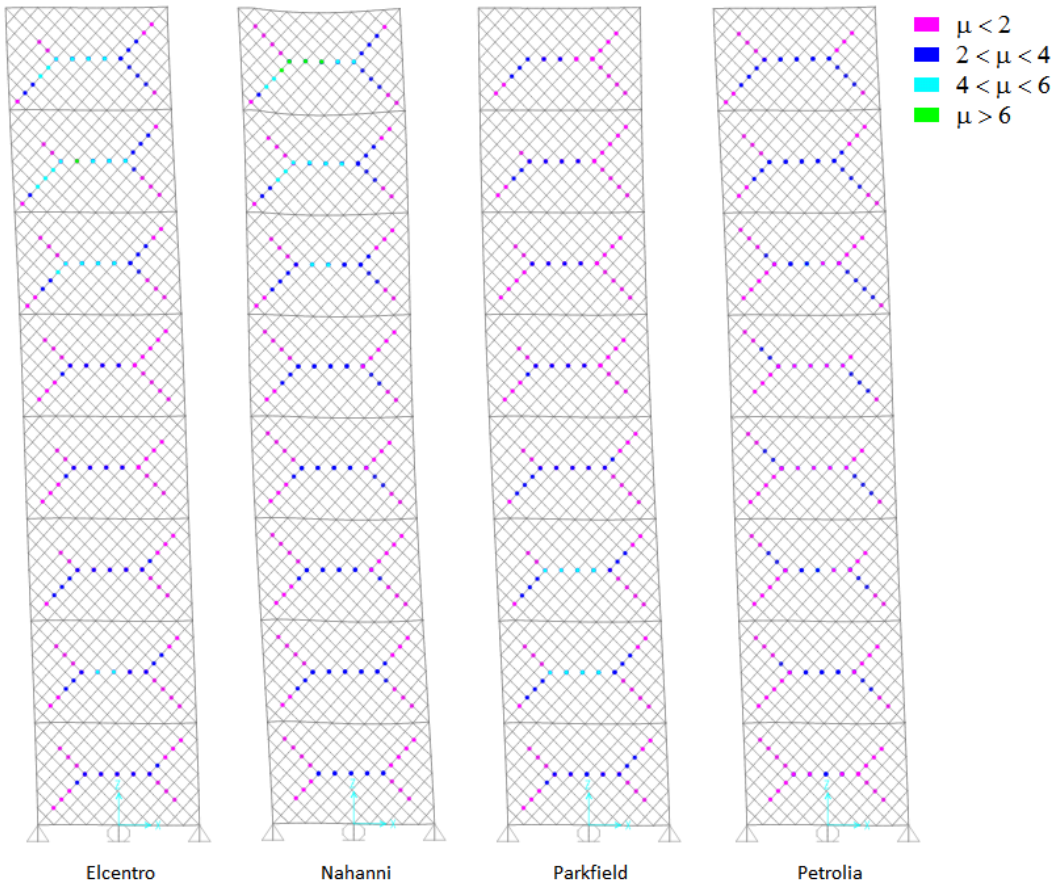

Figure 3.8 Plastic hinges in strip elements for the code-designed SPSW

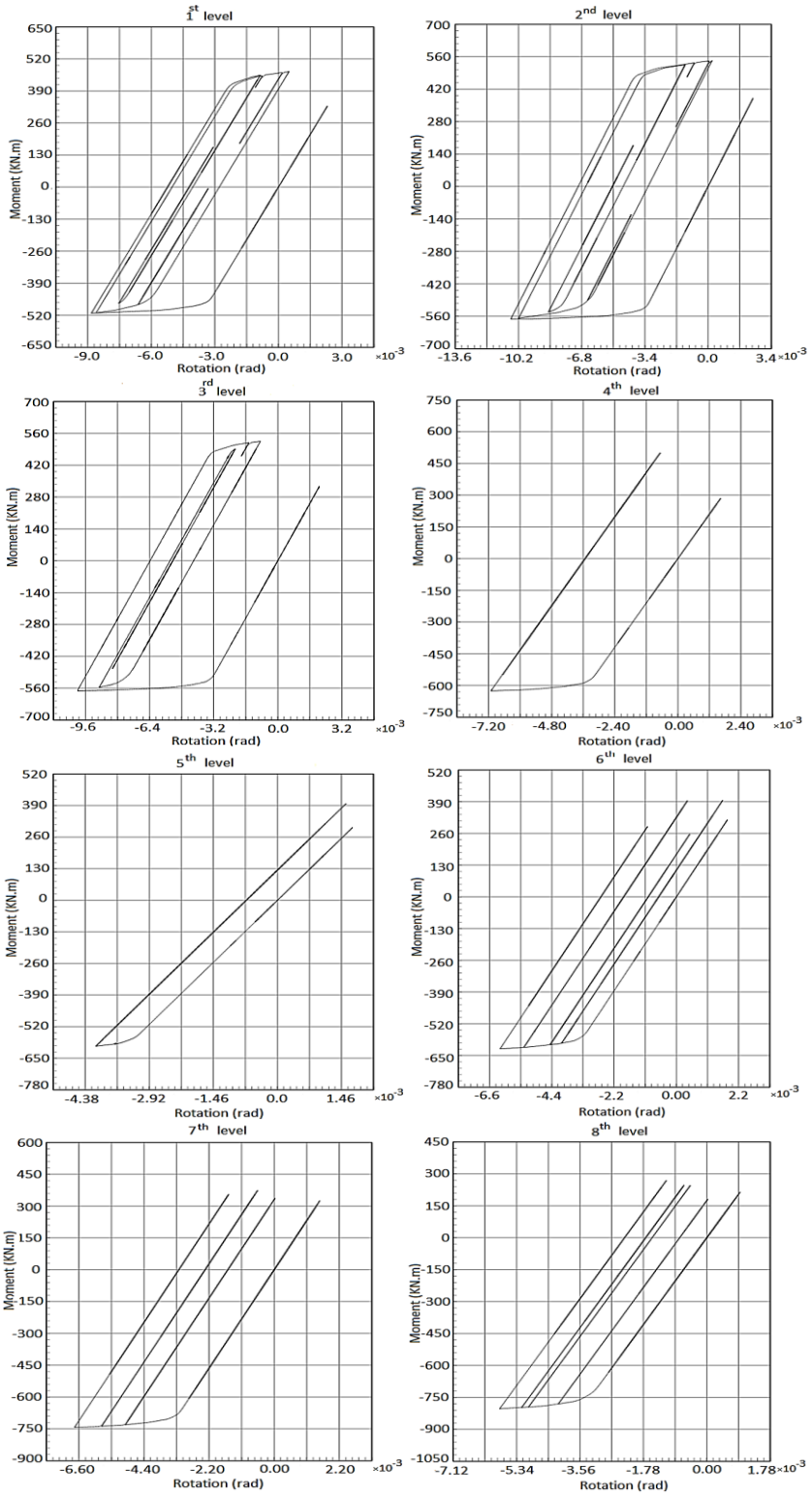

Figure 3.9 Moment rotation hysteresis of HBEs in PBOD-SPSW under modified Nahanni earthquake

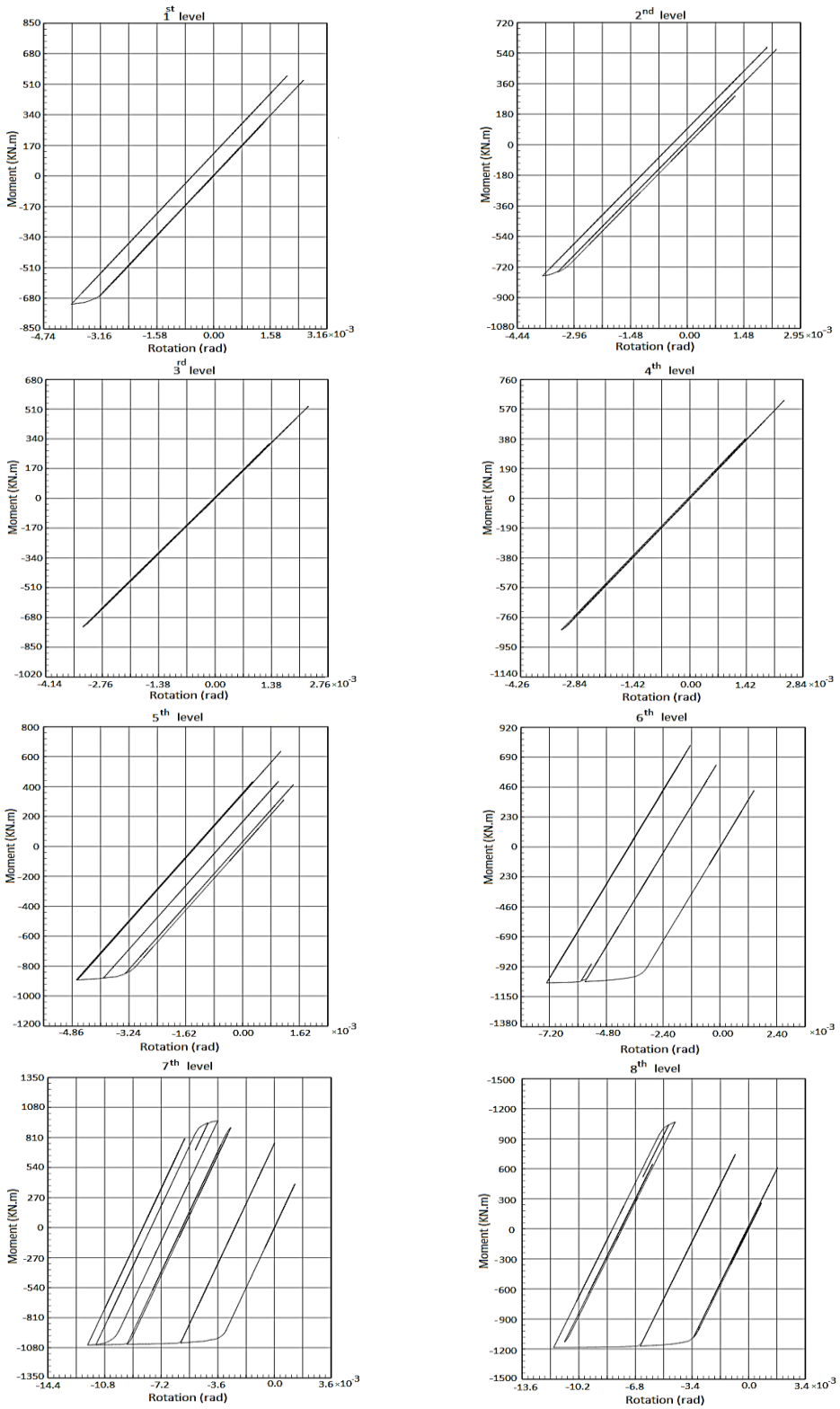

Figure 3.10 Moment rotation hysteresis of HBEs in code-designed SPSW under modified Nahanni earthquake

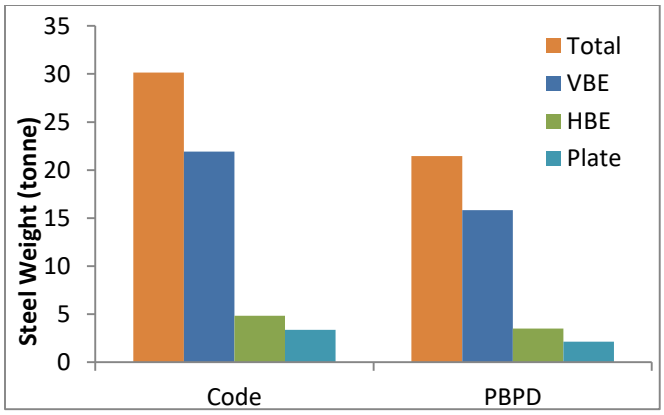

Figure 3.11 Comparison of steel weight for SPSWs

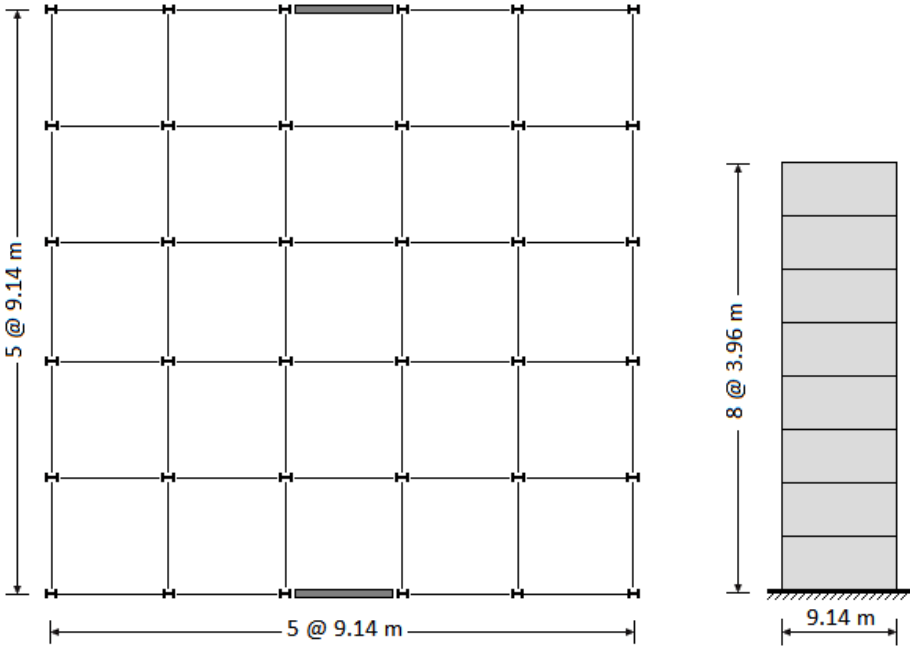

Figure 3.12 Floor plan and SPSW dimensions

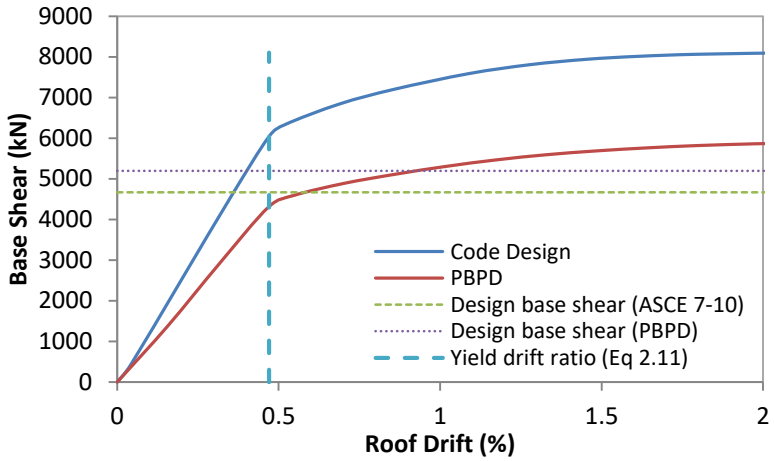

Figure 3.13 Roof drift versus base shear from pushover analyses

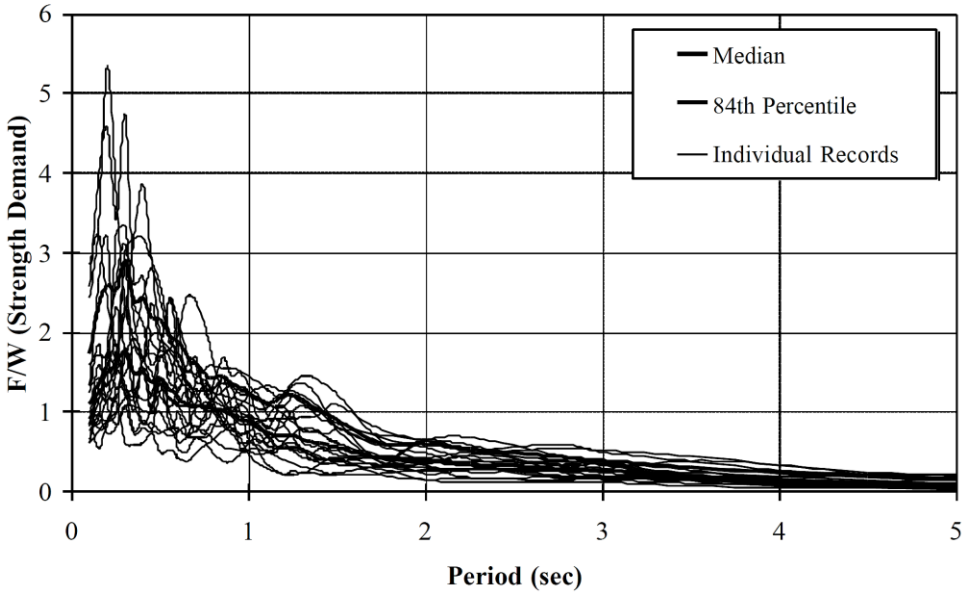

Figure 3.14 2% damped elastic acceleration spectra for the 20 earthquakes with 10% probability of exceedance in 50 years (Gupta and Krawinkler 1999)

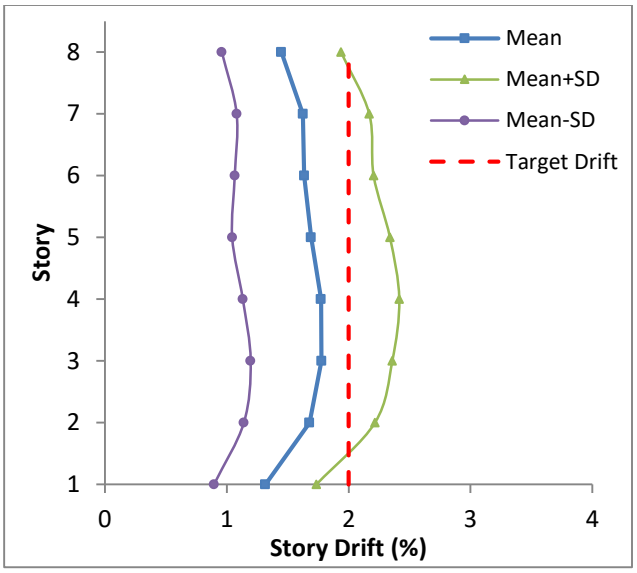

Figure 3.15 Maximum story drift profile for SPSW designed using the proposed approach

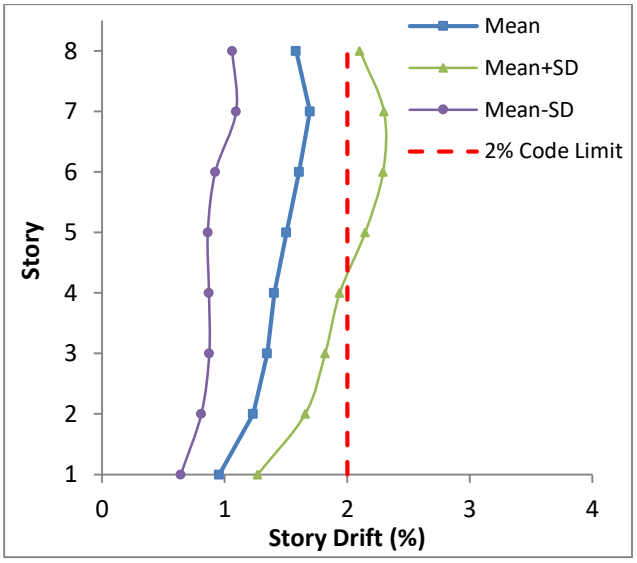

Figure 3.16 Maximum story drift profile for code designed SPSW

3.3 References

AISC. (2010). Seismic provisions for structural steel buildings, Chicago.

ASCE. (2010). Minimum design loads for buildings and other structures. SEI/ASCE 7-10, Reston, VA.

ASTM. (2008). Standard specification for Carbon structural steel. A36, West Conshohocken, PA.

Bhowmick, A.K. (2009). Seismic analysis and design of steel plate shear walls. Ph.D Dissertation, Department of Civil and Environmental Engineering, University of Alberta, Edmonton, Canada.

Berman, J.W., and Bruneau, M. (2005). Experimental investigation of light-gauge steel plate shear walls. Journal of Structural Engineering, 131 (2), 259-267.

Canadian Standards Association. (2014), Design of steel structures, CAN/CSA S16-14.

FEMA. (2000). FEMA355 State of the art report on systems performance of steel moment frames subject to earthquake ground shaking. Report No. FEMA-355C, FEMA, Washington, DC.

NBCC. (2010) National building code of Canada. National Research Council of Canada, Ottawa, ON, Canada.

Neilson, D.A.H., Grondin, G.Y., and Driver, R.G. (2010). Welding of light gauge infill panels for steel plate shear walls. Structural Engineering Report No. 290, Department of Civil and Environmental Engineering, University of Alberta, Edmonton, Canada.

Purba, R., and Bruneau, M. (2009). Finite element investigation and design recommendations for perforated steel plate shear walls. Journal of Structural Engineering, ASCE, Vol. 135, No. 11, 1367-1376.

Roberts, T., and Sabouri-Ghomi, S. (1992). Hysteretic characteristics of unstiffened perforated steel plate shear panels." Thin Walled Structures, Vol. 14, 139-151.

Saatcioglu, M., and Humar, J. (2003). Dynamic analysis of building for earthquake resistant design. Canadian Journal of Civil Engineering, 30:338-359.

Somerville P., Smith N., Punyamurthula S., and Sun, J. (1997). Development of ground motion time histories for phase 2 of the FEMA/SAC steel project. SAC background document. Report no. SAC/BD-97/04. SAC Joint Venture. 1997.

Vian, D., Bruneau, M., Tsai, K.-C., and Lin, U.C. (2009). Special perforated steel plate shear walls with reduced beam section anchor beams I: experimental investigation & II: analysis and design recommendations, Journal of Structural Engineering, ASCE, 135, 3, 211-228.

4. PLASTIC ANALYSIS AND BEHAVIOUR OF STEEL PLATE SHEAR WALLS WITH OUTRIGGERS[1]

4.1 Introduction

Steel plate shear wall (SPSW) systems are one of the most efficient and economical seismic force resisting systems for buildings located in high-risk earthquake zones. A typical thin unstiffened SPSW resists lateral loads, mainly through the formation of tension fields in infill plates, which buckle in shear in transverse direction at low load levels. The boundary moment frame, which is designed to anchor the fully yielded infill panels according to the capacity design principles, provides additional resistance to the system through the frame action. In conventional SPSWs, the overturning moments resulting from lateral loads are essentially resisted through the couple formed by the axial forces in vertical boundary elements (VBEs) at each level. The axial demands imposed by overturning moments, which can become extremely large in taller walls, together with flexural demands resulting from plastic hinging of the beam ends and pull-in forces of the tension field, can lead to unreasonably heavy VBEs. Furthermore, the extremely large axial demands can cause VBE failure and poor system performance when subjected to severe ground motions (Berman et al. 2008). In addition, the large concentrated force can cause foundation design issues. On the other hand, the relatively low overturning stiffness of conventional SPSWs compared to that of reinforced concrete walls is an important factor reducing the desirability of the system, especially in mid- to high-rise buildings (Berman et al. 2008).

In taller buildings, where the wall flexure dominates over shear, the overturning stiffness of SPSWs can be improved using outrigger systems. In modern tall buildings, core-and-outrigger systems are commonly used to resist high

[1] A version of this chapter has been accepted for publication in the *Journal of Constructional Steel Research*, Elsevier.

lateral forces and overturning moments due to earthquake and wind (Taranath 2012). In steel and composite constructions, the outriggers typically take the form of single- or multiple-story-tall trusses connecting the core (braced frame or shear wall) to perimeter frames where the axial stiffness of the outrigger columns is employed to enhance the flexural stiffness of the system (Taranath 2012). However, even for relatively shorter SPSWs, the low overturning stiffness may result in undesirable system characteristics. Therefore, practical and cost effective solutions are needed.

One practical option for improving the overturning stiffness of conventional SPSWs is to rigidly connect the beams of adjacent bays to the VBEs of SPSW at floor levels forming a dual structural system, herein referred to as steel plate shear walls with outriggers (SPSW-O). The moment-connected adjacent beams act as outriggers and work to reduce the bending in the SPSW by coupling it to the outrigger columns (OC). Furthermore, since the axial demands on the VBEs stem primarily from overturning moments due to lateral loads, the reduced overturning in SPSW would consequently result in lighter VBE sections, thus improving the desirability of the system in taller walls. Another potential application of SPSW-O configuration is in buildings with large bay widths, in which architectural constraints often do not allow the full width of the bay to be filled by a solid SPSW. In such cases, a narrower SPSW may be centrally placed within the bay to accommodate openings, and the adjacent beams may be designed as outriggers to improve the overturning stiffness of the narrow wall. As theoretically discussed above, the SPSW-O configuration can provide improved system performance as well as architectural flexibility for SPSWs to be more commonly used as lateral force resisting system in mid- to high-rise buildings. However, only limited work has been performed to investigate the efficiency and behaviour of such a structural system. Gholipour et al. (2015) investigated various arrangements of outrigger beam locations along the height of the SPSW. The researchers reported that the use of outrigger beams results in reduced VBE sizes and more uniform distribution of stiffness along the height of the system. However, the amount of VBE axial force

reduction and the overturning stiffness provided by the outrigger elements depend highly on the level of interaction between SPSW and the outrigger system, which is a function of the outrigger beam (OB) properties (i.e., strength, stiffness and length) and the rigidity of their connections to the VBEs and outrigger columns.

On the other hand, the SPSW-O configuration is a dual system in which the outrigger elements provide substantial lateral resistance to the system through the moment-resisting action of the connections. The levels of overturning stiffness and lateral strength provided by the outrigger elements are two important factors that should be quantified to achieve efficient design procedures for the SPSW-O systems. The current project undertakes this work through a combined analytical and numerical investigation aiming to provide design recommendations for desired levels of overturning stiffness and lateral load resistance, as described in this chapter and the following one. Several potential SPSW-O options are discussed, and their characteristics, particularly in terms of overturning stiffness and ultimate lateral strength, are studied. A parameter called the outrigger efficiency factor (OEF) is defined to quantify the level of overturning stiffness provided by the outrigger system within a SPSW-O. The OEF represents the level of interaction between SPSW and outrigger system in a SPSW-O configuration, which allows for the comparison of different SPSW-O options on a consistent basis. Analytical expressions are derived for the OEF and ultimate lateral strength of the systems and are verified using the results from numerical models. Sixty-four SPSW-O systems are designed to investigate the effects of various parameters on system behaviour. Parameters subject to investigation include outrigger beam (OB) properties, the height of the system, and OB-to-OC and HBE-to-VBE connection types.

4.2 SPSW-O System Configurations and Nomenclatures

In this chapter, several SPSW-O options are considered that are designed specifically to improve the overturning stiffness of SPSW systems. Figure 4.1 schematically shows four potential SPSW-O options having different combinations of simple and rigid HBE-to-VBE and OB-to-OC connections. The main

characteristic of all of these options is that they include moment-connected adjacent beams, which act as outriggers for SPSW by coupling it to the outer (outrigger) columns (OCs). Figure 4.1a shows the first SPSW-O option, herein referred to as SPSW-O (RR), in which all the connections in the system are rigid. In this option, while the outrigger system works to reduce the bending in the SPSW, it also provides significant lateral resistance to the system due to the moment-resisting action of the OB-to-OC and OB-to-VBE connections.

In the second option, named SPSW-O (RP), shown in Figure 4.2b, the outrigger beams are connected to the outrigger columns using pinned connections, and all other connections are moment resistant. Although the outrigger beams in this option transfer no moments to the outrigger columns, resulting in less interaction between the two systems, they effectively take part in restraining the rotation of the SPSW at floor levels. Therefore, they are expected to reduce the lateral drift corresponding to the flexural mode of deformation in the SPSW. The third option, called SPSW-O (PR), consists of a SPSW with pinned HBE-to-VBE connections and outrigger beams that are rigidly connected at both ends (Figure 4.1c). While the American Institute of Steel Construction (AISC) Seismic Provisions (2010) requires moment-resisting HBE-to-VBE connections for SPSWs, the Canadian Standards Association (CSA) Standard S16 (2009) permits simple connections to be used in the limited ductility (Type LD Plate Wall) category of SPSWs. Although SPSWs with simple connections have been shown to exhibit a highly pinched hysteretic behaviour, when they are used in conjunction with moment-connected outrigger beams, as shown in Figure 4.1c, a dual system is formed in which the outrigger elements not only improve resistance to overturning but also provide complementary energy dissipation to the system.

Yet another option is the SPSW-O system with pinned HBE-to-VBE and OB-to-OC connections, as shown in Figure 4.1d. This option, herein referred to as SPSW-O (PP), is intended to enhance the overturning stiffness of the system while reducing the fabrication costs associated with the high number of moment-resisting connections used in the previous options. In addition, the pinned HBE-to-VBE

connections used in the SPSW-O (PR) and SPSW-O (PP) options are aimed at reducing the large demands on the VBEs by eliminating the portions of the axial and flexural demands that are imposed by boundary frame moment-resisting action if rigid connections are used. Although the SPSW-O (PP) configuration would have lower redundancy and energy dissipation capacity compared to the previous options, it can be still considered an economical option for low to moderate, if not high, seismic areas.

For the purpose of brevity, throughout Chapters 4 and 5, the SPSW-O (RR), SPSW-O (RP), SPSW-O (PR) and SPSW-O (PP) options introduced above may be simply referred to as RR, RP, PR, and PP, respectively.

The level of overturning stiffness provided by the outrigger elements within a SPSW-O depends on various parameters such as the rigidity of OB-to-OC connections, outrigger beam properties and width of the outrigger bay. However, the lateral strength provided by these elements depends only on the first two parameters and is independent of the latter. In order to quantify the level of interaction between SPSW and the outrigger system, and to allow for the comparison of the four different SPSW-O options on a consistent basis, a simple parameter named the outrigger efficiency factor (OEF) is defined as the proportion of the overall overturning that is resisted by the outrigger system:

$$\mathrm{OEF} = \frac{\mathrm{M_{Outrigger}}}{\mathrm{M_{Total}}} \tag{4.1}$$

4.3 Plastic Analysis and Mechanisms of SPSW-O Systems

The plastic method of structural analysis is used herein to investigate behaviour, mechanisms and efficiency of the four SPSW-O options discussed earlier. As previously mentioned, although the primary objective for using the SPSW-O configuration is to enhance the overturning stiffness of the conventional SPSW systems, the lateral strength arising from moment-resisting action of the connections is inevitable and must be accounted for in an efficient design. As such, the lateral strength and flexural stiffness provided by such systems under desired

plastic mechanism are the basic building blocks used in understanding the behaviour of SPSW-Os; they are thus helpful in developing design procedures for such systems.

4.3.1 Single-Story SPSW-O

Statical and kinematic methods of plastic analysis are used in this section to derive the analytical expressions for ultimate lateral strength and outrigger efficiency factor of the SPSW-O systems introduced earlier. Although these parameters can be evaluated using nonlinear numerical simulations of the systems, reasonable estimates of them without performing such detailed analyses can greatly facilitate the design process. In order to better understand the behaviour of the system, equations are first developed for single story SPSW-Os and are then extended to the more complex cases of multi-storey systems. A single-story SPSW-O with moment-resisting HBE-to-VBE and OB-to-OC connections under a concentrated lateral load is shown in Figure 4.2.

Note that the expressions are first developed for the SPSW-O (RR) system, and are then used to derive the corresponding equations for the three other SPSW-O options described earlier. The desirable plastic mechanism of the system involves uniform yielding of the infill plate and plastic hinging at the ends of the HBEs and outrigger beams as well as at the bases of columns (i.e., VBEs and OCs). As shown in Figure 4.2, the overturning resistance of the SPSW-O system is provided by four different components, namely (1) the couple formed by the axial forces of the left and right VBEs, (2) the plastic flexural strength of the VBEs at their bases, (3) the couple formed by the axial forces of the left and right OCs and (4) the plastic flexural strength of the OCs at their bases. It should be noted that the overturning moment in conventional SPSWs is resisted only by the first two of these components.

4.3.1.1. **Equilibrium Method (Statical Method)**

In the plastic analysis method, it is assumed that the plasticity in the beam and column elements is lumped at plastic hinge locations. Assuming the desirable plastic mechanism shown above, Figure 4.3 illustrates the free body diagrams of individual elements of the single-story SPSW-O (RR). Note that the horizontal forces are not shown for clarity. In the statical method of plastic analysis, the expressions for ultimate lateral strength and OEF are derived using statics and the equilibrium equations of the forces and moments acting on individual elements, as well as on the whole structure. At the ultimate strength level, the overturning resistance of the system is equal to sum of the flexural resistances of the individual columns (i.e., VBEs and OCs) and the couples formed by the tensile and compressive forces within VBEs and OCs (Figure 4.3). Therefore, the overall overturning moment of the system can be written as:

$$M_{Total} = 2M_{VBE} + M_{SPSW} + M_{OT} + 2M_{OC} \quad (4.2)$$

where M_{VBE} is the plastic flexural strength of VBEs at their base; M_{SPSW} is the couple formed by axial forces of left and right VBEs; and M_{OT} is the couple formed by axial forces of the left and right outrigger columns. Since the plastic hinges have formed at both ends of the outrigger beams, the resulting shear forces in these elements can be calculated as:

$$V_{OB} = P_{OC} = \frac{2M_{OB}}{L'} \quad (4.3)$$

where, M_{OB} is the plastic flexural resistance of the outrigger beams and L' is the outrigger bay width, which is assumed to be the same for the left and right bays. The vertical component of the tension field along HBE is given by the following equation (Bruneau et al. 2011):

$$\omega_v = F_y t \cos^2\alpha \quad (4.4)$$

where F_y and t are the yield stress and thickness of the infill plate, respectively, and α is the tension field angle of inclination proposed by Timler and Kulak (1983):

$$\tan^4(\alpha) = \frac{1 + \frac{tL}{2A_c}}{1 + \text{ th } \left(\frac{1}{A_b} + \frac{h^3}{360I_cL}\right)} \tag{4.5}$$

where A_b and A_c are the cross-sectional areas of the HBE and VBE, respectively; h is the story height; L is the SPSW bay width, and I_c is the moment of inertia of the VBE. The internal shears at the left (V_{LHBE}) and right (V_{RHBE}) ends of the HBE are found to be:

$$V_{LHBE} = \frac{2M_{HBE}}{L} - \frac{F_y tL\cos^2\alpha}{2} \tag{4.6}$$

$$V_{RHBE} = \frac{2M_{HBE}}{L} + \frac{F_y tL\cos^2\alpha}{2} \tag{4.7}$$

where M_{HBE} is the plastic flexural strength of the HBEs. It can be assumed that the bottom horizontal boundary element (HBE0) is connected to the VBEs by simple connections. The tension field forces resulting from the fully yielded infill plate impose equal internal shear forces (V_{HBE0}) at both ends of the bottom HBE:

$$V_{HBE0} = \frac{F_y tL\cos^2\alpha}{2} \tag{4.8}$$

The axial (tensile) force in the left VBE, which is the summation of the vertical forces acting on this element resulting from the moment-resisting action of the connections and tension field action of the web plate, can be written as:

$$\begin{aligned} P_{LVBE} &= \frac{1}{2}F_y tH\sin 2\alpha + V_{LHBE} + V_{HBE0} - V_{OB} \\ &= \frac{1}{2}F_y tH\sin 2\alpha + \frac{2M_{HBE}}{L} - \frac{2M_{OB}}{L'} \end{aligned} \tag{4.9}$$

It is notable that the equilibrium equations of the right VBE yield the same value of the axial force in the opposite direction (compression). Therefore, the couple formed by the axial forces of the left and right VBE can be expressed as:

$$M_{SPSW} = P_{LVBE} \times L = \left(\frac{1}{2}F_y tH\sin 2\alpha + \frac{2M_{HBE}}{L} - \frac{2M_{OB}}{L'}\right)L \tag{4.10}$$

The axial (tensile) force in the left outrigger column is equal to the shear in the outrigger beam:

$$P_{OC} = V_{OB} = \frac{2M_{OB}}{L'} \tag{4.11}$$

Note that the right outrigger column is in compression; therefore, the couple formed by the axial forces of outrigger columns is represented by:

$$M_{OT} = P_{OC}(L + 2L') = \frac{2M_{OB}}{L'}(L + 2L') \tag{4.12}$$

Substituting the expressions derived for different terms in Eq. (4.1), the outrigger efficiency factor can be expressed as:

$$OEF = \frac{\frac{2M_{OB}}{L'}(L + 2L') + 2M_{OC}}{4M_{OB} + 2M_{HBE} + 2M_{VBE} + 2M_{OC} + \frac{1}{2}F_y tLH \sin 2\alpha} \tag{4.13}$$

On the other hand, the plastic lateral strength of the system (V_P) is the amount of force needed for the system to develop the desirable plastic mechanism shown in Figure 4.2. Therefore, the lateral load resistance of the single-story SPSW-O (RR) is calculated using the equilibrium equations of the system and is given by:

$$V_P = \frac{1}{H}M_{Total} = \frac{1}{H}(2M_{VBE} + 2M_{OC} + M_{SPSW} + M_{OT}) \tag{4.14}$$

Substituting the expression derived for different terms in Eq. (4.14), plastic lateral strength can be expressed as:

$$V_P = \frac{1}{H}\left(4M_{OB} + 2M_{HBE} + 2M_{VBE} + 2M_{OC} + \frac{1}{2}F_y tHL \sin 2\alpha\right) \tag{4.15}$$

4.3.1.2. **Kinematic Method (Virtual-Work Method)**

Simply stated, equating the amount of work done by the external forces needed to cause a plastic mechanism in the system and the internal work done by the plastic deformations in the elements of the structure provides an exact solution for the corresponding collapse loads for that mechanism. This is the main concept behind

the kinematic method of plastic analysis and is used in this section to derive the analytical expression for the plastic lateral strength and OEF of the single-story SPSW-O system. Assuming that the desirable plastic mechanism shown in Figure 4.2 has formed, the external work done by the concentrated lateral force is given by:

$$W_{Ex} = V_P H\theta \tag{4.16}$$

where, θ is the plastic rotation in the mechanism condition. The internal work of the system is the summation of the internal work done by plastic deformations of the infill panel and plastic rotations of the beam and column elements. These components of the internal work are given by Eqs. (4.17) and (4.18), respectively.

$$W_{In}(\text{plate}) = \frac{1}{2} F_y t L \sin 2\alpha \times H\theta \tag{4.17}$$

$$W_{In}(\text{frame action}) = (2M_{HBE} + 2M_{VBE} + 4M_{OB} + 2M_{OC})\,\theta \tag{4.18}$$

The total internal work is represented by the sum of these components as:

$$W_{In(SPSW-O)} = \left(\frac{1}{2} F_y t L H \sin 2\alpha + 2M_{HBE} + 2M_{VBE} + 4M_{OB} + 2M_{OC}\right)\theta \tag{4.19}$$

Equating internal and external work yields the same equation for the plastic lateral strength of the SPSW-O (RR) system as derived by the equilibrium method (Equation 4.15) as follows:

$$V_P = \frac{1}{H}\left(4M_{OB} + 2M_{HBE} + 2M_{OC} + 2M_{VBE} + \frac{1}{2} F_y H t L \sin 2\alpha\right) \tag{4.20}$$

At the assumed uniform plastic mechanism, the outrigger efficiency factor represents the relative contribution of the outrigger system to the overall overturning resistance of the SPSW-O system, and can be stated in terms of internal work as follows:

$$OEF = \frac{W_{In(Outrigger)}}{W_{In(SPSW-O)}} \tag{4.21}$$

The internal work done by the moment resistance provided by the outrigger system consists of two components, namely (1) the work done by the couple formed by the axial forces of the outrigger columns (M_{OT}) and (2) that due to the plastic hinging at the bases of the outrigger columns (M_{OC}). These moments and couple are subjected to a rotation θ, resulting in the internal work of:

$$W_{In(Outrigger)} = (M_{OT} + 2M_{OC})\,\theta \tag{4.22}$$

Substituting Eqs. (4.12), (4.19) and (4.22) into Eq. (4.21) yields the following expression for the OEF, which is the same as that derived using the equilibrium method:

$$OEF = \frac{\frac{2M_{OB}}{L'}(L + 2L') + 2M_{OC}}{4M_{OB} + 2M_{HBE} + 2M_{OC} + 2M_{VBE} + \frac{1}{2}F_y tLH \sin 2\alpha} \tag{4.23}$$

4.3.2 Multi-Story SPSW-O

The expressions developed for the ultimate lateral load resistance and outrigger efficiency factor of the single-story SPSW-O (RR) are extended to the more complicated case of the multi-story system. Figure 4.4 shows two possible plastic collapse mechanisms for the multi-story SPSW-O (RR) system.

A soft-story collapse mechanism can form when inelastic activities in a multistory structure subjected to lateral loads concentrate in a single or a few stories, resulting in undesirable system behaviour due to the formation of plastic hinges in the columns (Figure 4.4a). Equating the external work to the internal work for this plastic mechanism yields the following equation for the lateral load resistance of the system:

$$\sum_{j=i}^{n} F_j = \frac{1}{2}F_y t_i L \sin 2\alpha_i + \frac{4M_{OC\,i} + 4M_{VBE\ i}}{H_i} \tag{4.24}$$

Note that the external work in this case is essentially done by the lateral forces above the soft-story (level *i*), as there is no displacement below that level. The

internal work in this case stems only from the yielding of the infill panel and the formation of plastic hinges in the outrigger columns, as well as the VBEs, in soft-story. The strong-column and weak-beam concept has been incorporated into seismic design codes to prevent such undesirable collapse mechanisms in buildings. On the other hand, the desired plastic mechanism for a multi-story SPSW-O (RR) consists of uniformly yielded infill plates at all stories and plastic hinges formed at the ends of all HBEs and OBs, as well as at the bases of VBEs and OCs, as shown in Figure 4.4b.

The expression for the ultimate strength of this desirable plastic mechanism is derived by equating the amount external work and the internal work as:

$$\sum_{i=1}^{n} F_i h_i = 2M_{OC} + 2M_{VBE} + \sum_{i=1}^{n} [\, 4M_{(OB)i} + 2M_{(HBE)i} + \frac{1}{2} F_y L h_i \, (t_i \sin 2\alpha_i - t_{i+1} \sin 2\alpha_{i+1})] \qquad (4.25)$$

As in the procedure used for single-story SPSW-O, assuming that the anticipated desirable plastic mechanism is formed, and considering the sub-frame of the i^{th} story, as shown in Figure 4.5, the outrigger efficiency factor for the i^{th} story is defined as:

$$OEF_i = \frac{W_{In(Outrigger)i}}{W_{(In)i}} \qquad (4.26)$$

where the numerator indicates the amount of internal work due to the coupling action of the outrigger columns to resist overturning at story level i, and the denominator indicates the total internal work done by the sub-frame of the i^{th} story to resist overturning. Substituting the corresponding expressions of the internal work into Eq. (4.26), the outrigger efficiency factor for story level i takes the following format:

$$OEF_i = \frac{\sum_{j=i}^{n} \frac{2M_{(OB)j}}{L'}(L + 2L')}{\sum_{j=i}^{n}[\,4M_{(OB)j} + 2M_{(HBE)j} + \frac{1}{2}F_y L h_j\,(t_j \sin 2\alpha_j - t_{j+1} \sin 2\alpha_{j+1})]} \quad (4.27)$$

Note that the plastic hinges at bases of the outrigger columns and VBEs do not contribute to the overturning resistance of all stories above the base; therefore, their corresponding internal work do not appear in the expressions of the OEF for these story levels. Considering the entire system the OEF at the base of a multi-story SPSW-O (RR) system is expressed as:

$$OEF = \frac{2M_{OC} + \sum_{j=1}^{n} \frac{2M_{(OB)j}}{L'}(L + 2L')}{2M_{OC} + 2M_{VBE} + \sum_{j=1}^{n}[\,4M_{(OB)j} + 2M_{(HBE)j} + \frac{1}{2}F_y L h_j\,(t_j \sin 2\alpha_j - t_{j+1} \sin 2\alpha_{j+1})]} \quad (4.28)$$

As mentioned earlier in this section, the expressions of strength and outrigger efficiency factor for the SPSW-O system were derived assuming that all HBE-to-VBE and OB-to-OC connections are moment-resistant (i.e., SPSW-O (RR)). However, the level of interaction between SPSW and the outrigger system, as well as their relative contributions to the lateral load resistance, will be significantly affected by using pinned OB-to-OC and/or HBE-to-VBE connections in the systems, as shown in Figures 4.1b, 4.1c and 4.1d. Following the same procedure, the analytical expressions for plastic lateral strength of the SPSW-O (RP), SPSW-O (PR) and SPSW-O (PP) systems are given by Eqs. (4.29), (4.30) and (4.31), respectively.

$$\sum_{i=1}^{n} F_i h_i = 2M_{OC} + 2M_{VBE} + \sum_{i=1}^{n}[\,2M_{(OB)i} + 2M_{(HBE)i} + \frac{1}{2}F_y L h_i\,(t_i \sin 2\alpha_i - t_{i+1} \sin 2\alpha_{i+1})] \quad (4.29)$$

$$\sum_{i=1}^{n} F_i h_i = 2M_{OC} + 2M_{VBE} + \sum_{i=1}^{n}[\,4M_{(OB)i} + \frac{1}{2}F_y L h_i\,(t_i \sin 2\alpha_i - t_{i+1} \sin 2\alpha_{i+1})] \quad (4.30)$$

$$\sum_{i=1}^{n} F_i h_i = 2M_{OC} + 2M_{VBE} + \sum_{i=1}^{n}[\,2M_{(OB)i} + \frac{1}{2}F_y L h_i\,(t_i \sin 2\alpha_i - t_{i+1} \sin 2\alpha_{i+1})] \quad (4.31)$$

Also, using the same approach, the outrigger efficiency factors for the SPSW-O (RP), SPSW-O (PR) and SPSW-O (PP) systems are expressed by Eqs. (4.32), (4.33) and (4.34), respectively.

$$OEF = \frac{2M_{OC} + \sum_{j=1}^{n} \frac{M_{(OB)j}}{L'}(L + 2L')}{2M_{OC} + 2M_{VBE} + \sum_{j=1}^{n}[\,2M_{(OB)j} + 2M_{(HBE)j} + \frac{1}{2}F_y L h_j\,(t_j \sin 2\alpha_j - t_{j+1}\sin 2\alpha_{j+1})]} \quad (4.32)$$

$$OEF = \frac{2M_{OC} + \sum_{j=1}^{n} \frac{2M_{(OB)j}}{L'}(L + 2L')}{2M_{OC} + 2M_{VBE} + \sum_{j=1}^{n}[\,4M_{(OB)j} + \frac{1}{2}F_y L h_j\,(t_j \sin 2\alpha_j - t_{j+1}\sin 2\alpha_{j+1})]} \quad (4.33)$$

$$OEF = \frac{2M_{OC} + \sum_{j=1}^{n} \frac{M_{(OB)j}}{L'}(L + 2L')}{2M_{OC} + 2M_{VBE} + \sum_{j=1}^{n}[\,2M_{(OB)j} + \frac{1}{2}F_y L h_j\,(t_j \sin 2\alpha_j - t_{j+1}\sin 2\alpha_{j+1})]} \quad (4.34)$$

4.4 Verification Using Pushover Analyses

Prior sections introduced different SPSW-O options and presented the corresponding analytical expressions for their ultimate lateral load resistance and outrigger efficiency factors. To verify the validity of these analytical expressions, numerical models were developed for the four SPSW-O configurations introduced in this research. Eight- and 12-story SPSW-O systems were designed for modified versions of the 9-story SAC buildings (Gupta and Krawinkler 1999) according to the design procedure developed in the next chapter. A total of 16 SPSW-O systems consisting of 3.6-m-wide SPSWs and outrigger bays of either 3.2 m or 5.2 m, were considered in this section. The outrigger columns and VBEs were assumed to be pinned to the ground (since the SPSW-O configuration is expected to resist overturning primarily by the axial forces of the outrigger columns and VBEs, it is assumed that these elements are pinned to the ground). The uniform story height of 3.96 m was considered for all systems. In this section, the outrigger beams were selected to have the same size as HBEs at all stories. The structures were designed for a class D soil located in Los Angeles, California. The dead and live loads were matched with those of the 9-story SAC buildings. To have reasonable plate

thicknesses and VBE sizes, the seismic weights assigned to the walls were assumed to be 13100 kN and 19580 kN for the 8- and 12-story systems, respectively (i.e., six SPSW-Os in each direction). The design base shears were calculated using the performance-based plastic design method presented in Chapter 2. The periods of the structures were estimated using the equation proposed by Bhowmick et al. (2011), and were found to be 0.95 and 1.43 s for 8- and 12-story structures, respectively. The design short and one-second spectral acceleration parameters, S_{DS} and S_{D1}, were 1.07 g and 0.79 g, respectively. Summaries of the 8-story and 12-story SPSW-O designs are presented in Tables 4.1 and 4.2, respectively.

The commonly accepted strip models were created in SAP2000 (CSI 2010) to investigate the ultimate lateral strength and outrigger efficiency factor of the SPSW-O systems using nonlinear static analysis. The accuracy of the strip models to capture the inelastic response of SPSWs has been extensively verified by previous researchers (Driver et al. 1997; Elgaaly 1998; Berman 2003). The infill panels at all stories were represented by 15 pin-ended tension-only elements, where the compression strength of these elements was set to zero. The HBEs, VBEs, OBs and OCs were modeled using regular frame elements. To capture the nonlinearity in the models, lumped axial hinges were inserted at the midpoint of the strips, and axial-flexural fiber hinges were defined along the boundary frame members and outrigger elements. ASTM A572 Gr. 50 and A36 steels were selected for frame elements and infill panels, respectively. Idealized elasto-plastic material models were considered for all elements assuming no strain hardening. As commonly done in the strip modelling technique, it was assumed that the tension fields in all infill panels form at a single inclination angle equal to the average tension field angle of the plates at all stories. As such, a constant inclination angle of 42º was used for all strips in the numerical models for expediency. Pushover analyses were performed using the lateral force distribution method proposed by Chao et al. (2007).

Figure 4.6 shows a comparison of analytical and numerical simulations in estimating the ultimate lateral load resistance of the SPSW-O systems considered in this section. For each SPSW-O option, the base shear from pushover analysis

was normalized by the ultimate lateral load resistance, calculated using the corresponding analytical expressions (Equations 4.25 and 4.29-4.31). As shown in Figure 4.6, the normalized base shears obtained from pushover analyses and the theoretical calculations are in good agreement for all SPSW-O systems. The mean value of numerical/analytical ratio and the standard deviation of the ultimate lateral strength for the 16 SPSW-O systems are 0.97 and 0.015, respectively.

Figures 4.7 show plots of the outrigger efficiency factor versus roof drift for the 8- and 12-story SPSW-O systems, respectively. The mean value of the numerical/analytical ratio and the standard deviation of the OEF, for the sixteen SPSW-O systems are 1.02 and 0.02, respectively. Therefore, the analytical expressions presented in the previous section can be used by the design engineer as valid tools to obtain reasonable estimates of the lateral load resistance and the OEFs of the four SPSW-O configurations introduced in this chapter, without performing detailed nonlinear analyses.

In the 8-story systems, it was observed that the OEFs are lower in smaller drifts for all SPSW-O options, indicating that the contribution of the outrigger system to the overturning stiffness is smaller in the elastic region. As the systems deflect beyond the elastic region at approximately 0.75% roof drift, the OEFs start to increase and approach the OEF values predicted using the analytical expressions. This variation is more clearly observed in the SPSW-O systems with longer outrigger lengths (i.e., 5.2 m). However, for the 12-story systems, the opposite trend is generally observed, indicating that the outrigger system is more efficient in smaller drifts.

The reason behind this trend stems from the difference between the predominant modes of deflection in SPSWs and moment frames, and the associated yielding sequence. While the lateral deformation pattern in a moment frame is dominated by the shear mode, the lateral deflection of a SPSW is similar to that of a vertical cantilever plate girder, in which the contribution of the flexural mode of deformation to the overall drift can be significant. In taller SPSWs, the lateral deflection of the wall increases rapidly with the building height due primarily to

cumulative axial deformation of the VBEs. This results in significantly larger drifts in upper stories. However, the outrigger frames with predominant shear-type deformation tend to drift uniformly along the building height. Therefore, when drifting as a unit, the outrigger system tends to restrain these excessive elastic drifts due to the wall flexure by pulling back the SPSW in upper stories. Hence, when the 12-story SPSW-O systems are pushed to larger drifts, the outrigger beam ends (where rigid) at upper stories start to yield before other elements (i.e., infill plates and HBEs) at these levels; therefore, the OEF drops as the system behaviour deviates from the elastic range. As yielding progresses in the system, the infill plates and HBE ends start to plasticize in several stories, and OEF curves tend to become steady, approaching the theoretically estimated values of the OEF. However, in the 8-story SPSW-Os, since the height of the wall is relatively shorter, the cumulative axial deformation of the VBEs is less, resulting in smaller flexural deflection in the SPSWs. Therefore, the yielding of the outrigger beams occurs at larger drifts when numerous elements of the SPSW have partially yielded.

4.5 **Parametric Study**

To investigate the influence of a number of parameters on system characteristics and overall performance, 64 SPSW-Os were designed. The parameters subjected to investigation include outrigger beam length and flexural strength, the types of OB-to-OC and HBE-to-VBE connections, and the number of stories (i.e., height of the system). Eight- and 12-story SPSW-O systems were designed for the building structures described in the previous section. Two outrigger lengths, 3.2 m and 5.2 m, were considered for each of the four SPSW-O options. The outrigger beams were designed for four levels of flexural strength, and were selected based on the size of HBE at each story. By defining a parameter (λ) as the ratio of the outrigger beam plastic section modulus to that of HBE ($\lambda = Z_{OC}/Z_{HBE}$), these elements were proportioned to achieve the following λ values: $0.5, 1, 1.5$ and 2. Summaries of the designs for SPSW-O systems with $\lambda = 0.5, 1.5$ and 2 are given in Tables 4.3-4.10.

Note that the design details of all other SPSW-O systems with $\lambda = 1$ were presented in previous section (Tables 4.1 and 4.2).

As expected, the PP and RR systems required the largest and smallest plate thicknesses, respectively, indicating that the contributions of the frame action to overall strength within such systems are the least and the greatest among the SPSW-O options. A detailed discussion of the relative and respective contributions of the tension field action and moment resisting action to the overall strength of each SPSW-O option is provided in the next chapter; procedures for the preliminary design of the systems are also described. The validated analytical expressions presented earlier were used to estimate the outrigger efficiency factors and ultimate lateral strengths of the 64 SPSW-O systems designed in this section. Tables 4.11 and 4.12 show the calculated OEFs for the 8- and 12-story SPSW-O systems, respectively.

For each SPSW-O option, the analytically predicted OEFs were similar for the 8- and 12-story systems designed with the same outrigger length and λ value (i.e., the OEFs were not influenced by the building height). Clearly, SPSW-Os with rigid OB-to-OC connections possess significantly higher OEFs compared to their counterparts having pinned OB-to-OC connections with identical λ values. While the former systems employ bending moments and shear forces of the OBs to transfer overturning moments from the SPSW to the outrigger columns, the latter systems use only the OBs' shear forces for this purpose.

Figure 4.8 shows the variation of the outrigger efficiency factors for SPSW-Os with two different outrigger lengths and various outrigger beam strength levels. It is noteworthy that the variation of OEFs in the RR and RP systems are very similar to those of the PR and PP systems, respectively. This indicates that the type of HBE-to-VBE connections (i.e., pinned or rigid) does not have a significant impact on the OEF. It should be mentioned that this observation is valid for the systems designed according to the design procedure proposed in Chapter 5 (i.e., all SPSW-O systems were proportioned to have the same lateral load resistance). The validated equations derived for the strength of the systems (Eqs. 4.25, 4.29-4.31)

were used to calculate the overstrength of the 64 SPSW-O systems under consideration. Tables 4.13 and 4.14 present the estimated values of system overstrength for the 8- and 12-story SPSW-O systems, respectively.

The mean values of the overstrength were 1.07, 1.08, 1.09 and 1.10 for the RR, RP, PR and PP systems, respectively, with corresponding standard deviations of 0.012, 0.015, 0.010 and 0.012. The mean overstrength values calculated herein are generally lower than that prescribed by ASCE-7 (2010) for conventional SPSWs ($\Omega_o = 2$). This is the case for three main reasons: (1) the material strain hardening of the steel plates, boundary frame and outrigger elements was not taken into account in the calculations; (2) the strength provided by the frame action of the outrigger system and boundary frame was explicitly taken into account when designing infill plates using the proposed design method presented in Chapter 5; and (3) for comparison purposes, the calculated plate thicknesses were used in all designs in lieu of commercially available plate thickness (i.e., it was assumed that the theoretically required plate thicknesses were available in all cases).

However, it is recalled that the overstrength value in the code was suggested for the code-designed SPSWs, in which the infill panels are conventionally designed to resist 100% of the design story shears, resulting in heavier boundary elements and higher system overstrength. A more detailed discussion of the overstrength calculated for different SPSW-O options will be provided in Chapter 5.

It should be noted from the designs that the VBE sizes in the SPSW-O systems with simple HBE-to-VBE connections (i.e., PR and PP) are generally slightly heavier than those in their counterparts, having moment-resisting HBE-to-VBE connections (i.e., RR and RP). It is well understood that the axial and flexural demands on the VBEs within SPSW-O systems results from the tension field action of the infill plates and the moment-resisting actions of the outrigger frame and boundary frame (if rigid connections are used). Although the pinned HBE-to-VBE connections used in the PR and PP configurations help to reduce the flexural and axial demands on VBEs due to the frame action, on the other hand, the thicker infill

plates required in such systems (to achieve the same strength) impose larger tension field forces on these elements. Therefore, the increased demands caused by the tension fields in most cases outweigh the reduced demands due to the frame action, resulting in slightly larger VBE sections compared to those in the RR and RP systems, respectively.

Figure 4.9 shows a comparison of the resulting steel weights for the SPSW-O systems designed assuming four different levels of strength for the outrigger beams. For the same λ values, the SPSW-O systems with moment-resisting HBE-to-VBE connections (i.e., RR and RP) were slightly lighter than their counterparts having pinned HBE-to-VBE connections (i.e., PR and PP, respectively), with the RR and PP systems being the lightest and heaviest systems, respectively. As shown, for the SPSW-O systems considered herein, the level of interaction between the SPSW and the outrigger system did not generally have a significant impact on the system weight when proportioned for the same overall strength. However, in the RR and PR configurations, the use of stronger OBs, which leads to higher OEFs, resulted in slightly lighter systems, especially in the 12-story buildings. It should be recalled that the above conclusions are valid for the SPSW-O systems that were designed using the design procedures developed in the next chapter.

Figure 4.10 shows the calculated steel weights for different elements of SPSW-O systems that possess the same outrigger efficiency factors. The OEFs of the systems considered in this comparison were 0.4 and 0.33 for SPSW-Os with outrigger bays of 3.2 m and 5.2 m, respectively. As expected, the VBEs were the heaviest elements in all designs, which constituted about 55% and 60% of the total weights in the 8- and 12-story systems, respectively.

4.6 **Summary and Conclusion**

This chapter employed the principles of plastic analysis to investigate the behaviour and efficiency of the SPSW-O systems in which moment-connected outrigger beams are invoked to enhance the flexural stiffness of conventional SPSWs. Four potential SPSW-O options were introduced, and their characteristics in terms of

plastic collapse mechanisms, overturning stiffness and lateral load resistance were discussed. A parameter called the outrigger efficiency factor (OEF) was defined to quantify the contribution of the outrigger system to the overall overturning resistance; this allows for the comparison of various SPSW-Os on a consistent basis. Simple expressions that capture the OEF and ultimate strength of the single and multistory SPSW-O systems were developed and compared with the results of numerical analyses, with fairly reasonable agreement. These analytical expressions derived based on the force transfer mechanism and principals of plastic analysis provide a useful tool for the preliminary design of SPSW-O systems to achieve the desired strength and level of coupling between SPSWs and the outrigger systems. Sixty-four SPSW-O systems were designed in order to explore the characteristics of different options discussed in this research, and to study the influence of various parameters on the plastic behaviour of the systems.

The knowledge generated herein, which is based on the fundamental principles of plastic analysis and nonlinear static analysis, serves as an essential starting point in developing the seismic design procedure for the SPSW-O systems proposed in the next chapter. Although several SPSW-O options discussed in this research were shown to be effective under static monotonic loading, their seismic performance under earthquake excitations needs to be evaluated in order to support the theoretical discussions and conclusions.

On the other hand, the outrigger elements in different SPSW-O configurations not only improve their resistance to overturning, but also provide significant strength to the systems, which should be quantified to achieve an efficient design. These issues will be addressed in the next chapter.

Table 4.1 Summary of the designs for 8-story SPSW-O systems with outrigger lengths of either 3.2 m or 5.2 m

SPSW-O (PP)							
Story	Plate (mm)	HBE	OB	VBE (3.2 m)	OC (3.2 m)	VBE (5.2m)	OC (5.2m)
1	5.79	W18×55	W18×55	W14×426	W12×87	W14×426	W12×79
2	5.66	W18×55	W18×55	W14×426	W12×87	W14×426	W12×79
3	5.35	W18×55	W18×55	W14×311	W12×65	W14×342	W10×60
4	4.99	W18×50	W18×50	W14×311	W12×65	W14×342	W10×60
5	4.44	W18×50	W18×50	W14×233	W10×49	W14×233	W8×48
6	3.80	W18×46	W18×46	W14×233	W10×49	W14×233	W8×48
7	2.94	W18×40	W18×40	W14×132	W8×31	W14×132	W8×28
8	1.87	W18×46	W18×46	W14×132	W8×31	W14×132	W8×28

SPSW-O (PR)							
Story	Plate (mm)	HBE	OB	VBE (3.2 m)	OC (3.2 m)	VBE (5.2m)	OC (5.2m)
1	4.96	W18×46	W18×46	W14×342	W14×132	W14×370	W14×109
2	4.85	W18×46	W18×46	W14×342	W14×132	W14×370	W14×109
3	4.60	W18×46	W18×46	W14×257	W14×109	W14×283	W14×90
4	4.29	W18×46	W18×46	W14×257	W14×109	W14×283	W14×90
5	3.83	W18×46	W18×46	W14×193	W12×87	W14×193	W12×79
6	3.27	W18×40	W18×40	W14×193	W12×87	W14×193	W12×79
7	2.53	W18×40	W18×40	W14×109	W12×58	W14×109	W12×53
8	1.61	W18×40	W18×40	W14×109	W12×58	W14×109	W12×53

SPSW-O (RP)							
Story	Plate (mm)	HBE	OB	VBE (3.2 m)	OC (3.2 m)	VBE (5.2m)	OC (5.2m)
1	4.62	W18×50	W18×50	W14×370	W12×87	W14×398	W12×79
2	4.53	W18×50	W18×50	W14×370	W12×87	W14×398	W12×79
3	4.30	W18×50	W18×50	W14×311	W12×72	W14×311	W10×60
4	4.01	W18×50	W18×50	W14×311	W12×72	W14×311	W10×60
5	3.57	W18×50	W18×50	W14×233	W10×49	W14×233	W8×48
6	3.05	W18×50	W18×50	W14×233	W10×49	W14×233	W8×48
7	2.36	W18×50	W18×50	W14×145	W8×31	W14×145	W8×31
8	1.51	W18×55	W18×55	W14×145	W8×31	W14×145	W8×31

SPSW-O (RR)							
Story	Plate (mm)	HBE	OB	VBE (3.2 m)	OC (3.2 m)	VBE (5.2m)	OC (5.2m)
1	4.07	W16×45	W16×45	W14×311	W14×132	W14×342	W14×109
2	3.98	W16×45	W16×45	W14×311	W14×132	W14×342	W14×109
3	3.79	W16×45	W16×45	W14×257	W14×109	W14×257	W14×90
4	3.53	W16×45	W16×45	W14×257	W14×109	W14×257	W14×90
5	3.15	W16×45	W16×45	W14×176	W12×87	W14×193	W12×72
6	2.69	W16×45	W16×45	W14×176	W12×87	W14×193	W12×72
7	2.09	W16×45	W16×45	W14×120	W12×65	W14×120	W12×58
8	1.33	W18×50	W18×50	W14×120	W12×65	W14×120	W12×58

Table 4.2 Summary of the designs for 12-story SPSW-O systems with outrigger lengths of either 3.2 m or 5.2 m

SPSW-O (PP)							
Story	Plate (mm)	HBE	OB	VBE (3.2 m)	OC (3.2 m)	VBE (5.2m)	OC (5.2m)
1	7.59	W18×71	W18×71	W14×730	W14×132	W14×730	W14×120
2	7.52	W18×71	W18×71	W14×730	W14×132	W14×730	W14×120
3	7.39	W18×71	W18×71	W14×730	W14×132	W14×730	W14×120
4	7.05	W18×65	W18×65	W14×550	W14×99	W14×550	W12×87
5	6.78	W18×65	W18×65	W14×550	W14×99	W14×550	W12×87
6	6.43	W18×65	W18×65	W14×550	W14×99	W14×550	W12×87
7	5.88	W18×60	W18×60	W14×342	W12×72	W14×370	W10×60
8	5.37	W18×55	W18×55	W14×342	W12×72	W14×370	W10×60
9	4.77	W18×55	W18×55	W14×342	W12×72	W14×370	W10×60
10	3.98	W18×50	W18×50	W14×193	W10×45	W14×193	W10×39
11	3.12	W18×46	W18×46	W14×193	W10×45	W14×193	W10×39
12	2.03	W18×46	W18×46	W14×193	W10×45	W14×193	W10×39

SPSW-O (PR)							
Story	Plate (mm)	HBE	OB	VBE (3.2 m)	OC (3.2 m)	VBE (5.2m)	OC (5.2m)
1	6.50	W18×60	W18×60	W14×550	W14×211	W14×605	W14×176
2	6.44	W18×60	W18×60	W14×550	W14×211	W14×605	W14×176
3	6.33	W18×60	W18×60	W14×550	W14×211	W14×605	W14×176
4	6.09	W18×60	W18×60	W14×455	W14×176	W14×455	W14×145
5	5.86	W18×55	W18×55	W14×455	W14×176	W14×455	W14×145
6	5.56	W18×55	W18×55	W14×455	W14×176	W14×455	W14×145
7	5.09	W18×50	W18×50	W14×283	W14×120	W14×311	W14×99
8	4.65	W18×50	W18×50	W14×283	W14×120	W14×311	W14×99
9	4.13	W18×46	W18×46	W14×283	W14×120	W14×311	W14×99
10	3.46	W18×46	W18×46	W14×159	W12×79	W14×159	W12×65
11	2.71	W18×40	W18×40	W14×159	W12×79	W14×159	W12×65
12	1.76	W18×40	W18×40	W14×159	W12×79	W14×159	W12×65

SPSW-O (RP)							
Story	Plate (mm)	HBE	OB	VBE (3.2 m)	OC (3.2 m)	VBE (5.2m)	OC (5.2m)
1	6.30	W18×60	W18×60	W14×665	W14×132	W14×665	W14×109
2	6.24	W18×60	W18×60	W14×665	W14×132	W14×665	W14×109
3	6.13	W18×60	W18×60	W14×665	W14×132	W14×665	W14×109
4	5.86	W18×60	W18×60	W14×500	W14×109	W14×550	W12×87
5	5.63	W18×60	W18×60	W14×500	W14×109	W14×550	W12×87
6	5.35	W18×60	W18×60	W14×500	W14×109	W14×550	W12×87
7	4.91	W18×55	W18×55	W14×342	W12×72	W14×342	W12×65
8	4.48	W18×55	W18×55	W14×342	W12×72	W14×342	W12×65
9	3.98	W18×55	W18×55	W14×342	W12×72	W14×342	W12×65
10	3.32	W18×50	W18×50	W14×193	W10×45	W14×193	W10×39
11	2.60	W18×50	W18×50	W14×193	W10×45	W14×193	W10×39
12	1.69	W18×65	W18×65	W14×193	W10×45	W14×193	W10×39

Table 4.2 continued

SPSW-O (RR)							
Story	Plate (mm)	HBE	OB	VBE (3.2 m)	OC (3.2 m)	VBE (5.2m)	OC (5.2m)
1	5.39	W18×55	W18×55	W14×500	W14×211	W14×550	W14×176
2	5.34	W18×55	W18×55	W14×500	W14×211	W14×550	W14×176
3	5.25	W18×55	W18×55	W14×500	W14×211	W14×550	W14×176
4	5.05	W18×50	W18×50	W14×398	W14×159	W14×426	W14×132
5	4.85	W18×50	W18×50	W14×398	W14×159	W14×426	W14×132
6	4.60	W18×50	W18×50	W14×398	W14×159	W14×426	W14×132
7	4.25	W18×50	W18×50	W14×283	W14×120	W14×283	W14×99
8	3.88	W18×50	W18×50	W14×283	W14×120	W14×283	W14×99
9	3.45	W18×50	W18×50	W14×283	W14×120	W14×283	W14×99
10	2.89	W18×46	W18×46	W14×176	W12×87	W14×176	W12×72
11	2.26	W18×46	W18×46	W14×176	W12×87	W14×176	W12×72
12	1.47	W18×55	W18×55	W14×176	W12×87	W14×176	W12×72

Table 4.3 Summary of the designs for 8-story SPSW-O (PP) systems with outrigger lengths of either 3.2 m or 5.2 m

$\lambda = 0.5$							
Story	Plate (mm)	HBE	OB	VBE (3.2 m)	OC (3.2 m)	VBE (5.2m)	OC (5.2m)
1	6.28	W18×60	W16×36	W14×455	W12×79	W14×455	W12×72
2	6.15	W18×60	W16×36	W14×455	W12×79	W14×455	W12×72
3	5.81	W18×60	W16×36	W14×342	W10×60	W14×370	W10×54
4	5.42	W18×55	W16×31	W14×342	W10×60	W14×370	W10×54
5	4.81	W18×55	W16×31	W14×233	W10×45	W14×233	W10×45
6	4.11	W18×50	W16×31	W14×233	W10×45	W14×233	W10×45
7	3.18	W18×46	W16×26	W14×132	W8×28	W14×132	W8×28
8	2.03	W18×46	W16×26	W14×132	W8×28	W14×132	W8×28

$\lambda = 1.5$							
Story	Plate (mm)	HBE	OB	VBE (3.2 m)	OC (3.2 m)	VBE (5.2m)	OC (5.2m)
1	5.37	W18×50	W18×71	W14×398	W14×99	W14×398	W12×87
2	5.25	W18×50	W18×71	W14×398	W14×99	W14×398	W12×87
3	4.98	W18×50	W18×71	W14×311	W12×79	W14×311	W12×65
4	4.64	W18×50	W18×71	W14×311	W12×79	W14×311	W12×65
5	4.13	W18×46	W18×65	W14×211	W10×54	W14×233	W10×49
6	3.52	W18×46	W18×65	W14×211	W10×54	W14×233	W10×49
7	2.73	W18×40	W18×60	W14×132	W8×35	W14×132	W8×31
8	1.74	W18×40	W18×60	W14×132	W8×35	W14×132	W8×31

Table 4.3 Continued

$\lambda = 2$							
Story	Plate (mm)	HBE	OB	VBE (3.2 m)	OC (3.2 m)	VBE (5.2m)	OC (5.2m)
1	4.99	W18×46	W18×86	W14×370	W14×109	W14×370	W12×87
2	4.88	W18×46	W18×86	W14×370	W14×109	W14×370	W12×87
3	4.63	W18×46	W18×86	W14×283	W12×87	W14×311	W12×65
4	4.31	W18×46	W18×86	W14×283	W12×87	W14×311	W12×65
5	3.85	W18×46	W18×86	W14×211	W10×60	W14×211	W10×49
6	3.28	W18×40	W18×71	W14×211	W10×60	W14×211	W10×49
7	2.55	W18×40	W18×71	W14×132	W8×35	W14×132	W8×31
8	1.62	W18×40	W18×71	W14×132	W8×35	W14×132	W8×31

Table 4.4 Summary of the designs for 8-story SPSW-O (PR) systems with outrigger lengths of either 3.2 m or 5.2 m

$\lambda = 0.5$							
Story	Plate (mm)	HBE	OB	VBE (3.2 m)	OC (3.2 m)	VBE (5.2m)	OC (5.2m)
1	5.76	W18×55	W16×31	W14×398	W14×99	W14×426	W14×90
2	5.64	W18×55	W16×31	W14×398	W14×99	W14×426	W14×90
3	5.34	W18×55	W16×31	W14×311	W12×87	W14×311	W12×72
4	4.98	W18×50	W16×31	W14×311	W12×87	W14×311	W12×72
5	4.43	W18×50	W16×31	W14×211	W12×65	W14×211	W12×58
6	3.78	W18×46	W16×26	W14×211	W12×65	W14×211	W12×58
7	2.93	W18×40	W16×26	W14×120	W10×45	W14×120	W10×45
8	1.87	W18×46	W16×26	W14×120	W10×45	W14×120	W10×45

$\lambda = 1.5$							
Story	Plate (mm)	HBE	OB	VBE (3.2 m)	OC (3.2 m)	VBE (5.2m)	OC (5.2m)
1	4.42	W18×40	W18×60	W14×342	W14×159	W14×398	W14×132
2	4.33	W18×40	W18×60	W14×342	W14×159	W14×398	W14×132
3	4.10	W18×40	W18×55	W14×257	W14×132	W14×311	W14×109
4	3.82	W18×40	W18×55	W14×257	W14×132	W14×311	W14×109
5	3.42	W18×40	W18×55	W14×176	W14×99	W14×233	W12×87
6	2.92	W18×35	W18×50	W14×176	W14×99	W14×233	W12×87
7	2.26	W18×35	W18×50	W14×109	W12×72	W14×132	W12×65
8	1.44	W18×35	W18×50	W14×109	W12×72	W14×132	W12×65

$\lambda = 2$							
Story	Plate (mm)	HBE	OB	VBE (3.2 m)	OC (3.2 m)	VBE (5.2m)	OC (5.2m)
1	3.96	W16×40	W18×71	W14×257	W14×176	W14×283	W14×145
2	3.88	W16×40	W18×71	W14×257	W14×176	W14×283	W14×145
3	3.69	W16×36	W18×65	W14×211	W14×145	W14×233	W14×120
4	3.44	W16×36	W18×65	W14×211	W14×145	W14×233	W14×120
5	3.07	W16×36	W18×65	W14×159	W14×109	W14×176	W14×90
6	2.63	W16×36	W18×60	W14×159	W14×109	W14×176	W14×90
7	2.04	W16×31	W18×55	W14×99	W12×79	W14×99	W12×72
8	1.30	W16×36	W18×60	W14×99	W12×79	W14×99	W12×72

Table 4.5 Summary of the designs for 8-story SPSW-O (RP) systems with outrigger lengths of either 3.2 m or 5.2 m

$\lambda = 0.5$							
Story	Plate (mm)	HBE	OB	VBE (3.2 m)	OC (3.2 m)	VBE (5.2m)	OC (5.2m)
1	5.07	W18×55	W16×31	W14×426	W12×79	W14×426	W12×72
2	4.97	W18×55	W16×31	W14×426	W12×79	W14×426	W12×72
3	4.69	W18×55	W16×31	W14×311	W10×60	W14×342	W10×54
4	4.37	W18×55	W16×31	W14×311	W10×60	W14×342	W10×54
5	3.90	W18×55	W16×31	W14×233	W8×48	W14×233	W10×45
6	3.33	W18×50	W16×31	W14×233	W8×48	W14×233	W10×45
7	2.58	W18×50	W16×31	W14×145	W8×31	W14×145	W8×28
8	1.64	W18×60	W16×36	W14×145	W8×31	W14×145	W8×28

$\lambda = 1.5$							
Story	Plate (mm)	HBE	OB	VBE (3.2 m)	OC (3.2 m)	VBE (5.2m)	OC (5.2m)
1	4.31	W18×46	W18×65	W14×342	W14×99	W14×370	W12×87
2	4.22	W18×46	W18×65	W14×342	W14×99	W14×370	W12×87
3	4.00	W18×46	W18×65	W14×283	W12×79	W14×283	W12×65
4	3.74	W18×46	W18×65	W14×283	W12×79	W14×283	W12×65
5	3.33	W18×46	W18×65	W14×211	W10×60	W14×211	W10×49
6	2.85	W18×46	W18×65	W14×211	W10×60	W14×211	W10×49
7	2.21	W18×46	W18×65	W14×145	W8×35	W14×145	W8×31
8	1.41	W18×55	W18×86	W14×145	W8×35	W14×145	W8×31

$\lambda = 2$							
Story	Plate (mm)	HBE	OB	VBE (3.2 m)	OC (3.2 m)	VBE (5.2m)	OC (5.2m)
1	4.09	W16×45	W18×76	W14×342	W14×109	W14×370	W12×87
2	4.00	W16×45	W18×76	W14×342	W14×109	W14×370	W12×87
3	3.80	W16×45	W18×76	W14×257	W12×87	W14×283	W12×72
4	3.54	W16×45	W18×76	W14×257	W12×87	W14×283	W12×72
5	3.16	W16×45	W18×76	W14×211	W12×65	W14×211	W10×49
6	2.70	W16×45	W18×76	W14×211	W12×65	W14×211	W10×49
7	2.10	W16×45	W18×76	W14×145	W8×40	W14×145	W8×31
8	1.34	W18×50	W18×97	W14×145	W8×40	W14×145	W8×31

Table 4.6 Summary of the designs for 8-story SPSW-O (RR) systems with outrigger lengths of either 3.2 m or 5.2 m

$\lambda = 0.5$							
Story	Plate (mm)	HBE	OB	VBE (3.2 m)	OC (3.2 m)	VBE (5.2m)	OC (5.2m)
1	4.64	W18×46	W16×26	W14×370	W14×99	W14×370	W14×90
2	4.55	W18×50	W16×31	W14×370	W14×99	W14×370	W14×90
3	4.31	W18×50	W16×31	W14×283	W12×87	W14×311	W12×79
4	4.01	W18×50	W16×31	W14×283	W12×87	W14×311	W12×79
5	3.58	W18×50	W16×31	W14×211	W12×65	W14×211	W12×58
6	3.06	W18×50	W16×31	W14×211	W12×65	W14×211	W12×58
7	2.37	W18×46	W16×26	W14×132	W10×49	W14×132	W10×45
8	1.51	W18×55	W16×31	W14×132	W10×49	W14×132	W10×45

$\lambda = 1.5$							
Story	Plate (mm)	HBE	OB	VBE (3.2 m)	OC (3.2 m)	VBE (5.2m)	OC (5.2m)
1	3.58	W16×36	W18×46	W14×257	W14×145	W14×283	W14×120
2	3.51	W16×40	W18×55	W14×257	W14×145	W14×283	W14×120
3	3.34	W16×40	W18×55	W14×211	W14×132	W14×233	W14×109
4	3.11	W16×40	W18×55	W14×211	W14×132	W14×233	W14×109
5	2.78	W16×40	W18×55	W14×159	W14×99	W14×176	W14×90
6	2.37	W16×40	W18×55	W14×159	W14×99	W14×176	W14×90
7	1.85	W16×40	W18×55	W14×120	W12×79	W14×120	W12×65
8	1.18	W18×46	W18×65	W14×120	W12×79	W14×120	W12×65

$\lambda = 2$							
Story	Plate (mm)	HBE	OB	VBE (3.2 m)	OC (3.2 m)	VBE (5.2m)	OC (5.2m)
1	3.11	W18×35	W18×65	W14×233	W14×176	W14×257	W14×145
2	3.05	W18×35	W18×65	W14×233	W14×176	W14×257	W14×145
3	2.90	W18×35	W18×65	W14×176	W14×145	W14×211	W14×120
4	2.70	W18×35	W18×65	W14×176	W14×145	W14×211	W14×120
5	2.42	W18×35	W18×65	W14×145	W14×109	W14×159	W14×90
6	2.07	W18×35	W18×65	W14×145	W14×109	W14×159	W14×90
7	1.61	W18×35	W18×65	W14×109	W12×87	W14×109	W12×79
8	1.03	W18×40	W18×76	W14×109	W12×87	W14×109	W12×79

Table 4.7 Summary of the designs for 12-story SPSW-O (PP) systems with outrigger lengths of either 3.2 m or 5.2 m

$\lambda = 0.5$							
Story	Plate (mm)	HBE	OB	VBE (3.2 m)	OC (3.2 m)	VBE (5.2m)	OC (5.2m)
1	8.19	W18×76	W16×40	W14×730	W14×109	W14×730	W14×99
2	8.12	W18×76	W16×40	W14×730	W14×109	W14×730	W14×99
3	7.97	W18×76	W16×40	W14×730	W14×109	W14×730	W14×99
4	7.65	W18×71	W16×40	W14×605	W12×87	W14×605	W12×79
5	7.36	W18×71	W16×40	W14×605	W12×87	W14×605	W12×79
6	6.98	W18×71	W16×40	W14×605	W12×87	W14×605	W12×79
7	6.36	W18×65	W16×36	W14×370	W10×60	W14×398	W10×54
8	5.81	W18×60	W16×36	W14×370	W10×60	W14×398	W10×54
9	5.16	W18×55	W16×31	W14×370	W10×60	W14×398	W10×54
10	4.29	W18×50	W16×31	W14×193	W10×39	W14×193	W10×33
11	3.37	W18×46	W16×31	W14×193	W10×39	W14×193	W10×33
12	2.19	W18×50	W16×31	W14×193	W10×39	W14×193	W10×33

$\lambda = 1.5$							
Story	Plate (mm)	HBE	OB	VBE (3.2 m)	OC (3.2 m)	VBE (5.2m)	OC (5.2m)
1	7.02	W18×65	W18×97	W14×665	W14×159	W14×665	W14×132
2	6.96	W18×65	W18×97	W14×665	W14×159	W14×665	W14×132
3	6.83	W18×65	W18×97	W14×665	W14×159	W14×665	W14×132
4	6.53	W18×60	W18×86	W14×500	W14×120	W14×550	W14×99
5	6.28	W18×60	W18×86	W14×500	W14×120	W14×550	W14×99
6	5.96	W18×60	W18×86	W14×500	W14×120	W14×550	W14×99
7	5.47	W18×55	W18×76	W14×342	W12×79	W14×342	W12×65
8	5.00	W18×50	W18×71	W14×342	W12×79	W14×342	W12×65
9	4.44	W18×50	W18×71	W14×342	W12×79	W14×342	W12×65
10	3.70	W18×46	W18×65	W14×176	W10×49	W14×193	W10×39
11	2.90	W18×40	W18×60	W14×176	W10×49	W14×193	W10×39
12	1.88	W18×46	W18×65	W14×176	W10×49	W14×193	W10×39

$\lambda = 2$							
Story	Plate (mm)	HBE	OB	VBE (3.2 m)	OC (3.2 m)	VBE (5.2m)	OC (5.2m)
1	6.55	W18×60	W18×106	W14×605	W14×176	W14×605	W14×132
2	6.49	W18×60	W18×106	W14×605	W14×176	W14×605	W14×132
3	6.38	W18×60	W18×106	W14×605	W14×176	W14×605	W14×132
4	6.10	W18×60	W18×106	W14×455	W14×132	W14×500	W14×109
5	5.87	W18×55	W18×106	W14×455	W14×132	W14×500	W14×109
6	5.57	W18×55	W18×106	W14×455	W14×132	W14×500	W14×109
7	5.13	W18×50	W18×97	W14×342	W14×90	W14×342	W12×72
8	4.69	W18×50	W18×97	W14×342	W14×90	W14×342	W12×72
9	4.16	W18×46	W18×86	W14×342	W14×90	W14×342	W12×72
10	3.47	W18×46	W18×86	W14×176	W10×49	W14×193	W10×45
11	2.72	W18×40	W18×76	W14×176	W10×49	W14×193	W10×45
12	1.77	W18×40	W18×76	W14×176	W10×49	W14×193	W10×45

Table 4.8 Summary of the designs for 12-story SPSW-O (PR) systems with outrigger lengths of either 3.2 m or 5.2 m

$\lambda = 0.5$							
Story	Plate (mm)	HBE	OB	VBE (3.2 m)	OC (3.2 m)	VBE (5.2m)	OC (5.2m)
1	7.57	W18×71	W16×40	W14×730	W14×159	W14×730	W14×145
2	7.51	W18×71	W16×40	W14×730	W14×159	W14×730	W14×145
3	7.37	W18×71	W16×40	W14×730	W14×159	W14×730	W14×145
4	7.00	W18×65	W16×36	W14×500	W14×120	W14×550	W14×109
5	6.73	W18×65	W16×36	W14×500	W14×120	W14×550	W14×109
6	6.39	W18×65	W16×36	W14×500	W14×120	W14×550	W14×109
7	5.86	W18×60	W16×36	W14×342	W14×90	W14×342	W12×79
8	5.36	W18×55	W16×31	W14×342	W14×90	W14×342	W12×79
9	4.75	W18×55	W16×31	W14×342	W14×90	W14×342	W12×79
10	3.95	W18×46	W16×26	W14×176	W10×60	W14×176	W10×54
11	3.10	W18×46	W16×26	W14×176	W10×60	W14×176	W10×54
12	2.02	W18×46	W16×26	W14×176	W10×60	W14×176	W10×54

$\lambda = 1.5$							
Story	Plate (mm)	HBE	OB	VBE (3.2 m)	OC (3.2 m)	VBE (5.2m)	OC (5.2m)
1	5.71	W18×55	W18×76	W14×500	W14×257	W14×550	W14×211
2	5.66	W18×55	W18×76	W14×500	W14×257	W14×550	W14×211
3	5.56	W18×55	W18×76	W14×500	W14×257	W14×550	W14×211
4	5.33	W18×50	W18×71	W14×370	W14×211	W14×398	W14×159
5	5.13	W18×50	W18×71	W14×370	W14×211	W14×398	W14×159
6	4.86	W18×50	W18×71	W14×370	W14×211	W14×398	W14×159
7	4.49	W18×46	W18×65	W14×257	W14×145	W14×283	W14×120
8	4.10	W18×46	W18×65	W14×257	W14×145	W14×283	W14×120
9	3.64	W18×40	W18×60	W14×257	W14×145	W14×283	W14×120
10	3.05	W18×40	W18×60	W14×145	W14×90	W14×145	W12×87
11	2.39	W18×35	W18×55	W14×145	W14×90	W14×145	W12×87
12	1.55	W18×40	W18×60	W14×145	W14×90	W14×145	W12×87

$\lambda = 2$							
Story	Plate (mm)	HBE	OB	VBE (3.2 m)	OC (3.2 m)	VBE (5.2m)	OC (5.2m)
1	5.17	W18×46	W18×86	W14×426	W14×283	W14×500	W14×233
2	5.12	W18×46	W18×86	W14×426	W14×283	W14×500	W14×233
3	5.03	W18×46	W18×86	W14×426	W14×283	W14×500	W14×233
4	4.85	W18×46	W18×86	W14×342	W14×233	W14×370	W14×176
5	4.66	W18×46	W18×86	W14×342	W14×233	W14×370	W14×176
6	4.46	W18×46	W18×86	W14×342	W14×233	W14×370	W14×176
7	4.08	W18×40	W18×71	W14×233	W14×159	W14×257	W14×132
8	3.73	W18×40	W18×71	W14×233	W14×159	W14×257	W14×132
9	3.31	W18×40	W18×71	W14×233	W14×159	W14×257	W14×132
10	2.78	W18×35	W18×65	W14×132	W14×99	W14×145	W14×90
11	2.18	W18×35	W18×65	W14×132	W14×99	W14×145	W14×90
12	1.42	W18×35	W18×65	W14×132	W14×99	W14×145	W14×90

Table 4.9 Summary of the designs for 12-story SPSW-O (RP) systems with outrigger lengths of either 3.2 m or 5.2 m

$\lambda = 0.5$							
Story	Plate (mm)	HBE	OB	VBE (3.2 m)	OC (3.2 m)	VBE (5.2m)	OC (5.2m)
1	6.80	W18×65	W16×36	W14×665	W14×109	W14×730	W14×99
2	6.74	W18×65	W16×36	W14×665	W14×109	W14×730	W14×99
3	6.62	W18×65	W16×36	W14×665	W14×109	W14×730	W14×99
4	6.36	W18×65	W16×36	W14×550	W12×87	W14×550	W12×79
5	6.11	W18×65	W16×36	W14×550	W12×87	W14×550	W12×79
6	5.80	W18×65	W16×36	W14×550	W12×87	W14×550	W12×79
7	5.31	W18×60	W16×36	W14×370	W10×60	W14×370	W10×54
8	4.86	W18×60	W16×36	W14×370	W10×60	W14×370	W10×54
9	4.31	W18×60	W16×36	W14×370	W10×60	W14×370	W10×54
10	3.59	W18×55	W16×31	W14×211	W10×39	W14×211	W10×33
11	2.82	W18×55	W16×31	W14×211	W10×39	W14×211	W10×33
12	1.83	W18×65	W16×36	W14×211	W10×39	W14×211	W10×33

$\lambda = 1.5$							
Story	Plate (mm)	HBE	OB	VBE (3.2 m)	OC (3.2 m)	VBE (5.2m)	OC (5.2m)
1	5.83	W18×55	W18×76	W14×605	W14×159	W14×605	W14×120
2	5.78	W18×55	W18×76	W14×605	W14×159	W14×605	W14×120
3	5.67	W18×55	W18×76	W14×605	W14×159	W14×605	W14×120
4	5.43	W18×55	W18×76	W14×455	W14×120	W14×455	W14×99
5	5.22	W18×55	W18×76	W14×455	W14×120	W14×455	W14×99
6	4.95	W18×55	W18×76	W14×455	W14×120	W14×455	W14×99
7	4.55	W18×55	W18×76	W14×311	W12×87	W14×342	W12×72
8	4.16	W18×50	W18×76	W14×311	W12×87	W14×342	W12×72
9	3.69	W18×50	W18×76	W14×311	W12×87	W14×342	W12×72
10	3.09	W18×50	W18×76	W14×193	W10×49	W14×211	W10×45
11	2.42	W18×50	W18×76	W14×193	W10×49	W14×211	W10×45
12	1.58	W18×60	W18×86	W14×193	W10×49	W14×211	W10×45

$\lambda = 2$							
Story	Plate (mm)	HBE	OB	VBE (3.2 m)	OC (3.2 m)	VBE (5.2m)	OC (5.2m)
1	5.41	W18×55	W18×97	W14×550	W14×176	W14×605	W14×132
2	5.36	W18×55	W18×97	W14×550	W14×176	W14×605	W14×132
3	5.26	W18×55	W18×97	W14×550	W14×176	W14×605	W14×132
4	5.05	W18×50	W18×97	W14×426	W14×132	W14×455	W14×109
5	4.86	W18×50	W18×97	W14×426	W14×132	W14×455	W14×109
6	4.61	W18×50	W18×97	W14×426	W14×132	W14×455	W14×109
7	4.25	W18×50	W18×97	W14×311	W14×90	W14×311	W12×72
8	3.88	W18×50	W18×97	W14×311	W14×90	W14×311	W12×72
9	3.45	W18×50	W18×97	W14×311	W14×90	W14×311	W12×72
10	2.89	W18×46	W18×86	W14×211	W10×54	W14×211	W10×45
11	2.26	W18×46	W18×86	W14×211	W10×54	W14×211	W10×45
12	1.47	W18×55	W18×97	W14×211	W10×54	W14×211	W10×45

Table 4.10 Summary of the designs for 12-story SPSW-O (RR) systems with outrigger lengths of either 3.2 m or 5.2 m

$\lambda = 0.5$							
Story	Plate (mm)	HBE	OB	VBE (3.2 m)	OC (3.2 m)	VBE (5.2m)	OC (5.2m)
1	6.24	W18×60	W16×36	W14×605	W14×159	W14×665	W14×132
2	6.18	W18×60	W16×36	W14×605	W14×159	W14×665	W14×132
3	6.07	W18×60	W16×36	W14×605	W14×159	W14×665	W14×132
4	5.84	W18×60	W16×36	W14×500	W14×120	W14×500	W14×109
5	5.61	W18×60	W16×36	W14×500	W14×120	W14×500	W14×109
6	5.33	W18×60	W16×36	W14×500	W14×120	W14×500	W14×109
7	4.89	W18×55	W16×31	W14×342	W14×90	W14×342	W12×79
8	4.47	W18×55	W16×31	W14×342	W14×90	W14×342	W12×79
9	3.96	W18×55	W16×31	W14×342	W14×90	W14×342	W12×79
10	3.30	W18×50	W16×31	W14×176	W10×60	W14×176	W10×54
11	2.59	W18×50	W16×31	W14×176	W10×60	W14×176	W10×54
12	1.68	W18×65	W16×36	W14×176	W10×60	W14×176	W10×54

$\lambda = 1.5$							
Story	Plate (mm)	HBE	OB	VBE (3.2 m)	OC (3.2 m)	VBE (5.2m)	OC (5.2m)
1	4.77	W18×50	W18×71	W14×455	W14×257	W14×500	W14×193
2	4.73	W18×50	W18×71	W14×455	W14×257	W14×500	W14×193
3	4.64	W18×50	W18×71	W14×455	W14×257	W14×500	W14×193
4	4.46	W18×46	W18×65	W14×342	W14×193	W14×370	W14×159
5	4.29	W18×46	W18×65	W14×342	W14×193	W14×370	W14×159
6	4.07	W18×46	W18×65	W14×342	W14×193	W14×370	W14×159
7	3.75	W18×46	W18×65	W14×233	W14×145	W14×257	W14×120
8	3.43	W18×46	W18×65	W14×233	W14×145	W14×257	W14×120
9	3.04	W18×40	W18×60	W14×233	W14×145	W14×257	W14×120
10	2.56	W18×40	W18×60	W14×145	W14×90	W14×159	W12×87
11	2.00	W18×40	W18×60	W14×145	W14×90	W14×159	W12×87
12	1.30	W18×50	W18×76	W14×145	W14×90	W14×159	W12×87

$\lambda = 2$							
Story	Plate (mm)	HBE	OB	VBE (3.2 m)	OC (3.2 m)	VBE (5.2m)	OC (5.2m)
1	4.24	W18×46	W18×86	W14×370	W14×283	W14×426	W14×233
2	4.20	W18×46	W18×86	W14×370	W14×283	W14×426	W14×233
3	4.13	W18×46	W18×86	W14×370	W14×283	W14×426	W14×233
4	3.99	W18×40	W18×76	W14×311	W14×233	W14×342	W14×176
5	3.83	W18×40	W18×76	W14×311	W14×233	W14×342	W14×176
6	3.64	W18×40	W18×76	W14×311	W14×233	W14×342	W14×176
7	3.36	W18×40	W18×76	W14×211	W14×159	W14×233	W14×132
8	3.07	W18×40	W18×71	W14×211	W14×159	W14×233	W14×132
9	2.72	W18×40	W18×71	W14×211	W14×159	W14×233	W14×132
10	2.29	W18×40	W18×71	W14×145	W14×109	W14×159	W14×90
11	1.80	W18×35	W18×65	W14×145	W14×109	W14×159	W14×90
12	1.17	W18×46	W18×86	W14×145	W14×109	W14×159	W14×90

Table 4.11 Estimated outrigger efficiency factors for 8-Story SPSW-O systems

	SPSW-O (PP)		SPSW-O (PR)		SPSW-O (RP)		SPSW-O (RR)	
λ	3.2 m	5.2 m	3.2 m	5.2 m	3.2 m	5.2 m	3.2 m	5.2 m
0.5	0.13	0.10	0.23	0.19	0.13	0.11	0.24	0.20
1	0.23	0.19	0.41	0.33	0.24	0.20	0.40	0.33
1.5	0.32	0.26	0.53	0.43	0.33	0.27	0.54	0.44
2	0.40	0.33	0.63	0.51	0.40	0.33	0.66	0.54

Table 4.12 Estimated outrigger efficiency factors for 12-Story SPSW-O systems

	SPSW-O (PP)		SPSW-O (PR)		SPSW-O (RP)		SPSW-O (PP)	
λ	3.2 m	5.2 m	3.2 m	5.2 m	3.2 m	5.2 m	3.2 m	5.2 m
0.5	0.13	0.11	0.24	0.19	0.12	0.10	0.23	0.19
1	0.23	0.19	0.41	0.33	0.23	0.19	0.41	0.33
1.5	0.33	0.27	0.55	0.45	0.32	0.26	0.54	0.44
2	0.40	0.33	0.65	0.53	0.41	0.33	0.66	0.54

Table 4.13 Estimated system overstrength for 8-story SPSW-O systems

	SPSW-O (RR)		SPSW-O (RP)		SPSW-O (PR)		SPSW-O (PP)	
λ	3.2 m	5.2 m	3.2 m	5.2 m	3.2 m	5.2 m	3.2 m	5.2 m
0.5	1.08	1.08	1.09	1.09	1.10	1.10	1.11	1.11
1	1.07	1.07	1.08	1.08	1.08	1.08	1.10	1.10
1.5	1.06	1.06	1.07	1.07	1.07	1.07	1.09	1.09
2	1.05	1.05	1.07	1.07	1.06	1.06	1.08	1.08

Table 4.14 Estimated system overstrength for 12-story SPSW-O systems

	SPSW-O (RR)		SPSW-O (RP)		SPSW-O (PR)		SPSW-O (PP)	
λ	3.2 m	5.2 m	3.2 m	5.2 m	3.2 m	5.2 m	3.2 m	5.2 m
0.5	1.09	1.09	1.10	0.11	1.11	1.11	1.12	1.12
1	1.08	1.08	1.09	1.09	1.09	1.09	1.11	1.11
1.5	1.07	1.07	1.08	1.08	1.08	1.08	1.10	1.10
2	1.06	1.06	1.08	1.08	1.07	1.07	1.10	1.10

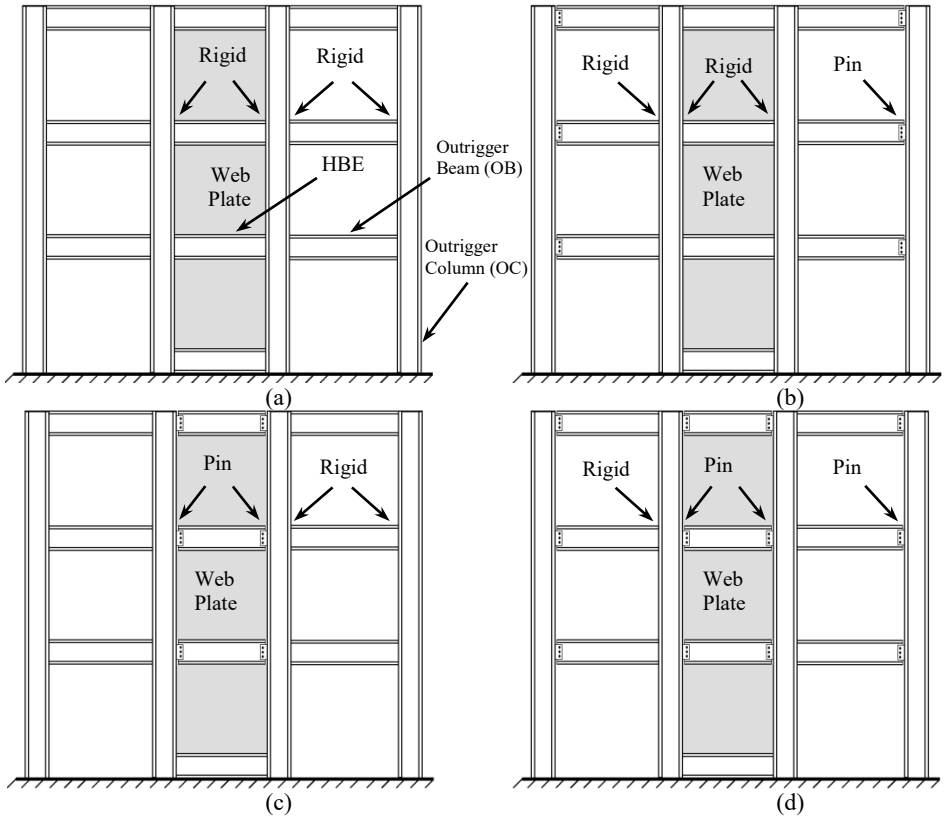

Figure 4.1 Schematic representation of different SPSW-O options: (a) SPSW-O (RR); (b) SPSW-O (RP); (c) SPSW-O (PR); and (d) SPSW-O (PP).
(Note: the first and second terms in the parentheses represent the type of HBE-to-VBE and OB-to-OC connections, respectively. R: rigid; P: pinned)

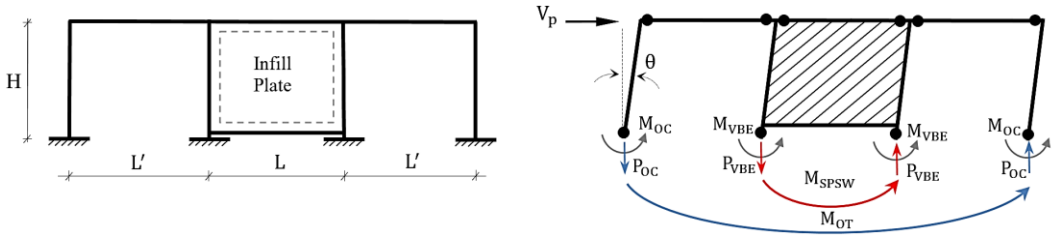

Figure 4.2 Single-story SPSW-O (RR) and the desirable plastic mechanism of the system

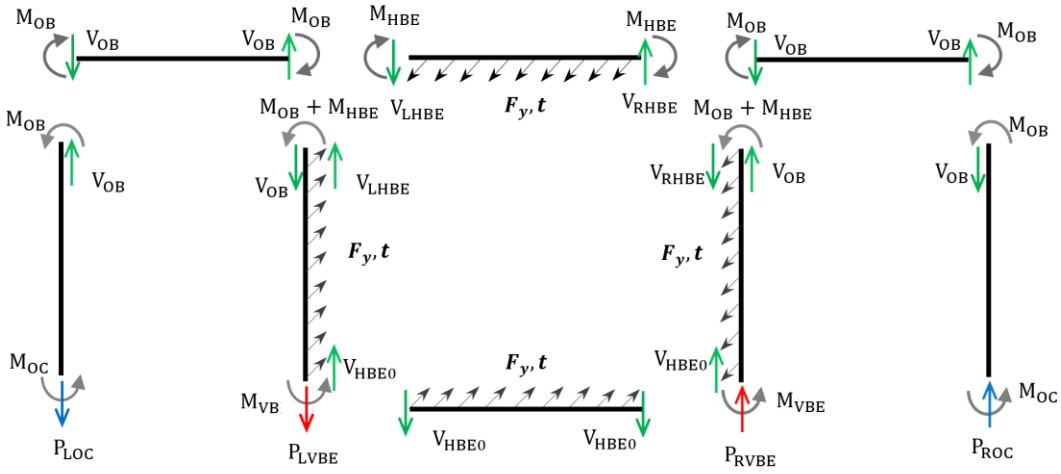

Figure 4.3 Free body diagram of single-story SPSW-O (RR) under assumed plastic mechanism (horizontal forces not shown)

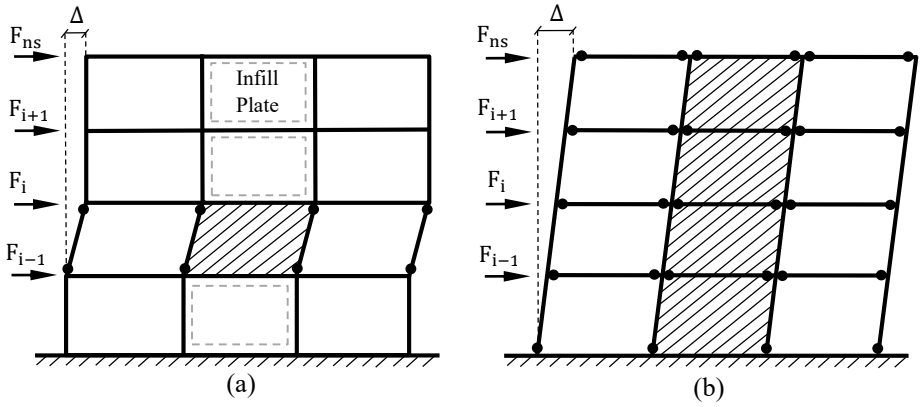

Figure 4.4 Plastic collapse mechanisms of typical multi-story SPSW-O (RR): (a) soft-story mechanism; (b) desirable uniform collapse mechanism.

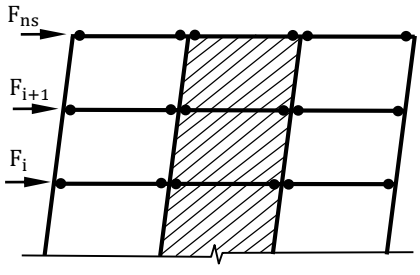

Figure 4.5 SPSW-O (RR) sub-frame

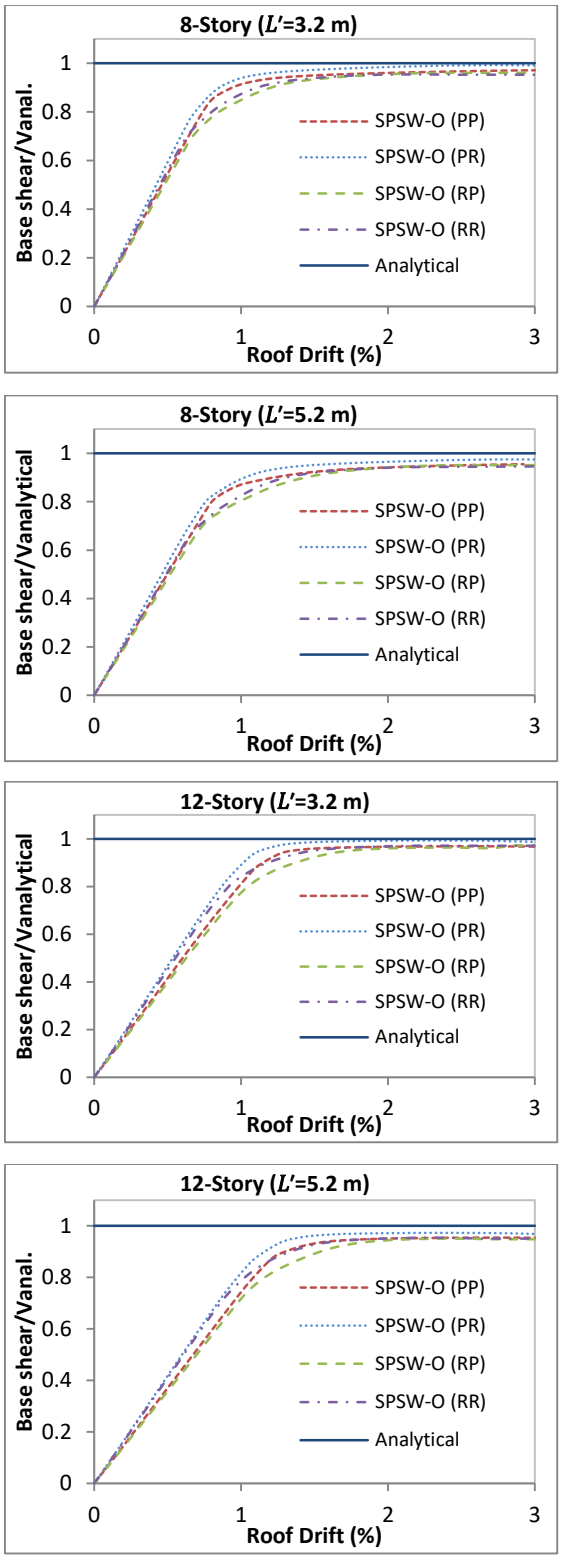

Figure 4.6 Comparison of lateral strength obtained using analytical and numerical methods

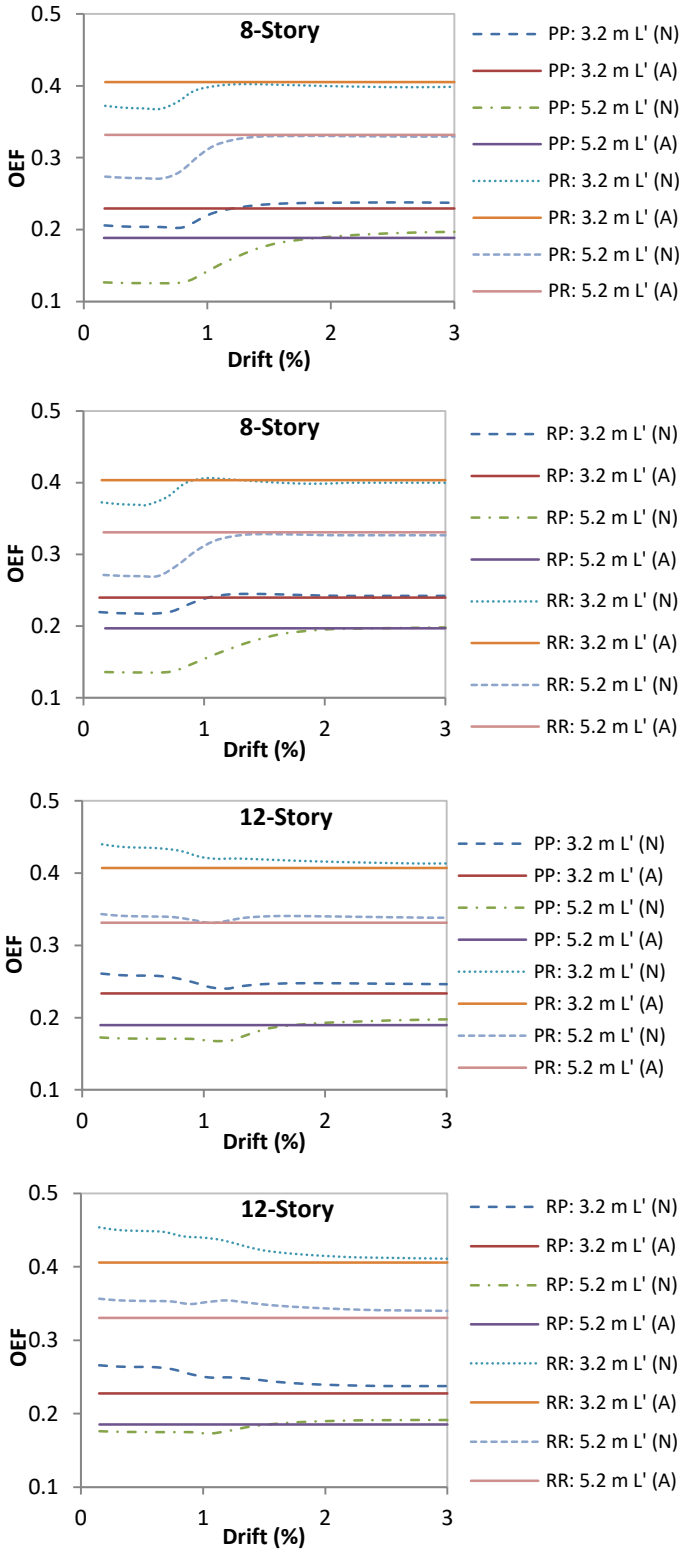

Figure 4.7 Comparison of OEF obtained using analytical and numerical methods (N: numerical; A: Analytical)

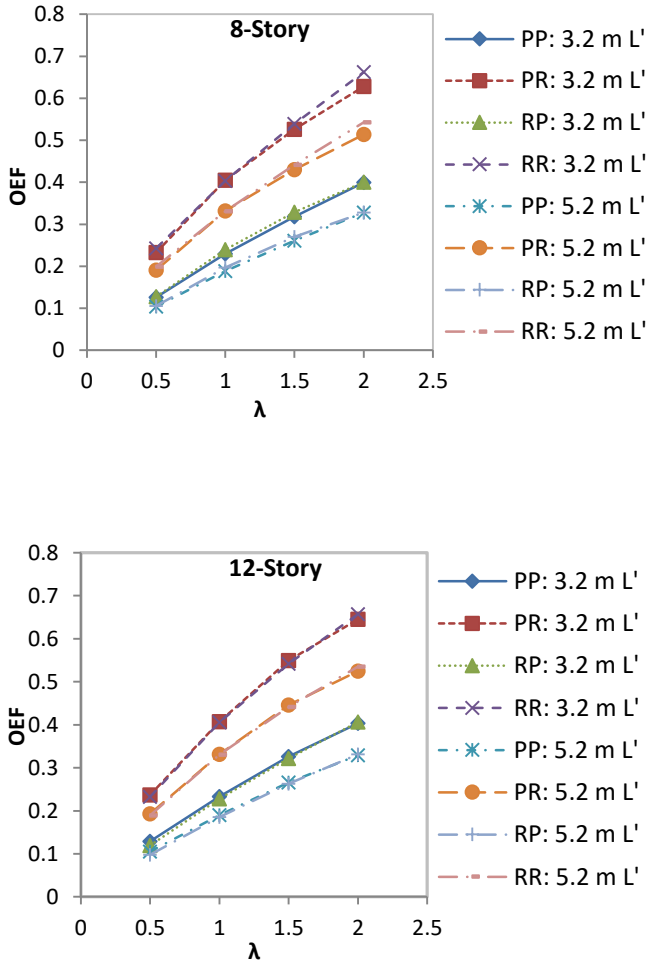

Figure 4.8 Variation of OEF for various levels of outrigger beams strength

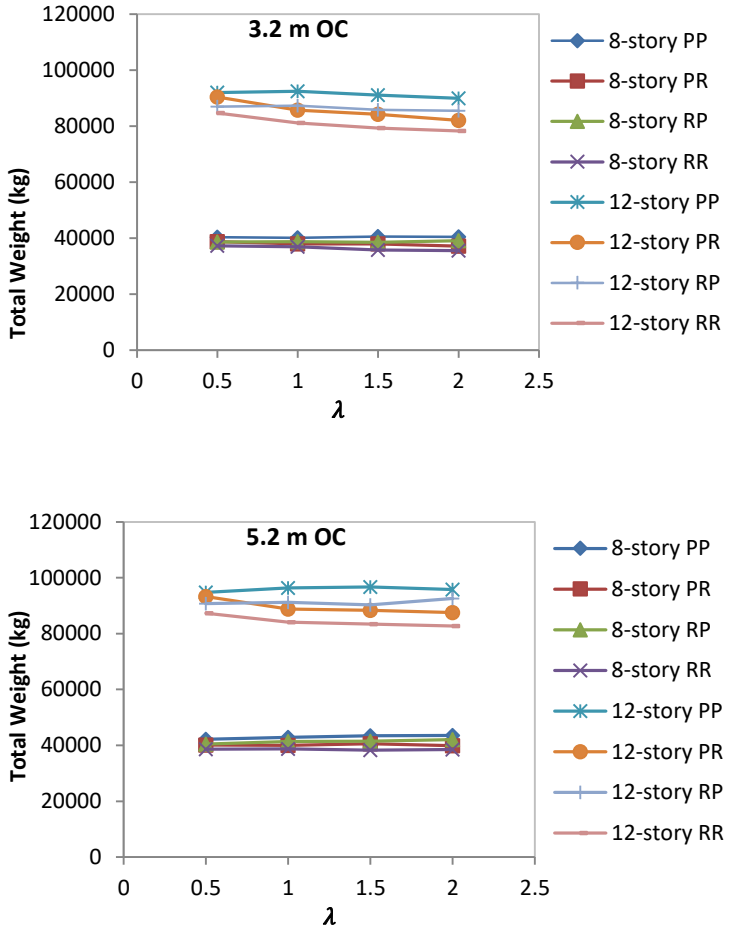

Figure 4.9 Variation of the system weight for different outrigger beam strength levels

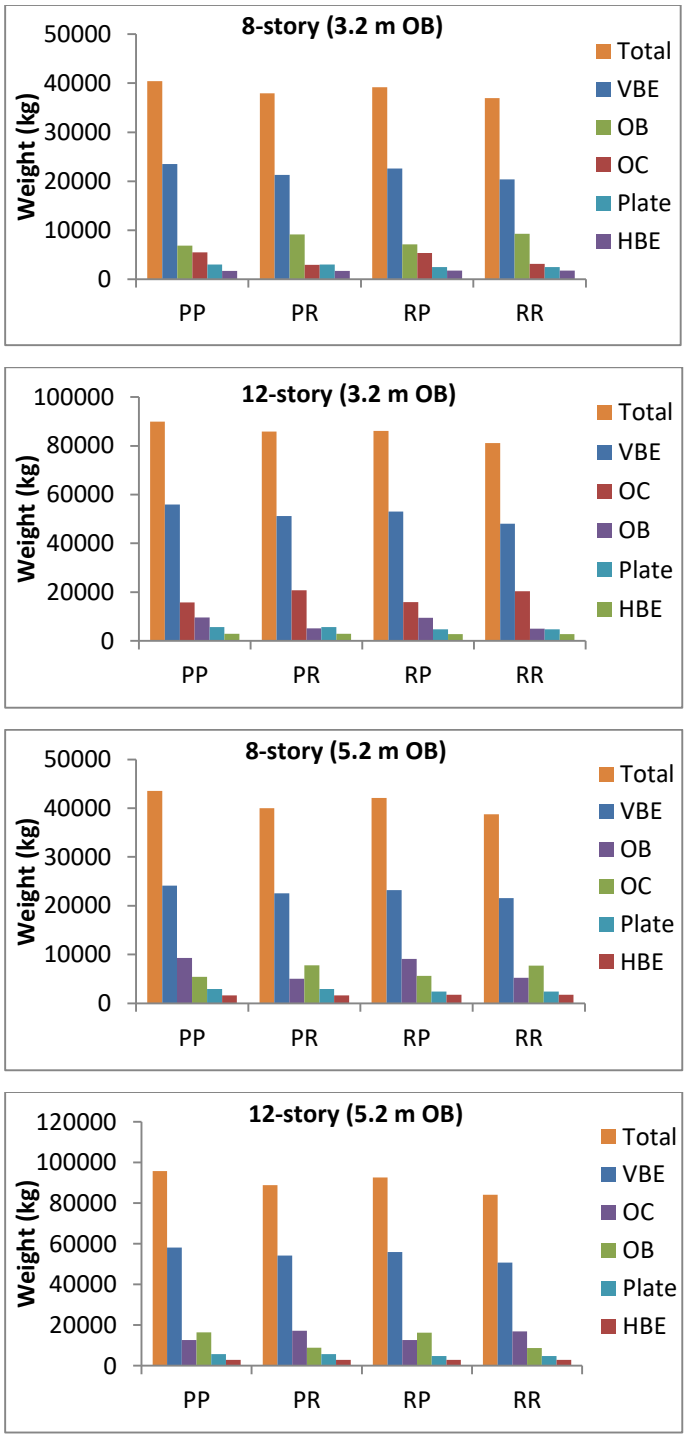

Figure 4.10 Comparison of steel weight for different elements of the systems

4.7 References

AISC. (2010). Seismic Provisions for structural steel buildings. American Institute of Steel Construction, Chicago.

ASCE. (2010) Minimum design loads for buildings and other structures. ASCE/SEI 7-10. American Society of Civil Engineers.

Berman, J.W., and Bruneau, M. (2003). Plastic analysis and design of steel plate shear walls. Journal of Structural Engineering, 129(11), 1448–1456.

Berman, J., Lowes, L.N., Okazaki, T., Bruneau, M., Tsai, K-C., Driver, R.G., and Sabelli, R. (2008). Research needs and future directions for steel plate shear walls. ASCE Structures Congress: Crossing Borders.

Bruneau, M., Uang, C.M., and Sabelli, R. (2011). Ductile design of steel structures. Second Edition, Mc Graw Hill.

Bhowmick, A.K., Grondin, G.Y., and Driver, R.G. (2011). Estimating fundamental periods of steel plate shear walls, Engineering Structures, Vol. 33, pp. 1883-1893.

Canadian Standards Association, (2014), Design of steel structures, CAN/CSA S16-14.

Chao, S.H., Goel, S.C., and Lee, S.S. (2007). A seismic design lateral force distribution based on inelastic state of structures. Earthquake Spectra, Vol. 23, pp. 547-569.

Driver, R.G., Kulak, G.L., Elwi, A.E. and Kennedy, D.J.L. (1998). FE and simplified models of steel plate shear walls. Journal of Structural Engineering, 124 (2), 121-130

Driver, R.G., Kulak, G.L., Kennedy, D.J.L., and Elwi, A.E. (1997). Seismic behavior of steel plate shear walls. Structural Engineering Rep. 215, Deptartment of Civil Engineering, University of Alberta, Edmonton, Alberta, Canada.

Elgaaly, M. (1998). Thin steel plate shear walls behavior and analysis. Thin-Walled Structures, 32(1–3), 151–180.

Gholipour, M., Asadi, E., and Alinia, M.M. (2015). The use of outrigger system in steel plate shear wall structures. Advances in Structural Engineering Vol. 18 No. 6: 853-872

Goel, S.C., and Chao, S.H. (2008). Performance-based plastic design: earthquake resistant steel structures. International Code Council.

Gupta, A., and Krawinkler, H. (1999). Seismic demands for performance evaluation of steel moment-resisting frame structures. Report no. 132. John A. Blume earthquake engineering center. Stanford University.

Kurban, C.O., and Topkaya, C. (2009). A numerical study on response modification, overstrength, and displacement amplification factors for steel plate shear wall systems. Earthquake Engineering and Structural Dynamics, 38: 497-516.

Safari Gorji, M., and Cheng, J.J.R. (2015). Improving overturning stiffness of steel plate shear walls, Proc., Structures Congress, Structural Engineering Institute, ASCE, Portland.

SAP2000 Version 14.2. Computer and Structures, Berkeley, CA.

Timler, P.A., and Kulak, G.L. (1983). Experimental study of steel plate shear walls. Structural Engineering Rep., No. 114, Department of Civil Engineering, University of Alberta, Edmonton, AB, Canada.

Taranath, B.S. (2012). Structural analysis and design of tall buildings; steel and composite construction. International Code Council. CRC Press, Taylor & Francis Group.

5. SEISMIC DESIGN AND PERFORMANCE OF STEEL PLATE SHEAR WALLS WITH OUTRIGGERS[2]

5.1 Introduction

In the previous chapter, analytical studies were performed to investigate the behaviour and efficiency of SPSW-Os, focusing on system configurations, plastic mechanisms, plastic strength and overturning stiffness. An attempt was made to quantify the level of interaction between the SPSW and its outrigger system by defining a simple metric indicating the contribution of the outrigger elements to the overall overturning stiffness of the SPSW-O system. Some valuable knowledge covering a relatively wide range of parameters influencing the behaviour and efficiency of such systems was thus generated; this was useful in the development of the proposed design procedure that is presented in this chapter. As demonstrated in the analytical expressions presented in Chapter 4, the lateral load resistance of a SPSW-O system is provided by three components, namely: (1) the tension field action of the infill panel; (2) the moment-resisting action of the boundary frame; and (3) the moment-resisting action of the outrigger frames. It is recalled that the boundary frame in a SPSW-O with ideal pinned HBE-to-VBE connections (i.e., SPSW-O (PR) and SPSW-O (PP)) obviously does not contribute to the lateral load resistance of the system. In this chapter, analytical studies are extended to quantify the relative contributions of these components to the overall strength of the four SPSW-O options introduced in Chapter 4, with the primary aim of achieving efficient designs for such systems. Procedures developed for the seismic design of the SPSW-O systems are described; numerical studies of several prototype designs verifying the effectiveness of the proposed design approach are then presented.

---

[2] A version of this chapter has been submitted for publication in the *Journal of Constructional Steel Research*, Elsevier.

5.2 Optimum Design for Lateral Load Resistance

In the conventional design of SPSWs in North America (AISC 2010; CSA-S16 2014), the infill plate at every story is designed to resist 100% of the factored story shear force; hence, the lateral strength of the boundary moment frame, which substantially contributes to the overall lateral load resistance, is neglected. Qu and Bruneau (2009) investigated the relative and respective contributions of these components to the overall strength of the conventional SPSW and showed that the overstrength provided by the boundary frame moment-resisting action can be significant. As discussed in Chapter 4, the outrigger frames within a SPSW-O adds even more strength to the system, especially in cases where the outrigger beams are moment-connected at both ends (i.e., SPSW-O (RR) and SPSW-O (PR) systems). Hence, it would be overly conservative to neglect the lateral load resistance provided by the outrigger system, as well as by the boundary frame, and to design the infill plates for the full lateral design loads. Therefore, in order to achieve material efficient designs for each of the four SPSW-O options discussed in this research, procedures are needed to quantify the contribution of each component (i.e., the tension field action and frame moment-resisting action) to the overall lateral load resistance of the systems. Such procedures are studied in the following sections by employing the principles of plastic analysis and capacity design. Both single-story and multi-story systems are considered for this purpose. Based on this study, a design procedure is developed for the SPSW-O systems by extending the conventional capacity design procedures used for SPSWs, while minimizing the overstrength of the system.

5.2.1 Single-Story SPSW-O Systems

To better understand the concepts and procedures presented in this section, the expressions are first developed for the case of a single-story SPSW-O, and are then extended to the more complex case of a multi-story system in the next section. The principles of plastic analysis and capacity design are employed to investigate the relative contributions of the tension field action and frame moment-resisting action

to the global lateral strength of the four different SPSW-O options discussed in this research. Moreover, procedures are developed to achieve an efficient design approach for each of these options by minimizing their structural overstrength.

5.2.1.1. **Single-Story SPSW-O (RR) Systems**

The single-story SPSW-O with rigid HBE-to-VBE and OB-to-OC connections, shown in Figure 5.1, is assumed to be pinned to the ground. This simplifying assumption is made to reduce the complexity of the expressions developed next. Since the plastic strength of the VBE bases are greatly reduced due to the presence of significant axial loads in these elements, they contribute very little to the global strength of multi-story SPSW-O systems with a high degree of redundancy. On the other hand, since the SPSW-O configuration is intended to improve the flexural stiffness of the system primarily through the couple formed by the axial forces of the outrigger columns, these elements can be connected to the ground using pinned connections.

In order to design the infill panel within the SPSW-O system shown in Figure 5.1a, it is assumed that a fraction of the total lateral design load ($\kappa_{RR}F_D$) is resisted by this element through the formation of tension field. Considering the plastic mechanism shown in Figure 1.c, this portion of the design load is resisted by the horizontal component of the tension field in the fully yielded infill panel. Note that the flexural rigidities of the OB-to-OC, OB-to-HBE and HBE-to-VBE connections in frame (5.1b) are removed; therefore, the required thickness of the infill panel can be calculated using Eq. (5.1) (Qu and Bruneau 2009):

$$\kappa_{RR}F_D = \frac{1}{2}F_y L t \sin 2\alpha \qquad (5.1)$$

where t and F_y are the thickness and yield strength of the infill panels, respectively; L is the SPSW bay width and α is the tension field inclination angle estimated using the following equation (Timler and Kulak 1983):

$$\tan^4(\alpha) = \frac{1 + \frac{tL}{2A_c}}{1 + \text{ th } \left(\frac{1}{A_b} + \frac{h^3}{360I_cL}\right)} \tag{5.2}$$

where A_b and A_c are the cross-sectional areas of the HBE and VBE, respectively; h is the story height, and I_c is the moment of inertia of the VBE.

The vertical and horizontal components of the distributed force along the HBE due to the yielding of the infill panel are given by Eqs. (5.3) and (5.4), respectively, and are related to each other through Eq. (5.5) (Bruneau et al. 2011):

$$\omega_v = F_y t \cos^2\alpha \tag{5.3}$$

$$\omega_h = \frac{1}{2} F_y t \sin 2\alpha \tag{5.4}$$

$$\omega_v = \omega_h \cot\alpha \tag{5.5}$$

Substituting Eq. (5.4) into Eq. (5.1) results in the following:

$$\kappa_{RR} F_D = \omega_h L \tag{5.6}$$

On the other hand, equating internal and external work and assuming the desirable yield mechanism shown in Figure 5.1c, the plastic lateral strength of the system can be expressed as:

$$F_p H = \omega_h LH + 2M_{HBE} + 4M_{OB} \tag{5.7}$$

where M_{OB} and M_{HBE} are the plastic flexural strengths of the outrigger beams and HBEs, respectively. For preliminary design purposes, it is assumed that the outrigger beams are proportioned based on the size of HBE, and the parameter λ is defined as follows:

$$\lambda = \frac{Z_{OB}}{Z_{HBE}} = \frac{M_{OB}}{M_{HBE}} \tag{5.8}$$

where Z_{OB} and Z_{HBE} are the plastic section moduli of the outrigger beams and HBEs, respectively. Substituting λ in Eq. (5.7), the expression for the plastic strength of the system takes the following format:

$$F_p H = \omega_h L H + 2M_{HBE}(1 + 2\lambda) \tag{5.9}$$

On the other hand, as discussed by Vian and Bruneau (2005), in order to prevent in-span plastic hinging of the HBEs, which results in an undesirable plastic mechanism, these elements should be designed to resist the flexural demand given by Eq. (5.10).

$$M_{HBE} = \frac{1}{4}\omega_v L^2 \times \frac{\eta}{1 + \sqrt{1 - \eta^2}} \tag{5.10}$$

In this equation, η is the plastic section modulus reduction ratio in cases where reduced-beam section (RBS) HBE-to-VBE connections are used, and is defined as:

$$\eta = \frac{Z_{RBS}}{Z} \tag{5.11}$$

where Z_{RBS} and Z are the plastic section moduli of the reduced section and the full section, respectively. Substituting Eq. (5.10) into Eq. (5.9), the plastic strength of the system is given by:

$$F_p = \omega_h L + \frac{\omega_v L^2}{2H}(1 + 2\lambda)\frac{\eta}{1 + \sqrt{1 - \eta^2}} \tag{5.12}$$

Considering the relationship between horizontal and vertical components of the tension field given by Eq. (5.5), the ultimate strength of the system can be rewritten as:

$$F_p = \omega_h L[1 + \frac{(1 + 2\lambda)}{2}\frac{L}{H}\cot\alpha \times \frac{\eta}{1 + \sqrt{1 - \eta^2}}] \tag{5.13}$$

Substituting Eq. (5.5) into Eq. (5.13), the expression for the plastic strength takes the following format:

$$F_p = \kappa_{RR} F_D[1 + \frac{(1 + 2\lambda)}{2}\frac{L}{H}\cot\alpha \times \frac{\eta}{1 + \sqrt{1 - \eta^2}}] \tag{5.14}$$

The overstrength of the SPSW-O (RR) system (Ω_{RR}) is calculated as the ratio of the ultimate strength of the system (F_p) to the design lateral load (F_D):

$$\Omega_{RR} = \frac{F_P}{F_D} \tag{5.15}$$

Substituting Eq. (5.14) into Eq. (5.15) yields the expression for the overstrength of the single-story SPSW-O (RR) system.

$$\Omega_{RR} = \kappa_{RR}[1 + \frac{(1+2\lambda)}{2}\frac{L}{H}\cot\alpha \times \frac{\eta}{1+\sqrt{1-\eta^2}}] \tag{5.16}$$

As described by Qu and Bruneau (2009), an optimum design for lateral load resistance is achieved by setting the overstrength of the system equal to unity. Solving for κ_{RR}, an equation is derived indicating the percentage of the design lateral load that should be assigned to the infill panel to achieve the optimum design of a single-story SPSW-O (RR) system, given by:

$$\kappa_{optimum(RR)} = [1 + \frac{(1+2\lambda)}{2}\frac{L}{H}\cot\alpha \times \frac{\eta}{1+\sqrt{1-\eta^2}}]^{-1} \tag{5.17}$$

5.2.1.2. **Single-Story SPSW-O (RP) Systems**

In the case of SPSW-O (RP) systems, since the outrigger beams are pin-connected to the outrigger columns, the outrigger system provides less strength to the system compared to that in the SPSW-O (RR) configuration; therefore, a larger portion of the lateral load is carried by the infill panel. In this case, using the same procedure, the expression of the $\kappa_{optimum}$ takes the following format:

$$\kappa_{optimum(RP)} = [1 + \frac{(1+\lambda)}{2}\frac{L}{H}\cot\alpha \times \frac{\eta}{1+\sqrt{1-\eta^2}}]^{-1} \tag{5.18}$$

Note that for a typical SPSW-O system, $\kappa_{optimum}$ is a function of a series of parameters, including the relative flexural strength of outrigger beams and HBEs, the infill panel aspect ratio, reduced beam section properties, the type of OB-to-OC and HBE-to-VBE connections, and the angle of the tension field in the fully yielded infill panel.

5.2.1.3. **Single-Story SPSW-O (PR) Systems**

In the case of SPSW-O (PR) systems, simple HBE-to-VBE connections are used (Figure 5.2a); therefore, the lateral load resistance is essentially provided by the tension field action and the moment-resisting action of the OB-to-VBE and OB-to-OC connections. Assuming the plastic mechanism shown in Figure 5.2c, the following equation can be written for the lateral load resistance by equating the internal and external work in the system:

$$F_p H = \omega_h L H + 4M_{OB} \tag{5.20}$$

As assumed in the previous section, the outrigger beams are proportioned based on the size of HBEs. Since the HBEs are pin-connected to the VBEs within the SPSW-O (PR) system, they act as simply supported beams. Thus, they should be designed for the flexural demands resulting from the vertical component of the tension field given by:

$$M_{HBE} = \frac{1}{8}\omega_v L^2 \tag{5.21}$$

Substituting Eqs. (5.8) and (5.21) into Eq. (5.20), and following the same approach used in previous section, the expression of $\kappa_{optimum}$ for the SPSW-O (PR) system takes the following format:

$$\kappa_{optimum(PR)} = [1 + \frac{\lambda}{2}\frac{L}{H}\cot\alpha]^{-1} \tag{5.22}$$

5.2.1.4. **Single-Story SPSW-O (PP) Systems**

In the case of SPSW-O (PP) systems, both the HBE-to-VBE and OB-to-OC connections are pinned and hence do not contribute to the lateral load resistance. Therefore, the following equation can be obtained for the strength of the system:

$$F_p H = \omega_h L H + 2M_{OB} \tag{5.23}$$

The lateral design load in this case is resisted through the tension field action of the infill plate and moment-resisting action of the OB-to-VBE connections. Following

the procedure used in prior sections, the expression of $\kappa_{optimum}$ for the SPSW-O (PP) system can be obtained as follows:

$$\kappa_{optimum\ (PP)} = [1 + \frac{\lambda}{4}\frac{L}{H}\cot\alpha]^{-1} \tag{5.24}$$

Figure 5.3 shows the variation of $\kappa_{optimum}$ for different SPSW-O options, assuming various values of λ and typical range of infill panel aspect ratios. Note that a constant value of 45° was assumed for the tension field angle in all cases. As expected, assuming the same λ in all systems, the largest and smallest percentages of the design lateral loads are assigned to the infill plates in the PP and RR systems, respectively, indicating that the frame actions within these systems provide the least and the greatest relative contributions to the overall strength.

Note that $\kappa_{optimum}$ is inversely correlated to λ and to the infill panel aspect ratio in all cases. Also, $\lambda = 0$ theoretically indicates that the adjacent frames provide no strength and overturning resistance to the system; this is the case when both OB-to-VBE and OB-to-OC connections are pinned, resulting in a free-standing SPSW system.

5.2.2 Multi-Story SPSW-O Systems

In this section, the expressions derived for the optimum design of the single-story SPSW-Os are extended to more complex cases involving multi-story systems. The detailed derivations for the design of multi-story SPSW-O (RR) systems are presented, and the corresponding expressions for three other options are briefly discussed. Figure 5.4a illustrates a multi-story SPSW-O (RR) system subjected to design lateral loads. In order to design the infill panels, it is assumed that a portion of the design lateral loads at each story level ($\kappa_i F_{Di}$) is assigned to frame b, in which the flexural rigidities of moment connections are removed; therefore, these modified lateral loads are only resisted by the infill plates within this frame (Figure 5.4b). As such, the modified lateral design force applied at the floor level (i) is equal to the resultant of horizontal components of tension field forces acting at the top

and bottom of HBE (i) (Figure 5.5), as given in the following equation (Qu and Bruneau 2009):

$$(\omega_{h(i)} - \omega_{h(i+1)})L = \kappa_{RRi} F_{Di} \tag{5.25}$$

Considering an intermediate floor of the system in the uniform sway plastic mechanism condition (Figure 5.6), the equation of virtual work tributary to this floor can be written as:

$$F_{Pi} h_i = (\omega_{h(i)} - \omega_{h(i+1)})Lh_i + 4M_{OBi} + 2M_{HBEi} \tag{5.26}$$

As previously defined for the single-story systems, parameter λ_i, corresponding to story level (i) in a multi-story SPSW-O, is given by:

$$\lambda_i = \frac{M_{OBi}}{M_{HBEi}} \tag{5.27}$$

Substituting λ_i into Eq. (5.26) results in following equation:

$$F_i h_i = (\omega_{h(i)} - \omega_{h(i+1)})Lh_i + 2M_{HBEi}(1 + 2\lambda_i) \tag{5.28}$$

Considering Eq. (5.10), in order to prevent the formation of in-span plastic hinges in HBEs, these elements are required to have flexural strength given by Eq. (5.29) (Bruneau et al. 2011).

$$M_{HBEi} = \frac{1}{4}(\omega_{v(i)} - \omega_{v(i+1)})L^2 \times \frac{\eta}{1 + \sqrt{1 - \eta^2}} \tag{5.29}$$

Substituting Eq. (5.29) into Eq. (5.28) and solving for F_{Pi} results in the following expression:

$$F_{Pi} = \kappa_{RRi} F_{Di} \left[1 + \frac{(1 + 2\lambda_i)}{2} \frac{L}{h_i} \cot \alpha_i \times \frac{\eta}{1 + \sqrt{1 - \eta^2}}\right] \tag{5.30}$$

The optimum design of the system is achieved by setting $F_{Pi} = F_{Di}$; therefore, the corresponding expression of the optimum design case for the SPSW-O (RR) system ($\kappa_{optimum(RR)i}$) is obtained as:

$$\kappa_{optimum(RR)i} = \left[1 + \frac{(1 + 2\lambda_i)}{2} \frac{L}{h_i} \cot \alpha_i \times \frac{\eta}{1 + \sqrt{1 - \eta^2}}\right]^{-1} \tag{5.31}$$

Following the same approach and considering the equations derived for the single-story SPSW-O systems in previous sections, the expressions of $\kappa_{optimum(i)}$ for the multi-story SPSW-O (RP), SPSW-O (PR) and SPSW-O (PP) systems are given by Eqs. (5.32), (5.33) and (5.34), respectively.

$$\kappa_{optimum(RP)i} = [1 + \frac{(1+\lambda_i)}{2}\frac{L}{h_i}\cot\alpha_i \times \frac{\eta}{1+\sqrt{1-\eta^2}}]^{-1} \quad (5.32)$$

$$\kappa_{optimum(PR)i} = [1 + \frac{\lambda_i}{2}\frac{L}{h_i}\cot\alpha_i]^{-1} \quad (5.33)$$

$$\kappa_{optimum(PP)i} = [1 + \frac{\lambda_i}{4}\frac{L}{h_i}\cot\alpha_i]^{-1} \quad (5.34)$$

Note that since reduced beam section HBE-to-VBE connections are not feasible for the SPSW-O (PR) and SPSW-O (PP) options, the term η does not appear in the expressions of the $\kappa_{optimum(i)}$ for such systems. In the derivations above, it was assumed that the outrigger beams are employed in all floor levels. However, if the designer decides to use the moment-connected outrigger beams only in particular floor levels, for example in every other story, then the percentage of design lateral load assigned to the infill plate in stories without outriggers is calculated by setting $\lambda_i = 0$ in Equations 5.31-5.34.

Figure 5.7 shows a comparison of design story shears assigned to the infill panels in different SPSW-O options, according to the optimum design expressions derived in this section. Four-story SPSW-O systems were considered, with infill panel aspect ratio of L/H=1 in all cases. To demonstrate the impact of outrigger beams' strength on the relative contributions of the infill plates to the lateral load resistance, two values, 1.5 and 0.5, were considered for λ. An inverted triangular lateral load distribution pattern was assumed for all cases. Note that a constant tension field inclination angel of $\alpha = 45^{\circ}$ was assumed for the infill plates at all stories. It is clear that the infill panels within the SPSW-O (PP) and SPSW-O (RR) options provide the largest and smallest contributions, respectively, to the lateral force resistance of the systems. The relative flexural strength of the HBEs and OBs

also has a considerable impact on the story shear assigned to the infill plates. For each SPSW-O option, once the modified story shear associated with the optimum design case is determined, the infill plates can be sized using Eq. (5.1).

5.3 Design of SPSW Boundary Frame and Outrigger Elements

Once the infill plates are sized using the modified design loads corresponding to the optimum design cases presented in the previous section, the boundary frame elements of the SPSW can be proportioned according to the capacity design principles assuming uniform plastic mechanism shown in Figure 5.4c. The capacity design procedures outlined in current codes for conventional SPSWs are extended herein to include the SPSW-O systems under consideration. According to the North American steel design codes, HBEs within SPSWs must be designed to withstand tension field forces of the fully yielded infill plates, while allowing for the development of plastic hinges only at their ends. This requirement remains valid for HBEs within SPSW-O systems with rigid HBE-to-VBE connections (i.e., RR and RP systems). As mentioned earlier, in order to prevent the formation of in-span plastic hinges along HBEs within the SPSW-O (RR) and SPSW-O (RP) systems, these elements should be proportioned to resist a flexural demand given by $\frac{1}{4}\omega_v L^2$ (Vian and Bruneau 2005) (ω_v represents the resultant vertical component of the tension field acting above and below a given HBE). However, since HBEs within the SPSW-O options with simple HBE-to-VBE connections (i.e., PR and PP) act as simply supported beams, they are required to resist only half of this flexural demand (i.e., $\frac{1}{8}\omega_v L^2$).

In SPSW-O (RR) and SPSW-O (RP) systems, assuming that the uniform sway plastic mechanism is formed, the shear forces resulting from the formation of plastic hinges at the ends of the HBEs and OBs act in opposite directions. As discussed in Chapter 4, while the shear forces induced by the OB plastic hinges work to reduce the overall axial demands in the VBEs due to overturning moments, their plastic moments are additive to the local flexural demands imposed by the

HBEs. However, the simple HBE-to-VBE connections used in the SPSW-O (PR) and SPSW-O (PP) options eliminate the forces and moments due to boundary frame action, thus reducing the local flexural and axial demands in the VBEs as compared to SPSW-O options in which rigid HBE-to-VBE connections are used. As in conventional planar SPSWs, the VBEs within the SPSW-O systems must remain essentially elastic, with the exception of the plastic hinging that is allowed at their bases to develop the desirable sway plastic mechanism. As such, the capacity design procedures used for the VBEs in conventional SPSWs can be extended to the design of VBEs within the SPSW-O systems. Detailed discussions of the design procedures for the HBEs and VBEs can be found elsewhere (Sabelli and Bruneau 2007; Bruneau et al. 2011).

As assumed in the design procedures presented in earlier sections, the outrigger beams at each story are proportioned based on the size of HBEs considering parameter λ, which represents the relative flexural strength of OBs and HBEs (Equation 4.27). The outrigger beams within the SPSW-O (RR) and SPSW-O (PR) systems impose both axial and flexural demands on the outrigger columns through the moment-resisting actions of OB-to-OC connections. Hence, the outrigger columns in these systems must be designed for the combined effects of axial, flexural and shear demands due to the frame action and gravity loads, assuming that the plastic mechanism shown in Figure 5.4 is formed. However, in the cases of SPSW-O (RP) and SPSW-O (PP) systems, since pinned OB-to-OC connections are used, the reduced overturning moment of the SPSW is transferred to the outrigger columns essentially by means of shear at the ends of outrigger beams, ideally imposing no flexural demands on these elements. Therefore, outrigger columns in such systems are required to resist axial demands imposed by the outrigger beams as well as gravity loads.

Once the boundary frame and outrigger elements are selected, the plate thicknesses may be revised in order to avoid unnecessary overstrength, and to ensure that the assumed plastic mechanism will form. The inherent overstrength in SPSW systems is inevitable to some extent, partly because the calculated plate

thicknesses needed to resist design story shear can be impractical due to unavailability or welding and handling requirements; therefore, thicker infill plates are usually selected by the design engineer, resulting in heavier boundary elements. However, where practicable, attempts can be made to minimize unnecessary overstrength by revising plate thicknesses, the boundary frame and outrigger elements. The principle of virtual work (Neal 1977) can be used herein to calculate the portion of the design story shear to be carried by the infill plate at story i (V_i). The plate thicknesses can be updated using V_i calculated from Equations 5.35-5.39 for the RR, RP, PR and PP systems, respectively.

$$\left(\sum_{i=1}^{n} F_i h_i\right) = 2M_{OC} + 2M_{VBE} + 4\sum_{i=1}^{n} M_{OBi} + 2\sum_{i=1}^{n} M_{HBEi} + \sum_{i=1}^{n} V_i h_{si} \tag{5.35}$$

$$\left(\sum_{i=1}^{n} F_i h_i\right) = 2M_{OC} + 2M_{VBE} + 2\sum_{i=1}^{n} M_{OBi} + 2\sum_{i=1}^{n} M_{HBEi} + \sum_{i=1}^{n} V_i h_{si} \tag{5.36}$$

$$\left(\sum_{i=1}^{n} F_i h_i\right) = 2M_{OC} + 2M_{VBE} + 4\sum_{i=1}^{n} M_{OBi} + \sum_{i=1}^{n} V_i h_{si} \tag{5.37}$$

$$\left(\sum_{i=1}^{n} F_i h_i\right) = 2M_{OC} + 2M_{VBE} + 2\sum_{i=1}^{n} M_{OBi} + \sum_{i=1}^{n} V_i h_{si} \tag{5.38}$$

Where, M_{OC} and M_{VBE} are the plastic moments at the bases of the outrigger columns and VBEs, respectively, and h_{si} is the height of *i*-th story.

5.4 Case Study Designs

In order to evaluate and compare the seismic performances of the four different SPSW-O options introduced in previous chapter, 12- and 20-story SPSW-Os were designed according to the proposed design procedure. In addition, two SPSWs (without outriggers), herein referred to as free-standing SPSWs, were designed for comparison purposes. The case studies considered herein were designed for modified versions of the SAC model buildings (Gupta and Krawinkler 1999). The

12-story buildings were the same as those considered in Chapter 4. The dimensions, floor masses, and dead and live loads for the 20-story systems were matched exactly with those of the 20-story SAC building.

Two SPSW-O layouts were considered for the case study buildings (see Figure 5.8 and 5.9). As described in Chapter 4, the 12-story SPSW-O systems consisted of narrow SPSWs centrally placed within relatively large bays of gravity columns, and adjacent beams designed as outrigger elements (Figure 5.8). This design case could be expected for a given building layout if openings were required due to architectural demands for doorways or windows within the bay. However, the 20-story SPSW-O systems comprised of 6.1-meter-wide SPSWs placed in the central bays of the frames (in the north-south direction), as shown in Figure 5.9, in which the girders of the adjacent bays were designed as outriggers.

The symmetrical prototype buildings were assumed to be located in Los Angeles, CA (site class D), and all other design assumptions remain the same as those considered in Chapter 4. Considering rigid floor diaphragms and neglecting the effects of torsion, it was assumed that all SPSW-Os equally resist the same seismic loads in each direction. Four different SPSW-O options were designed according to the preliminary design procedure described in previous sections, along with free-standing SPSWs for comparison.

To allow for the comparison of the seismic performances of the different SPSW-O options on a consistent basis, design process sough to achieve the same levels of overall strength and OEF for all systems. In addition, the outrigger beams were of the same size at all stories in each SPSW-O system. Summaries of the designs for different SPSW-O options are presented in Tables 5.1 and 5.2 for the 20- and 12-story systems, respectively.

5.4.1 System Overstrength and OEF

As mentioned earlier, the OEF is an important metric quantifying the level of interaction between SPSW and the outrigger system; it allows for the comparison of different SPSW-O systems on a consistent basis. As such, the design process

sought to achieve the same OEF in all case study SPSW-O options. Analytical expressions developed in Chapter 4 were used to estimate the overall strength and OEF for all SPSW-O systems considered in this study, and are given in Table 5.3.

In the preliminary design procedure described earlier, the expressions presented for optimum design cases were derived by setting the overstrength of the systems equal to unity. In addition, further attempts were made to minimize possible overstrength by calculating the share of the frame action after the initial design and revising plate thicknesses to resist the remaining portion of the lateral load (i.e., Equations 5.35-5.38). However, although the prototype SPSW-Os were designed assuming that calculated plate thicknesses are available in all cases, the systems possess slight overstrength, as shown in Table 5.3. These overstrengths stem from the resistance factor ($\Phi = 0.9$) used in the design of infill plates, which results in slightly higher values for SPSW-Os in which the infill panels make relatively larger contributions to the lateral load resistance (i.e., PP and PR systems). It is worth noting that the overstrength values given in the Table 5.1 are consistent with those observed in parametric studies presented in Chapter 4.

5.4.2 Nonlinear Response History Analyses

A series of nonlinear response history analyses were conducted to evaluate and compare the seismic performance of the four SPSW-O options designed using the proposed design method presented earlier. The SPSW-O systems were modelled using the commonly accepted dual strip model in which the infill plates are represented by a series of pin-ended tension-only members oriented in the directions of the tension fields. All modelling assumptions are similar to those considered in Chapter 4.

The case study structures were analysed under earthquake acceleration time-histories developed for the SAC buildings located in Los Angeles (Somerville et al. 1997). The suite of 20 ground motions considered herein are those associated with the design basis earthquake (DBE) with a 10% probability of exceedance in 50 years (10/50). Rayleigh damping (corresponding to 2% of critical damping) was

incorporated into the models, and appropriate constraints were defined at all floor levels to simulate rigid diaphragms. Lean-on gravity columns with tributary seismic weights were included in the models to account for the P-Delta effects. The direct integration method was used to solve the nonlinear dynamic equations in SAP2000.

5.4.2.1. **Fundamental Period and Inelastic Drift**

Table 5.4 presents the calculated fundamental periods of the systems, and the mean maximum story drifts obtained from the nonlinear response history analyses. The fundamental periods of the SPSW-O systems were generally smaller than those of the free-standing SPSWs, indicating higher initial stiffness in such systems.

Figure 5.10 shows the pushover curves resulting from nonlinear static analysis of the 12-story systems. As can be seen in this figure, while the free-standing wall and SPSW-Os possess similar overall strength, their initial stiffnesses are different due mainly to the difference in their predominant modes of deformation. The free-standing SPSWs, with a predominantly flexural mode of deformation resulting from the cumulative elongation and shortening of the VBEs, exhibited lower initial stiffness compared to the SPSW-O systems, in which the outrigger elements work to reduce the cumulative drifts by restraining the cantilever bending of the plate wall, as shown in Figure 5.11.

It is noteworthy that the fundamental periods calculated herein were consistent with those reported by previous research (Gupta and Krawinkler 1999; Brman 2011). For example, the fundamental period of the 20-story Los Angeles SAC buildings calculated using different analytical models were reported to be in the range of 3.45 s to 3.98 s (Gupta and Krawinkler 1999). In another study (Berman 2011), three 20-story SPSWs having different bay widths were designed for the same building and seismicity (as described above), and fundamental periods ranging from 2.97 s to 3.78 s were reported. Note that the slight differences stem from the fact that the code-designed SPSWs studied by Berman (2011) possess

considerable overstrengths, while the SPSW systems designed herein were aimed at minimizing system overstrength.

Figure 5.12 shows the mean values of maximum story drifts over the height of the systems from nonlinear response history analyses of the 20 earthquake excitations. As shown, the peak story drifts occurred at the upper stories in all cases, due to the presence of higher vibration modes; this is especially true in the free-standing SPSWs, in which these effects were more significant. It is evident that all the four SPSW-O options were effective in limiting excessive drift demands in upper stories by restraining the overturning-type deformations in both the 12- and 20-story SPSW systems. Considering the results, the mean maximum drifts at several upper stories exceeded the 2% drift limit in both 12- and 20-story SPSWs, with maximums of 2.5% and 2.18%, respectively (Table 5.4). In contrast, the mean maximum story drifts for all SPSW-O systems were less than 2% under the design earthquakes.

Furthermore, results from the nonlinear response history analyses indicated that the SPSW-O configurations resulted in more uniform distributions of the story drifts over the height of the systems compared to those of the free-standing SPSWs, indicating improved seismic performance in such systems. While all SPSW-Os considered performed well within the 2% limit, the SPSW-O (RR) configuration exhibited the most uniform response in terms of drift, and appeared to be more effective in reducing the cantilever-type deformations in upper stories. Both the 12- and 20-story SPSW-O (PP) systems exhibited slightly larger drifts at the upper stories compared to other options. The 20-story SPSW-Os performed similarly in all stories up to the 16^{th} floor, with somewhat different drifts at stories above that level. This highlights the importance of outrigger beam strength and stiffness distributions in upper levels. On the other hand, slightly larger drifts were observed at stories below floor level 10 in the 20-story SPSW-Os, compared to those in the free-standing SPSW. These larger drifts are due in part to the difference between predominant modes of deformation in SPSWs and moment frames, resulting in the development of interaction forces between the two systems, as shown schematically

in Figure 5.13. When drifting as a unit, the outrigger frames with predominant racking-type deformation tend to push the SPSW to larger drifts in the lower stories.

However, Figure 5.12 shows that the mean story drifts of the 12-story SPSW-Os were all, with the exception of first two stories of the RR and RP systems, less than those of the free-standing SPSWs. This may be attributed to smaller interaction forces developed in these systems.

5.4.2.2. **VBE Demands**

Figure 5.14 shows maximum axial force demands at the base of the VBEs observed during nonlinear response history analyses of the suite of 20 ground motions considered in this study. As expected, the SPSW-O configurations were significantly effective in reducing large VBE axial demands caused primarily by the overturning moments. Note that the axial force reduction trends in SPSW-Os with the same type of HBE-to-VBE connections (i.e., pinned for PP & PR and rigid for RP & RR) were similar under the majority of earthquakes for both the 12- and 20-story systems. The reduction of VBE axial demands by the SPSW-O configuration depends on the level of interaction between the SPSW and the outrigger system, as quantified by the OEF.

As such, the VBE axial force reduction due to the presence of outriggers is more clearly observed in the 12-story systems, which were designed for a higher level of OEF than the 20-story SPSW-Os (i.e., OEF=0.3 versus 0.24).

Table 5.5 presents the overall axial force reduction at the bases of the VBEs in different SPSW-O options, as compared to the case of the free-standing SPSWs. As shown, the RR and PP configurations were, respectively, the most and least effective systems, in terms of reducing VBE axial force demands.

Table 5.6 shows the ratios of maximum axial force demands at the base of the VBEs to those calculated using the capacity design method. As described earlier, in the capacity design of the VBEs within the SPSW-O configurations, it was assumed that all infill panels yield at the same time, and that plastic hinges form at the ends of HBEs and OBs at all story levels. However, the nonlinear

responses of the systems indicated that the capacity design procedure results in conservative VBE designs, especially in the 20-story systems, in which the assumed simultaneous yielding of all designated energy dissipating elements is unlikely due to the presence of higher vibration modes. The mean maximum axial forces observed at the bases of the VBEs were approximately 75% and 55% of those used in the capacity design of these elements for the 12- and 20-story systems, respectively. However, the peak VBE axial force demands observed in the 12-story systems during earthquakes were about 96% and 90% of those used in capacity design for the SPSW and SPSW-O systems, respectively.

Figure 5.15 shows VBE displacement profiles at the time of maximum roof drift for the SPSWs and SPSW-O (RR) systems. It is evident that the SPSW-O configurations have effectively limited excessive cantilever-type VBE deformations, especially in the top third of the building, and have resulted in more uniform VBE displacement profiles.

5.4.2.3. **Outrigger Column Demands**

Figure 5.16 shows the maximum axial demands at the base of outrigger columns, obtained from nonlinear response history analyses of the 20 earthquake excitations considered. As shown, the outrigger columns experienced similar axial force demands in all SPSW-O options under the majority of earthquakes. However, slightly larger axial demands were observed in outrigger columns within the 20-story SPSW-O systems with rigid OB-to-OC connections (i.e., PR & RR) than in the two other options.

Table 5.7 shows maximum axial forces at the bases of the outrigger columns, normalized by those obtained from the capacity design of the 12- and 20-story systems. The nonlinear analysis results indicated that the assumption of simultaneous yielding of all outrigger beams, used in the capacity design of the outrigger columns, leads to conservative designs for such elements, especially in the 20-story SPSW-Os. The mean values of maximum axial force demands are less

than 80% and 50% of those used in the design of the 12- and 20-story systems, respectively.

5.4.2.4. **Plate Ductility Demands and Outrigger Beam Rotations**

A summary of the mean values of the maximum plate ductility demands and outrigger beam rotations is given in Table 5.8. For each earthquake, the plate maximum ductility demand (μ_{max}) at a given story was calculated by dividing the maximum plastic elongation of the strips by the yield elongation (e_y) as follows:

$$\mu_{max} = \frac{e_{max} - e_y}{e_y} \tag{5.39}$$

The mean peak ductility demands on the infill plates in the 12-story SPSW-Os were, with the exception of the PR system, larger than that of the free-standing SPSW. In contrast, the infill plates in the 20-story SPSW-O systems exhibited smaller peak ductility demands compared to that of the free-standing wall. These differences stem from a number of key factors influencing system performance, including infill plate aspect ratio, the height of the systems, and the level of interaction between the outrigger system and the plate wall.

Figure 5.17 shows the distribution of ductility demands on the plates along the height of the systems. It is evident that higher vibrational modes imposed larger ductility demands on the plates at the upper- and lower-level stories and, as shown, middle story levels experienced less ductility demands during earthquakes. It should be noted that the plate ductility demand is due primarily to racking-type deformations in the system.

The SPSW-O configurations have generally decreased the plate ductility demands in the upper stories of both the 12- and 20-story systems. However, slightly increased ductility demands were observed in the lower stories of SPSW-Os with moment-resisting HBE-to-VBE connections (i.e., RP & RR). These larger demands are due partly to the relatively thinner infill plates used in such systems

(e.g., 5.9 mm versus 7.4 mm plates, used in the first stories of the SPSW-O (RR) and SPSW systems, respectively), which require larger inelastic elongations to dissipate earthquake-induced energy. Another reason for these larger ductility demands may be attributed to the greater contribution of the shear resistance from the frame action and the interaction forces developed between the outrigger frames and the plate wall at the lower stories. It should be mentioned that the plate ductility demands and their distribution patterns observed herein are consistent with those reported in previous research (Berman 2011) for mid- and high-rise SPSWs.

As shown in Figure 5.17, for both the 12- and 20-story buildings, the SPSW-O systems that have same type of HBE-to-VBE connections exhibited similar distributions of ductility demand in their infill plates. The SPSW-O (PR) systems experienced smaller ductility demands compared to all other systems, whereas the SPSW-O (RP) systems were found to exhibit the largest plate ductility demands, especially in the lower stories.

Figure 5.18 shows the mean maximum nonlinear rotations of the outrigger beams experienced during earthquakes. The rotation demands on the outrigger beams follow, to a large extent, the distribution of story drifts over the height of the systems (see Figure 5.12). As shown, SPSW-O systems with the same types of OB-to-OC connection exhibited somewhat similar rotation demands on their outrigger beams. The outrigger beams in the SPSW-O systems with rigid OB-to-OC connections generally experienced larger inelastic rotations. At first glance, this may seem contradictory, considering the fact that the rotational stiffness of a beam rigidly connected at both ends is higher than that of a beam with a rigid connection at one end and a pinned connection at the other end. However, it should be noted that the plastic section modulus of the outrigger beams in the PR and RR systems were generally selected about half of those used in the PP and RP systems to achieve the same level of OEF in all designs. Therefore, these elements experienced larger rotations when working to reduce the overturning in the plate walls. As the graphs reveal, while the outrigger beams with similar boundary conditions performed similarly in the lower and medium levels, they experienced somewhat different

rotation demands at the upper stories. This highlights the higher importance of the outrigger beams' strength distributions at these story levels. The nonlinear analysis results indicated that the mean peak outrigger beams rotation demands did not exceed 0.011 radians.

5.4.3 System Weight Comparison

Figure 5.19 shows the calculated system weight for each prototype design. For comparison purposes, the steel weights of different elements of the systems are also shown. For both building heights, the SPSW-O configurations generally resulted in lighter systems compared to the free-standing SPSWs, with the RR systems being the lightest.

For instance, the total steel weights of the PP, PR, RP and RR systems were, respectively, 95%, 0.91%, 93% and 90% of that of the free-standing SPSW in the 20-story buildings. While the RR option resulted in slightly higher material efficiency compared with the other options, on the other hand, the fabrication costs associated with the higher number of moment-resisting connections used in such system, would probably outweigh the saving in steel tonnage and can be a potential detraction to the system's use. However, although the improved seismic performance often justifies the increased cost of the system, the three other options considered, each with slightly different characteristics, can alternatively be used as more economical options, while still meeting the desired performance objectives.

5.5 Summary and Conclusion

Steel plate shear walls with outrigger (SPSW-O) systems have been investigated in this chapter; several alternative configurations aiming to improve overturning stiffness of slender and tall SPSWs have been considered. A preliminary design procedure was developed for the SPSW-O systems with explicit consideration of the frame action and employing the principles of plastic analysis and capacity design. The relative contributions of the frame action and tension field action to the

overall strength were quantified for the four SPSW-O options discussed in this research, and key design parameters were identified.

The applications of the SPSW-O systems in mid-rise and high-rise building structures were studied by considering 12- and 20-story case studies, designed using the proposed design approach. The 12-story SPSW-Os consisted of a slender SPSW centrally placed within the relatively large bay of gravity columns, and the adjacent beams were designed as outriggers. This case study was intended to examine the application of the SPSW-O configuration in cases where the use of a solid shear wall is not feasible due to architectural restrictions, which is not uncommon in typical buildings with large bays. However, the 20-story case studies comprised of solid SPSWs placed in the central bays of frames in which the girders of adjacent bays were designed as outriggers. In addition, 12- and 20-story free-standing SPSWs were designed for the purpose of comparison.

A series of nonlinear response history analyses were carried out to investigate the behaviour of several SPSW-O options and to verify the validity of the preliminary design procedures proposed in this research. The seismic performance of the case study designs was evaluated in terms of story drifts, plate ductility demands, outrigger beam rotations, and the axial demands on the VBEs and outrigger columns. The results of response history analyses indicated that the four different SPSW-O options considered experienced fairly uniform response under the design-level earthquakes (i.e., earthquakes with 10% probability of exceedance in 50 years), and were comparably effective in limiting excessive drift demands due to the overturning moments.

The results also indicated that different SPSW-O options designed for the same levels of strength and OEF were similarly effective in reducing VBE axial force demands. Additionally, very similar axial force demands were observed at the base of the outrigger columns in all SPSW-O options with the same level of OEF. Therefore, the OEF, which quantifies the level of interaction between SPSW and the outrigger system, was found to be an important factor influencing system performance. Moreover, it allows for the comparison of SPSW-Os on a consistent

basis. As such, this parameter can be used by the design engineer to facilitate the design process when proportioning SPSW-Os for desired levels of overturning resistance.

The nonlinear analysis results indicated that all SPSW-O options were effective in reducing VBE axial demands, with the RR system being the most effective. The reduced axial forces allow for the use of lighter VBE sections, especially in taller systems, in which the SPSW-O configuration greatly improves the overturning stiffness of the SPSW by coupling it to the outrigger columns. On the other hand, the SPSW-O configuration increases the effective depth of the system and helps avoid concentrating extremely large forces at the base of the SPSW, and can reduce foundation design issues.

Considering the results, it appears that the capacity design procedure used for the design of VBEs and outrigger columns within the SPSW-O systems resulted in conservative design for these elements, especially in the 20-story case studies. The SPSW-O configurations generally reduced infill plate ductility demands at the upper stories. However, slightly greater ductility demands were observed at the lower story plates in some cases, especially in the SPSW-O systems with moment-resisting HBE-to-VBE connections (i.e., RP and RR). The plate ductility demands in all cases were well within the acceptable limits reported by previous experimental and analytical research. The inelastic rotation demands on the outrigger beams were all less than 0.02 rad under design-level earthquakes. The distribution patterns of the outrigger beam rotation demands along the height of the systems were similar in shape to those of the story drift demands, albeit with considerably smaller values.

This study extends the current understanding of the SPSW-O systems, and provides design recommendations to further the implementation of SPSWs in mid- to high-rise building structures. However, while several SPSW-O options discussed in this research, each with slightly different characteristics, were found to be effective in achieving design objectives under the earthquake hazard level

considered here, further experimental and analytical research is warranted to support the findings of this research.

Table 5.1 Summary of the designs for 20-story systems

SPSW					
Story	Plate (mm)	HBE	Adjacent Girder	VBE	Outer column
1	4.01	W14×48	W14×22	W36×800	W14×109
2	4.00	W14×48	W14×22	W36×800	W14×109
3	3.97	W14×48	W14×22	W36×800	W14×109
4	3.91	W14×48	W14×22	W36×652	W14×90
5	3.86	W14×48	W14×22	W36×652	W14×90
6	3.80	W14×53	W14×22	W36×652	W14×90
7	3.70	W14×53	W14×22	W36×529	W12×79
8	3.62	W14×53	W14×22	W36×529	W12×79
9	3.51	W14×53	W14×22	W36×529	W12×79
10	3.38	W14×53	W14×22	W36×395	W12×65
11	3.25	W14×53	W14×22	W36×395	W12×65
12	3.10	W14×53	W14×22	W36×395	W12×65
13	2.92	W14×53	W14×22	W36×282	W10×49
14	2.73	W14×53	W14×22	W36×282	W10×49
15	2.53	W14×53	W14×22	W36×282	W10×49
16	2.29	W14×53	W14×22	W36×194	W8×35
17	2.03	W14×53	W14×22	W36×194	W8×35
18	1.73	W14×61	W14×22	W36×194	W8×35
19	1.37	W14×61	W14×22	W36×194	W8×35
20	0.91	W24×68	W14×22	W36×194	W8×35

SPSW-O (PP)					
Story	Plate (mm)	HBE	OG	VBE	OC
1	3.60	W14×38	W18×55	W36×652	W14×145
2	3.58	W14×38	W18×55	W36×652	W14×145
3	3.56	W14×38	W18×55	W36×652	W14×145
4	3.51	W14×38	W18×55	W36×529	W14×132
5	3.46	W14×38	W18×55	W36×529	W14×132
6	3.41	W14×38	W18×55	W36×529	W14×132
7	3.33	W14×38	W18×55	W36×441	W14×109
8	3.25	W14×38	W18×55	W36×441	W14×109
9	3.16	W14×38	W18×55	W36×441	W14×109
10	3.03	W14×38	W18×55	W36×302	W12×87
11	2.92	W14×38	W18×55	W36×302	W12×87
12	2.79	W14×38	W18×55	W36×302	W12×87
13	2.63	W14×38	W18×55	W36×231	W12×65
14	2.46	W14×38	W18×55	W36×231	W12×65
15	2.28	W14×38	W18×55	W36×231	W12×65
16	2.06	W14×34	W18×55	W36×150	W10×49
17	1.83	W14×34	W18×55	W36×150	W10×49
18	1.55	W14×34	W18×55	W36×150	W10×49
19	1.23	W14×34	W18×55	W36×150	W10×49
20	0.83	W14×53	W18×55	W36×150	W10×49

Table 5.1 Continued

SPSW-O (PR)					
Story	Plate (mm)	HBE	OG	VBE	OC
1	3.62	W14×38	W16×31	W36×652	W14×159
2	3.58	W14×38	W16×31	W36×652	W14×159
3	3.56	W14×38	W16×31	W36×652	W14×159
4	3.50	W14×38	W16×31	W36×529	W14×145
5	3.46	W14×38	W16×31	W36×529	W14×145
6	3.41	W14×38	W16×31	W36×529	W14×145
7	3.32	W14×38	W16×31	W36×395	W14×120
8	3.24	W14×38	W16×31	W36×395	W14×120
9	3.15	W14×38	W16×31	W36×395	W14×120
10	3.03	W14×38	W16×31	W36×302	W14×99
11	2.91	W14×38	W16×31	W36×302	W14×99
12	2.78	W14×38	W16×31	W36×302	W14×99
13	2.63	W14×38	W16×31	W36×231	W12×87
14	2.46	W14×38	W16×31	W36×231	W12×87
15	2.27	W14×34	W16×31	W36×231	W12×87
16	2.06	W14×34	W16×31	W36×150	W12×65
17	1.83	W14×34	W16×31	W36×150	W12×65
18	1.55	W14×34	W16×31	W36×150	W12×65
19	1.23	W14×38	W16×31	W36×150	W12×65
20	0.82	W14×53	W16×31	W36×150	W12×65

SPSW-O (RP)					
Story	Plate (mm)	HBE	OG	VBE	OC
1	3.09	W14×38	W18×55	W36×588	W14×145
2	3.08	W14×38	W18×55	W36×588	W14×145
3	3.06	W14×43	W18×55	W36×588	W14×145
4	3.03	W14×43	W18×55	W36×529	W14×132
5	3.00	W14×43	W18×55	W36×529	W14×132
6	2.95	W14×43	W18×55	W36×529	W14×132
7	2.87	W14×43	W18×55	W36×395	W14×109
8	2.80	W14×43	W18×55	W36×395	W14×109
9	2.73	W14×43	W18×55	W36×395	W14×109
10	2.62	W14×43	W18×55	W36×302	W12×87
11	2.52	W14×43	W18×55	W36×302	W12×87
12	2.41	W14×43	W18×55	W36×302	W12×87
13	2.27	W14×43	W18×55	W36×231	W12×65
14	2.13	W14×43	W18×55	W36×231	W12×65
15	1.97	W14×43	W18×55	W36×231	W12×65
16	1.79	W14×43	W18×55	W36×160	W10×49
17	1.58	W14×48	W18×55	W36×160	W10×49
18	1.35	W14×48	W18×55	W36×160	W10×49
19	1.07	W14×53	W18×55	W36×160	W10×49
20	0.71	W14×74	W18×55	W36×160	W10×49

Table 5.1 Continued

SPSW-O (RR)					
Story	Plate (mm)	HBE	OG	VBE	OC
1	3.12	W14×38	W16×31	W36×588	W14×159
2	3.11	W14×38	W16×31	W36×588	W14×159
3	3.09	W14×38	W16×31	W36×588	W14×159
4	3.06	W14×43	W16×31	W36×529	W14×145
5	3.02	W14×43	W16×31	W36×529	W14×145
6	2.98	W14×43	W16×31	W36×529	W14×145
7	2.90	W14×43	W16×31	W36×395	W14×120
8	2.83	W14×43	W16×31	W36×395	W14×120
9	2.75	W14×43	W16×31	W36×395	W14×120
10	2.65	W14×43	W16×31	W36×302	W14×99
11	2.55	W14×43	W16×31	W36×302	W14×99
12	2.43	W14×43	W16×31	W36×302	W14×99
13	2.29	W14×43	W16×31	W36×231	W12×87
14	2.15	W14×43	W16×31	W36×231	W12×87
15	1.99	W14×43	W16×31	W36×231	W12×87
16	1.80	W14×43	W16×31	W36×160	W12×65
17	1.60	W14×48	W16×31	W36×160	W12×65
18	1.36	W14×48	W16×31	W36×160	W12×65
19	1.07	W14×53	W16×31	W36×160	W12×65
20	0.72	W14×74	W16×31	W36×160	W12×65

Table 5.2 Summary of the designs for 12-story systems

SPSW			
Story	Plate (mm)	HBE	VBE
1	7.41	W18×71	W14×730
2	7.34	W18×71	W14×730
3	7.21	W18×71	W14×730
4	6.92	W18×71	W14×605
5	6.65	W18×71	W14×605
6	6.31	W18×71	W14×605
7	5.77	W18×65	W14×398
8	5.27	W18×65	W14×398
9	4.68	W18×65	W14×398
10	3.89	W18×60	W14×211
11	3.05	W18×60	W14×211
12	1.98	W18×71	W14×211

Table 5.2 continued

SPSW-O (PP)					
Story	Plate (mm)	HBE	OB	VBE	OC
1	7.09	W18×65	W18×76	W14×665	W14×159
2	7.03	W18×65	W18×76	W14×665	W14×159
3	6.90	W18×65	W18×76	W14×665	W14×159
4	6.60	W18×65	W18×76	W14×500	W14×120
5	6.34	W18×60	W18×76	W14×500	W14×120
6	6.02	W18×60	W18×76	W14×500	W14×120
7	5.51	W18×55	W18×76	W14×311	W12×87
8	5.03	W18×55	W18×76	W14×311	W12×87
9	4.47	W18×55	W18×76	W14×311	W12×87
10	3.73	W18×46	W18×76	W14×193	W10×49
11	2.92	W18×46	W18×76	W14×193	W10×49
12	1.90	W18×46	W18×76	W14×193	W10×49

SPSW-O (PR)					
Story	Plate (mm)	HBE	OB	VBE	OC
1	7.16	W18×65	W18×40	W14×665	W14×176
2	7.09	W18×65	W18×40	W14×665	W14×176
3	6.97	W18×65	W18×40	W14×665	W14×176
4	6.63	W18×60	W18×40	W14×455	W14×132
5	6.37	W18×60	W18×40	W14×455	W14×132
6	6.05	W18×60	W18×40	W14×455	W14×132
7	5.56	W18×55	W18×40	W14×311	W14×99
8	5.08	W18×55	W18×40	W14×311	W14×99
9	4.51	W18×50	W18×40	W14×311	W14×99
10	3.76	W18×46	W18×40	W14×159	W12×72
11	2.95	W18×46	W18×40	W14×159	W12×72
12	1.92	W18×46	W18×40	W14×159	W12×72

SPSW-O (RP)					
Story	Plate (mm)	HBE	OB	VBE	OC
1	5.87	W18×55	W18×76	W14×605	W14×159
2	5.81	W18×55	W18×76	W14×605	W14×159
3	5.71	W18×55	W18×76	W14×605	W14×159
4	5.46	W18×55	W18×76	W14×455	W14×120
5	5.25	W18×55	W18×76	W14×455	W14×120
6	4.98	W18×55	W18×76	W14×455	W14×120
7	4.60	W18×55	W18×76	W14×342	W12×87
8	4.20	W18×55	W18×76	W14×342	W12×87
9	3.71	W18×50	W18×76	W14×342	W12×87
10	3.11	W18×50	W18×76	W14×193	W10×49
11	2.43	W18×50	W18×76	W14×193	W10×49
12	1.58	W18×60	W18×76	W14×193	W10×49

Table 5.2 continued

SPSW-O (RR)					
Story	Plate (mm)	HBE	OB	VBE	OC
1	5.91	W18×55	W18×40	W14×605	W14×176
2	5.86	W18×55	W18×40	W14×605	W14×176
3	5.75	W18×55	W18×40	W14×605	W14×176
4	5.50	W18×55	W18×40	W14×455	W14×132
5	5.29	W18×55	W18×40	W14×455	W14×132
6	5.02	W18×55	W18×40	W14×455	W14×132
7	4.61	W18×55	W18×40	W14×311	W14×99
8	4.22	W18×55	W18×40	W14×311	W14×99
9	3.74	W18×50	W18×40	W14×311	W14×99
10	3.13	W18×50	W18×40	W14×176	W12×72
11	2.45	W18×50	W18×40	W14×176	W12×72
12	1.60	W18×60	W18×40	W14×176	W12×72

Table 5.3 Calculated system overstrength and outrigger efficiency factor

	SPSW		SPSW-O (PP)		SPSW-O (PR)		SPSW-O (RP)		SPSW-O (RR)	
Story	12	20	12	20	12	20	12	20	12	20
Overstrength	1.11	1.11	1.10	1.10	1.10	1.09	1.08	1.08	1.09	1.08
OEF	-	-	0.31	0.24	0.30	0.24	0.31	0.23	0.30	0.24

Table 5.4 Fundamental periods, and mean peak drifts from response history analyses

	SPSW		SPSW-O (PP)		SPSW-O (PR)		SPSW-O (RP)		SPSW-O (RR)	
Story	12	20	12	20	12	20	12	20	12	20
Period (s)	2.57	3.92	2.19	3.74	2.13	3.64	2.27	3.86	2.21	3.73
Story Drift (%)	2.50	2.18	1.88	1.94	1.82	1.86	1.78	1.82	1.69	1.77
Roof Drift (%)	1.57	1.20	1.27	1.12	1.19	1.09	1.31	1.11	1.23	1.08

Table 5.5 Reduction of VBE axial force demands by SPSW-O configurations

	SPSW-O (PP)		SPSW-O (PR)		SPSW-O (RP)		SPSW-O (RR)	
Story	12	20	12	20	12	20	12	20
Mean (%)	23	16	26	18	29	23	31	24
Max (%)	34	28	37	31	39	32	42	35

Table 5.6 Ratios of the mean and peak VBE axial force demands observed during earthquakes to those calculated using capacity design procedure

	SPSW		SPSW-O (PP)		SPSW-O (PR)		SPSW-O (RP)		SPSW-O (RR)	
System	Mean	Peak	Mean	Peak	Mean	Peak	Mean	Peak	Mean	Peak
12-story	0.75	0.96	0.73	0.87	0.7	0.86	0.77	0.92	0.74	0.91
20-story	0.55	0.81	0.58	0.81	0.56	0.79	0.56	0.79	0.55	0.77

Table 5.7 Ratios of the mean and peak outrigger column axial force demands observed during earthquakes to those calculated using capacity design procedure

	SPSW-O (PP)		SPSW-O (PR)		SPSW-O (RP)		SPSW-O (RR)	
System	Mean	Peak	Mean	Peak	Mean	Peak	Mean	Peak
12-story	0.77	0.85	0.78	0.86	0.77	0.85	0.79	0.86
20-story	0.41	0.51	0.44	0.52	0.41	0.51	0.44	0.52

Table 5.8 Mean peak outrigger beam rotations and infill plate ductility demands from response history analyses

	SPSW		SPSW-O (PP)		SPSW-O (PR)		SPSW-O (RP)		SPSW-O (PP)	
Story	12	20	12	20	12	20	12	20	12	20
Plate ductility	3.52	4.63	3.74	3.71	3.50	3.50	4.18	4.41	3.80	4.21
OB rotation (rad)	-	-	0.009	0.007	0.011	0.010	0.008	0.005	0.011	0.090

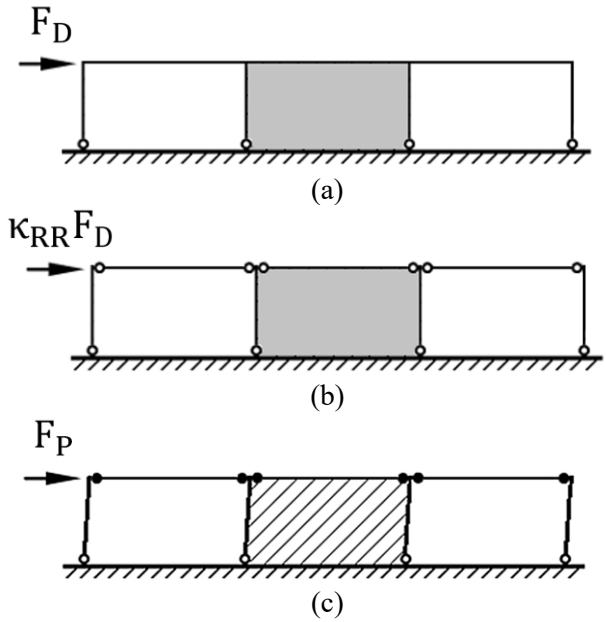

Figure 5.1 Single-story SPSW-O (RR): (a) system subjected to full lateral design load; (b) assigning a portion of the design load to the infill panel; (c) lateral force needed to develop plastic mechanism of the system

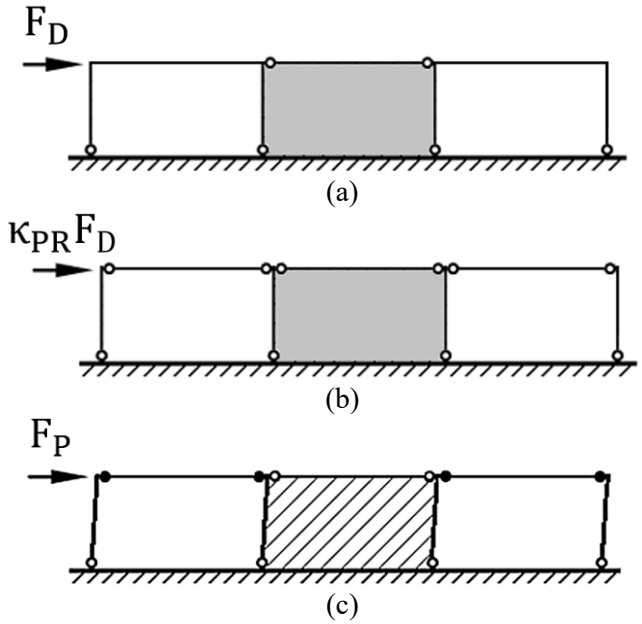

Figure 5.2 Single-story SPSW-O (PR): (a) system subjected to full lateral design load; (b) assigning a portion of the design load to the infill panel; (c) lateral force needed to develop plastic mechanism of the system

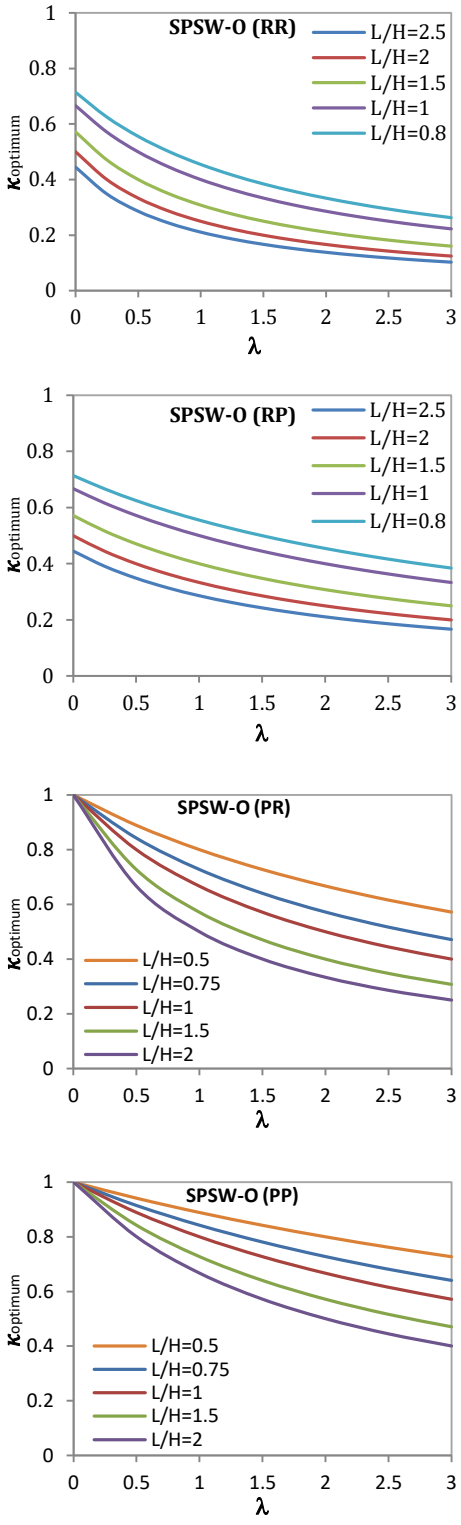

Figure 5.3 Relationship between $\kappa_{optimum}$ and λ in different SPSW-O option

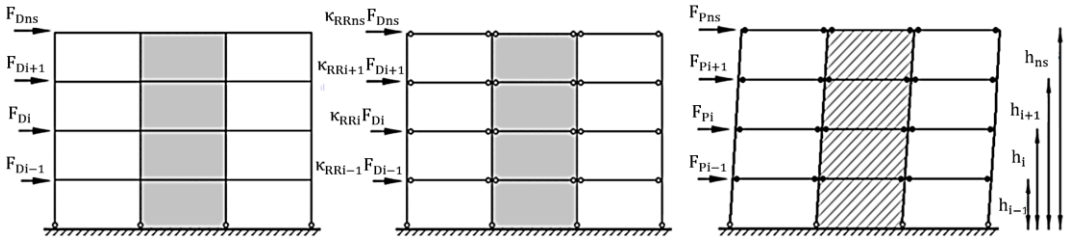

(a) (b) (c)

Figure 5.4 Multi-story SPSW-O with rigid HBE-to-VBE and OB-to-OC connections: (a) Design lateral force; (b) Modified lateral force to size infill panel; (c) Lateral force needed to develop desirable plastic mechanism

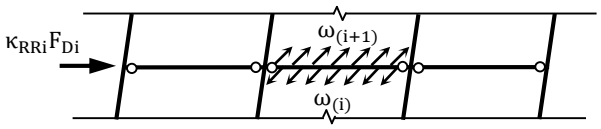

Figure 5.5 Tension field forces and modified design load in an intermediate floor of frame 5.4b

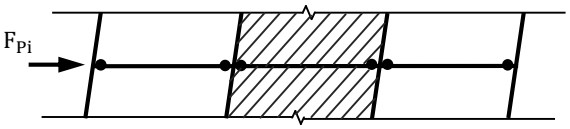

Figure 5.6 An intermediate floor in a multi-story SPSW-O (RR) system in mechanism condition

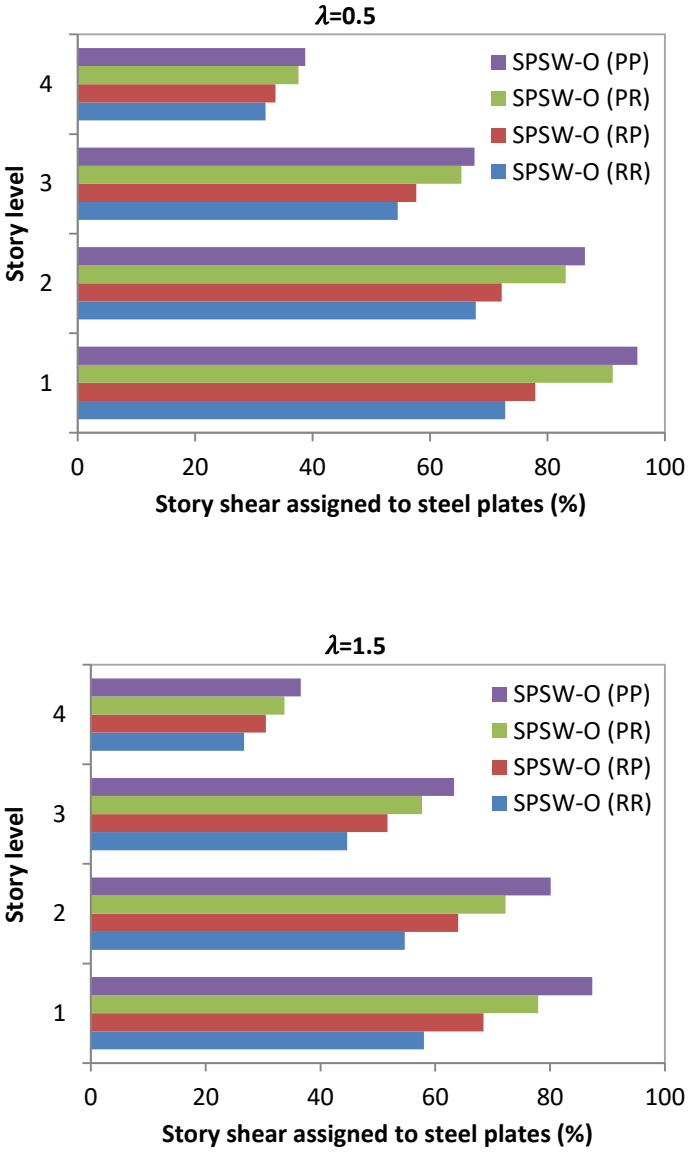

Figure 5.7 Comparison of story shear resisted by steel plates for 4-story SPSW-O systems (no RBS connections)

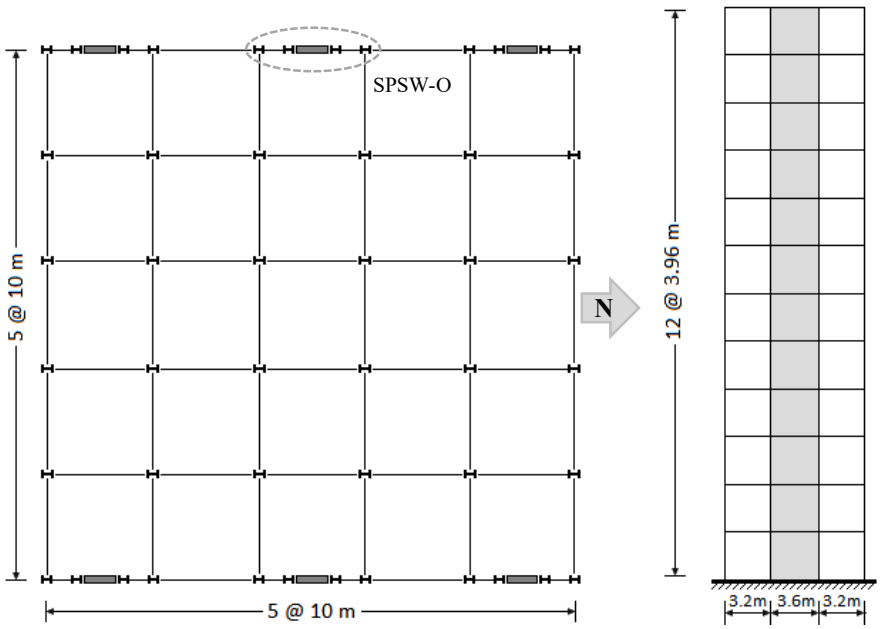

Figure 5.8 12-story case study buildings and SPSW-O system

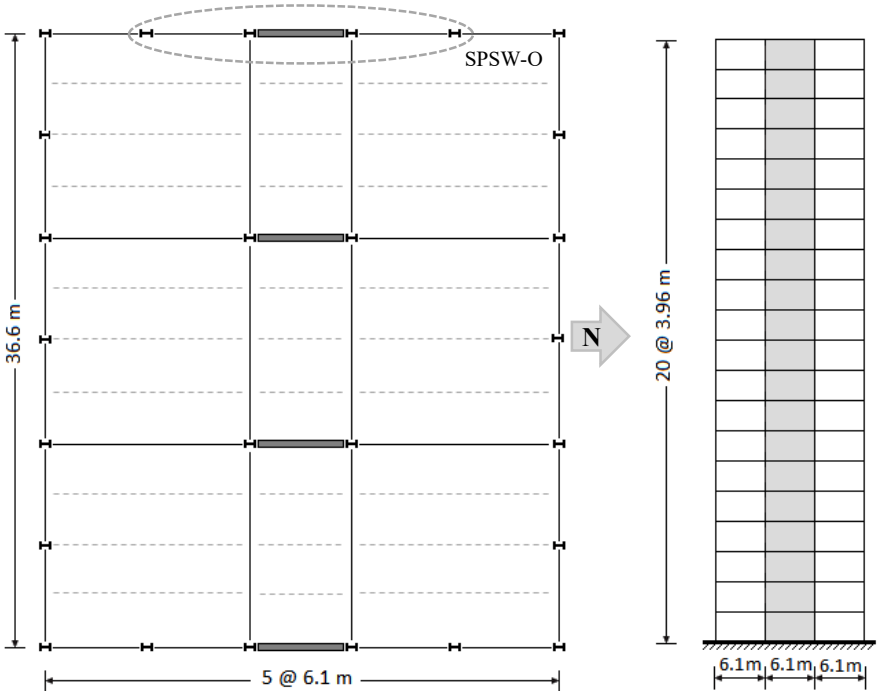

Figure 5.9 20-story case study buildings and SPSW-O system

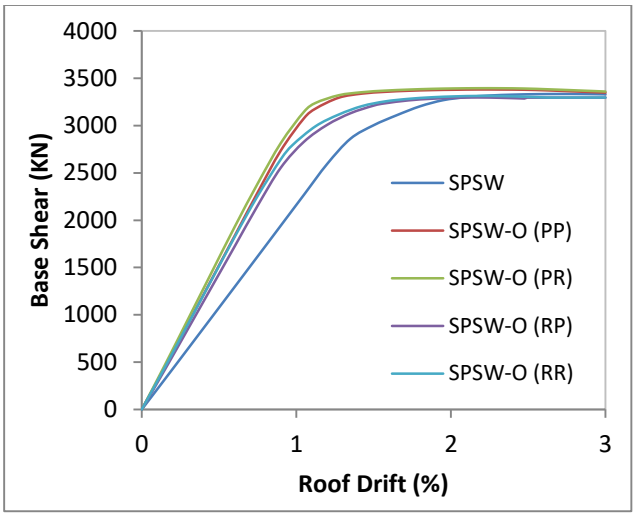

Figure 5.10 Pushover curves of 12-story systems from nonlinear static analyses

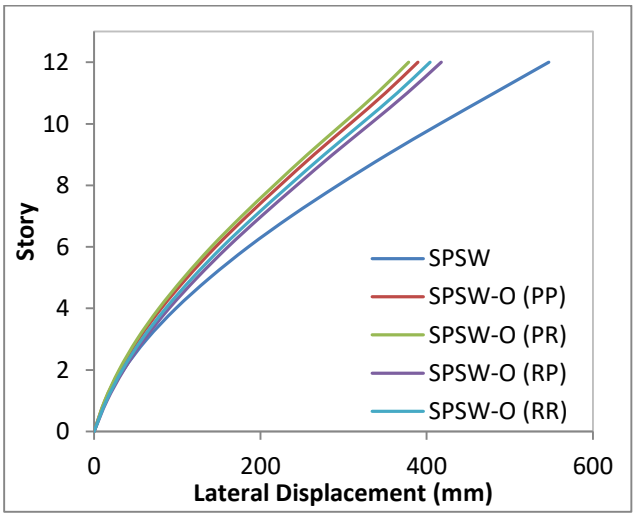

Figure 5.11 Lateral displacement profiles of the 12-story systems subjected to design load

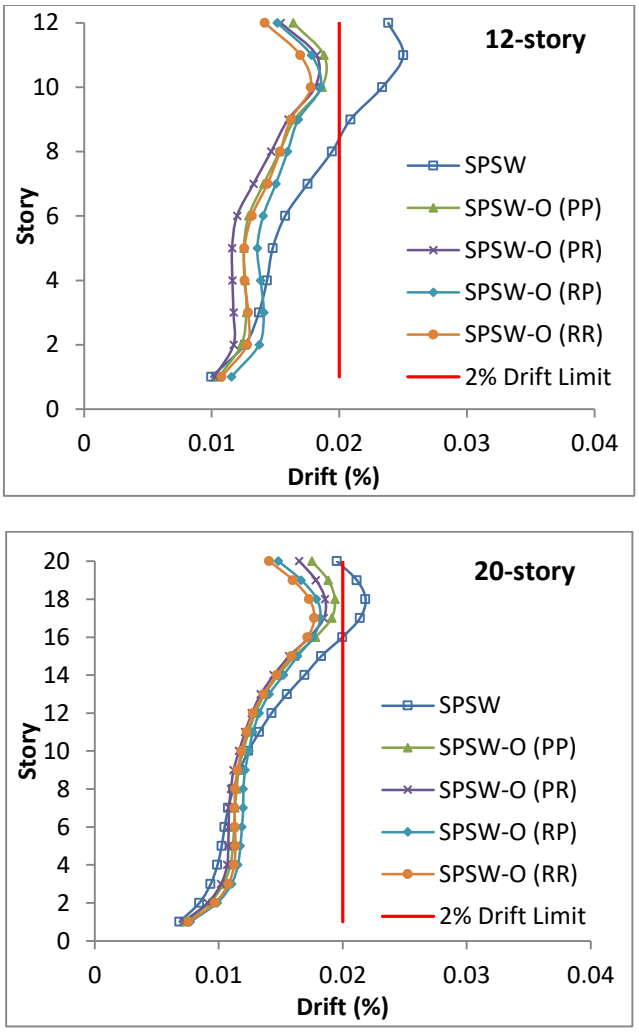

Figure 5.12 Mean drift demands from nonlinear response history analyses

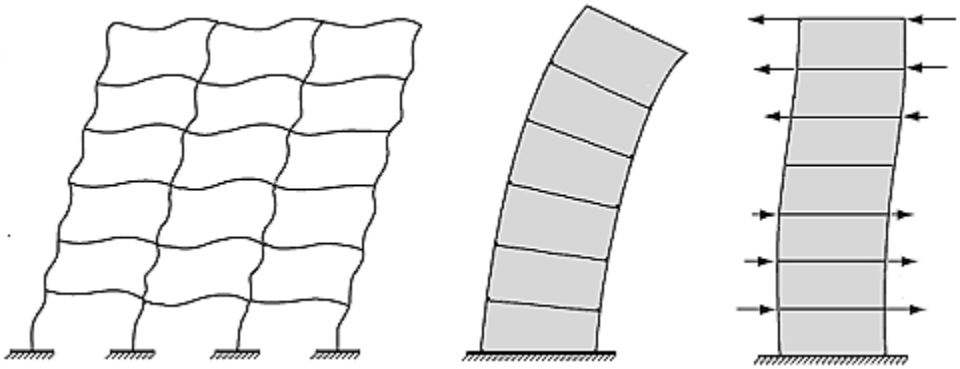

Figure 5.13 Predominant mode of deformation in moment frame and SPSW, and interaction forces

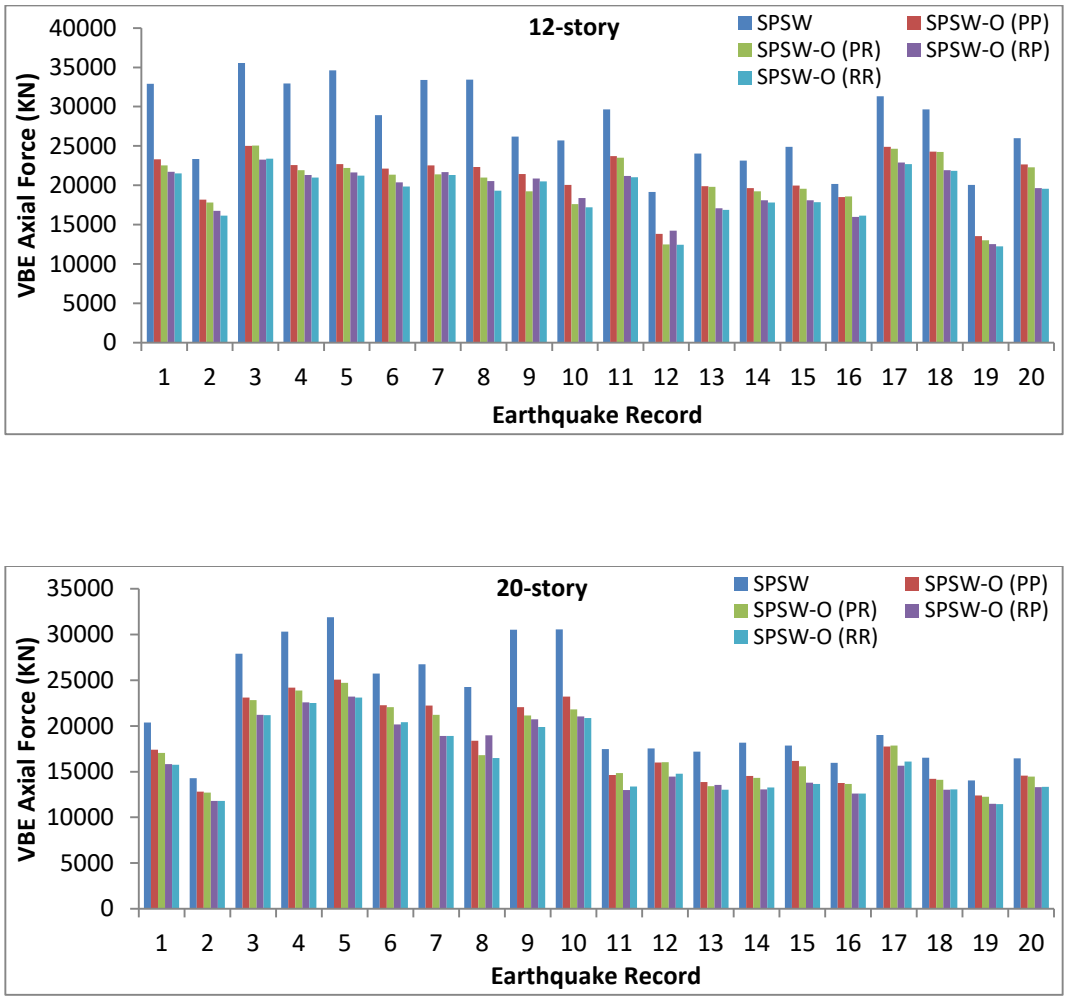

Figure 5.14 Maximum axial force demands at the base of VBEs observed during earthquakes

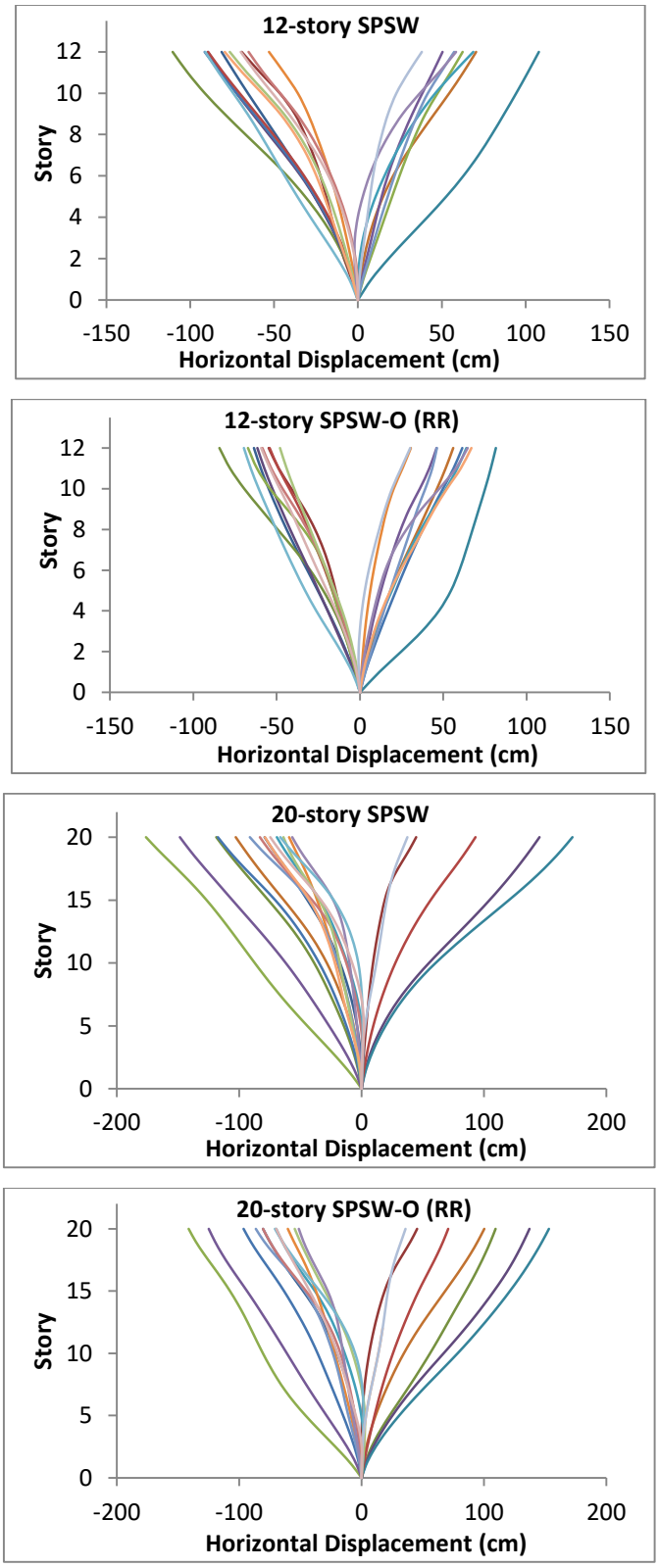

Figure 5.15 VBE displacement profile at the time of maximum roof drift

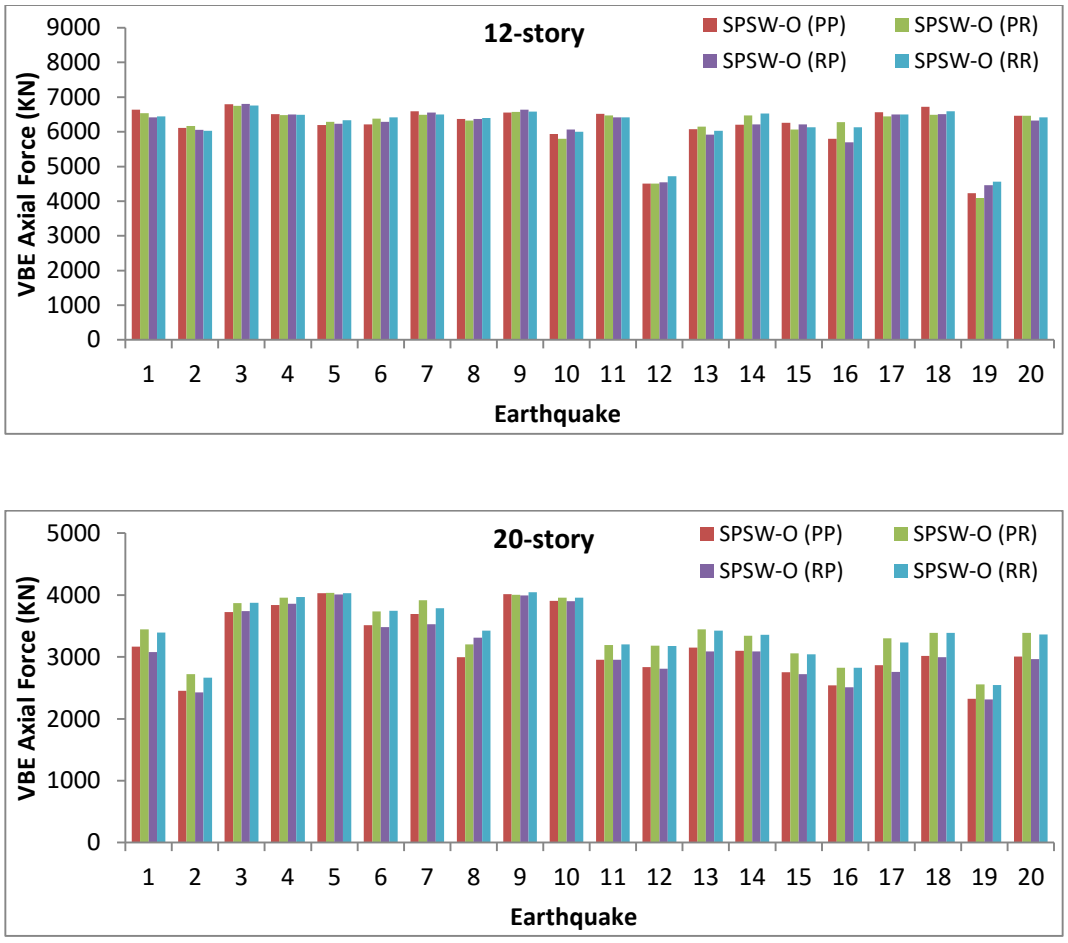

Figure 5.16 Maximum axial force demands at the base of outrigger columns observed during earthquakes

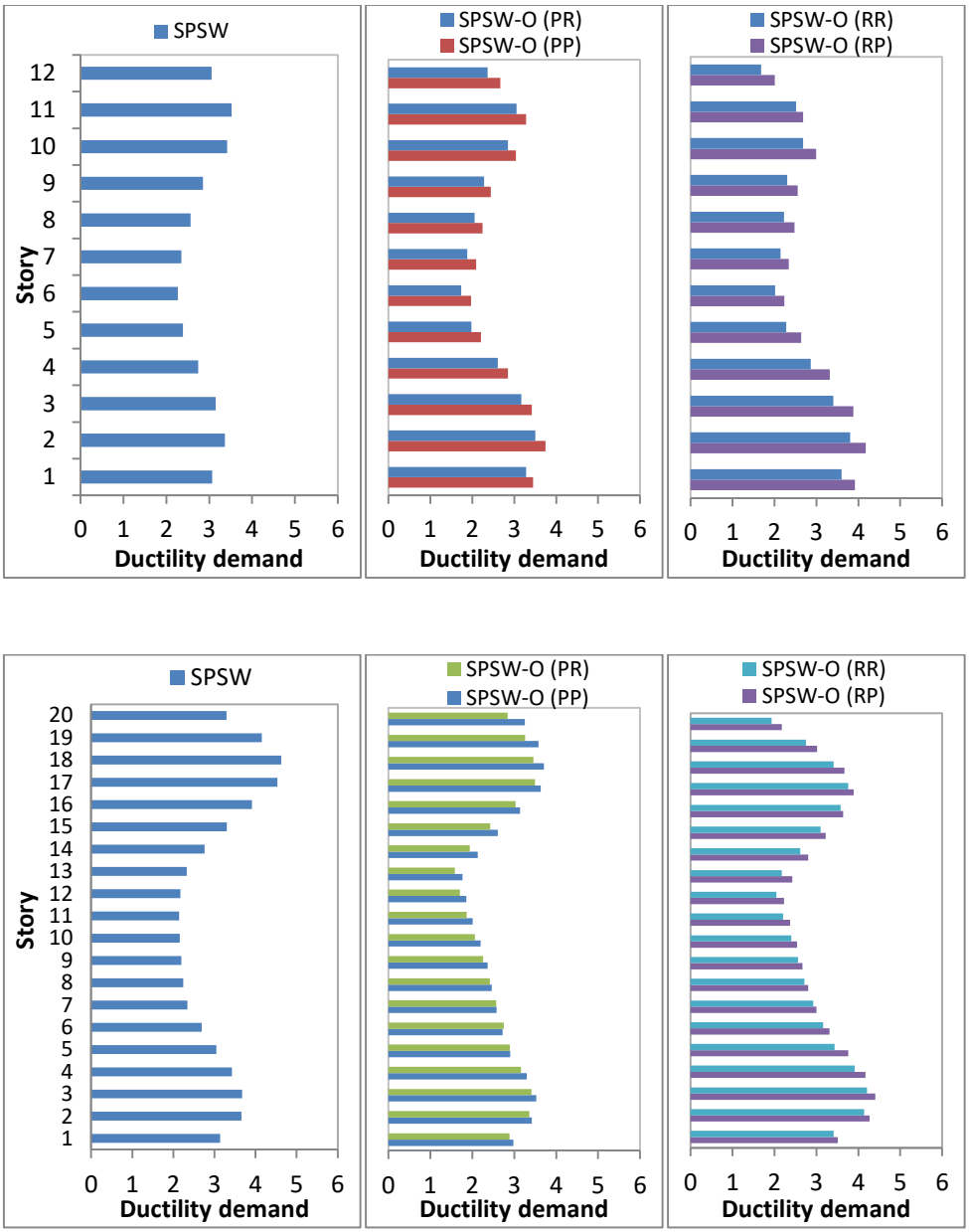

Figure 5.17 Mean infill plates ductility demands from response history analyses

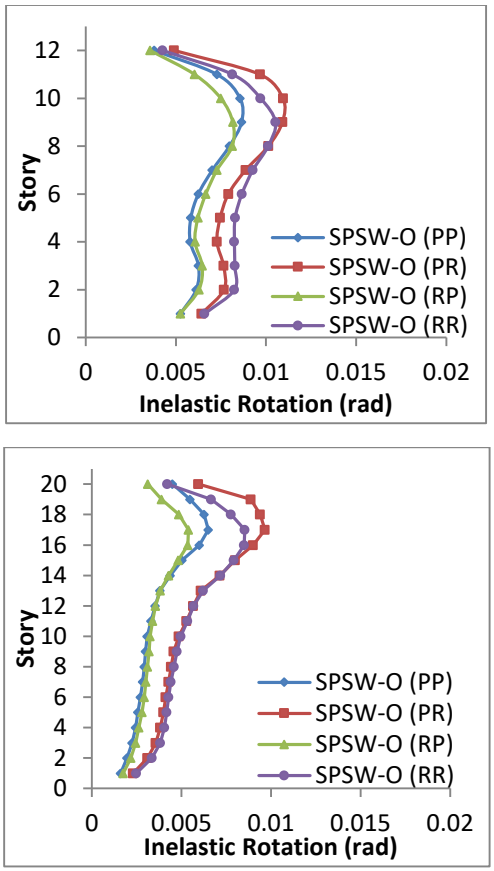

Figure 5.18 Outrigger beams inelastic rotation demands from response history analyses

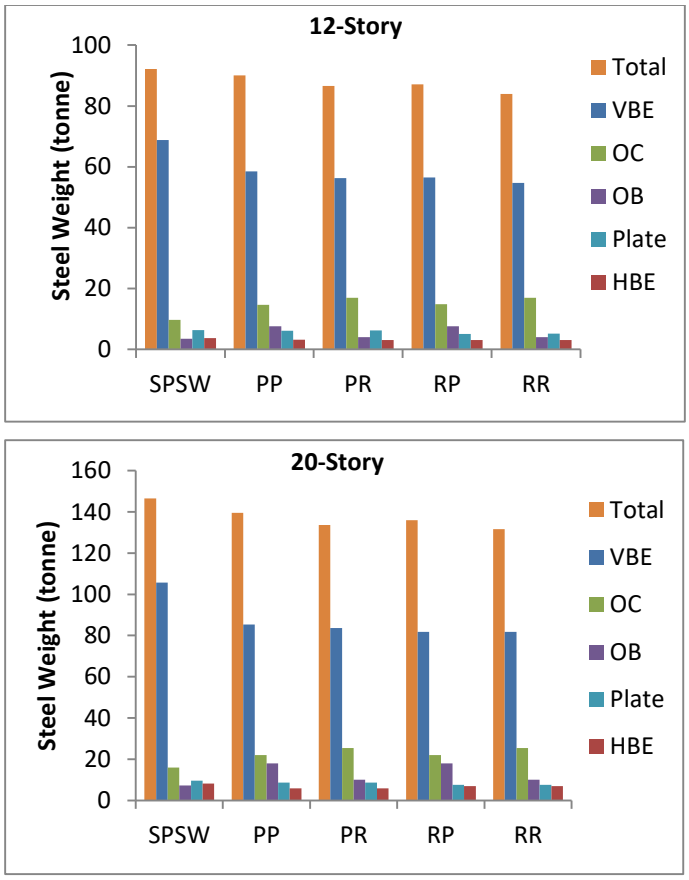

Figure 5.19 Steel weight comparison of the prototype designs

5.6 References

AISC. (2010). Seismic Provisions for structural steel buildings. American Institute of Steel Construction, Chicago.

Berman, J., Lowes, L.N., Okazaki, T., Bruneau, M., Tsai, K-C., Driver, R.G. and Sabelli, R. (2008). Research needs and future directions for steel plate shear walls. ASCE Structures Congress: Crossing Borders.

Bruneau, M., Uang, C.M. and Sabelli, R. (2011). Ductile design of steel structures. Second Edition, Mc Graw Hill.

Canadian Standards Association. (2014). Design of Steel Structures, CAN/CSA S16-14.

Driver, R.G., Kulak, G.L., Elwi, A.E. and Kennedy, D.J.L. (1998). FE and simplified models of steel plate shear walls. Journal of Structural Engineering, 124 (2), 121-130

Driver, R.G., Kulak, G.L., Kennedy, D.J.L. and Elwi, A.E. (1997). Seismic behavior of steel plate shear walls. Structural Engineering Rep. 215, Deptartment of Civil Engineering, University of Alberta, Edmonton, Alberta, Canada.

Neal, B.G. (1977). The plastic method of structural analysis, Chapman & Hall, London.

Gupta, A. and Krawinkler, H. (1999). Seismic demands for performance evaluation of steel moment-resisting frame structures. Report no. 132. John A. Blume earthquake engineering center. Stanford University.

Safari Gorji, M. and Cheng, J.J.R. (2015). Improving overturning stiffness of steel plate shear walls, Proc., Structures Congress, Structural Engineering Institute, ASCE, Portland.

Safari Gorji, M. and Cheng, J.J.R. (2013). Performance-based plastic design of Type D steel plate shear walls. Proc. Canadian Society for Civil Engineering Annual Conference, Montreal.

SAP2000 Version 14.2. Computer and Structures, Berkeley, CA.

Timler, P.A., and Kulak, G.L. (1983). Experimental study of steel plate shear walls. Structural Engineering Rep., No. 114, Department of Civil Engineering, University of Alberta, Edmonton, AB, Canada.

Taranath, B.S. (2012). Structural analysis and design of tall buildings; steel and composite construction. International Code Council. CRC Press, Taylor & Francis Group.

Vian, D. and Bruneau, M. (2005). Steel plate shear walls for seismic design and retrofit of building structures. Technical Report No. MCEER-05-0010,

Multidisciplinary Center for Earthquake Engineering Research, Buffalo, New York.

6. PLASTIC ANALYSIS AND DESIGN OF COUPLED STEEL PLATE SHEAR WALLS[3]

6.1 Introduction

Steel plate shear walls (SPSWs) have been efficiently used as robust and economical seismic force resisting systems for buildings located in earthquake-prone areas. A conventional SPSW consists of thin unstiffened infill panels surrounded by horizontal and vertical boundary elements (HBEs and VBEs). The shear strength of a typical SPSW is provided by the tension field action of the infill panel and the moment-resisting action of the HBE-to-VBE connections. Unlike reinforced concrete shear walls, in which the entire width contributes to overturning resistance, SPSWs resist overturning moments primarily through the axial forces in their VBEs. The relatively low overturning stiffness of SPSWs in comparison to reinforced concrete shear walls is considered a potential drawback and a major detraction to the system's application, especially in taller buildings (Berman et al. 2008). On the other hand, architectural requirements (e.g., openings to accommodate doorways and windows) often do not allow the entire width of the bay to be infilled with solid steel panels.

A number of researchers investigated the coupled steel plate shear wall (C-SPSW) configuration as an alternative to address the above-mentioned issues (Zhao and Astaneh 2004; Li et al. 2012; Borello and Fahnestock 2012). A C-SPSW consists of two SPSW piers linked by coupling beams (CB) at the floor levels. The C-SPSW configuration allows for the placement of two adjacent SPSWs within a single span, accommodating doorways and windows. Previous researchers have reported that the C-SPSW system maintains the ductile and robust seismic performance of conventional SPSWs while improving material efficiency (Borello

[3]A version of this chapter has been submitted for publication in the *Journal of Structural Engineering*, ASCE.

and Fahnestock 2012). These researchers extended the capacity design method used for conventional SPSWs to design the C-SPSW systems and investigated the degree of coupling (DC) as an important metric, which affects the behaviour and efficiency of C-SPSWs.

The C-SPSW configuration is inherently a dual system in which a substantial portion of the story shear is carried through the moment-resisting action of the boundary frames of the individual SPSW piers and the CB-to-VBE connections. Therefore, procedures are needed to quantify this strength and estimate the portion of the total lateral design force to be resisted by the steel plates in order to achieve an efficient design of C-SPSWs. Borello and Fahnestock (2012) employed the procedure proposed by Sabelli and Bruneau (2006) for planar SPSWs to size the infill panels within the C-SPSW systems. According to this procedure, it is preliminarily assumed that the total lateral design force is resisted by the infill panels, and the initial plate thicknesses are selected accordingly. The boundary frame elements are then designed according to the capacity design procedure to resist the maximum tension field forces generated by the infill plates. Next, an elastic analysis is performed to determine the portion of the total story shear that is resisted by the infill panels. The plate thicknesses and the boundary frame elements are subsequently revised based on the updated story shear. The procedure is repeated to optimize the design in an iterative manner.

However, since the lateral load resistance provided by the frame action in a C-SPSW is significant, many design iterations may be needed to arrive at the final design. Because any changes in the plate thickness and consequently the boundary elements in each design iteration require recalculation of the tension field angles and reanalysis of sharing of story shear forces between the infill panels and frames, this procedure can result in a lengthy and time-consuming design process. To minimize the number of design iterations and possibly achieve an optimum design of C-SPSWs, this research employs principles of the plastic analysis and capacity design to quantify the sharing of story shear forces between the infill panels and frames within C-SPSW systems. A preliminary design procedure is proposed that

explicitly accounts for the strength provided by the frame action in the C-SPSW configurations right from the beginning of the design process.

As discussed earlier, improved architectural flexibility, material efficiency and overturning stiffness over planar SPSWs are the three key factors contributing to the desirability of the C-SPSW configuration. However, the fabrication cost associated with the higher number of moment-resisting connections required in such systems is a potential drawback for their use as an economical option. One potential solution is to use simple HBE-to-VBE connections in the SPSW piers, as shown in Figure 6.1, allowing for less stringent detailing requirements and reduced fabrication costs. While the AISC Seismic Provisions (2010) require moment-resisting boundary frames in SPSWs for seismic applications, CSA-S16 (2014) permits the use of simple shear HBE-to-VBE connections in the limited-ductility (Type LD) category of SPSWs. Moghimi and Driver (2013) tested a full-scale modular SPSW with simple boundary frame connections and reported a stable cyclic performance with a high level of ductility. The specimen exhibited hysteresis loops comparable with those of a SPSW with a moment-resisting frame cyclically tested by Driver et al. (1997). As such, when a pair of SPSWs with simple boundary frames is used in a C-SPSW configuration, the resulting dual system is expected to perform in a ductile manner similar to that of a SPSW with moment resisting frame. When such a C-SPSW is subjected to cyclic loading, the rigidly connected coupling beams would provide complementary energy dissipation to the system through the formation of plastic hinges, and prevent excessive pinching of the hysteresis loops. As theoretically discussed above, such a C-SPSW option could offer the potential for a desirable seismic performance at a reduced fabrication cost.

However, at the time of this writing no research has been conducted on the behavior and design of such C-SPSW systems; therefore, this type of C-SPSW is also studied in this chapter. For this purpose, the C-SPSW systems considered in this research are categorized into two types: (1) C-SPSWs with pinned HBE-to-VBE connections, herein referred to as C-SPSW (P), and (2) C-SPSWs with rigid HBE-to-VBE connections, herein referred to as C-SPSW (R). Case studies of 8-

and 12-story C-SPSWs are designed using the proposed design approach for a selected degree of coupling. The performances of the prototype designs and the validity of the proposed design approach are evaluated using nonlinear static and response history analyses.

6.2 Optimum Design for Lateral Load Resistance

As discussed in the previous section, the moment-resisting actions of the CB-to-VBE and HBE-to-VBE connections in a C-SPSW configuration provide significant lateral load resistance to the system. Hence, when designing C-SPSW systems, it would be overly conservative to neglect this lateral strength and design the infill panels for full lateral design loads. Therefore, in order to achieve an efficient design of such systems, procedures are needed to consider and quantify the contribution of the frame action to the overall lateral load resistance of the system. Such procedures are studied in the following sections for the two C-SPSW options discussed in this research, by employing the principles of plastic analysis and capacity design.

6.2.1 Single-Story C-SPSW Systems

For ease of understanding, the expressions presented in this section are first developed for the case of single-story C-SPSWs, and are extended in the next section to the more complex case of multi-story systems. Qu and Bruneau (2009) used the plastic method of structural analysis to investigate the overstrength provided by the boundary frame moment-resisting action in planar SPSWs, and introduced a balanced design case in which the strength provided by the frame is exactly equal to that required to anchor the fully yielded infill plates (i.e., the boundary frame provides no overstrength for the system). The same concept is extended here to develop procedures for the efficient design of the two types of C-SPSWs discussed in this research.

6.2.1.1. **Single-Story C-SPSW (R)**

Figure 6.2 shows a single-story C-SPSW with moment-resisting boundary frames subjected to a lateral design load (F_D). For simplicity, the system is assumed to have pinned VBE connections at the support. In order to design the infill panels within the single-story C-SPSW (R) system, it is assumed that a fraction of the total lateral design load ($\kappa_R F_D$) is resisted by the two infill panels within the SPSW piers, as shown in Figure 6.2b, and that the remaining portion of the load is carried by the frame action. Assigning a portion of the lateral load to the infill panels, the required thickness of the plate within each SPSW pier can be calculated using the following equation:

$$\frac{1}{2}\kappa_R F_D = \frac{1}{2} F_y L t \sin 2\alpha \tag{6.1}$$

where t and F_y are the thickness and yield strength of the infill panels, respectively. α is the tension field inclination angle estimated by the following equation proposed by Timler and Kulak (1983):

$$\tan^4(\alpha) = \frac{1 + \frac{tL}{2A_c}}{1 + \text{ th}\left(\frac{1}{A_b} + \frac{h^3}{360 I_c L}\right)} \tag{6.2}$$

Where h is the story height, L is the bay width, I_c is moment of inertia of the VBE, and $A_b$is the cross-sectional area of the HBE. It is important to note that the flexural rigidities of the HBE-to-VBE and CB-to-VBE connections in Figure 6.2b is removed; therefore, half of the load assigned to this system ($\frac{1}{2}\kappa_R F_D$) is resisted by each infill panel. Equations (6.3) and (6.4) give the vertical and horizontal components, respectively, of the web plate yielding along HBEs (Bruneau et al. 2011).

$$\omega_v = F_y t \cos^2\alpha \tag{6.3}$$

$$\omega_h = \frac{1}{2} F_y t \sin 2\alpha \tag{6.4}$$

Substituting Eq. (6.4) into Eq. (6.1) results in:

$$\kappa_R F_D = 2\omega_h L \tag{6.5}$$

On the other hand, equating internal and external work, and assuming the desirable yield mechanism for the system, as shown in Figure 6.2c, the plastic lateral strength of the system can be expressed as:

$$F_p H = 2\omega_h LH + 4M_{HBE} + 2M_{CB} \tag{6.6}$$

where H is the height of the system, and M_{CB} and M_{HBE} are the plastic flexural strength of the coupling beams and HBEs, respectively. For preliminary purposes, it is assumed that the coupling beams are proportioned based on the size of the HBEs, and the parameter λ is defined as:

$$\lambda = \frac{Z_{CB}}{Z_{HBE}} = \frac{M_{CB}}{M_{HBE}} \tag{6.7}$$

Substituting λ in Eq. (6.6), the expression for plastic lateral strength of the system takes the following format:

$$F_p H = 2\omega_h LH + 2M_{HBE}(2 + \lambda) \tag{6.8}$$

On the other hand, as discussed by Vian and Bruneau (2005), in order to prevent HBEs from developing in-span plastic hinges, which can lead to undesirable plastic mechanism, these elements should be proportioned for a flexural strength given by Eq. (6.9).

$$M_{HBE} = \frac{1}{4}\omega_v L^2 \times \frac{\eta}{1 + \sqrt{1 - \eta^2}} \tag{6.9}$$

In this equation, η is the plastic section modulus reduction ratio in cases where reduced beam section (RBS) connections are used, and is defined as:

$$\eta = \frac{Z_{RBS}}{Z} \tag{6.10}$$

where Z_{RBS} and Z are the plastic section modulus of the reduced section and the full section, respectively. Substituting Eq. (6.9) into Eq. (6.8), the lateral load resistance of the system is given by:

$$F_p = 2\omega_h L + \frac{\omega_v L^2}{2H}(2+\lambda)\frac{\eta}{1+\sqrt{1-\eta^2}} \tag{6.11}$$

Given the expressions presented earlier in this section (Equations 6.3 and 6.4), the vertical and horizontal components of the tension field forces on the HBEs are related by:

$$\omega_v = \omega_h \cot\alpha \tag{6.12}$$

Substituting Eq. (6.12) into Eq. (6.11), the plastic lateral strength of the system can be rewritten as:

$$F_p = 2\omega_h L + \frac{(2+\lambda)}{2H}\frac{\eta}{1+\sqrt{1-\eta^2}}\,\omega_h L^2 \cot\alpha$$

$$= 2\omega_h L\left[1 + \frac{(2+\lambda)}{4}\frac{L}{H}\cot\alpha \times \frac{\eta}{1+\sqrt{1-\eta^2}}\right] \tag{6.13}$$

Substituting Eq. (6.5) into Eq. (6.13), the expression for the plastic strength of the single-story C-SPSW (R) takes the following format:

$$F_p = \kappa_R F_D\left[1 + \frac{(2+\lambda)}{4}\frac{L}{H}\cot\alpha \times \frac{\eta}{1+\sqrt{1-\eta^2}}\right] \tag{6.14}$$

The structural overstrength of the C-SPSW (R) system (Ω_R) can be written as:

$$\Omega_R = \frac{F_P}{F_D} \tag{6.15}$$

Substituting Eq. (6.14) into Eq. (6.15) yields the expression for the overstrength of the single-story C-SPSW (R) system.

$$\Omega_R = \kappa_R\left[1 + \frac{(2+\lambda)}{4}\frac{L}{H}\cot\alpha \times \frac{\eta}{1+\sqrt{1-\eta^2}}\right] \tag{6.16}$$

An optimum design for lateral load resistance is achieved by setting the overstrength of the system equal to unity. Solving for κ_R, an equation is derived for

$\kappa_{optimum}$ indicating the percentage of the design lateral load that should be assigned to the infill panels to achieve the optimum design of a single-story C-SPSW (R) system.

$$\kappa_{optimum\ (R)} = [1 + \frac{(2+\lambda)}{4}\frac{L}{H}\cot\alpha \times \frac{\eta}{1+\sqrt{1-\eta^2}}]^{-1} \quad (6.17)$$

Note that for a typical C-SPSW system, $\kappa_{optimum}$ is a function of a series of parameters including the relative strengths of coupling beams and HBEs, the infill panel aspect ratio, and reduced beam section properties, as well as the tension field inclination angle. It should be mentioned that the coupling beam is assumed to be long enough to develop flexural plastic hinges rather than shear hinges. As suggested by Borello and Fahnestock (2012), the classification of AISC (2010) and CSA-S16 (2014) for eccentrically braced frame (EBF) links can be used for the coupling beams. According to this classification, when the CBs are longer than $2.6M_p/V_p$ they develop plastic hinges dominated by flexure. In cases where no RBS connection is used; $\eta = 1$ and Eq. (6.17) takes the following format:

$$\kappa_{optimum\ (R)} = [1 + \frac{(2+\lambda)}{4}\frac{L}{H}\cot\alpha]^{-1} \quad (6.18)$$

Assuming that the coupling beams and HBEs are of the same size (i.e., $\lambda = 1$), Figure 6.3a shows the variation of $\kappa_{optimum\ (R)}$ (Eq. 6.18) for the typical range of tension field angles (α) and infill panel aspect ratios within the SPSW piers. According to these graphs, a smaller portion of the design lateral load is assigned to the infill panels for larger infill panel aspect ratios. In other words, the contribution of the frame strength (due to the moment-resisting actions of the CB-to-VBE and HBE-to-VBE connections) to the global lateral load resistance becomes greater as the panel aspect ratio increases. Figure 6.3b illustrates the relationship between $\kappa_{optimum(R)}$ and η for various values of the infill panel aspects ratio in cases where RBS connections are used.

6.2.1.2. **Single-Story C-SPSW (P)**

Figure 6.4 shows a single-story C-SPSW system with pinned HBE-to-VBE connections, subjected to lateral design load. Following the procedure used in the previous sub-section, assigning a portion of the lateral load to the infill panels (Figure 6.4b), the required thickness of the plate within each SPSW pier in a single-story C-SPSW (P) can be calculated using the following equation:

$$\frac{1}{2}\kappa_P F_D = \frac{1}{2} F_y L t \sin 2\alpha \tag{6.19}$$

It is recalled that the flexural rigidity of the CB-to-VBE connections in Figure 6.4b is removed; therefore, half of the load assigned to this system ($\frac{1}{2}\kappa_P F_D$) is resisted by each infill panel. Using the procedure described above for C-SPSW (R) results in the same equations for C-SPSW (P)—i.e., Eqs. (6.3), (6.4) and (6.5). Considering the desirable plastic mechanism shown in Figure 4.c, and equating the internal and external work, the plastic strength of the system can be expressed as:

$$F_p H = 2\omega_h L H + 2M_{CB} \tag{6.20}$$

As was assumed in the previous section, the coupling beams are proportioned based on the size of the HBEs. Substituting Eq. (6.7) into Eq. (6.20), the expression for lateral load resistance of the C-SPSW (P) system takes the following format:

$$F_p H = 2\omega_h L H + 2M_{HBE}\lambda \tag{6.21}$$

Since the HBEs are pinned to the VBEs within each SPSW pier, they act as simply supported beams. As such, the minimum flexural strength required for these elements to resist tension field forces is calculated as:

$$M_{HBE} = \frac{1}{8}\omega_v L^2 \tag{6.22}$$

Substituting Eq. (6.22) into Eq. (6.21), the plastic strength of the system is given by:

$$F_p = 2\omega_h L + \lambda \frac{\omega_v L^2}{4H} \tag{6.23}$$

Considering the relation between the horizontal and vertical components of the tension field (Equation 6.12), the equation of plastic lateral strength can be rewritten as:

$$F_p = 2\omega_h L + \frac{\lambda}{4H}\omega_h L^2 \cot\alpha = 2\omega_h L[1 + \frac{\lambda}{8}\frac{L}{H}\cot\alpha] \quad (6.24)$$

Substituting Eq. (6.5) into Eq. (6.24), the expression of the plastic strength takes the following format:

$$F_p = \kappa_P F_D[1 + \frac{\lambda}{8}\frac{L}{H}\cot\alpha] \quad (6.25)$$

Substituting Eq. (6.25) into Eq. (6.15) yields the following equation for the overstrength of the single-story C- SPSW (P) system:

$$\Omega_P = \kappa_P[1 + \frac{\lambda}{8}\frac{L}{H}\cot\alpha] \quad (6.26)$$

By setting the overstrength of the system equal to unity, the following equation is derived for the percentage of the lateral design force that should be assigned to the infill panels to achieve an optimum design of C-SPSW (P):

$$\kappa_{optimum(P)} = [1 + \frac{\lambda}{8}\frac{L}{H}\cot\alpha]^{-1} \quad (6.27)$$

Assuming a constant value of 45° for the tension field angle in all cases, Figure 6.5 shows the variation of $\kappa_{optimum}$ for different values of λ and infill panel aspect ratios for the two types of C-SPSWs discussed in this research. As expected, since the boundary frames within C-SPSW (P) do not contribute to the lateral load resistance, a larger portion of the design lateral load is assigned to the infill panels within such a system than in C-SPSW (R). For example, for an infill panel aspect ratio equal to unity (L/H=1), when the flexural strength of the coupling beam is selected twice that of the HBEs, 50% and 80% of the lateral design load is assigned to the infill panels within the C-SPSW (R) and C-SPSW (P) systems, respectively.

Obviously, the values of $\kappa_{optimum}$ decrease as the flexural strength of the coupling beam increases, resulting in a larger contribution of moment-resisting

action to the overall strength of the systems. Also, $\lambda = 0$ represents the cases in which the pair of SPSWs is uncoupled.

6.2.2 Multi-Story C-SPSW Systems

The expressions derived for single-story C-SPSW (R) and C-SPSW (P) are extended to more complex cases of multi-story systems in the following sub-sections.

6.2.2.1. Multi-Story C-SPSW (R) Systems

Figure 6.6a shows a multi-story C-SPSW with moment-resisting frames subjected to lateral design loads. It is assumed here that these lateral forces are modified so that a portion of the total load at each story level is assigned to the infill plates, as illustrated in Figure 6.6b. κ_{Ri} represents the percentage of the design lateral load assigned to the infill panel at story level i. Note that the flexural rigidities of all connections are removed in Figure 6.6b so that the modified lateral loads are essentially resisted through the tension field action of the infill panels within each SPSW pier, and the corresponding story shears are used to size the plates.

For any story level in frame (b), shown in Figure 6.6, the story shear is resisted by the horizontal components of the tension fields in fully yielded infill plates within the two SPSW piers. The corresponding equations for two consecutive stories (i) and (i+1) can be written as:

$$2\omega_{h(i)}L = \sum_{j=i}^{n} \kappa_{Rj} F_{Dj} \tag{6.28}$$

$$2\omega_{h(i+1)}L = \sum_{j=i+1}^{n} \kappa_{Rj} F_{Dj} \tag{6.29}$$

Subtracting Eq. (6.29) from Eq. (6.28) yields the modified lateral force assigned to story level (i) (Figure 6.7):

$$2(\omega_{h(i)}L - \omega_{h(i+1)})L = \kappa_{Ri} F_{Di} \tag{6.30}$$

Considering an intermediate floor along the height of the C-SPSW (R) system for the assumed uniform plastic mechanism (Figure 6.6c and Figure 6.8), and employing principles of virtual work, the following expression is derived by equating the internal and external work tributary to this floor:

$$F_{Pi}h_i = 2\left(\omega_{h(i)} - \omega_{h(i+1)}\right)Lh_i + 4M_{HBEi} + 2M_{CBi} \tag{6.31}$$

It should be noted that Eq. (6.30) is also valid for the top HBEs by setting $\omega_{h(i+1)} = 0$. As previously defined for a single-story system, parameter λ_i, representing the relative flexural strengths of the CB and HBEs at floor level (i) in a multi-story C-SPSW, is given by:

$$\lambda_i = \frac{M_{CBi}}{M_{HBEi}} \tag{6.32}$$

Substituting λ_i into Eq. (6.31) results in following equation:

$$F_{Pi}h_i = 2\left(\omega_{h(i)} - \omega_{h(i+1)}\right)Lh_i + 2M_{HBEi}(2 + \lambda_i) \tag{6.33}$$

In order to prevent the formation of in-span plastic hinges in HBEs, these elements are required to have a minimum flexural strength given by Equation 6.34 (Vian and Bruneau 2005):

$$M_{HBEi} = \frac{1}{4}\left(\omega_{v(i)} - \omega_{v(i+1)}\right)L^2 \times \frac{\eta}{1 + \sqrt{1 - \eta^2}} \tag{6.34}$$

Substituting Eq. (6.34) into Eq. (6.33) and solving for F_{Di} results in the following expression:

$$F_{Pi} = \kappa_{Ri}F_{Di}\left[1 + \frac{(2 + \lambda_i)}{4}\frac{L}{h_i}\cot\alpha_i \times \frac{\eta}{1 + \sqrt{1 - \eta^2}}\right] \tag{6.35}$$

An optimum design is achieved by setting $F_{Pi} = F_{Di}$; therefore, the corresponding value for $\kappa_{optimum(R)i}$ is obtained as:

$$\kappa_{optimum(R)i} = \left[1 + \frac{(2 + \lambda_i)}{4}\frac{L}{h_i}\cot\alpha_i \times \frac{\eta}{1 + \sqrt{1 - \eta^2}}\right]^{-1} \tag{6.36}$$

Assigning a percentage of the lateral design force (corresponding to the optimum design case estimated by Equation 6.36) to the infill panels at each story level ($\kappa_{optimum(R)i}F_{Di}$), the steel plates within each SPSW pier are sized to resist half of the modified design story shear.

6.2.2.2. **Multi-Story C-SPSW (P) Systems**

In the case of C-SPSW (P) configuration, since the HBEs are pin-connected to the VBEs, the boundary frames within the SPSW piers do not contribute to the lateral load resistance, and the story shear is essentially resisted by the tension field actions of the infill panels and moment-resisting action of the CB-to-VBE connections. Following the same procedure used in previous section, and considering an intermediate floor of the C-SPSW (P) system in mechanism condition, as shown in Figure 6.9, the equation of the virtual work tributary to this floor can be expressed as:

$$F_{Pi}h_i = 2\left(\omega_{h(i)} - \omega_{h(i+1)}\right)Lh_i + 2M_{CBi} \tag{6.37}$$

Since the HBEs within each SPSW pier act as simply supported beams, they need to be proportioned for a flexural strength given by:

$$M_{HBEi} = \frac{1}{8}\left(\omega_{v(i)} - \omega_{v(i+1)}\right)L^2 \tag{6.38}$$

Substituting Eqs. (6.32) and (6.38) into Eq. (6.37) and setting $F_{Pi} = F_{Di}$ result in the following expression for the C-SPSW (P) systems:

$$\kappa_{optimum(P)i} = \left[1 + \frac{\lambda_i}{8}\frac{L}{h_i}\cot\alpha_i\right]^{-1} \tag{6.39}$$

Note that, since reduced beam section (RBS) HBE-to-VBE connections are not feasible for the C-SPSW (P) systems, the term η does not appear in the expressions of $\kappa_{optimum(i)}$ for such systems. Figure 6.10 shows a comparison between the percentages of the design story shear assigned to the infill panels in the two types of C-SPSW systems according the optimum design expressions presented in this section (Equations 6.36 and 6.39). For comparison purpose, four 4-story C-SPSWs

were considered along with two cases of uncoupled SPSWs with simple and moment-resisting boundary frames for comparison purposes. Two different cases were considered for the C-SPSW systems as follows: (1) the coupling beam and HBEs at each floor level were of the same size (i.e., λ=1); and (2) plastic section modulus of the coupling beam was twice that of the HBEs at each floor level (i.e., λ=2).

An infill panel aspect ratio of L/H=1 and a constant tension field inclination angel of $\alpha = 45^{\circ}$ were assumed for all cases. Also, an inverted triangular lateral load distribution was employed to distribute the lateral load along the height of the systems. Obviously, 100% of the story shears were assigned to the infill plates in the uncoupled pair of SPSWs with simple boundary frames, herein referred to as Uncoupled (P). As an example, consider the first story of C-SPSWs in which the coupling beams and HBEs were of the same size ($\text{i.e.}, \lambda_i = 1$). The optimum designs were achieved by assigning 78% and 95% of the story shears to the infill panels in the C-SPSW (R) and C-SPSW (P) systems, respectively. Also, in the case of uncoupled SPSWs with moment-resisting boundary frames, referred to as Uncoupled (R), 84% of the design story shear was assigned to the infill panels. By doubling the flexural strength of the coupling beams, the story shears assigned to the infill plates were reduced by 5% and 7% in the C-SPSW (R) and C-SPSW (P) systems, respectively.

6.3 Design of Boundary Frame Elements and Coupling Beams

Once the infill plates are sized using the modified design forces corresponding to the optimum design cases presented in previous section, the boundary frame elements within each SPSW pier are designed according to capacity design procedures assuming the uniform plastic mechanism for the system, as shown in Figure 5c. As in the conventional SPSWs, the HBEs within a C-SPSW (R) must be designed to resist the tension field forces generated by the infill panels while allowing the development of plastic hinges at their ends. As discussed in prior sections, in order to prevent the formation of in-span plastic hinges along HBEs

within the C-SPSW (R) and C-SPSW (P) systems, these elements must be proportioned to resist bending moments of $\frac{1}{4}\omega_v L^2$ and $\frac{1}{8}\omega_v L^2$, respectively (ω_v representing the resultant vertical component of the tension field acting above and below a given HBE).

On the other hand, unlike those in the conventional planar SPSWs, the VBEs within each SPSW pier of a C-SPSW system are not identical due to the coupling actions, which result in different demands on the internal and external VBEs. However, the code requirements for VBEs in the conventional SPSWs (CSA S16 2014 and AISC 2010) are valid for both the internal and external VBEs in C-SPSWs, where these elements must remain essentially elastic, with the exception of inelastic deformations that are allowed at their bases to develop the desirable sway plastic mechanism. As such, the internal VBEs in a C-SPSW (R) must be designed to withstand the combined effects of flexural, axial and shear demands resulting from the tension field actions of the infill panels and the moment-resisting actions of the boundary frame and CB-to-VBE connections. Assuming that the desirable uniform plastic mechanism in the C-SPSW (R) system is formed, the shear forces resulting from the formation of plastic hinges at the ends of HBEs and coupling beams act in opposite directions. While the shear forces induced by the coupling beams work to reduce the overall axial demands on the internal VBEs, their plastic moments are additive to the local flexural demands imposed by the HBEs. However, the capacity design forces and moments in the external VBEs in such systems are calculated in the same manner as used for VBEs in the conventional SPSWs.

On the other hand, since the HBEs in a C-SPSW (P) are pin-connected to the VBEs, ideally they do not impose flexural demands on these elements. Therefore, considering a uniform plastic mechanism for such a system, the axial and flexural demands on the internal VBEs result primarily from the yielding of the infill panels and plastic hinging of the coupling beams. Obviously, the additional

demands due to the frame actions are not present in the capacity design forces of the external VBEs in a C-SPSW (P).

As discussed above, the capacity design procedures outlined in current seismic design provisions for conventional SPSWs (AISC 2010 and CSA S16 2014) can be extended to design the boundary frame elements in both C-SPSW configurations discussed in this research. Detailed discussions of the capacity design procedures for the HBEs and VBEs can be found elsewhere (Berman and Bruneau 2008; Qu and Bruneau 2009; Bruneau et al. 2011).

For preliminary purposes, the coupling beams are proportioned based on the size of HBEs at each floor level considering the parameter λ, which reflects the strength of the CBs relative to the HBEs (Equation 6.32). As illustrated in Figure 6.5, the variation of λ values has substantial impacts on the relative contributions of the infill panels and frame actions to the lateral load resistance of the C-SPSW systems. In addition, the level of coupling between the two SPSW piers is directly related to the strength of the coupling beams (Borello and Fahnestock 2012), which is described in detail in the next section.

Once the boundary frame elements and the coupling beams are selected, the plate thicknesses may be revised in order to avoid unnecessary overstrength in the system, and to ensure that the assumed plastic mechanism will form. The inherent overstrength in the SPSW systems is to some extent inevitable, partly because the calculated plate thicknesses needed to resist design story shear can be impractical due to unavailability or welding and handling requirements. Therefore, thicker infill plates are usually selected by the design engineer, resulting in heavier boundary elements. However, where practicable, attempts can be made to minimize unnecessary overstrength by updating the plate thicknesses, boundary frame elements and coupling beams. The principle of virtual work (Neal 1977) can be used herein to calculate the overall strength due to the frame action and the remaining portion of the story shear to be resisted by the infill plates at the *i*-th story (V_i). Hence, the initial plate thicknesses are updated using V_i at each story level,

calculated from Equations (6.40) and (6.41) for the C-SPSW (R) and C-SPSW (P) systems, respectively:

$$\left(\sum_{i=1}^{n} F_i h_i\right) = 2M_{VBE\,(Ext)} + 2M_{VBE(Int)} + 4\sum_{i=1}^{n} M_{HBEi} + 2\sum_{i=1}^{n} M_{CBi} + \sum_{i=1}^{n} V_i h_{si} \tag{6.40}$$

$$\left(\sum_{i=1}^{n} F_i h_i\right) = 2M_{VBE\,(Ext)} + 2M_{VBE(Int)} + 2\sum_{i=1}^{n} M_{CBi} + \sum_{i=1}^{n} V_i h_{si} \tag{6.41}$$

where $M_{VBE\,(Ext)}$ and $M_{VBE(Int)}$ are the plastic moments at the bases of the external and internal VBEs, respectively; h_{si} is the height of the *i*-th story; h_i is the elevation of the *i*-th floor; and M_{HBEi} and M_{CBi} are, respectively, the plastic moments of the HBEs and coupling beam at level *i*. Subsequently, the boundary frame elements can be revised to optimize the design.

6.4 Degree of Coupling and Lateral Load Resistance in C-SPSWs

In coupled wall systems, the degree of coupling (DC) is defined as the fraction of the total overturning moment that is resisted by the coupling action (CSA A23.3 1994; Chaallal et al. 1996). The coupling mechanism in a C-SPSW is formed by the net axial forces within the two SPSW piers when the system undergoes a lateral displacement. The degree of coupling of a C-SPSW, which reflects the level of interaction between the two SPSW piers, is expressed as follows (Borello and Fahnestock 2012):

$$DC = \frac{M_{Coupling}}{M_{Total}} = \frac{M_{Coupling}}{\sum M_{VBE} + \sum M_{Pier} + M_{Coupling}} \tag{6.42}$$

In a typical C-SPSW system, the total overturning moment is resisted through three different mechanisms, namely: (1) the flexure of each individual VBE (M_{VBE}), (2) couples formed by the opposite axial forces of internal and external VBEs within each SPSW pier (M_{Pier}), and (3) a couple formed by the net axial force of each shear wall pier ($M_{Coupling}$). Assuming a uniform sway plastic mechanism, and considering the contribution of each of the above-mentioned components to the

overall overturning resistance, Borello and Fahnestock (2012) derived the following analytical expression for the degree of coupling of C-SPSWs with moment-resisting boundary frames:

$$DC = \frac{\sum_{i=1}^{n} \frac{2M_{CB_i}}{e}(L+e)}{2M_{IVBE} + 2M_{EVBE} + \sum_{i=1}^{n}[4M_{HBE_i} + 2M_{CB_i} + F_y h_i L\,(t_i \sin(2\alpha_i) - t_{i+1}\sin(2\alpha_{i+1}))]} \quad (6.43)$$

where, t and F_y are the thickness and yield strength of the infill panels; M_{IVBE} and M_{EVBE} are plastic moments of the internal and external VBEs, respectively; L is the width of the SPSW piers; e is the coupling length; h_i is the elevation of the *i*-th floor level; and α is tension field inclination angle as defined in Eq. (6.2). The DC equation indicates that this metric is a function of a series of parameters including coupling length (e), infill plate thicknesses, and the flexural strengths of the HBEs, VBEs and CBs.

It is noteworthy that the denominator in Eq. (6.43) indicates the total internal work done by the inelastic deformations of elements in the system. By equating the amount of external work to the internal work, Borello and Fahnestock (2012) presented the following equation for the ultimate strength of C-SPSWs with moment resisting boundary frames:

$$\sum_{i=1}^{n} F_i h_i = 2M_{IVBE} + 2M_{EVBE} + \sum_{i=1}^{n}[2M_{CB_i} + 4M_{HBE_i} + F_y h_i L\,(t_i \sin(2\alpha_i) - t_{i+1}\sin(2\alpha_{i+1}))] \quad (6.44)$$

The above expressions were validated against numerical results by the researchers, and were used in a comprehensive parametric study to investigate the impact of coupling on the behaviour and efficiency of C-SPSWs. It was suggested by the authors that the C-SPSW systems should be designed for a DC range between 0.4 and 0.6 to achieve the optimum material efficiency.

In the C-SPSW (P) systems, however, since simple HBE-to-VBE connections are used, the HBEs do not contribute to the internal work; therefore, the expressions of the DC for such systems take the following format:

$$DC = \frac{\sum_{i=1}^{n} \frac{2M_{CB_i}}{e}(L+e)}{2M_{IVBE} + 2M_{EVBE} + \sum_{i=1}^{n}[2M_{CB_i} + F_y h_i L\,(t_i \sin(2\alpha_i) - t_{i+1}\sin(2\alpha_{i+1}))]} \tag{6.45}$$

Also, the lateral load resistance of the C-SPSW (P) systems can be estimated using the following equation:

$$\sum_{i=1}^{n} F_i h_i = 2M_{IVBE} + 2M_{EVBE} + \sum_{i=1}^{n}[2M_{CB_i} + F_y h_i L\,(t_i \sin(2\alpha_i) - t_{i+1}\sin(2\alpha_{i+1}))] \tag{6.46}$$

Equations (6.43) through (6.46) can be used to facilitate the design process when proportioning C-SPSWs for desired levels of coupling and lateral load resistance.

6.5 Case Study Designs

In order to evaluate the seismic performances of the two C-SPSW options discussed in this research, and to verify the validity of the proposed design approach, 8- and 12-story buildings were considered. The hypothetical buildings under consideration were assumed to be located on firm soil (site class D) in Los Angeles, California. The buildings had four identical C-SPSWs in each direction; thus, each system was assumed to resist one-quarter of the total seismic load (torsion neglected). Both the 8- and 12-story model buildings were designed with the C-SPSW (P) and C-SPSW (R) systems. In addition, two uncoupled pairs of SPSWs were designed for the purpose of comparison. The plan layout, which was adopted with slight modification from Gupta and Krawinkler (1999), and elevations of the C-SPSW systems are shown in Figure 6.11. As shown, the SPSW piers were assumed to be 3.5-m-wide, linked by 3 m coupling beams at floor levels. The seismic masses, dead loads and live loads were the same as those considered in Chapter 5. To allow comparison between the seismic performances of the two C-SPSW options on a consistent basis, attempts were made to achieve the same level of coupling in all C-SPSW designs. As assumed in prior sections, the coupling beams were proportioned based on the size of HBEs at each floor level. Note that for comparison purposes and to preclude the overstrength due to unavailability of the required plate sizes, the calculated plate thicknesses were used in all designs in lieu of

commercially available plate thickness. Summaries of the designs for the 8- and 12-story systems are presented in Tables 6.1 and 6.2, respectively. As expected, the internal VBEs in both the C-SPSW (P) and C-SPSW (R) systems were substantially lighter than the external VBEs. This is primarily due to the coupling action, which greatly reduces the axial demands on the internal VBEs. In addition, since the external VBEs were designed to carry additional axial loads due to gravity, larger sections were required for these elements, even in the uncoupled walls. Note that the VBEs in both the C-SPSW (P) and C-SPSW (R) systems were generally lighter than those in uncoupled SPSWs, especially in the 12-story buildings.

6.5.1 System Overstrength and Degree of Coupling

As mentioned earlier, the degree of coupling (DC), which quantifies the level of coupling between the two SPSW piers, allows for the comparison of the two different C-SPSW options on a consistent basis. As such, the design process sought to achieve the same levels of DC as well as lateral load resistance for both types of C-SPSWs studied in this research. The analytical expressions presented in the previous section (i.e., Eqs. 6.43 through 6.46) were used to estimate the degree of coupling and overall strength of the C-SPSW systems considered in this study. The resulting values are presented in Table 6.3.

Although the expressions presented for optimum design cases (i.e., Eqs. 6.36 and 6.39) were derived by setting the system overstrength equal to unity, the prototype designs possessed slight overstrengths. As described in Chapter 5, this overstrength arose from the resistance factor ($\Phi = 0.9$) used for steel in the design process. It should be noted that the overstrength values given in Table 6.3 are consistent with those of the SPSW-O systems presented in Chapter 4.

6.5.2 Nonlinear Analyses

A series of pushover and nonlinear response history analyses were conducted to evaluate and compare the seismic performances of the case studies designed using the proposed design procedure presented earlier. The C-SPSW systems were

modelled using the dual strip models described in previous chapters. The infill plates within each of the SPSW piers were represented by 13 inclined pin-ended tension-only members oriented in each direction. The coupling beams, HBEs and VBEs were modeled using regular frame elements in which fiber axial-flexural plastic hinges were defined to capture inelastic deformations. All other modelling assumptions were the same as those used in previous chapters.

The strip model of an 8-story C-SPSW is shown in Figure 6.12 (P-Delta column not shown). The case study structures were nonlinearly analysed under a suite of 20 earthquake acceleration time-histories with a 10% probability of exceedance in 50 years (Somerville et al. 1997). Rayleigh damping and P-Delta effects were incorporated into the models and seismic masses were lumped at floor levels. Nonlinear dynamic equations were solved using the direct integration method in SAP2000. Furthermore, pushover analyses of the systems were performed employing the lateral force distribution pattern used in the design for the purpose of comparison.

6.5.2.1. **Fundamental Period and Inelastic Drift Demands**

Table 6.4 shows the calculated fundamental periods of the systems, and the mean peak story drifts obtained from nonlinear response history analyses of 20 earthquake ground motions. As shown, the fundamental periods of the C-SPSW systems were generally smaller than those of the uncoupled SPSW, indicating a higher elastic stiffness in such systems. Considering the pushover curves shown in Figure 6.13, it appears that the C-SPSW (P) and C-SPSW (R) systems, which were designed for the same level of coupling, exhibited similar initial stiffnesses in both the 8- and 12-story buildings.

As shown, the coupling action substantially increased the elastic stiffness of the walls, especially in the 12-story systems. Since the coupling of the two SPSW piers helps reduce the cantilever bending component of the deformation, resulting in improved flexural stiffness of the system, the first yields (i.e., the point where

the pushover curves deviate from elastic region) in the C-SPSW systems occur at smaller roof drifts compared to that of the uncoupled walls (see Figure 6.13).

It is worth mentioning that the fundamental periods calculated herein are slightly higher than those reported by Borello and Fahnestock (2012) (e.g., 1.9 sec versus 1.6 sec for 12-story coupled SPSW). The slight differences are due to the fact that the C-SPSWs considered in their research were designed using code-prescribed force and response modification factors, resulting in significant overstrength and thus, smaller periods (a mean overstrength of 1.71 was reported by Borello and Fahnestock [2012]). In contrast, the C-SPSW systems designed herein were aimed at minimizing system overstrength, as shown in Table 6.3, in which the mean value is 1.1.

Figure 6.14 shows the mean values of the maximum story drifts over the height of the systems obtained from nonlinear response history analyses of the 20 earthquake excitations. As shown, the peak story drifts occur at upper stories in all systems due to the presence of higher vibration modes, especially in uncoupled SPSWs, in which these effects are more significant.

It is evident that both the C-SPSW (P) and C-SPSW (R) configurations were effective in limiting excessive drift demands (caused by overturning moments) in the upper stories by restraining the cantilever-type deformations in the systems. The analysis results indicate that the mean maximum drifts at several upper stories exceeded the 2% drift limit in both the 8- and 12-story uncoupled SPSWs, with the maximums of 2.32% and 2.41%, respectively (Table 6.4). In contrast, the mean maximum story drifts for all C-SPSWs were well within the 2% limit for the seismic hazard level considered in this research. Furthermore, the C-SPSW systems exhibited more uniform distributions of the story drifts compared to the uncoupled SPSWs, resulting in improved seismic performances. While both C-SPSW options performed well within the 2% limit, the C-SPSW (R) systems experienced more uniform responses in terms of drift, and appeared to be more effective in reducing the cantilever bending deformations in the upper stories. Both the 8- and 12-story C-SPSW (P) systems exhibited slightly larger drifts at upper stories compared to

the C-SPSW with rigid HBE-to-VBE connections. On the other hand, for both building heights, slightly larger drifts were observed at stories below mid-levels in the C-SPSW (R) systems than in the C-SPSW (P) systems.

6.5.2.2. **VBE Demands**

Figures 6.15 and 6.16 show the maximum axial force demands at the bases of the internal and external VBEs, respectively, observed during nonlinear response history analyses of the suite of 20 ground motions. As expected, the axial demands on the internal VBEs were significantly reduced due to the coupling action in the C-SPSW configurations, as compared to the cases of uncoupled walls. It should be noted that both C-SPSW options designed for the same level of coupling were comparably effective in reducing the large axial force demands in the internal VBEs. However, the internal VBEs within C-SPSW (P) systems experienced slightly larger axial demands in both the 8- and 12-story systems. Although the use of pinned HBE-to-VBE connections in the C-SPSW (P) configuration eliminated the demands due to the moment-resisting actions of the boundary frames, the thicker infill plates (compared to those in the C-SPSW (R) systems) used in such systems, on the other hand, resulted in increased VBE demands due to the tension field actions.

Figure 6.16 shows the maximum axial force demands at the base of external VBEs, obtained from response history analyses. Note that these axial demands were generally larger in the uncoupled walls than in C-SPSWs under the majority of earthquakes, for both the 8- and 12-story buildings. As shown in Tables 6.1 and 6.2, since the plate thicknesses in the C-SPSW (P) systems are very similar to those in the uncoupled SPSWs, the reduced axial demands in the external VBEs are primarily attributed to the use of pinned HBE-to-VBE connections in such systems. However, the reduction of axial demands in the external VBEs of the C-SPSW (R) systems was due in part to the thinner infill plates used in their design (compared to the plates used in uncoupled SPSWs), resulting in smaller tension field forces. In addition, since the HBEs in the C-SPSW (R) systems were slightly lighter than

those in the uncoupled walls, relatively smaller forces were imposed on the external VBEs by the frame action in such systems.

Table 6.5 presents the ratio of the mean maximum axial force demands at the base of the VBEs in C-SPSWs to those of the uncoupled SPSWs. When the pair of 8-story SPSWs were coupled (DC=0.3), overall axial force reductions of 45% and 51% were observed in the internal VBEs within the C-SPSW (P) and C-SPSW (R) configurations, respectively. However, when designed for the same level of coupling, the 12-story C-SPSW systems experienced relatively larger axial force reductions in their internal VBEs (i.e., 52% and 55%), compared to those in the 8-story systems. These slight differences may be attributed to the effects of higher modes in taller systems. The analysis results indicated that the reduction of axial force due to the coupling action was not affected by the height of the system in the external VBEs in both C-SPSW options.

Table 6.6 shows the ratios of maximum axial force demands at the base of the VBEs to those calculated using the capacity design method. As described earlier, in the capacity design of the VBEs within C-SPSWs, it was assumed that all infill panels yield at the same time and that plastic hinges form at the ends of the HBEs and coupling beams at all story levels. However, results of the nonlinear analyses indicate that the capacity design procedure results in conservative VBE designs, especially in the 12-story systems in which the assumed simultaneous yielding of all designated energy dissipating elements is unlikely, due to the presence of higher vibration modes. The mean maximum axial forces observed at the base of VBEs were approximately 80% and 70% of those calculated using capacity design of these elements in 8- and 12-story C-SPSW systems, respectively.

Figures 6.17 and 6.18 show the VBE lateral displacement profiles at the time of maximum roof drifts during earthquakes. It is evident that both C-SPSW configurations have effectively limited the excessive lateral deformations of the VBEs at the upper stories that are due primarily to the flexural mode of deformation of the walls. As such, the coupling of the walls results in more uniform VBE displacement profiles in both the 8- and 12-story systems.

6.5.2.3. **Plate Ductility Demands and Coupling Beam Rotations**

A summary of the mean values of the maximum plate ductility demands and coupling beam rotations is given in Table 6.7. The maximum plate ductility demand (μ_{max}) at a given story for each earthquake was calculated by dividing the maximum plastic elongation of a strip by its yield elongation, as described in Chapter 5.

The mean peak plate ductility demands in the C-SPSW systems were generally smaller than those of the uncoupled SPSWs for both the 8-story and 12-story buildings. The C-SPSW systems with moment-resisting boundary frames experienced slightly larger peak plate ductility demands compared to those with simple boundary frame connections. The largest peak ($\mu_{mean} = 5.0$) and smallest peak ($\mu_{mean} = 3.16$) plate ductility demands were observed in the 8-story uncoupled SPSWs and 12-story C-SPSW (P) systems, respectively.

Figure 6.19 shows the distributions of plate ductility demands along the heights of the systems. Note that higher vibrational modes imposed larger ductility demands on plates at the upper- and lower-level stories of the 12-story walls and, as shown, middle story levels experienced less ductility demands during earthquakes. The coupling actions generally decreased the plate ductility demands in the upper stories of both the 8- and 12-story systems. However, slightly increased ductility demands were observed in the lower stories of the 8-story C-SPSW (R) system.

Although both C-SPSW configurations were proportioned for the same overall strength as well as level of coupling, the ductility demands on their infill plates and their distribution patterns were slightly different. As shown, in the C-SPSW (R) systems, the peak plate ductility demand occurred in the second story for both the 8- and 12-story buildings; while in the C-SPSW (P) systems, the peak plate ductility demands occurred in the 7^{th} story and 11^{th} story for the 8- and 12-story buildings, respectively. Since the plate thicknesses used in the design of C-SPSW (P) and C-SPSW (R) systems, and consequently the relative contributions of the tension field

and frame actions, were different, the extent of inelastic deformation needed to dissipate the same amount of earthquake-induced energy was not the same.

It is noteworthy that the plate ductility demands and their distribution patterns observed herein are consistent with those reported by previous research (Berman 2011). The median plate ductility demands on the infill plates of the mid-rise SPSWs studied by Berman were all less than 5 under the 10/50 hazard level. In addition, the results of several past experimental research on SPSWs confirm that the ductility demands observed during the nonlinear analyses were within acceptable range. The 4-story SPSW tested by Driver et al. (1997) experienced an infill plate ductility of 9 prior to the failure of its first story column. Berman and Bruneau (2005) reported a ductility demand of 12 on the infill plate during the cyclic test of a single-story SPSW. In addition, 3-story SPSWs tested by Choi and Park (2008) experienced infill plate ductility of 11.7 prior to failure, which was governed by plate tearing.

Figure 6.20 shows the mean maximum inelastic rotations of the coupling beams experienced during earthquakes. The results of nonlinear analyses suggest that the rotation demands of the coupling beams to large extent follow the story drift distributions shown in Figure 6.14. As shown, the C-SPSW (R) systems exhibited more uniform CB rotation demand distributions (along the height) than the C-SPSW (P) systems in both the 8- and 12-story buildings. The CBs within the C-SPSW (P) systems generally experienced smaller inelastic rotations at stories below mid-height of the walls and exhibited larger rotation demands at stories above that, compared to those in the C-SPSW (R) systems. The peak CB rotation demands in the C-SPSW (P) systems were observed at the floor level immediately below the roof (i.e., 7^{th} and 11^{th} floors in 8- and 12-story walls, respectively). However, the coupling beams in the C-SPSW (R) systems experienced similar inelastic rotations at several upper stories.

It is noteworthy that the distributions of the inelastic rotation demands on the coupling beams observed herein are similar to those reported by Borello and Fahnestock (2012). It should also be noted that the mean maximum CB rotation

demands were well within the 0.02 (rad) limit associated with the 10/50 earthquake hazard level.

6.5.3 System Weight Comparison

Figures 6.21 and 6.22 show comparisons of steel weights for different elements of the 8- and 12-story systems, respectively. As shown, the C-SPSW configurations generally resulted in lighter systems compared to the uncoupled walls, with the C-SPSW (R) system being the lightest. The total steel weights of the 8- and 12-story C-SPSW (P) systems were respectively 92% and 90% of those of the uncoupled SPSWs. In the case of the C-SPSW (R) systems, the 8- and 12-story designs were respectively 14% and 16% lighter than the corresponding uncoupled walls.

Although the C-SPSW (R) cofiguration resulted in slighthy higher material efficiency in comparison with the C-SPSW (P) system, the fabrication costs associated with the higher number of moment-resisting connections (i.e., HBE-to-VBE connections) in such systems would likely offset or even outweigh the savings in steel tonnage.

6.6 Summary and Conclusion

The research presented in this chapter investigated two different coupled steel plate shear wall (C-SPSW) configurations, namely (1) coupled SPSWs with simple boundary frame connections (referred to as C-SPSW (P)); and (2) coupled SPSWs with moment-resisting boundary frame connections (referred to as C-SPSW (R)). A preliminary design procedure, which explicitly considers the frame moment-resisting actions, was developed for each of these C-SPSW systems, employing the principles of plastic analysis and capacity design. As such, the relative contributions of the frame actions—i.e., the moment-resisting actions of the CB-to-VBE and HBE-to-VBE connections—and tension field actions to the overall strength were quantified for the two C-SPSW configurations, and key design parameters were identified.

Eight- and 12-story case study C-SPSWs were designed according to the preliminary design procedure presented in this paper. A series of nonlinear static and response history analyses were carried out to investigate and compare the seismic behaviors of the C-SPSW configurations discussed in this study. The performances of the case study designs were evaluated in terms of story drifts, plate ductility demands, coupling beam rotations and VBE demands. The results of nonlinear analyses indicated that both C-SPSW configurations performed well under the seismic hazard representing the design-level earthquake, and were effective in limiting the excessive drift demands due to the overturning moments.

For both building heights, the two different C-SPSW configurations designed for the same level of coupling as well as overall strength were similarly effective in reducing the VBE axial force demands through the coupling actions. The degree of coupling (DC), which allows for the comparison of different C-SPSWs on a consistent basis, was recognized as an important factor influencing the behavioral characteristics of the systems. For the selected degree of coupling (DC=0.3), the mean maximum axial force demands at the bases of the internal and external VBEs in C-SPSWs were, respectively, approximately 50% and 90% of those in the corresponding uncoupled walls. These reduced axial forces allow for the use of lighter VBE sections, especially the internal ones. Furthermore, the capacity design procedure used for the VBEs within both the C-SPSW (P) and C-SPSW (R) systems resulted in conservative designs for these elements, especially in the 12-story buildings.

The C-SPSW configurations generally reduced plate ductility demands at the upper stories of the systems; however, slightly increased ductility demands were observed in the infill plates at the lower stories of the 8-story C-SPSW (R) system. The plate ductility demands in all C-SPSW designs were well within the acceptable limits reported in previous experimental and analytical studies (e.g., Driver et al. 1997; Berman 2011). Also, the nonlinear rotation demands on the coupling beams were all within the 0.02 radians limit under the design-level earthquakes (i.e., earthquake with a 10% probability of exceedance in 50 years). The distributions of

these rotation demands along the height of the systems were, to a large extent, similar to those of the drift demands.

This research expanded the current knowledge of the behavior and design of C-SPSWs through rational design procedures that acknowledge the fact that coupled SPSWs are inherently dual systems in which a substantial portion of the overall lateral load resistance is provided by the frame actions. Furthermore, an exploration of the potential to improve the economics of the C-SPSWs systems through the use of simple boundary frame connections was presented. However, while both C-SPSW options discussed in this research were found to be effective in achieving the design objectives with comparable seismic performances under the considered earthquake hazard, further experimental and analytical research is warranted to support the findings of this research.

Table 6.1: Summary of the designs for 8-story systems

Uncoupled SPSWs				
Story	Plate (mm)	HBE	VBE (int)	VBE (ext)
1	4.57	W18×46	W14×370	W14×426
2	4.47	W18×46	W14×370	W14×426
3	4.23	W18×46	W14×283	W14×311
4	3.94	W18×46	W14×283	W14×311
5	3.51	W18×46	W14×193	W14×233
6	3.00	W18×46	W14×193	W14×233
7	2.32	W18×46	W14×120	W14×132
8	1.48	W18×55	W14×120	W14×132

C-SPSW (P)					
Story	Plate (mm)	HBE	CB	VBE (int)	VBE (ext)
1	4.74	W18×46	W18×76	W14×311	W14×398
2	4.64	W18×46	W18×76	W14×311	W14×398
3	4.40	W18×46	W18×76	W14×233	W14×311
4	4.09	W18×40	W18×71	W14×233	W14×311
5	3.65	W18×40	W18×71	W14×176	W14×193
6	3.11	W18×40	W18×71	W14×176	W14×193
7	2.41	W18×40	W18×71	W14×109	W14×99
8	1.54	W18×40	W18×71	W14×109	W14×99

C-SPSW (R)					
Story	Plate (mm)	HBE	CB	VBE (int)	VBE (ext)
1	3.86	W18×40	W18×71	W14×257	W14×370
2	3.78	W18×40	W18×71	W14×257	W14×370
3	3.59	W18×40	W18×71	W14×211	W14×283
4	3.34	W18×40	W18×71	W14×211	W14×283
5	2.98	W18×40	W18×71	W14×176	W14×193
6	2.55	W18×40	W18×71	W14×176	W14×193
7	1.98	W18×40	W18×71	W14×120	W14×120
8	1.26	W18×46	W18×76	W14×120	W14×120

Table 6.2: Summary of the designs for 12-story systems

Uncoupled SPSWs				
Story	Plate (mm)	HBE	VBE (int)	VBE (ext)
1	5.85	W18×55	W14×605	W14×665
2	5.79	W18×55	W14×605	W14×665
3	5.69	W18×55	W14×605	W14×665
4	5.44	W18×55	W14×455	W14×500
5	5.23	W18×55	W14×455	W14×500
6	4.96	W18×55	W14×455	W14×500
7	4.56	W18×50	W14×311	W14×342
8	4.16	W18×50	W14×311	W14×342
9	3.70	W18×50	W14×311	W14×342
10	3.10	W18×50	W14×159	W14×176
11	2.41	W18×50	W14×159	W14×176
12	1.57	W18×55	W14×159	W14×176

C-SPSW (P)					
Story	Plate (mm)	HBE	CB	VBE (int)	VBE (ext)
1	5.92	W18×50	W18×97	W14×455	W14×665
2	5.87	W18×50	W18×97	W14×455	W14×665
3	5.77	W18×50	W18×97	W14×455	W14×665
4	5.52	W18×50	W18×97	W14×342	W14×500
5	5.31	W18×50	W18×97	W14×342	W14×500
6	5.04	W18×50	W18×97	W14×342	W14×500
7	4.63	W18×46	W18×86	W14×257	W14×311
8	4.23	W18×46	W18×86	W14×257	W14×311
9	3.76	W18×46	W18×86	W14×257	W14×311
10	3.14	W18×40	W18×76	W14×145	W14×145
11	2.46	W18×40	W18×76	W14×145	W14×145
12	1.60	W18×40	W18×76	W14×145	W14×145

C-SPSW (R)					
Story	Plate (mm)	HBE	CB	VBE (int)	VBE (ext)
1	4.93	W18×46	W18×86	W14×398	W14×605
2	4.89	W18×46	W18×86	W14×398	W14×605
3	4.80	W18×46	W18×86	W14×398	W14×605
4	4.60	W18×46	W18×86	W14×311	W14×455
5	4.43	W18×46	W18×86	W14×311	W14×455
6	4.20	W18×46	W18×86	W14×311	W14×455
7	3.87	W18×46	W18×86	W14×233	W14×311
8	3.54	W18×46	W18×86	W14×233	W14×311
9	3.14	W18×46	W18×86	W14×233	W14×311
10	2.63	W18×40	W18×76	W14×159	W14×159
11	2.06	W18×40	W18×76	W14×159	W14×159
12	1.34	W18×50	W18×97	W14×159	W14×159

Table 6.3: Calculated system overstrength and degree of coupling

	Uncoupled SPSW		C-SPSW (P)		C-SPSW (R)	
Story	8	12	8	12	8	12
Overstrength	1.10	1.11	1.10	1.11	1.08	1.09
DC	-	-	0.31	0.32	0.30	0.31

Table 6.4: Fundamental periods and mean peak drifts from response history analyses

	Uncoupled SPSW		C-SPSW (P)		C-SPSW (R)	
Story	8	12	8	12	8	12
Period (s)	1.51	2.49	1.25	1.86	1.30	1.94
Story Drift (%)	2.32	2.41	1.61	1.72	1.53	1.56
Roof Drift (%)	1.44	1.53	1.20	1.10	1.21	1.09

Table 6.5: Ratios of the axial force demands at the bases of VBEs in C-SPSWs to those of uncoupled SPSWs

	Internal VBE		External VBE	
Story	8	12	8	12
C-SPSW (P)	0.55	0.48	0.92	0.91
C-SPSW (R)	0.49	0.45	0.86	0.86

Table 6.6: Ratios of the mean maximum VBE axial force demands from response history analyses to those calculated using capacity design

	8-story		12-story	
	Int. VBE	Ex. VBE	Int. VBE	Ext. VBE
Uncoupled SPSW	0.85	0.80	0.78	0.73
C-SPSW (P)	0.76	0.77	0.62	0.69
C-SPSW (R)	0.80	0.79	0.68	0.72

Table 6.7: Mean maximum coupling beam rotations and infill plates ductility demands from response history analyses

	Plate ductility demand (μ)		CB inelastic rotation (rad)	
Story	8	12	8	12
Uncoupled SPSW	5.00	3.64	-	-
C-SPSW (P)	3.67	3.16	0.11	0.015
C-SPSW (R)	4.09	3.56	0.10	0.013

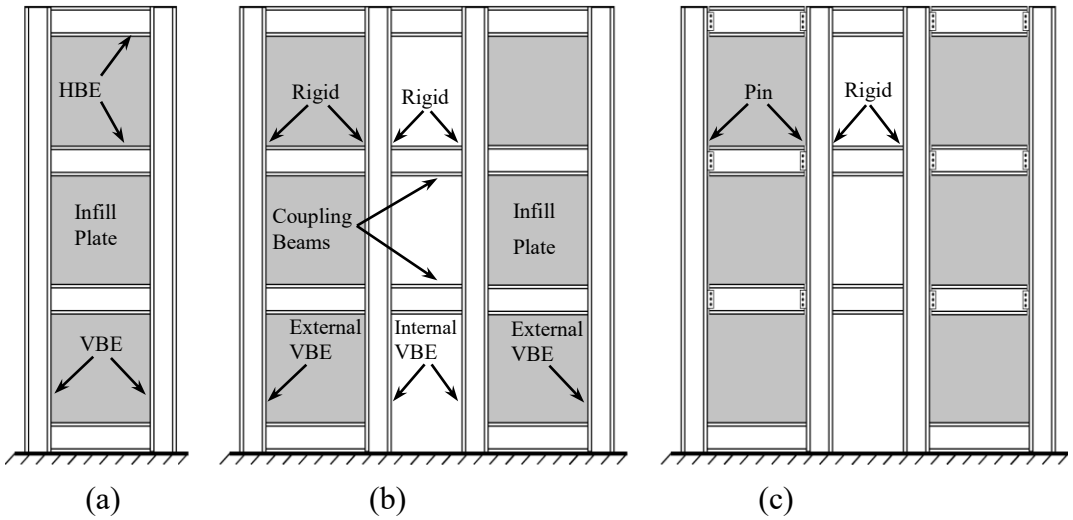

Figure 6.1: SPSW systems: (a) conventional (planar) SPSW; (b) C-SPSW (R); (c) C-SPSW (P)

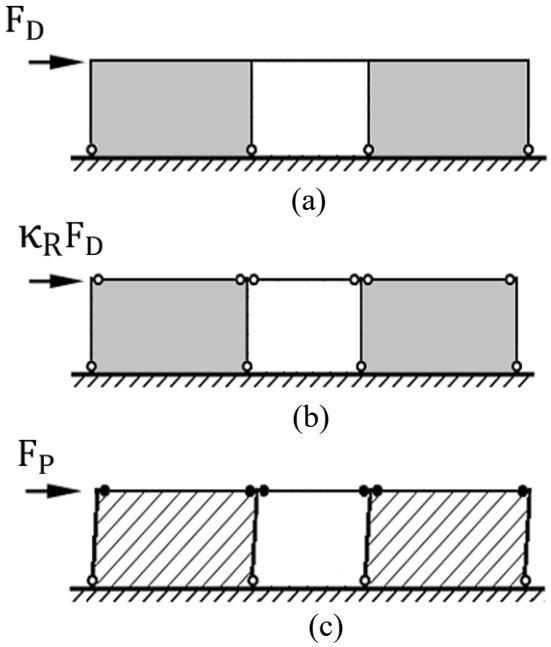

Figure 6.2 Single-story C-SPSW with rigid HBE-to-VBE connections: (a) system subjected to full lateral design load; (b) assigning a portion of the design load to infill panels; (c) lateral force needed to develop plastic mechanism for the system.

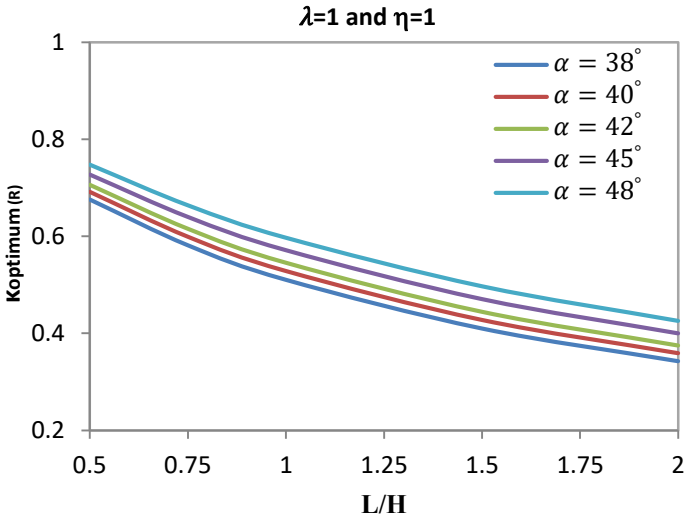

(a)

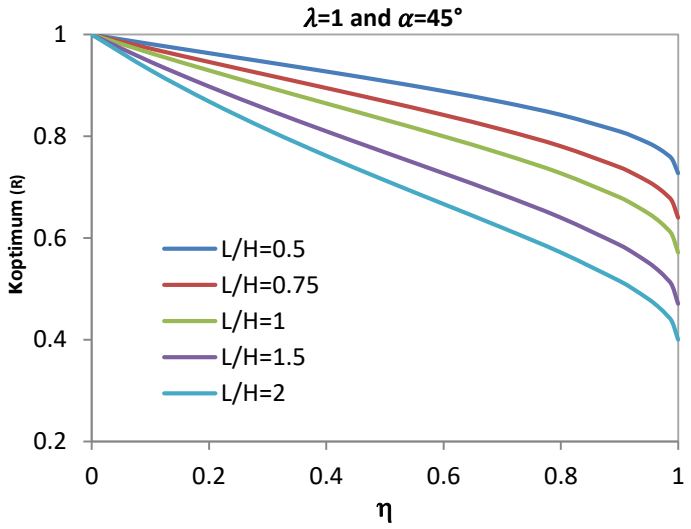

(b)

Figure 6.3 Variation of $\kappa_{optimum}$: (a) relationship between α, infill panel aspect ratio and $\kappa_{optimum}$ (assuming $\lambda = 1$ and $\eta = 1$); (b) relationship between η, infill panel aspect ratio and $\kappa_{optimum}$ (assuming $\lambda = 1$ and $\alpha = 45°$)

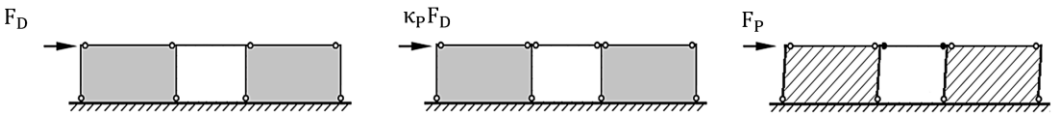

(a) (b) (c)

Figure 6.4 Single-story C-SPSW with pinned HBE-to-VBE connections: (a) system subjected to full lateral design load; (b) assigning a portion of the design load to infill panels; (c) lateral force needed to develop plastic mechanism for the system

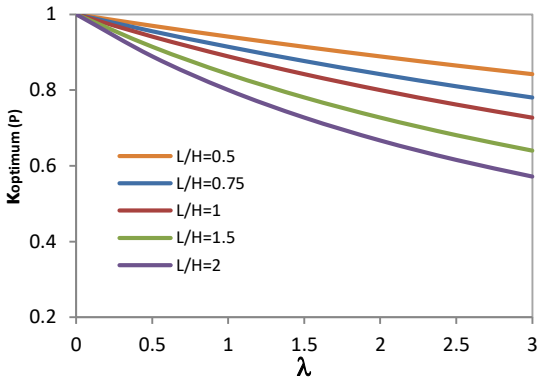

(a)

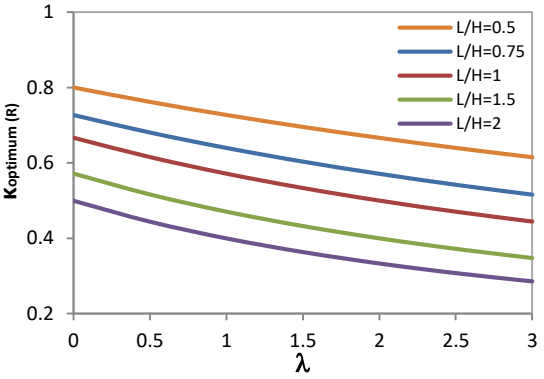

(b)

Figure 6.5 Relationship between $\kappa_{optimum}$, λ and infill panel aspect ratio: (a) single-story C-SPSW (P); (b) single-story C-SPSW (R)

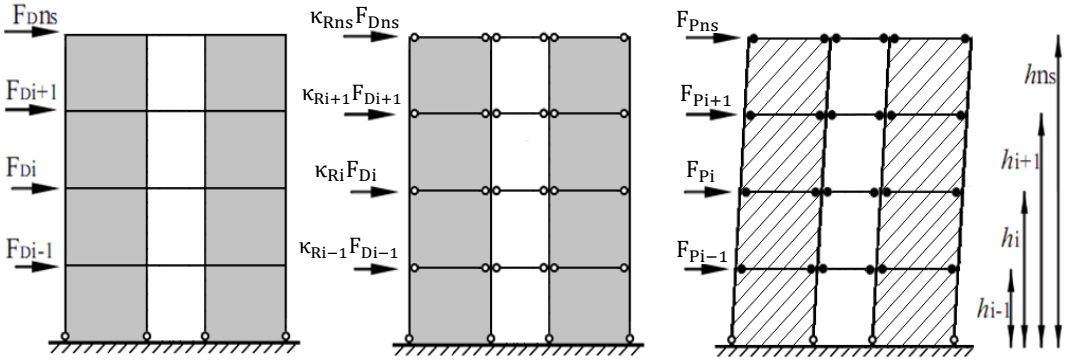

(a) (b) (c)

Figure 6.6 Multi-story C-SPSW (R): (a) system subjected to design lateral forces; (b) modified lateral force to size infill panel; (c) lateral force needed to develop desirable plastic mechanism

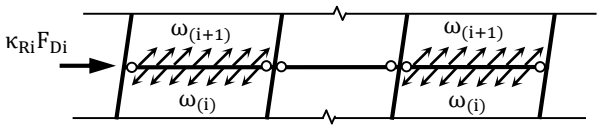

Figure 6.7 Tension field forces and modified design load in an intermediate floor of frame 6.6b

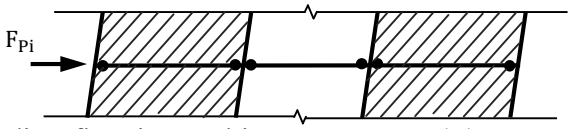

Figure 6.8 An intermediate floor in a multi-story C-SPSW (R) system in mechanism condition

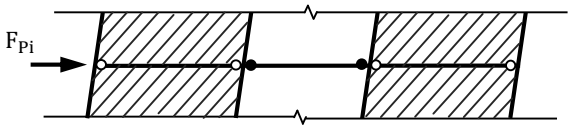

Figure 6.9 An intermediate floor in a multi-story C-SPSW (P)

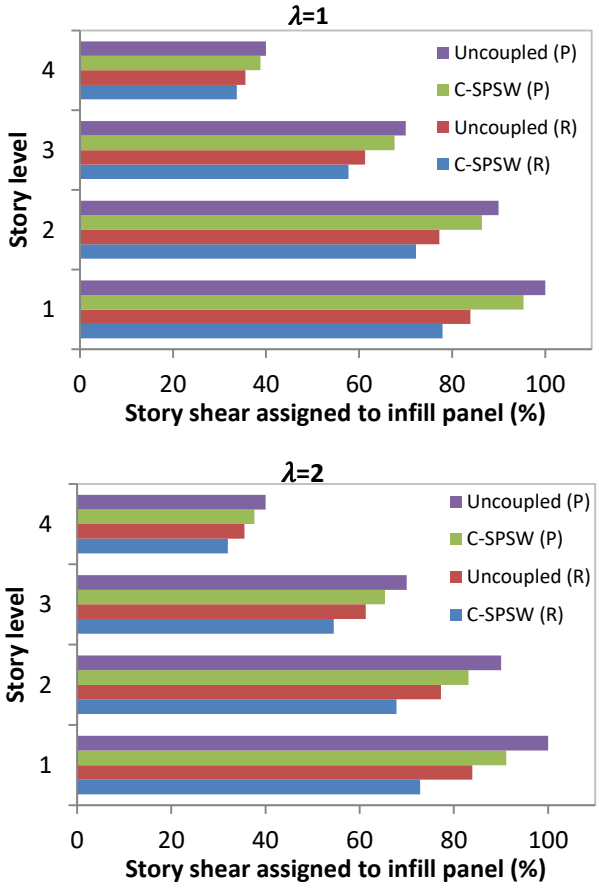

Figure 6.10 Comparison of story shears assigned to the infill panels in different SPSW systems (assuming $\eta = 1$)

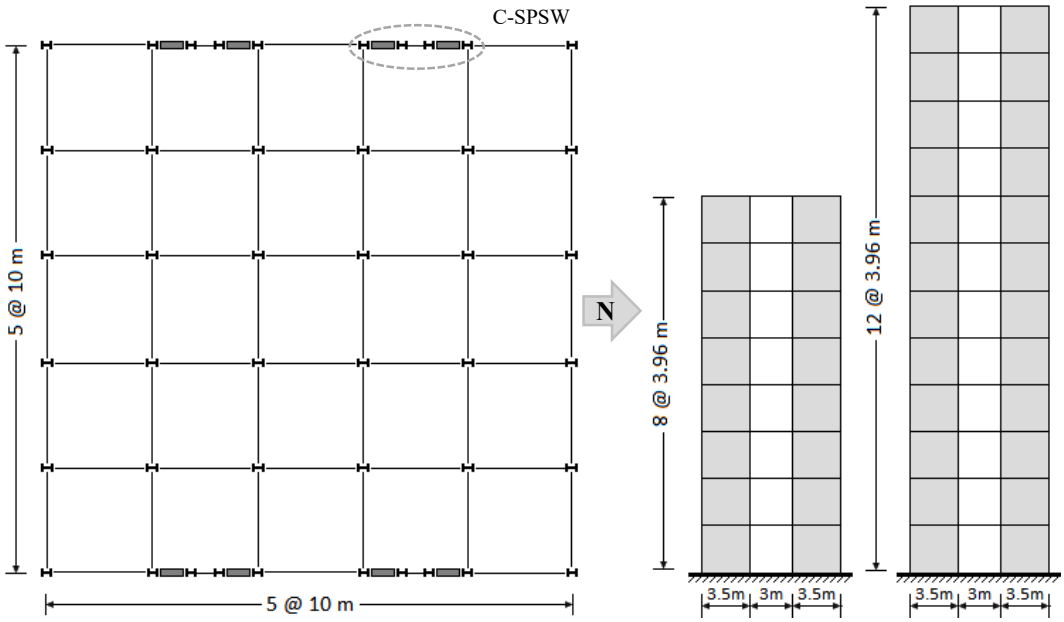

Figure 6.11 Building layout and C-SPSW systems

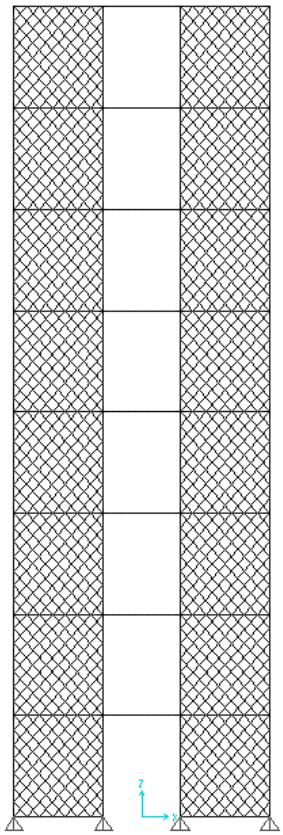

Figure 6.12 Strip model of an 8-story C-SPSW

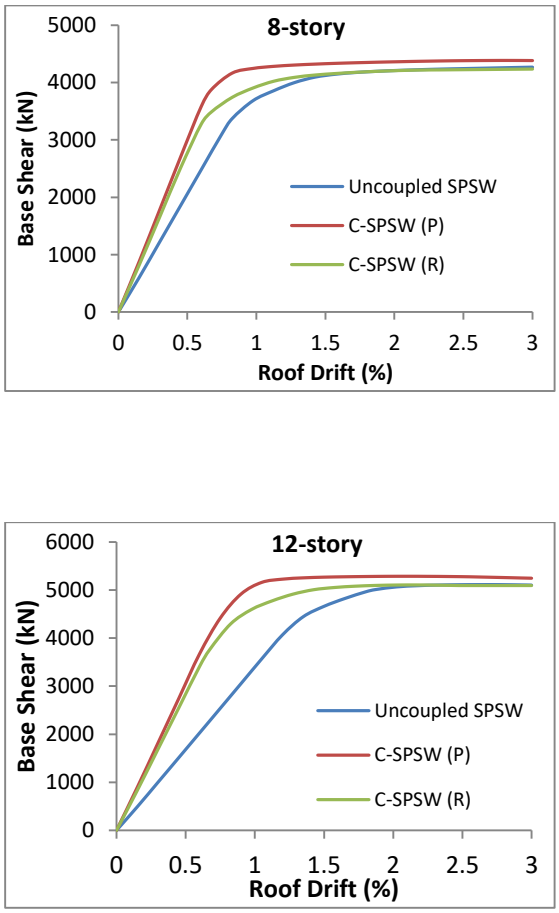

Figure 6.13 Pushover curves of the case study designs from nonlinear static analyses

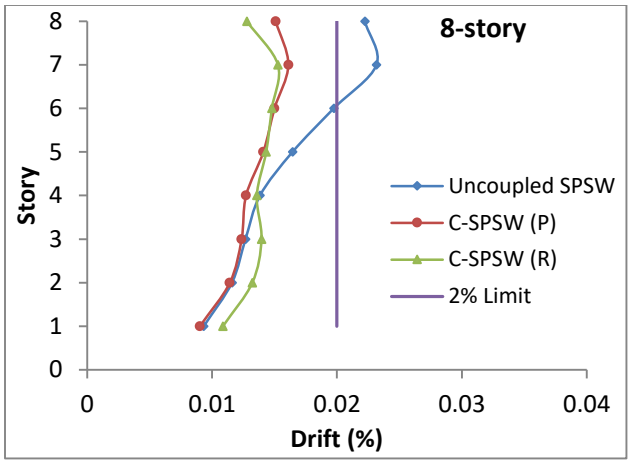

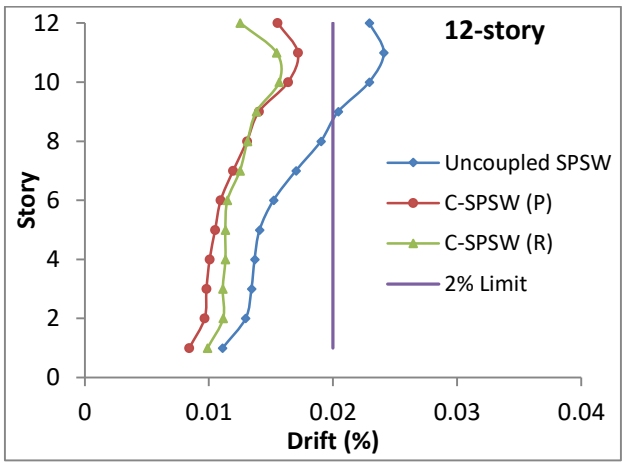

Figure 6.14 Mean drift demands from nonlinear response history analyses

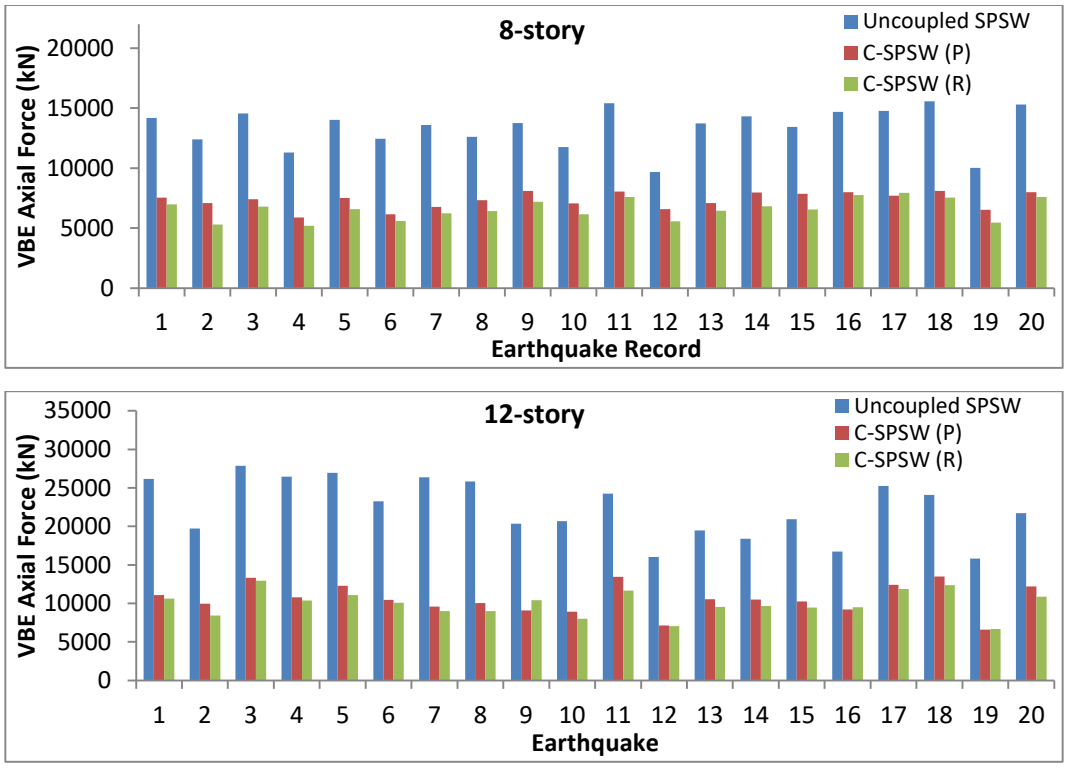

Figure 6.15 Maximum axial force demands at the base of internal VBEs

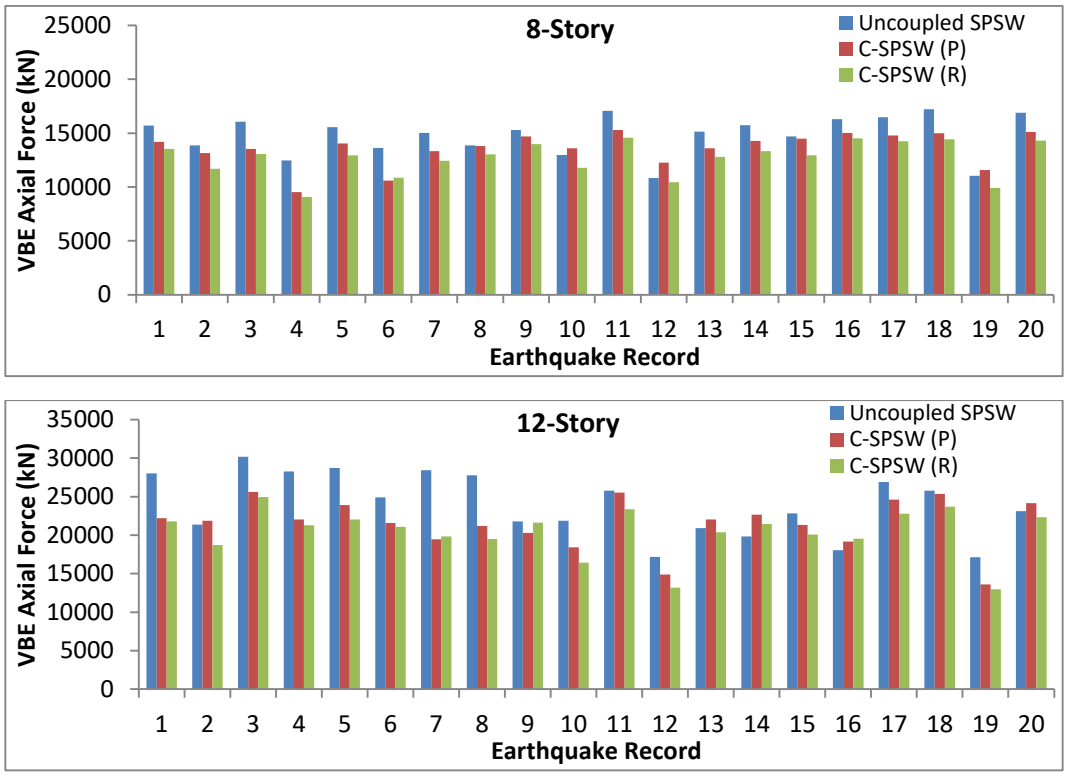

Figure 6.16 Maximum axial force demands at the base of external VBEs

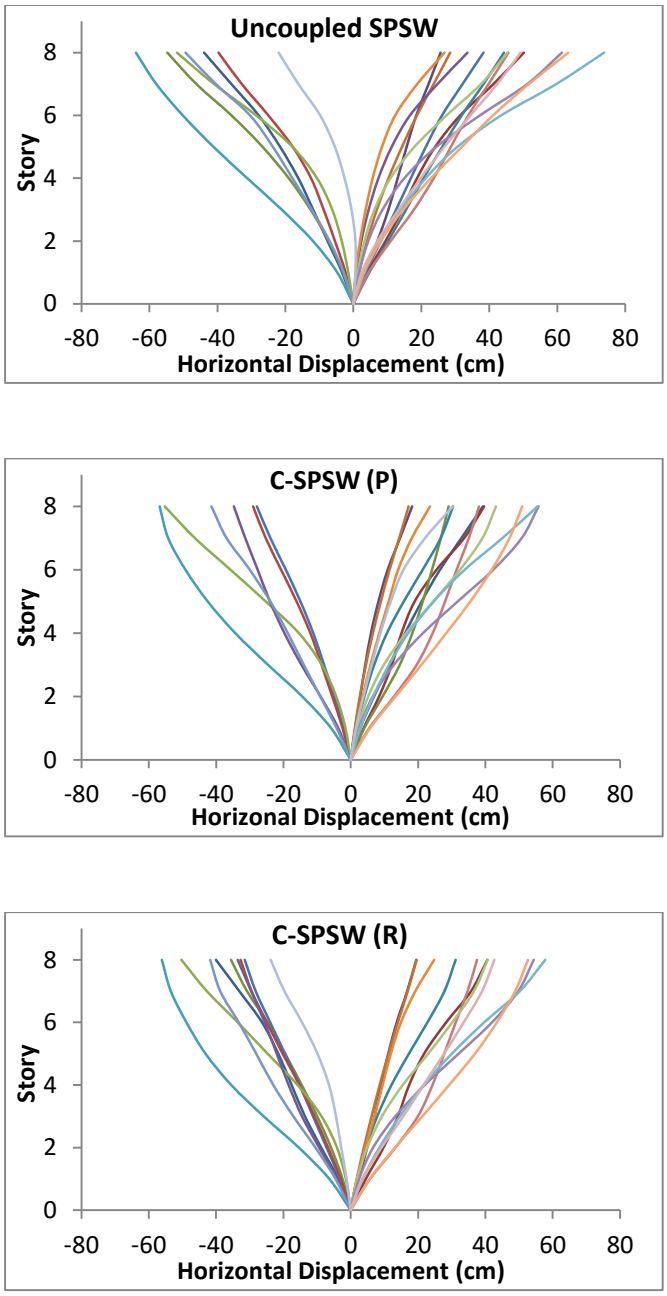

Figure 6.17 VBE displacement profile at the time of maximum roof drift in 8-story walls

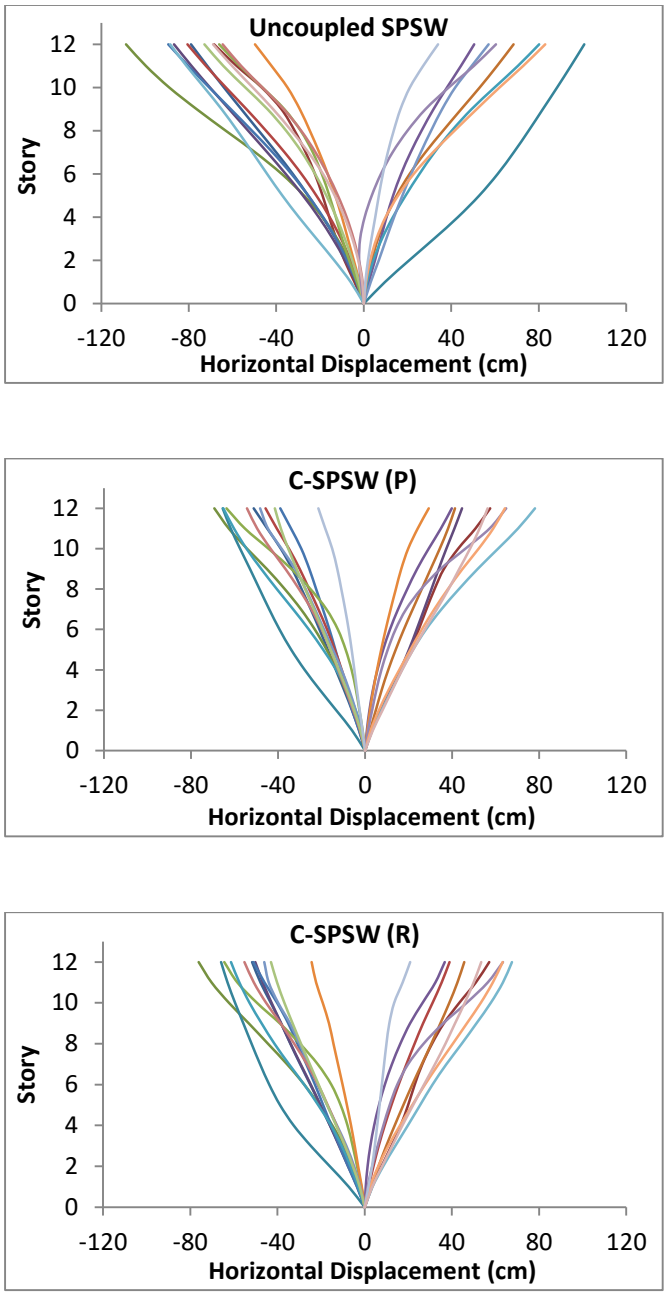

Figure 6.18 VBE displacement profile at the time of maximum roof drift in 12-story walls

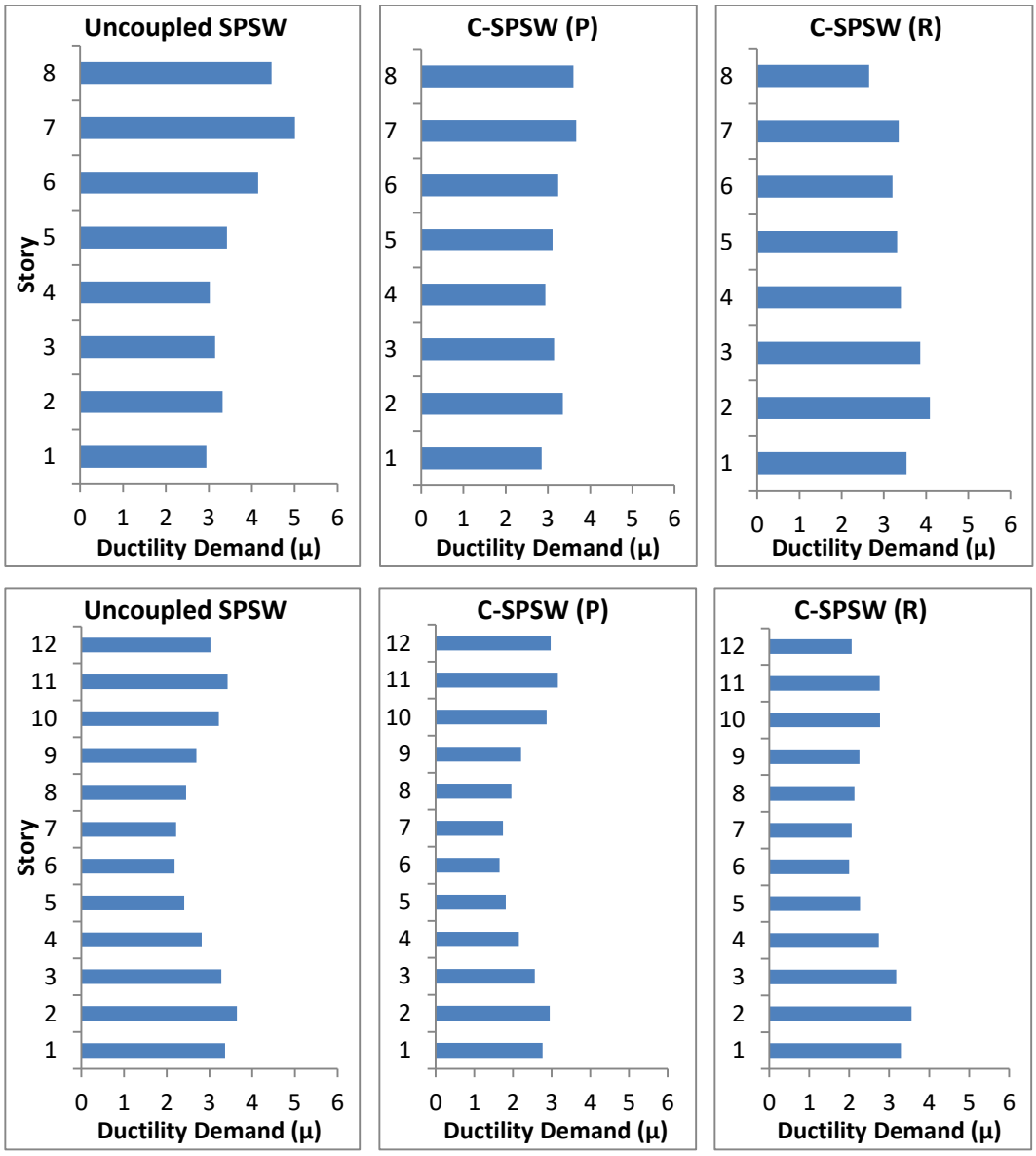

Figure 6.19 Mean infill plate ductility demands from response history analyses

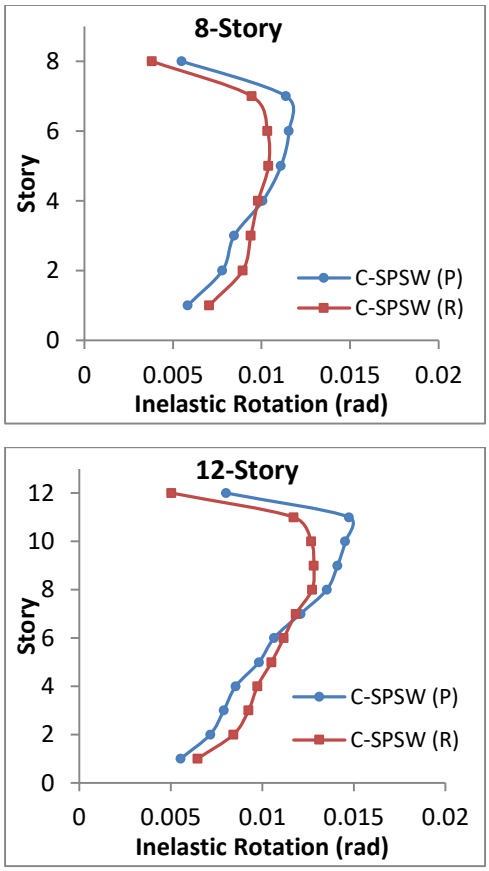

Figure 6.20 Coupling beam nonlinear rotation demands from response history analyses

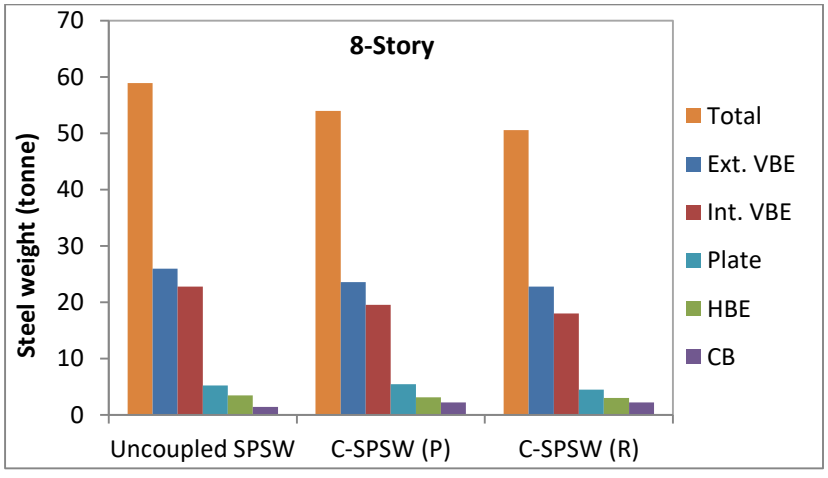

Figure 6.21 Steel weight comparisons of 8-story systems

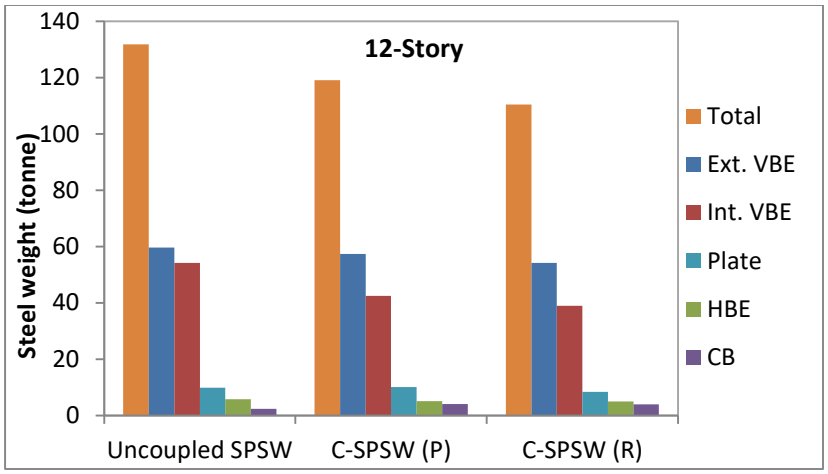

Figure 6.22 Steel weight comparisons of 12-story systems

6.7 References

AISC. (2010). Seismic provisions for structural steel buildings. ANSI/AISC 341-10, American Institute of Steel Construction, Chicago.

Berman, J.W., Lowes, L.N., Okazaki, T., Bruneau, M, Tsai, K-C., Driver, R.D., Sabelli, R. (2008). Research needs and future directions for steel plate shear walls. ASCE Structures Congress: Crossing Borders.

Berman, J.W., and Bruneau, M. (2003). Plastic analysis and design of steel plate shear walls. Journal of Structural Engineering, ASCE, 129 (11): 1448-1456.

Berman, J.W. and Bruneau, M. (2005). Experimental investigation of light-gauge steel plate shear walls. Journal of Structural Engineering; 131(2):259–267.

Berman, J.W. (2011). Seismic behavior of code designed steel plate shear walls. Engineering Structures, 33(1), 230–244.

Borello, D.J. and Fahnestock, L.A. (2012). Behaviour and mechanisms of steel plate shear walls with coupling. Journal of Constructional Steel Research, 74: 8–16.

Borello, D.J. and Fahnestock, L.A. (2012). Seismic design and analysis of steel plate shear walls with coupling, Journal of Structural Engineering, 139: 1263-1273.

Bruneau, M., Uang, C.M., and Sabelli, R. (2011). Ductile Design of Steel Structures. Second Edition, Mc Graw Hill.

Canadian Standards Association. (1994). Design of concrete structures. CSA A23.3-04, Canadian Portland Cement Association, Toronto.

Canadian Standards Association. (2014). Design of Steel Structures, CSA S16-14, Canadian Standards Association, Mississauga, ON.

Chaallal, O., Gauthier, D., and Malenfant, P. (1996). Classification methodology for coupled shear walls. Journal of Structural Engineering, ASCE, Vol. 122, No. 12.

Choi, I.R. and Park, H.G. (2008). Ductility and energy dissipation capacity of shear-dominated steel plate walls. Journal of Structural Engineering; 134(9):1495–507.

Driver, R.G., Kulak, G.L., Kennedy, D.J.L. and Elwi, A.E. (1997). Seismic behaviour of steel plate shear walls. Structural Engineering Report No. 215. Deptartment of Civil Engineering University of Alberta.

Li, C-H., Tsai, K-C., Chang, J-T., Lin, C-H., Chen, J-C., Lin, T-H. and Chen, P-C. (2012). Cyclic test of a coupled steel plate shear wall substructure. Journal of Earthquake Engineering and Structural Dynamics. 41:1277-1299.

Moghimi, H., Driver, R.G. (2013). Economical steel plate shear walls for low seismic regions. Journal of Structural Engineering, ASCE, Vol. 139, No. 3.

Qu, B. and Bruneau, M. (2009). Design of Steel Plate Shear Walls Considering Boundary Frame Moment-resisting Action. Journal of Structural Engineering, ASCE, Vol. 135, No. 12, pp. 1511-1521.

Vian, D. and Bruneau, M. (2005). Steel plate shear walls for seismic design and retrofit of building structures. Technical Rep. No. MCEER-05-0010, Multidisciplinary Center for Earthquake Engineering Research, Buffalo, N.Y.

Zhao, Q. and Astaneh-Asl, A. (2004). Cyclic behaviour of traditional and innovative composite shear walls. Journal of Structural Engineering, 130 (2): 271-284.

7. SUMMARY, CONCLUSIONS AND RECOMMENDATIONS

7.1 Summary

Steel plate shear walls (SPSWs) are ductile and efficient lateral force resisting systems available to the structural engineering community. However, despite the proven benefits of SPSWs, their implementation has been relatively limited, especially in mid- to high-rise buildings. The potential drawbacks to the system's use are attributed partly to some inherent structural characteristics of the conventional SPSW configuration (e.g., low overturning stiffness), and partly to some conservatism and ambiguities that still exist in current design practice.

A direct performance-based design procedure was presented for steel plate shear wall (SPSW) systems by explicitly taking into consideration the inelastic drift demands and dual action (infill panel-frame). The main objective was to tackle some of the shortcoming of current SPSW design practice, partly arising from the "indirect" force-based design approach and partly due to the conservative design assumptions (i.e., neglecting the lateral strength of the boundary frame).

The proposed design approach takes advantages of the philosophy of the performance-based plastic design (PBPD) methodology, which is built on an energy-work balance equation for a given structure. Several key design parameters were investigated by quantitatively and qualitatively examining SPSW system characteristics. The principles of plastic analysis and capacity design were extensively employed to achieve the intended yield mechanism and maximize material efficiency. As such, an "optimum" design concept was employed in this research to determine appropriate proportions of the lateral design loads that should be assigned to the infill panel in order to achieve an efficient design, while minimizing (or eliminating) the number of design iterations. A step-by-step design procedure was presented and the detailed description of each step was provided. Based on a series of nonlinear response history analyses of 12 SPSWs with different heights and infill panel aspect ratios, a simple empirical equation was presented to

predict the yield drift ratio in SPSW systems; this is an essential parameter that is used at the beginning of the design process.

Two eight-story SPSW structures were designed in order to investigate the effectiveness of the proposed design approach in achieving the desired performance objectives. For the purpose of comparison, these systems were also designed according to the applicable codes. The case study SPSWs were assumed to be located in high seismic zones in Canada and the U.S. The intention was to assess the behaviour of the SPSWs designed using the proposed approach for different seismic hazard levels. The seismic performances of the PBOD-SPSWs and code-SPSWs were evaluated under spectrum-compatible earthquake records for the given locations. Various characteristics of the seismic responses were investigated, especially in terms of story drift and inelastic deformation distributions in the energy dissipating elements (i.e., the infill plates and HBEs).

The behavioural characteristics and efficiency of SPSW with outriggers (SPSW-O) systems were studied, with an emphasis on the overturning stiffness and lateral load resistance. The SPSW-O system consists of a SPSW and two adjacent frames with rigidly connected beams which act as outriggers for the SPSW. Since a SPSW-O with all moment-resisting connections for the frame elements (i.e., the boundary frame and outrigger frames) is inherently a dual system with a high degree of redundancy (and high fabrication cost associated with the moment resisting connections), there was a significant incentive to provide potential economical options for such systems with comparable seismic performances. As such, several SPSW-O configurations were discussed that were specifically aimed at improving the flexural stiffness of the conventional SPSWs; these included various combinations of simple shear and moment-resisting HBE-to-VBE and OB-to-OC connections.

A parameter called the outrigger efficiency factor (OEF) was introduced in order to quantify the overturning stiffness provided by the outrigger system in a SPSW-O configuration. The OEF, which was defined as the proportion of the

overall overturning moment that is resisted by the outrigger elements, allows for the comparison of various SPSW-O systems on a consistent basis. The principles of plastic analysis were used to investigate the OEF and lateral load resistance of the four SPSW-O options discussed in this research. Closed-form analytical expressions of these two key design parameters were derived for each of the SPSW-O options and compared with numerical simulations with reasonable agreement. The simple expressions are valid tools, which allow the designer to reasonably estimate these parameters during the design process without the need to perform detailed numerical analysis during the design process. As such, they can significantly facilitate the design process when proportioning SPSW-O systems. A total of 16 SPSW-O designs were used to verify the analytical expressions of the OEF and ultimate lateral strength of the four SPSW-O configurations using numerical simulations. Nonlinear static analyses were conducted by employing strip models of the systems. The numerical results were then compared with those of the analytical equations with good accuracy. Next, a comprehensive parametric study was performed to investigate the influence of a number of parameters on the behaviour and efficiency of the SPSW-O systems. A total of 64 systems were designed considering the four SPSW-O options discussed in this research, with emphasis on varying the following parameters: the length and strength of the outrigger beams, the height of the systems, and the type of the beam-to-column connections.

Procedures were developed to achieve efficient designs for the four SPSW-O configurations, by explicitly taking into consideration the lateral load resistance provided by the outrigger system. For this purpose, the relative contributions of the outrigger frames and infill panels to the lateral strength of the systems were investigated, and appropriate shares of the lateral design load that should be used to size the infill plates within each of these configurations were estimated. In order to investigate the effectiveness of the proposed design approaches, 12- and 20-story SPSW-O structures were designed along with two free-standing SPSWs (i.e., no

outriggers) for the purpose of comparison. The seismic performances of the SPSW-O systems were evaluated under a suite of 20 earthquake time-history records, and compared with those of the free-standing walls.

Next, the proposed design approach was further extended to include the coupled SPSW (C-SPSW) systems. The C-SPSW configuration consists of two SPSW piers that are coupled through the coupling beams (CBs) at floor levels. Two C-SPSW options were considered in this research, namely (1) C-SPSW with pinned HBE-to-VBE connections, and (2) C-SPSW with moment-resisting HBE-to-VBE connections. A seismic design procedure was developed for these two options by employing the principles of plastic analysis and capacity design. The C-SPSWs are inherently dual systems in which the lateral loads are resisted through the tension field action of the infill plates and moment resisting actions of the HBE-to-VBE (if rigid) and CB-to-VBE connections. As such, the relative contribution of each of these components to the overall lateral load resistance was quantified for the both C-SPSW options, with the aim of achieving efficient designs for the systems. In order to assess the seismic performances of the two C-SPSW options discussed in this research, 8- and 12-story prototypes were designed using the proposed approach. In order to allow for the comparison of the two C-SPSW options on a consistent basis, both systems were proportioned to achieve the same levels of coupling as well as lateral load resistance. The seismic performances of the C-SPSWs were evaluated using nonlinear response history and pushover analyses. Various characteristics of the nonlinear response were evaluated, including the VBE axial force demands, infill plate ductility demands, coupling beam rotations, and story drifts. Furthermore, the seismic behaviour of the C-SPSWs were compared with those of the uncoupled SPSWs.

7.2 Conclusions

7.2.1 Free-Standing Steel Plate Shear Walls

It was demonstrated the proposed design approach is a promising alternative to the conventional design of SPSWs. The proposed procedure is capable of achieving SPSW performance objectives in a direct manner, while improving material efficiency and minimizing the need for design iterations. The two case study SPSWs designed using the proposed approach experienced fairly uniform story drifts within the pre-selected target values, while achieving the intended yield mechanism. Although slightly larger drift demands were observed in the PBOD-SPSWs compared to those of the code-designed SPSWs, especially in the lower half of the building heights, the mean responses were well-controlled within the 2% target drift, with fairly uniform distributions along the height of the systems.

The simple empirical equation presented for predicting yield drift ratio in SPSWs provided good estimates of this quantity, resulting in appropriate design base shears for the selected target drift and seismic hazard levels. The larger inelastic drifts experienced in the PBOD-SPSW prototypes were attributed to the considerably thinner infill panels used in their designs. While both the proposed procedure and code method resulted in similar design base shears, the former approach resulted in lighter system due to the explicit consideration of the boundary frame strength in the design process.

7.2.2 Steel Plate Shear Walls with Outriggers

The force transfer mechanisms and structural behaviour of the SPSW-O systems were studied by employing the statical and kinematic methods of plastic analysis. Closed-form expressions were derived for the lateral load resistance and the outrigger efficiency factor (OEF) of the four SPSW-O options discussed in this research. The validity of these analytical expressions was verified by using numerical simulations of multistory SPSW-O systems, and the results were found to be in close agreement. Therefore, these analytical expressions are valuable tools,

which can be used by the design engineers to facilitate the design process when proportioning SPSW-O systems for desired levels of strength and overturning stiffness. The OEF, which quantifies the effectiveness of the outrigger system in resisting overturning moments, allows for the comparison of different SPSW-O configurations on a consistent basis.

A comprehensive parametric study was conducted by designing 8- and 12-story SPSW-Os with various outrigger system characteristics. The outrigger beam lengths were either 3.2 m or 5.2 m. The outrigger beams within each SPSW-O option were proportioned for four different levels of flexural strength. For the SPSW-O systems designed using the proposed procedures, the level of interaction between the SPSW and the outrigger frames did not generally have a significant impact on the system weight when proportioned for the same overall strength. However, in the RR and PR configurations, the use of stronger outrigger beams, which leads to higher OEFs, resulted in slightly lighter systems, especially in the 12-story buildings. Also, the SPSW-O systems with moment-resisting HBE-to-VBE connections were slightly lighter than their counterparts having pinned HBE-to-VBE connections, with RR and PP being the lightest and heaviest systems in all cases, respectively. The results of the parametric study indicated that the type of HBE-to-VBE connections (i.e., pinned or rigid) within SPSW-Os does not have a considerable influence on the OEF when the systems are designed for the same overall strength. However, the use of pinned HBE-to-VBE connections within the SPSW-O systems (i.e., PP and RP systems) substantially reduces the share of the story shear that is resisted by the frame action. On the other hand, the type of OB-to-OC connections has significant impact on the level of interaction between the SPSW and the outrigger system. As such, to achieve the same level of OEF in all SPSW-O options, considerably stronger outrigger beams are needed in the systems with pinned OB-to-OC connections (i.e., RP and PP systems). In addition, for each SPSW-O option, the analytically predicted OEFs were similar for the 8- and 12-story systems designed with the same outrigger length and λ value (i.e., the OEFs were not influenced by the building height).

The mean values of the system overstrengths were 1.07, 1.08, 1.09 and 1.10 for the RR, RP, PR and PP systems, respectively, with corresponding standard deviations of 0.012, 0.015, 0.010 and 0.012. This indicates that material-efficient designs can be realized for such systems using the proposed procedures. The mean overstrength values calculated herein are generally lower than those of the code-designed SPSWs.

The relative contributions of the frame action and tension field action to the lateral load resistance were quantified for the four SPSW-O options discussed in this research, and key design parameters were identified. A preliminary design procedure was developed for the SPSW-O systems considering the frame moment-resisting action and employing principles of plastic analysis and capacity design. A series of nonlinear response history analyses were conducted to evaluate the seismic performances of mid-rise and high-rise SPSW-O systems designed according to the proposed design approaches. The behaviour of the case study designs was evaluated in terms of drifts, plate ductility demands, outrigger beam rotations, and the axial demands on the VBEs and outrigger columns. The results indicated that all of the case study SPSW-Os performed well under the seismic hazard level considered in this study (i.e., earthquakes with 10% probability of exceedance in 50 years). As such, all four SPSW-O configurations discussed in this research satisfied the desired performance objectives, and were comparably effective in limiting excessive drift demands due to the overturning moments.

The results also indicated that different SPSW-O options designed for the same level of strength as well as OEF were similarly effective in reducing VBE axial force demands. Therefore, the OEF was found to be an important factor influencing system performance that allows for the comparison of SPSW-O systems on a consistent basis. The reduced axial force demands on the VBEs in the SPSW-O configurations allows for the use of lighter VBE sections, especially in taller walls.

As in the conventional SPSWs, the capacity design procedure used for the design of VBEs and outrigger columns within the SPSW-O systems results in

conservative design for these elements, especially in the 20-story prototypes. The SPSW-O configurations generally reduced the ductility demands on the infill plates in the upper stories. However, slightly greater ductility demands were experienced in the lower story plates of the SPSW-Os with moment-resisting HBE-to-VBE connections (i.e., RP and RR systems). The ductility demands on the infill plates in all prototype designs were well within the acceptable limits determined by past experimental studies. The rotation demands on the outrigger beams were also well within the acceptable limits (0.02 rad) associated with the earthquake hazard level considered in this research. In summary, this study provided important insights on the behaviour and efficiency of the SPSW-Os, and helps further advance the implementation of the SPSW systems in mid- to high-rise building structures.

7.2.3 Coupled Steel Plate Shear Walls

This research covered C-SPSWs with either pinned or rigid HBE-to-VBE connections. A preliminary design procedure was developed for each of the two C-SPSW configurations by quantifying the relative contributions of the frame action (i.e., the moment-resisting action of the CB-to-VBE and HBE-to-VBE connections) and tension field action to the lateral load resistance of the systems.

A series of nonlinear static and response history analyses were performed to investigate the seismic behaviour of the two C-SPSW options discussed in this study. The performances of the 8- and 12-story prototype designs were evaluated in terms of drifts, plate ductility demands, coupling beam rotations and VBE demands. The results of nonlinear analyses indicated that both C-SPSW options performed well under the design-level ground motions, and were effective in meeting seismic performance objectives.

The results also indicated that both C-SPSW options designed for the same level of coupling as well as lateral load resistance were similarly effective in reducing the VBE axial force demands through the coupling action. As such, it was recognized that the degree of coupling (DC), which is an important factor

influencing the behavioural characteristics of the systems, allows for the comparison of the two C-SPSW options on a consistent basis.

The mean maximum axial force demands in the internal and external VBEs (at their bases) in C-SPSWs systems were, respectively, about 50% and 90% of those in the uncoupled walls. These reduced axial forces allow for the use of lighter VBE sections, especially the internal ones. It was recognized that the capacity design procedure used for the design of VBEs within the C-SPSW systems resulted in conservative design for these elements, especially in the 12-story buildings. The C-SPSW configuration generally reduced infill plate ductility demands in the upper stories of both the 8- and 12-story systems. However, slightly increased ductility demands were experienced in the infill plates at the lower stories of the 8-story C-SPSW with moment-resisting HBE-to-VBE connections. The inelastic demands on the infill plates were well within the acceptable limits in all C-SPSW designs. The nonlinear rotation demands on the coupling beams were all within the 0.02 radians limit under design-level earthquakes. This research extended the current understanding of the C-SPSW configurations and provided design recommendations to achieve efficient and cost-effective C-SPSW systems.

7.3 **Recommendation for Future Research**

While several SPSW-O options discussed in this research, each with slightly different characteristics, were found to be effective in achieving design objectives under the earthquake hazard level considered, further experimental and analytical research is warranted to support the findings of this research. Specifically, the seismic performances of these configurations under more severe earthquake excitations (e.g., maximum considered earthquake (MCE) with a 2% probability of exceedance in 50 years) also merit investigation. For this purpose, the analytical models of the systems must be capable of capturing deterioration of strips and fracture of components. It is also recommended that the FEMA P-695 approach for seismic performance assessment be used for such research.

It was demonstrated that the C-SPSW systems with simple HBE-to-VBE connections exhibited seismic performance comparable with that of the C-SPSWs with moment-resisting connections under the design-level earthquakes at a possibly reduced fabrication cost. Further, research is needed to evaluate the seismic behaviour of these systems under more severe hazard levels.

In the derivation of the analytical expressions presented for the design of C-SPSW and SPSW-O systems that included simple beam-to-column connections, it was assumed that these connections are ideally pinned. In reality, however, even simple shear connections (e.g., double angle and shear tab connections) possess non-negligible flexural rigidity. Therefore, further modification may be needed to account for this effect.

In this research, it was assumed that the beam-to-column connections in C-SPSW and SPSW-O systems (HBE-to-VBE and OB-to-OC connections are either pinned or rigid. Analytical and experimental research is needed to investigate the behaviour of such systems with semi-rigid connections.

8. REFERENCES

AISC (2010). Seismic Provisions for Structural Steel Buildings. ANSI/AISC 341-10, American Institute of Steel Construction, Incl., Chicago, Illinois.

ASCE. (2010). Minimum design loads for buildings and other structures. SEI/ASCE 7-10, Reston, VA.

Aschheim, M.A., and Black, E.F. (2000). Yield point spectra for seismic design and rehabilitation. Earthquake Spectra, Vol. 16, No. 2, 317-336.

ASTM. (2008). Standard specification for Carbon structural steel. A36, West Conshohocken, PA.

Bayat, M.R. (2010). Performance-based plastic design of earthquake resistant steel structures: concentrically braced frames, tall moment frames, plate shear wall frames. Ph.D. dissertation, Department of Civil Engineering, The University of Texas at Arlington, Texas.

Berman, J.W. (2011). Seismic behavior of code designed steel plate shear walls., Engineering Structures, 33(1), 230–244.

Berman, J.W. and Bruneau, M. (2005). Experimental Investigation of Light-Gauge Steel Plate Shear Walls. Journal of Structural Engineering, 131 (2), 259-267.

Berman, J.W., and Bruneau, M. (2003). Plastic analysis and design of steel plate shear walls. Journal of Structural Engineering, ASCE, 129 (11): 1448-1456.

Berman, J.W., Lowes, L.N., Okazaki, T., Bruneau, M, Tsai, K-C., Driver, R.D., Sabelli, R. (2008). Research needs and future directions for steel plate shear walls. ASCE Structures Congress: Crossing Borders.

Bhowmick, A.K. (2009). Seismic analysis and design of steel plate shear walls. Ph.D Dissertation, Department of Civil and Environmental Engineering, University of Alberta, Edmonton, Canada.

Bhowmick, A.K., Grondin, G.Y., and Driver, R.G. (2011). Estimating fundamental periods of steel plate shear walls., Engineering Structures, 33(6), 1883-1893.

Borello, D.J. and Fahnestock, L.A. (2012). Behaviour and mechanisms of steel plate shear walls with coupling. Journal of Constructional Steel Research, 74: 8–16.

Borello, D.J. and Fahnestock, L.A. (2012). Seismic design and analysis of steel plate shear walls with coupling, Journal of Structural Engineering, 139: 1263-1273.

Browning, J.P. (2001). Proportioning of earthquake-resistant RC building structures. Journal of the Structural Division, ASCE, Vol. 127, No.2, 145-151.

Bruneau, M., Uang, C.M. and Sabelli, R. (2011). Ductile design of steel structures. Second Edition, Mc Graw Hill.

Chaallal, O., Gauthier, D., and Malenfant, P. (1996). Classification methodology for coupled shear walls. Journal of Structural Engineering, ASCE, Vol. 122, No. 12.

Chao, S.-H., and Goel, S.C. (2006a). Performance-based design of eccentrically braced frames using target drift and yield mechanism. AISC Engineering Journal, Third quarter: 173–200.

Chao, S.-H., and Goel, S.C. (2006b). A seismic design method for steel concentric braced frames (CBF) for enhanced performance. In Proceedings of Fourth International Conference on Earthquake Engineering, Taipei, Taiwan, 12–13 October, Paper No. 227.

Chao, S.-H., Goel, S.C., and Lee, S.-S. (2007). A seismic design lateral force distribution based on inelastic state of structures. Earthquake Spectra 23: 3, 547–569.

Chao, S.-H., and Goel, S.C. (2008). Performance-based plastic design of seismic resistant special truss moment frames. AISC Engineering Journal, Second quarter: 127–150.

Choi, I-R., and Park, H-G. (2008). Ductility and energy dissipation capacity of shear-dominated steel plate walls. Journal of Structural Engineering, ASCE, Vol. 134, No. 9, pp. 1495-1507.

Choi, I-R., and Park, H-G. (2009). Steel plate shear walls with various infill plate designs. Journal of Structural Engineering, ASCE, Vol. 135, No. 7, pp. 785-796.

Choi, I-R., and Park, H-G. (2010). Hysteresis model of thin infill plate for cyclic nonlinear analysis of steel plate shear walls." Journal of Structural Engineering, ASCE, Vol. 136, No. 11, pp. 1423-1434.

Chopra, A.K., and Goel, R.K. (2001). Direct displacement-based design: use of inelastic vs. elastic design spectra. Earthquake Spectra, Vol. 17, No.1, 47-65.

Chopra, A.K., and Goel, R.K. (2002). A modal pushover analysis procedure for estimating seismic demands for buildings. Earthquake Engineering & Structural Dynamics, 31 (3), 561-582.

CSA (1994). Limit states design of steel structures. CAN/CSA S16-94, Canadian Standards Association, Rexdale, ON, Canada.

CSA (2009). Design of steel structures. CAN/CSA S16-14, Canadian Standards Association, Mississauga, ON, Canada.

CSA (1994). Design of concrete structures. CSA A23.3-04, Canadian Standards Association, Rexdale, ON, Canada.

Dasgupta, P., Goel, S.C., and Parra-Montesinos, G. (2004). Performance-based seismic design and behaviour of a composite buckling restrained braced frame (BRBF). In Proceedings of Thirteenth World Conference on Earthquake Engineering, Vancouver, Canada, 1–6 August 2004, Paper No. 497.

Dastfan, M., and Driver, R.G. (2008), Flexural stiffness limits for frame members of steel plate shear wall systems, Proceedings of Annual Stability Conference, Nashville, Structural Stability Research Council, Rolla, MO.

Della Corte, G. and Mazzolani, F.M. (2008). Theoretical developments and numerical verification of a displacement-based design procedure for steel braced structures. 14th World Conference on Earthquake Engineering, Beijing, China.

Driver, R.G., Kulak, G.L., Kennedy, D.J.L., and Elwi, A.E. (1997). Seismic behavior of steel plate shear walls. Structural Engineering Rep. 215, Deptartment of Civil Engineering, University of Alberta, Edmonton, Alberta, Canada.

Driver, R.G., Kulak, G.L., Kennedy, D.J.L., and Elwi, A.E. (1998a). Cyclic test of a four-story steel plate shear wall. Journal of Structural Engineering; 124(2):112–30.

Driver, R.G., Kulak, G.L., Elwi, A.E. and Kennedy, D.J.L. (1998b). FE and simplified models of steel plate shear walls. Journal of Structural Engineering, 124 (2), 121-130.

Elgaaly, M. (1998). Thin steel plate shear walls behavior and analysis. Thin-Walled Structures, 32(1–3), 151–180.

FEMA. (2000). FEMA355 State of the art report on systems performance of steel moment frames subject to earthquake ground shaking. Report No. FEMA-355C, FEMA, Washington, DC.

FEMA (2003). NEHRP recommended provisions for seismic regulations for new buildings and other structures. FEMA Report No. 450, Building Safety Council for FEMA, Washington, D.C.

Freeman, S.A. (1998). The capacity spectrum method as a tool for seismic design, Proceedings of the 11th European Conference on Earthquake Engineering, Sept 6-11, Paris.

Gholipour, M., Asadi, E., and Alinia, M.M. (2015). The use of outrigger system in steel plate shear wall structures. Advances in Structural Engineering Vol. 18 No. 6: 853-872.

Ghosh, S., Adam, F., and Das, A. (2009). Design of steel plate shear walls considering inelastic drift demand. Journal of Constructional Steel Research, Vol. 65, pp. 1431–1437.

Goel, S.C., and Chao, S.-H. (2008). Performance-based plastic design: earthquake resistant steel structures. International Code Council.

Goggins, J.G., and Sullivan, T.J. (2009). Displacement-based seismic design of SDOF concentrically braced frames, in STESSA 2009, Mazzolani, Ricles & Sause (eds), Taylor & Francis Group, pp. 685-692.

Gupta, A., and Krawinkler, H. (1999). Seismic demands for performance evaluation of steel moment-resisting frame structures. Report no. 132. John A. Blume earthquake engineering center. Stanford University.

Housner, G.W. (1956). Limit design of structures to resist earthquakes. In Proceedings of First World Conference on Earthquake Engineering, Earthquake Engineering Research Institute, Berkeley, CA, June; Part 5: 1–11.

International Code Council. (2012) International Building Code (IBC).

Kalkan, E., and Kunnath, S.K. (2006). Adoptive modal combination procedure for nonlinear static analysis of building structures. Journal of Structural Engineering. 132:11, 1721-1731.

Kharmale, S.B., and Ghosh, S. (2013). Performance-based plastic design of steel plate shear walls. Journal of Constructional Steel Research, Vol. 90, pp. 85–97.

Kurban, C.O., and Topkaya, C. (2009). A numerical study on response modification, overstrength, and displacement amplification factors for steel plate shear wall systems. Earthquake Engineering and Structural Dynamics, 38: 497-516.

Lee, S.-S., and Goel, S.C. (2001). Performance-based design of steel moment frames using target drift and yield mechanism. Research Report no. UMCEE 01-17, Dept. of Civil and Environmental Engineering, University of Michigan, Ann Arbor, MI.

Leelataviwat, S., Goel, S.C., and Stojadinovic, B. (1999). Toward performance-based seismic design of structures. Earthquake Spectra 15(3): 435–461.

Leelataviwat, S., Saewon, W., and Goel, SC. (2007). An energy based method for seismic evaluation of structures. In Proceedings of Structural Engineers Association of California Convention, SEAOC 2007, Lake Tahoe, CA, September 26–29, 2007; 21–31.

Liao, W-C., and Goel, S.C. (2012). Performance-based plastic design and energy-based evaluation of seismic resistant RC moment frame. Journal of Marine Science and Technology, Vol. 20, No. 3, pp. 304-310.

Li, C-H., Tsai, K-C., Chang, J-T., Lin, C-H., Chen, J-C., Lin, T-H. and Chen, P-C. (2012). Cyclic test of a coupled steel plate shear wall substructure. Journal of Earthquake Engineering and Structural Dynamics. 41:1277-1299.

Mazzoni, S., McKenna, F., Scott, M.H., and Fenves, GL. (2006). Open system for earthquake engineering simulation user command-language manual-opensees version 1.7.3. Pacific earthquake engineering research center.

Moghimi, H., and Driver, R.G. (2013). Economical steel plate shear walls for low seismic regions. Journal of Structural Engineering, 139, 379–388.

NBCC. (2010) National building code of Canada. National Research Council of Canada, Ottawa, ON, Canada.

Neal, B.G. (1977). The plastic method of structural analysis, Chapman & Hall, London.

Neilson, D.A.H., Grondin, G.Y., and Driver, R.G. (2010). Welding of light gauge infill panels for steel plate shear walls. Structural Engineering Report No. 290, Department of Civil and Environmental Engineering, University of Alberta, Edmonton, Canada.

Newmark, N.M., and Hall, W.J. (1982). Earthquake spectra and design, Engineering Monographs on Earthquake Criteria, Structural Design, and Strong Motion Records, Vol 3, Earthquake Engineering Research Institute, University of California, Berkeley, CA.

Panagiotakos, T.B., and Fardis, M.N. (1999). Deformation-controlled earthquake-resistant design of RC buildings. Journal of Earthquake Engineering, Vol. 3 No. 4, 498-518.

Priestley, M.J.N., and Kowalsky, M.J. (2000). Direct displacement-based design of concrete buildings. Bulletin of the New Zealand National Society for Earthquake Engineering, New Zealand National Society for Earthquake Engineering, Silverstream. Vol. 33, No.4.

Priestley, M.J.N., Calvi, G.M., and Kowalski, M.J. (2007). Displacement based seismic design of structures, IUSS Press, Pavia, Italy.

Purba, R., and Bruneau, M. (2012). Case study on the impact of horizontal boundary elements design on seismic behaviour of steel plate shear walls. Journal of Structural Engineering, Vol. 138, No. 5, 645-657.

Purba, R., and Bruneau, M. (2009). Finite element investigation and design recommendations for perforated steel plate shear walls. Journal of Structural Engineering, ASCE, Vol. 135, No. 11, 1367-1376.

Qu, B., Bruneau, M., Lin, C.H., and Tsai, K.C. (2008). Testing of full scale two-story steel plate shear walls with RBS connections and composite floor. Journal of Structural Engineering, 134 (3), 364–373.

Qu, B., and Bruneau, M. (2009). Design of steel plate shear walls considering boundary frame moment-resisting action. Journal of Structural Engineering, ASCE, Vol. 135, No. 12, pp. 1511-1521.

Roberts, T., and Sabouri-Ghomi, S. (1992). Hysteretic characteristics of unstiffened perforated steel plate shear panels." Thin Walled Structures, Vol. 14, 139-151.

Saatcioglu, M., and Humar, J. (2003). Dynamic analysis of building for earthquake resistant design. Canadian Journal of Civil Engineering, 30:338-359.

Safari Gorji, M. and Cheng, J.J.R. (2013). Performance-based plastic design of Type D steel plate shear walls. Proc. Canadian Society for Civil Engineering Annual Conference, Montreal.

Safari Gorji, M., and Cheng, J.J.R. (2015). Improving overturning stiffness of steel plate shear walls, Proc., Structures Congress, Structural Engineering Institute, ASCE, Portland.

Sahoo, D.R., and Chao, S-H. (2010). Performance-based plastic design method for buckling-restrained braced frames. Engineering Structures, Vol. 32: 2950-2958.

Salawdeh, S. (2012). Seismic design of concentrically braced steel frames. PhD thesis, National University of Ireland, Galway, Ireland, 280 pages.

SAP2000 Version 14.2 [Computer software]. Computer and Structures Inc., Berkeley, CA.

Shibata, A., and Sozen, M.A. (1976). Substitute structure method for seismic design in RC. Journal of Structural Division, ASCE, Vol. 102, ST1.

Shishkin, J.J., Driver, R.G., and Grondin, G.Y. (2009). Analysis of steel plate shear walls using the modified strip model. Journal of Structural Engineering, ASCE, Vol. 135, No. 11.

Somerville, P., Smith, N., Punyamurthula, S., and Sun, J. (1997). Development of ground motion time histories for phase 2 of the FEMA/SAC steel project. SAC background document. Report no. SAC/BD-97/04. SAC Joint Venture. 1997.

Sullivan, T.J., Maley, T., and Calvi, G.M. (2011). Seismic response of steel moment-resisting frames designed using a Direct DBD procedure. 8th International Conference on Structural Dynamics, Eurodyn2011, paper No.730.

Sullivan, T.J. (2012). Formulation of a direct displacement-based design procedure for steel eccentrically braced frame structures. 15th World Conference on Earthquake Engineering, Lisbon, Portugal.

Taranath, B.S. (2012). Structural analysis and design of tall buildings; steel and composite construction. International Code Council. CRC Press, Taylor & Francis Group.

Thorburn, L.J., Kulak, G.L., and Montgomery, C.J. (1983). Analysis of steel plate shear walls. Structural Engineering Report No. 107, Department of Civil Engineering, University of Alberta, Edmonton, Alberta, Canada.

Timler, P.A., and Kulak, G.L. (1983). Experimental study of steel plate shear walls. Structural Engineering Rep., No. 114, Department of Civil Engineering, University of Alberta, Edmonton, Alberta, Canada.

Topkaya, C., and Kurban, C.O. (2009). "Natural periods of steel plate shear wall systems." Journal of Constructional Steel Research, 65(3), 542-551.

Vian, D., and Bruneau, M. (2005). Steel plate shear walls for seismic design and retrofit of building structure. Technical Report No. MCEER-05-0010, Multidisciplinary Center for Earthquake Engineering Research, Buffalo, New York.

Vian, D., Bruneau, M., Tsai, K.-C., and Lin, U.C. (2009). Special perforated steel plate shear walls with reduced beam section anchor beams I: experimental investigation & II: analysis and design recommendations, Journal of Structural Engineering, ASCE, 135, 3, 211-228.

Wijesundara, K. (2009). Design of concentrically braced steel frame with RHS shape braces. PhD thesis, ROSE School, IUSS Pavia, Italy, 345pages.

Zhao, Q. and Astaneh-Asl, A. (2004). Cyclic behaviour of traditional and innovative composite shear walls. Journal of Structural Engineering, 130 (2): 271-284.